Nicolae BUZBUCHI **Liviu-Constantin STAN**

Cătălin FAITĂR

♦

DYNAMIC BEHAVIOR MODELING AND SIMULATION OF MARINE PROPULSION SYSTEMS

Nicolae BUZBUCHI **Liviu-Constantin STAN**

Cătălin FAITĂR

DYNAMIC BEHAVIOR MODELING AND SIMULATION OF MARINE PROPULSION SYSTEMS

Editura NAUTICA

Constanța 2022

Editura **NAUTICA**, 2011
Editură recunoscută de CNCSIS
Str. Mircea cel Bătrân nr.104
900663 Constanţa, România
tel.: +40-241-66.47.40
fax: +40-241-61.72.60
e-mail: info@cmu-edu.eu
www.edituranautica.org.ro

Descrierea CIP a Bibliotecii Naţionale a României

BUZBUCHI, NICOLAE
Dynamic behavior modeling and simulation of marine propulsion systems / Nicolae Buzbuchi, Liviu-Constantin Stan, Cătălin Faitar. - Constanţa : Nautica, 2022
Conţine bibliografie
ISBN 978-606-681-170-5

I. Stan, Liviu Constantin
II. Faitar, Cătălin

629.5

Acknowledgement

The work of Faitar Catalin was supported by the project "PROINVENT", Contract no. 62487/03.06.2022 - POCU/993/6/13 - Code 153299, financed by The Human Capital Operational Programme 2014–2020 (POCU), Romania.

Table of Contents

1. KINETICS AND DYNAMIC OF MARINE ENGINES

Piston internal combustion marine engines have a particular feature consisting in the transformation of the alternative translation motion of the piston, under the gas pressure generated by the burning process of fuel in the cylinders, in crank shaft a motion, through the mean of the crank gear.

In the following pages piston internal combustion engines dynamics general aspects will be presented. This category of engines includes the marine engines which will be analyzed in a modern analytical fashion this way offering the possibility of realizing fast connections between the present chapter and the next ones which are being devoted to an detailed analysis of the dynamic behavior of marine propulsion engines.

1.1 Kinetics of the engine drive

The necessity in studying the kinetics of the engine gear is being imposed by the necessity of knowing the forces and the stresses generated by them by calculating functions defining the displacement, the speed and the acceleration of main components that complete de engine gear.

1.1.1. Kinetics of normal engine gear

The normal engine gear is presented in the 1.1 diagram. Its main components are the crank with a R length, which has a rotation speed with an angular speed ω, having a constant value, the reciprocating rod with a L length, being articulated with the crank in a M defined point and having a plane-parallel motion; the piston is being articulated on the reciprocating rod by a bolt or a crosshead (this being a solution used for two stroke marine engines) having and alternative translation motion along the piston in the P point.

For the kinetic analysis of the normal engine gear as a general coordinate the rotation crank angle θ is being chosen, thus the mechanism position will be completely defined by two variable values: β – the reciprocating rod leaning angle and the y-coordinate. In this manner, from the theory of mechanism [2] and [9] the following formulas can be applied:

$$\begin{cases} \beta = \arcsin(\lambda \sin\theta) \\ y = R\cos\theta + L\cos\beta \end{cases}$$

Were the λ ratio has been inserted also known as the elongation of the reciprocating rod (gear compactness coefficient) being calculated with the following formula:

$$\lambda = R / L$$

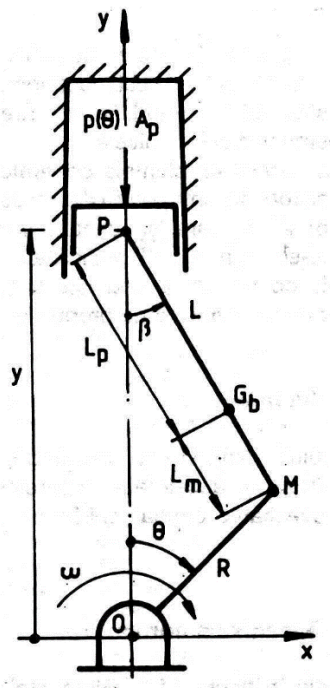

Figure 1.1: The normal engine gear diagram

Using those two formulas we can define the following coefficients:

$$\begin{cases} c_{w_p} = \dfrac{dy}{d\theta} = -ytg\beta \\ c_{\omega_b} = \dfrac{d\beta}{d\theta} = \lambda \dfrac{\cos\theta}{\cos\beta} \\ c_{a_p} = \dfrac{dc_{y_p}}{d\theta} = \\ \quad = -R\cos\beta - c_{\omega_b}^2 L\cos\beta - \\ \quad - c_{\varepsilon_b} L\sin\beta \\ c_{\varepsilon_b} = \dfrac{dc_{\omega_b}}{d\theta} = \\ \quad = -\lambda \dfrac{\sin\theta}{\cos\beta} + c_{\omega_b}^2 tg^2\beta \end{cases} \quad (1.3)$$

The coefficients above are known as:

w_p – the piston speed coefficient;

ω_b – reciprocating rod angular speed coefficient;

ε_b – reciprocating rod angular acceleration coefficient.

It should be noted that the β and y variables, as well as their derivatives are generalized coordinate functions θ, thus their values vary with the rotation movement of the reciprocating rod.

Depending on the previous defined coefficients we can calculate the kinematic values for the normal engine gear, in classical formulation [5], [11], [12]. [14], [17] as in (1.4) formulas.

It can be noticed that the piston motion is being noted as y_p, usual registered in p.m.i (lower dead center). Unlike the previous formulations the explicit dependency on the generalized coordinate is being highlighted by using coefficients defined by the (1.3) formulas.

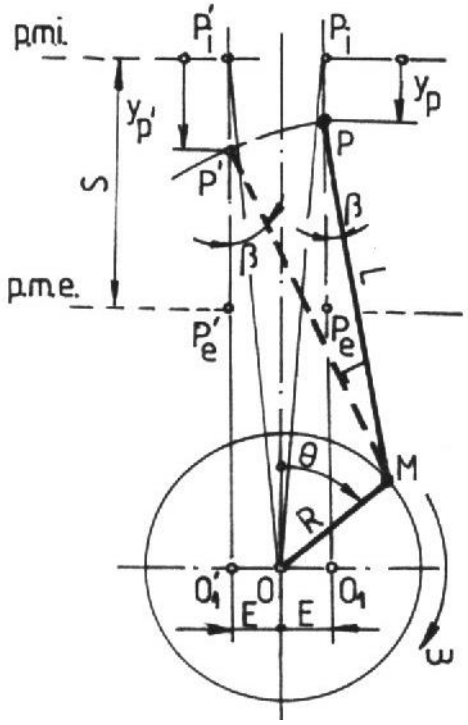

Figure 1.2: The calculus diagram for the normal gear kinetic dimensions

$$y_p = R + L - y$$

$$w_p = \frac{dy}{d\tau} = y_p = -y = \theta c_{wp}$$

$$a_p = \frac{dw_p}{d\tau} = \frac{d^2 y_p}{d\tau^2} = -\theta c_{wp} - \theta c_{ap} \quad (1.4)$$

$$\omega_b = \theta c_{wb}$$

$$\varepsilon_b = \theta c_{wb} + \theta c_{\varepsilon b}$$

Continuing, the reciprocating rod motion will be described, having a mass center, $G_{b,}$ pointed out at a distance L_m and L_p, faced with the crank articulation points, as well as with the piston (as pointed out in the 1.1 figure). The gravity center position for the reciprocating rod will be calculated using the following formula:

$$\begin{cases} x_{G_b} = R\sin\theta - L_m \sin\beta \\ y_{G_b} = R\cos\theta + L_m \cos\beta \end{cases} \quad (1.5)$$

The second formula can also be rewritten from a p.m.i perspective as:

$$y_b = R + L - y_{G_b} \quad (1.6)$$

Derivatives depending on the θ general coordinate of these coordinates are depending on the following coefficients as:

$$\begin{cases} c_{1_{b_x}} = \dfrac{dx_{G_b}}{d\theta} = R\cos\theta - c_{\omega_b} L_m \cos\beta \\ c_{1_{b_y}} = \dfrac{dy_{G_b}}{d\theta} = -R\sin\theta - c_{\omega_b} L_m \sin\beta \\ c_{2_{b_x}} = \dfrac{dc_{1_{b_x}}}{d\theta} = -R\cos\theta - c_{\varepsilon_b} L_m \cos\beta + c_{\omega_b}^2 L_m \sin\beta \\ c_{2_{b_y}} = \dfrac{dc_{1_{b_y}}}{d\theta} = R\cos\theta - c_{\varepsilon_b} L_m \sin\beta - c_{\omega_b}^2 L_m \sin\beta \end{cases} \quad (1.7)$$

Using these formulas the values of the components described in the 1.1 figure for reciprocating rod speed and angular acceleration can be calculated with:

$$\begin{aligned} \omega_{bx} &= \theta c_{1bx} \\ \omega_{by} &= \theta c_{1by} \\ a_{Gbx} &= \theta c_{1bx} + \theta c_{2bx} \\ a_{Gby} &= \theta c_{1by} + \theta c_{2by} \end{aligned} \quad (1.8)$$

Using the calculation scheme form the 1.2 figure usual formulas can be generated for kinematic dimensions of normal gear, taking into account the possibility of offsetting the gear, *E*, depending which a second coefficient can be defined along with λ, used in order to define the characteristics of this gear:

$$e = E / R \qquad (1.9)$$

and the above coefficient is called *relative offsetting (eccentricity)*.

By analyzing the first relation from the (1.4) set, the exact formula for the offset normal gear piston will be obtained as:

$$y_p = y_p(\theta) = R\left\{\sqrt{\left(1+\frac{1}{\lambda}\right)^2 - e^2} - \left[\cos\theta + \frac{1}{\lambda}\sqrt{1-\lambda^2(\sin\theta \mp e)^2}\right]\right\} \qquad (1.10)$$

In the above formula the + symbol stands for direct offsetting, while – stands for the reverse offsetting, since the cylinder axis beside the rotation axis of the crank shaft has the rotation direction of the cylinder or a reverse direction. The formula (1.10) can be developed in a Fourier series, such as:

$$y_p = R\left[a_0 + \sum_{k=1}^{\infty}(a_k \cos k\theta + b_k \sin k\theta)\right] \qquad (1.11)$$

This is a periodic function with a 2π period, continuous and odd, that is why the developing coefficients are as:

$$\begin{cases} a_0 = \dfrac{1}{\pi R}\displaystyle\int_0^{\pi} y_p(\theta)d\theta = \\ \quad = c_1 - c_1'\displaystyle\int_0^{\pi}\sqrt{1-\lambda^2(\sin\theta \mp e)^2}\,d\theta \\ a_k = \dfrac{2}{\pi R}\displaystyle\int_0^{\pi} y_p(\theta)\cos k\theta d\theta = \\ \quad = c_2\displaystyle\int_0^{\pi}\sqrt{1-\lambda^2(\sin\theta \mp e)^2}\,\cos k\theta d\theta \\ b_k = \dfrac{2}{\pi R}\displaystyle\int_0^{\pi} y_p(\theta)\sin k\theta d\theta = \\ \quad = c_3 - c_3'\displaystyle\int_0^{\pi}\sqrt{1-\lambda^2(\sin\theta \mp e)^2}\,\sin k\theta d\theta \end{cases} \qquad (1.12)$$

Were c_1, c_1', c_3, c_3' are coefficients that can be easily calculated; in exchange, the above integral equations are elliptical, but they are not complete elliptical

equations, being complex to develop if using the radicals from the (1.10) formula in exponential series.

It can be demonstrated from [4] and [17] that in these conditions the exact formula for normal piston displacement is as it follows:

$$y_p = R\left\{\sqrt{\left(1+\frac{1}{\lambda}\right)^2 - e^2} - \cos\theta - \sum_{k=0}^{\infty}(-1)^k C_{\frac{1}{2}}^{k}\lambda^{2k-1}\left\{\sum_{j=0}^{2k} C_{2k}^{2j} e^{2j}\left[\frac{1}{2^{2k-2j-1}}\times\right.\right.\right.$$
$$\left.\times\sum_{i=1}^{k-j}(-1)^i C_{2k-2j}^{k-j+1}\cos 2i\theta + \frac{1}{2^{2k-2j}} C_{2k-2j}^{k-j}\right] - \sum_{j=1}^{k} C_{2k}^{2j-1} e^{2j-1}\times$$
$$\left.\left.\times\sum_{i=1}^{k-j+1}(-1)^{i-1} C_{2k-2j+1}^{k-j-i+1}\sin(2i-1)\theta\right\}\right\}$$

(1.13)

using the known notation for combinations. Further on will analyze the normal axial gear, one the most common for marine engines, in the above formulas, keeping in mind the particularity e = 0 (corresponding with E = 0). In this case, the analytical formulas of kinematic dimensions for the normal axial gear are given in the 1.1 table. It can be noticed that, for the piston displacement only first order and odd harmonics occur in the developing process of this dimension.

The harmonic coefficients for the piston displacement can be expressed as:

$$a_0 = 1 + \frac{1}{4}\lambda + \frac{3}{64}\lambda^3 + \frac{5}{216}\lambda^5 + \frac{125}{16384}\lambda^7 + \mathrm{K}$$
$$a_1 = -1$$
$$a_2 = -\left(\frac{1}{4}\lambda + \frac{1}{16}\lambda^3 + \frac{15}{512}\lambda^5 + \frac{35}{2048}\lambda^7 + \mathrm{K}\right)$$
$$a_4 = \frac{1}{16}\lambda^3 + \frac{3}{216}\lambda^5 + \frac{35}{4096}\lambda^7 + \mathrm{K}$$
$$a_6 = -\left(\frac{1}{512}\lambda^5 + \frac{5}{2048}\lambda^7 + \mathrm{K}\right)$$
$$a_8 = \frac{5}{16384}\lambda^7 + \mathrm{K}$$

(1.14)

Practical speaking only first and second order harmonics are worthy and by overlapping them we can obtain the simplified values from 1.1 table were the values for the general coordinate θ have been presented for which the respective kinematic dimensions are 0, just as the ones for which these have extreme values.

Figures 1.3 to 1.5 present the variation waves for displacement values, speed and acceleration for the axial normal gear piston for the marine engine.

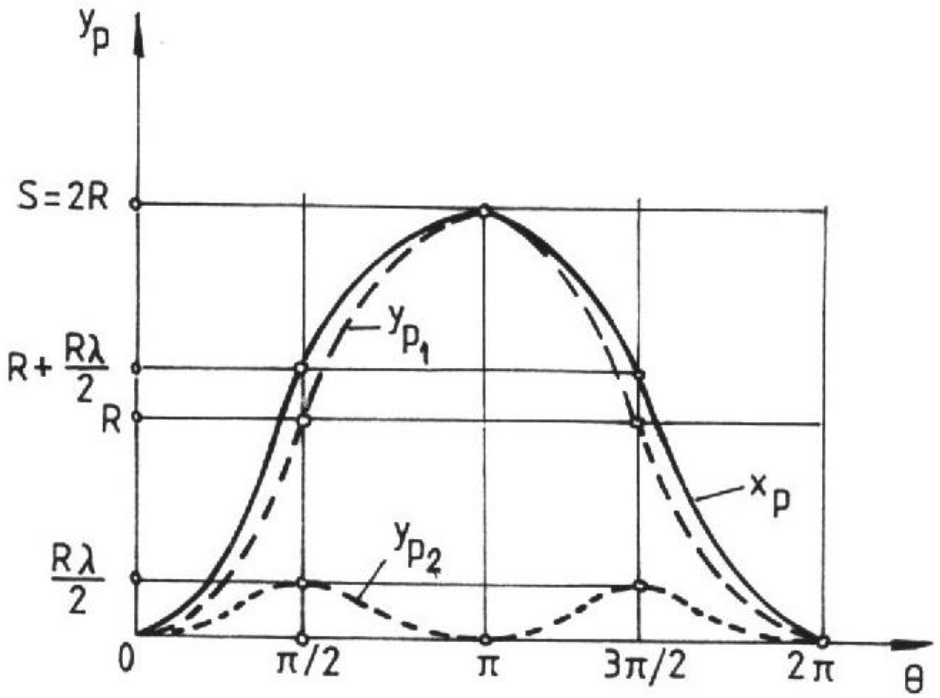

Figure 1.3: The piston displacement variation depending on the crank angle

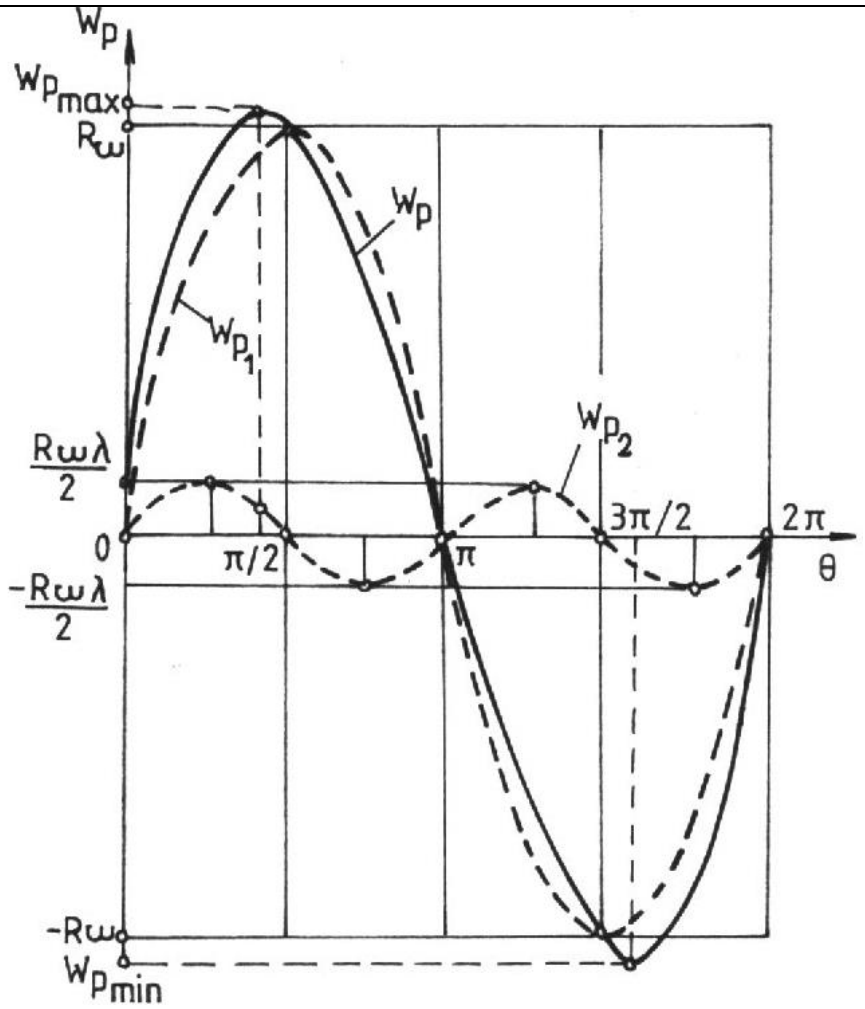

Figure 1.4: The variation of piston speed depending on the crank angle

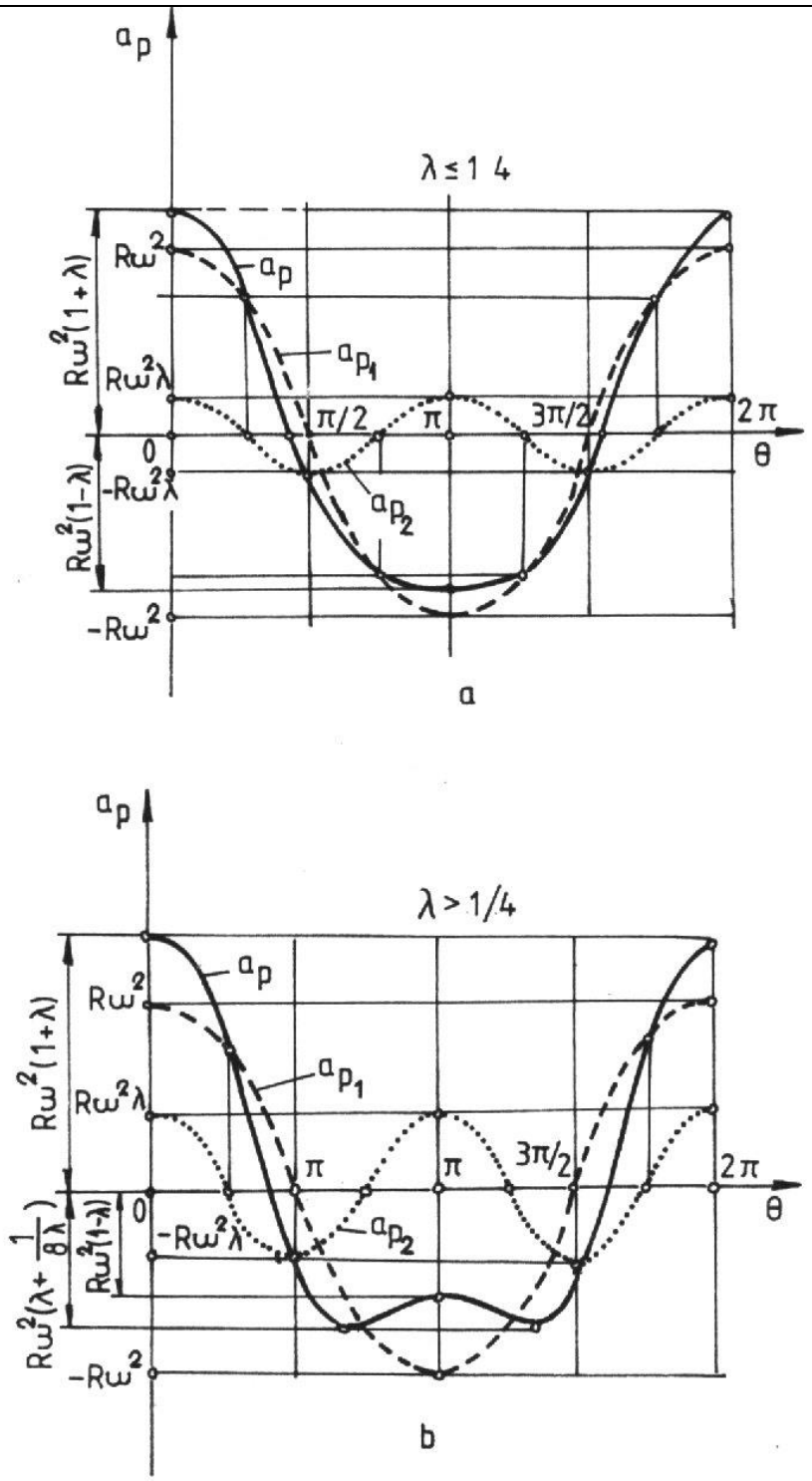

Figure 1.5: The variation of piston acceleration depending on the crank angle

1.1.2. Kinetics of the gear with main reciprocating rod and secondary reciprocating rods

The mechanism is specific for engines having at least two shaft lines and a single crank shaft, as well as engine with de star shape cylinder deployment. In the same time, the gear can be used for V shaped cylinder configuration when it has ascertained that the reciprocating rods side articulation mounted on the same twist can lead to higher lengths and a bigger dimension of the main engine. In the following part only the kinetics of the piston with a secondary reciprocating rod will be discussed, because the main reciprocating rod is a part of a normal mechanism. The gear with main reciprocating rod and secondary reciprocating rods are being described in the 1.6 figure. The main notations used are:

γ – the angle between the axis of the main cylinder and the one of the secondary cylinder (the first vertical position has been presented, in the γ position in order to make the symmetric multiplying process much easier for a W or star shaped mechanism);

γ_1 – the super positioning angle for the secondary reciprocating rod;

θ_1 – the crank rotation angle on the axis of the secondary cylinder;

β_1 – the leaning angle of the secondary reciprocating rod;

r – the distance from the crankshaft crankpin axis of to the secondary reciprocating rod;

l – secondary reciprocating rod length;

y_p – articulated piston displacement with the secondary reciprocating rod facing the lower dead center point P_{i1} on the secondary cylinder axis.

Table 1.1. Analytical formulas of kinematic dimensions of the normal axial engine gear

Component	Dimensions	Exact formula	Simplified formula	θ for 0 values	Extreme values
Crank	Displacement	$\theta = \omega\tau$	-	-	-
	Speed	$\omega = \frac{d\theta}{d\tau} = const.$	-	-	-
	Acceleration	$a_n = -R\omega^2$	-	-	-
Piston	Displacement	$y_p = R\left(a_0 + a_1 + \sum_{k=1}^{\infty} a_{2k}\cos 2k\theta\right)$	$y_p = R\left[(1-\cos\theta) + \frac{\lambda}{4}(1-\cos 2\theta)\right]$ $y_{p_1} = R(1-\cos\theta)$ $y_{p_2} = R\frac{\lambda}{4}(1-\cos 2\theta)$	$0, 2\pi$	$y_{p\max} = y_p(\pi) = S = 2R$
	Speed	$w_p = -R\omega\left[a_1\sin\theta + \sum_{k=1}^{\infty}(2k)a_{2k}\sin 2k\theta\right]$	$w_p = R\omega\left(\sin\theta + \frac{\lambda}{2}\sin 2\theta\right)$ $w_{p_1} = R\omega\sin\theta$ $w_{p_2} = R\omega\frac{\lambda}{2}\sin 2\theta$	$0, \pi, 2\pi$	$w_{p\max} = w_p\left(\theta_{w_{p\max}}\right)$ $w_{p\min} = w_p\left(\theta_{w_{p\min}}\right) = -w_{p\max}$ $\theta_{w_{p\max}} = \arccos\left(\frac{-1+\sqrt{1+8\lambda^2}}{4\lambda}\right)$ $\theta_{w_{p\min}} = 2\pi - \theta_{w_{p\max}}$
	Acceleration	$a_p = -R\omega^2\left[a_1\cos\theta + \sum_{k=1}^{\infty}(2k)^2 a_{2k}\cos 2\theta\right]$	$a_p = R\omega^2(\cos\theta + \lambda\cos 2\theta)$	$\theta_{w_{p\max}}$, $\theta_{w_{p\min}}$	$a_{p\max} = a_p(0) = a_p(2\pi) = R\omega^2(1+\lambda)$ $a_{p\min} = a_p(\pi) = -R\omega^2(1-\lambda)$ $a_{p_{extr_{1,2}}} = a_p\left(\theta_{a_{p_{extr_1}}}\right) = -R\omega^2\left(\lambda + \frac{1}{8\lambda}\right)$ $\theta_{a_{p_{extr_1}}} = \arccos\left(-\frac{1}{4\lambda}\right), \lambda \geq \frac{1}{4}$

			$a_{p_1} = R\omega^2 \cos\theta$ $a_{p_2} = R\omega^2 \cos 2\theta$		$\theta_{a_{p_{extr_2}}} = 2\pi - \theta_{a_{p_{extr_1}}}$

Reciprocating rod	Displacement	$\beta = \arcsin(\lambda \sin\theta)$	-	$0, \pi, 2\pi$	$\beta_{extr} = \pm\arcsin\lambda$, $\theta_{\beta_{extr}} = \frac{\pi}{2}, \frac{3\pi}{2}$
	Speed	$\omega_b = \lambda\omega \frac{\cos\theta}{\sqrt{1-\lambda^2 \sin^2\theta}}$	-	$\frac{\pi}{2}, \frac{3\pi}{2}$	$\omega_{b_{extr}} = \pm\lambda\omega$, $\theta_{b_{extr}} = 0, \pi, 2\pi$
	Acceleration	$\varepsilon_b = -\lambda\omega^2\left(1-\lambda^2\right)\frac{\sin\theta}{\sqrt{\left(1-\lambda^2 \sin^2\theta\right)^{3/2}}}$	-	$0, \pi, 2\pi$	$\varepsilon_{b_{extr}} = \pm\frac{\lambda\omega^2}{\sqrt{1-\lambda^2}}$, $\theta_{\varepsilon_{b_{extr}}} = \frac{\pi}{2}, \frac{3\pi}{2}$

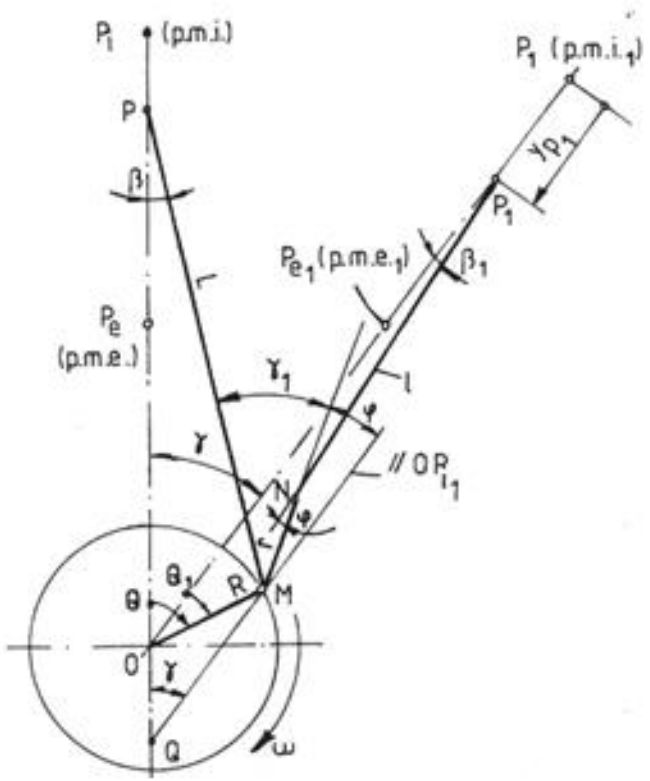

Figure 1.6: Calculus kinematic diagram for the gear with main reciprocating rod and secondary reciprocating rods

Piston internal combustion marine engines have a particular feature consisting in the transformation of the alternative translation motion of the piston, under the gas pressure generated by the burning process of fuel in the cylinders, in crank shaft a motion, through the mean of the crank gear.

If the main reciprocating rod is part of a normal type gear (reciprocating rod – crank) that has known kinematic characteristics, as mentioned in the previous subchapter, then the secondary reciprocating rod acts on the crank through the main reciprocating rod being part of a gear which differs from a kinematic point of view, having in mind the normal motion laws. Thus the calculus algorithm for this mechanism with a main reciprocating rod and a secondary reciprocating rod starts proceeds with mentioning the value of coefficient y_1 (as mentioned in the 1.1.1 subchapter):

$$OP_1 = y_1 = R\cos\theta_1 + r\cos(\beta - \varphi) + l\cos\beta_1 \qquad (1.15)$$

For which:

$$\varphi = \gamma_1 - \gamma \qquad (1.16)$$

The value for β is being given form the first set of equations (1.1), and the leaning angle of the secondary reciprocating rod β_1, according with [17], is being given by the following formula:

$$A = \left[\left(\frac{R}{l} - \lambda\frac{r}{l}\cos\gamma\cos\psi\right)^2 + \left(\lambda\frac{r}{l}\sin\gamma s\cos\psi\right)^2\right]^{\frac{1}{2}} \qquad (1.18a)$$

$$\mu = arctg\frac{\lambda\frac{r}{l}\cos\gamma\cos\psi}{\frac{R}{l} - \lambda\frac{r}{l}\cos\gamma\cos\psi} \qquad (1.18b)$$

$$x = -\frac{r}{Al}\sin\psi\cos\beta \qquad (1.18c)$$

In the (1.16) formula the following substitution are successively made: $\theta_1 = 0$ and $\theta_1 = \pi$. For these values the values for OP_{i1} and OP_{i2} (the distances from the center of the rotation axis to the inner dead center and the distance to the outer dead center) can be calculated.

By particularizing the angles that are specified in the (1.15) formula, $\beta = \beta_0$ and $\beta_1 = \beta_{10}$ for the first case and $\beta = \beta_0'$ and $\beta_1 = \beta_{10}'$ for the second case, as well as developing the trigonometrical series functions from the above mentioned formulas [4], [5], we can obtain the values for the following distances:

$$\begin{aligned}
OP_{i_1} &= R + r\left(1 - \frac{\lambda^2}{4}\right)\cos\psi + \lambda r \sin\gamma \sin\psi + \\
&+ \lambda^2 \frac{r}{4}\cos\psi\cos 2\gamma + l - -\frac{r^2}{2l}\sin^2\psi - \\
&+ \lambda^2 \frac{r}{4}\cos\psi\cos 2\gamma + l - -\frac{r^2}{2l}\sin^2\psi - \\
&- \lambda^2 \frac{r^2}{2l}\sin^2\gamma\cos 2\psi + \lambda\frac{r^2}{2l}\sin\gamma\sin 2\psi - \\
&- \lambda^3 \frac{r^2}{4l}\sin^3\gamma\sin 2\psi \\
OP_{e_1} &= -R + r\left(1 - \frac{\lambda^2}{4}\right)\cos\psi - \lambda r\sin\gamma\sin\psi + \\
&+ \lambda^2 \frac{r}{4}\cos\psi\cos 2\gamma + l - \frac{r^2}{2l}\sin^2\psi - \\
&- \lambda^2 \frac{r^2}{2l}\sin^2\gamma\cos 2\psi - \lambda\frac{r^2}{2l}\sin\gamma\sin 2\psi
\end{aligned} \tag{1.19}$$

In this manner we can express the analytical formulas for the engine gear that has a main reciprocating rod and secondary reciprocating rods, in which harmonic of any order can be found generated by de cosine and sine functions as well:

$$\begin{cases} y_{p_1} = OP_{i_1} - OP_1 = \\ \quad = R\left[a_0 + \sum_{k=1}^{\infty} \left(a_k \cos k\theta_1 + b_k \sin k\theta_1 \right) \right] \\ w_{p_1} = -R\omega \sum_{k=1}^{\infty} k(a_k \sin k\theta_1 + b_k \sin k\theta_1) \\ a_{p_1} = -R\omega^2 \sum_{k=1}^{\infty} k^2 (a_k \sin k\theta_1 - b_k \sin k\theta_1) \end{cases} \tag{1.20}$$

Thus, if for the normal mechanism piston the expression from the 1.1 table is being maintained, for the displacement of the secondary gear a more complex formula will be obtained which is in fact specific for a offset normal gear [17].

The harmonic coefficients for the secondary gear piston displacement expressed in a useful manner for a practical calculus will be:

$$\begin{aligned} a_0 &= \frac{1}{R}\left(R + \lambda r \sin\psi \sin\gamma + \lambda^2 \frac{r}{4}\cos\psi\cos 2\gamma - \lambda^2 \frac{r^2}{2l}\sin^2\gamma\cos 2\psi + \right. \\ &\quad \left. + \lambda \frac{r^2}{2l}\sin\gamma\sin 2\psi - \lambda^3 \frac{r^2}{4l}\sin^3\gamma\sin 2\psi + \frac{A^2 l}{4} - \lambda^2 \frac{r^2}{4l}\right) \\ a_1 &= \frac{1}{R}\left[-R - \lambda r \sin\gamma\sin\psi - Ar\left(1 - \frac{\lambda^2}{4}\right)\sin\psi\sin\mu - \lambda^2 \frac{rA}{8}\sin\psi\sin(2\gamma+\mu)\right] \\ a_2 &= \frac{1}{R}\left[\lambda^2 \frac{r}{4}\cos\psi\cos 2\gamma - \frac{A^2 l}{4}\cos 2\mu + \lambda^2 \frac{r^2}{4l}\cos 2\gamma\right] \\ a_3 &= \lambda^2 \frac{rA}{8R}\sin\psi\sin(2\gamma-\mu), \cdots \end{aligned}$$

(1.21)

$$\begin{aligned} b_1 &= \frac{1}{R}\left[-\lambda r \sin\psi\cos\gamma + Ar\left(1 - \frac{\lambda^2}{4}\right)\sin\psi\cos\mu - \lambda^2 \frac{rA}{8}\sin\psi\cos(2\gamma+\mu)\right. \\ b_2 &= \frac{1}{R}\left(\lambda^2 \frac{r}{4}\cos\psi\sin 2\gamma - \frac{A^2 l}{4}\sin 2\mu - \lambda^2 \frac{r^2}{4l}\sin 2\gamma\right) \\ b_3 &= \lambda^2 \frac{rA}{8R}\sin\psi\cos(2\gamma-\mu), \cdots \end{aligned}$$

As it was highlighted in [5] when projecting a gear with main and secondary reciprocating rods it is mandatory that the similarity condition to be maintained for the

compression ratio ε_1 from the secondary cylinder related with the compression ratio form the main cylinder ε, especially when the dimensions of these cylinders and pistons are identical. First of all the value of S_1, secondary piston stroke, is being calculated, as well as S_{c1}, the height of the combustion chamber from the secondary cylinder (which is considered as being included in the cylinder head):

$$\begin{cases} S_1 = OP_i - OP_{e_1} = S + \Delta \\ S_{c_1} = S_c + (OP_i - OP_e) = S_c + \Delta_1 \end{cases} \qquad (1.22)$$

In the above formulas Δ and Δ_1 are calculated with:

$$\begin{cases} \Delta = 2\lambda r \sin\gamma \sin\psi + \lambda \dfrac{r^2}{l^2} \sin\gamma \sin 2\psi - \lambda^3 \dfrac{r^2}{2l} \sin^3\gamma \sin 2\psi \\ \Delta_1 = L - r\left(1 - \dfrac{\lambda^2}{4}\right)\cos\psi - \lambda r \sin\gamma \sin\psi - \lambda^2 \dfrac{r}{4} \cos\psi \cos 2\gamma - l + \\ + \dfrac{r^2}{2l} \sin^2\psi + \lambda^2 \dfrac{r^2}{2l} \sin^2\gamma \cos 2\psi - \lambda \dfrac{r^2}{2l} \sin^2\gamma \sin 2\psi + \lambda^3 \dfrac{r^2}{4l} \sin^3\gamma \sin 2\psi \end{cases}$$

(1.23)

The similarity condition for the compression ratio for the two cylinders thus becomes:

$$\varepsilon - 1 = \frac{\Delta}{\Delta_1} \qquad (1.24)$$

from which, under the condition:

$$L = l + r \qquad (1.25)$$

mandatory for V and W engine configuration, the trigonometrical equation will be generated:

$$a\sin\psi + b\cos\psi + c\sin 2\psi + d\cos 2\psi + e = 0 \quad (1.26)$$

where the coefficients are given by the formulas:

$$a = \lambda(\varepsilon + 1)\sin\gamma$$

$$b = (\varepsilon - 1)\left(1 - \frac{\lambda^2}{2}\sin^2\gamma\right)$$

$$c = \lambda\frac{r}{2l}(\varepsilon + 1)\left(1 - \frac{\lambda^2}{2}\sin^2\gamma\right)$$

$$d = \frac{r}{4l}(\varepsilon - 1)(1 - 2\lambda\ \sin^2\gamma) \quad (1.27)$$

$$e = -(\varepsilon - 1)\left(1 + \frac{r}{4l}\right)$$

with the following notation:

$$x = tg\frac{\psi}{2} \qquad (1.28)$$

The equation (1.26) becomes an equation in x constant:

$$(b + 3d - e)x^4 - 2(a - 2c)x^3 + 2(d - e)x^2 - 2(a + 2c)x - (b + d + e) = 0 \quad (1.29)$$

that has a solution which subsequently leads to the values of the ψ angle, thus γ_1, more specific the angle at which the secondary reciprocating rod has to be fixed in order to ensure an equality between compression ratios; from these solutions the one that satisfies the condition $\psi = 5 \pm 10^0$.

For star shape configuration cylinder engines the basic condition is $\varphi = 0$ in the (1.22) and (1.23) equations and this results in:

$$L = l + r + \lambda^2\frac{r}{l}\left(1 + \frac{r}{l}\right)\sin^2\gamma \quad (1.30)$$

Finally, keeping in mind the mass features, generally the radius *r* sets the value for the length of the secondary reciprocating rod. The logical diagram of the calculus logarithm is being presented in the 1.7 figure. It can be noticed that the mechanism for the engines with a V configuration and neighboring reciprocating rods has an identical

kinematic feature for the secondary gear similar with the main gear, this being a practical solution for the engines used in the marine domain.

1.1.3. The kinematics of engine gears with opposite displayed pistons

The engines with opposite displayed pistons represent a special category which has not yet been studied in the technical literature [18] and can be found in many slow marine engines. The kinematic diagram for the engine gear with opposite pistons includes two gears with two different gears but each one of them acts on one crank shaft in the case of engines with two different crank shafts (as shown in the 1.8 figure) or both of them acting on the same crank shaft (as shown in the 1.9 figure).

In order to obtain an even distribution of gases one of the cranks has to be fitted offset facing the second one at a φ angle comparing with the positions at 0^0 and 180^0; thus the piston covers the evacuation chambers and is in advance, while the piston that closes the evacuation chambers is being delayed. The optimal scavenging value for the advance angle φ is usually in the $10 – 15^0$ RAC clearance.

For engines with opposite pistons included in the first category, for a crank angle θ_1 corresponding with an advance piston depending on the delaying gear, the following formula will be applied:

$$\theta_1 = \theta_2 + \varphi \qquad (1.31)$$

thus φ defines the crank position in advance towards the dead center of the most close moment in which the delayed piston is in p.m.i. The most important part is the calculus for the variable distance y between the two pistons.

Keeping in mind that the two values are identical the chosen calculus hypothesis states the fact the two pistons have a flat head and it can be noticed that the distance y is the one between the articulations between pistons and reciprocating rods, this hypothesis stands at the base of the calculation method of kinematic dimensions of normal gear with a single piston. Thus for the distances y between P_1 and P_2 the following formula will result:

$$y = y_{p_1} + y_{p_2} + y_0 \qquad (1.32)$$

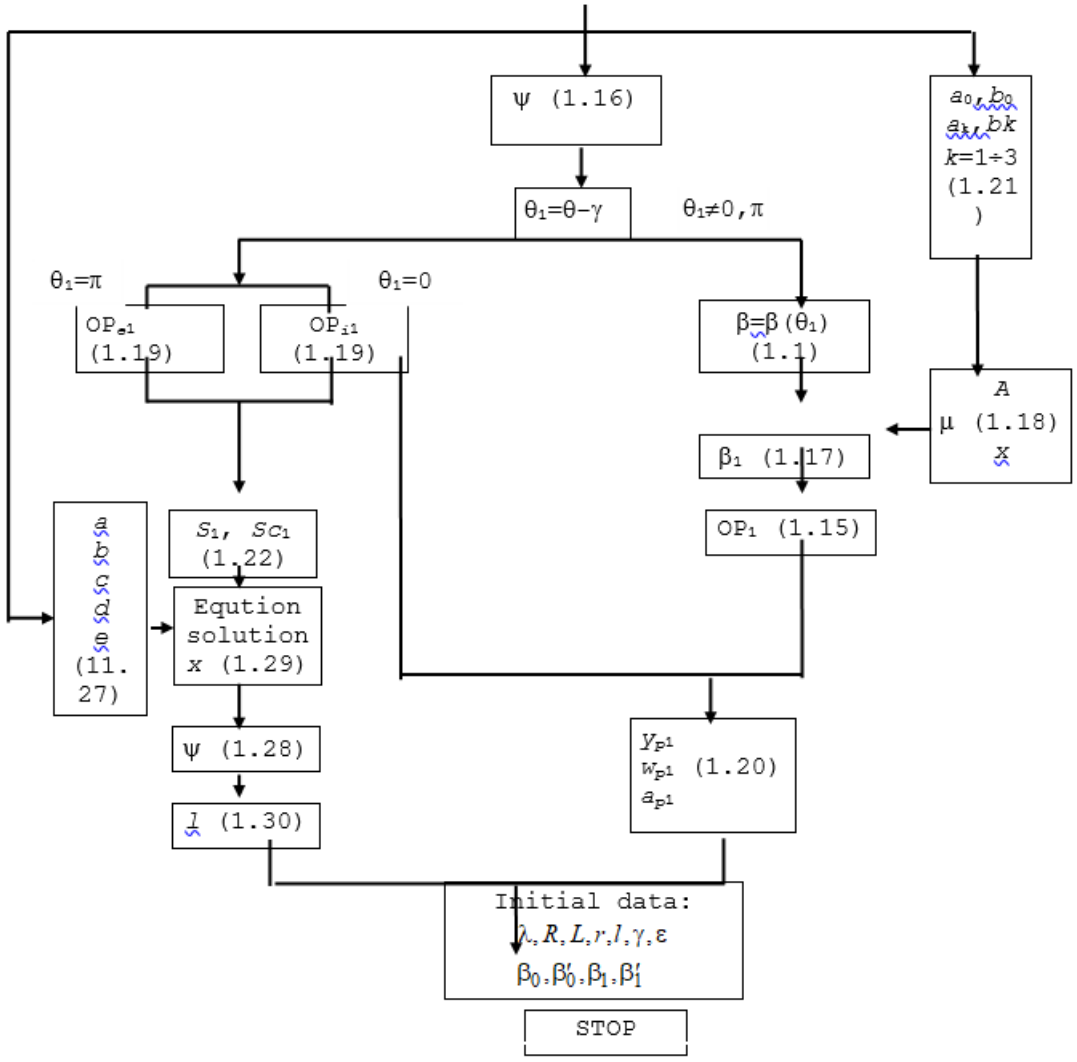

Figure 1.7: Logical diagram for the kinematic model of the gear fitted with main reciprocating rod and secondary reciprocating rods

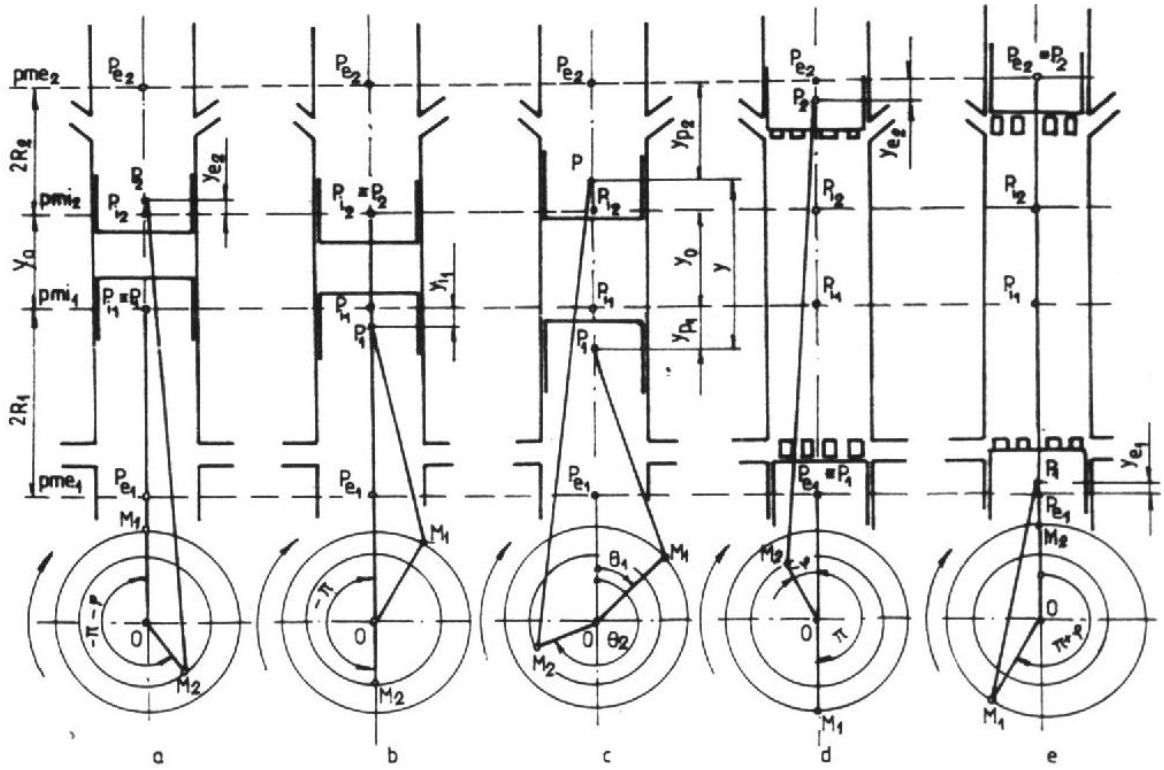

Figure 1.8: Kinematic calculus diagram for engines fitted with opposite pistons and two crank shafts

In the above figure y_{p1} and y_{p2} are the displacements for the two pistons facing the corresponding inner dead centers and they can be calculated by applying the formulas presented in the 1.1 table, while y_0 is the distance between the fixed positions of those two inner dead center points which are in fact the height of the combustion space, except two situations.

Thus the following formula will be obtained:

$$y = R_1\left[a_0 + \sum_{k=0}^{\infty}\left(a_k \cos k\theta_1 + b_k \sin k\theta_1\right)\right] \qquad (1.33)$$

For the practical case of limiting the first two harmonic coefficients the following formulas will be obtained:

$$
\begin{aligned}
a_0 &= 1 + k_R + \frac{\lambda_1}{4}\left(1 + k_R k_\lambda\right) + \frac{y_0}{R_1} \\
a_1 &= \left(1 + k_R \cos\ \right) \\
b_1 &= k_R \sin \\
a_2 &= \frac{\lambda_1}{4}\left(1 + k_R k_\lambda \cos 2\ \right) \\
b_2 &= \frac{\lambda_1}{4} k_R k_\lambda \sin 2 \\
&\ldots\ldots\ldots\ldots\ldots\ldots\ldots\ldots\ldots\ldots\ldots\ldots\ldots\ldots\ldots\ldots
\end{aligned}
\qquad (1.34)
$$

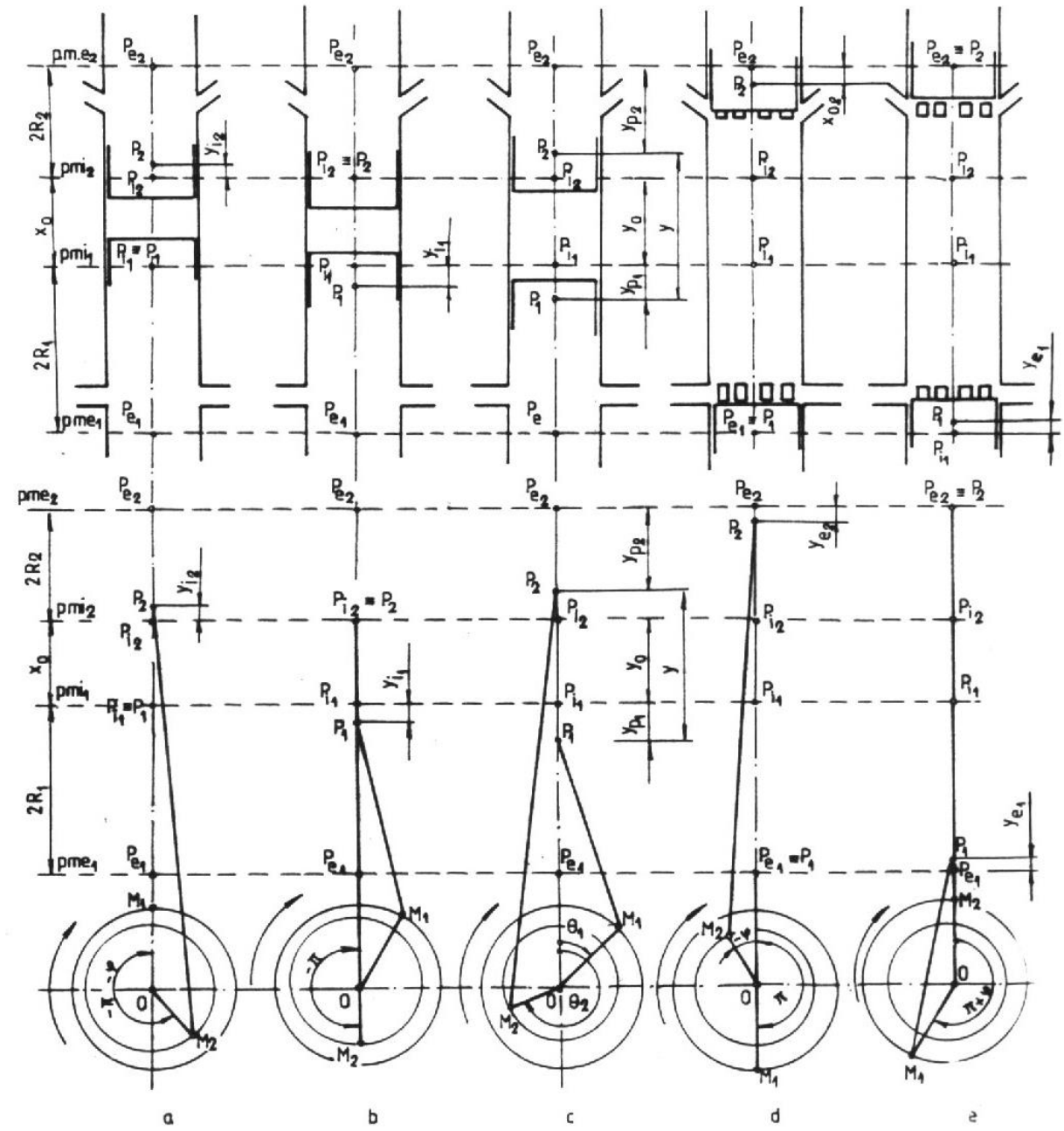

Figure 1.9: Kinematic calculus diagram for engines fitted with opposite pistons and one crank shaft

In which the ratios between radius and elongations of the two reciprocating rods have been inserted in the general hypothesis of some gears with generic different dimensions:

$$\begin{cases} k_R = R_2 / R_1 \\ k_\lambda = \lambda_2 / \lambda_1 \end{cases} \qquad (1.35)$$

With these harmonic coefficients the so-called *overall piston displacement, y*, can be rewritten as:

$$y = R_1 \left[a_0 + \sqrt{a_1^2 + b_1^2}\, \sin(\theta_1 + \mu_1) + \sqrt{a_2^2 + b_2^2}\, \sin(2\theta_1 + \mu_2) \right] \qquad (1.36)$$

But this formula is identical with the formula for the displacement of a fictional similar gear, normally offset, with the radius and crank angle R_1 and θ, with an angular speed noted with ω_1, this being a gear that has an piston speed and a piston acceleration equal with:

$$\begin{cases} w = R_1 \omega_1 \left[\sqrt{a_1^2 + b_1^2}\, \sin(\theta_1 + \mu_1) + 2\sqrt{a_2^2 + b_2^2}\, \sin(2\theta_1 + \mu_2) \right] \\ a = -R\omega_1^2 \left[\sqrt{a_1^2 + b_1^2}\, \sin(\theta_1 + \mu_1) + 4\sqrt{a_2^2 + b_2^2}\, \sin(2\theta_1 + \mu_2) \right] \end{cases} \qquad (1.37)$$

In the formulas above the initial stages have been inserted as:

$$\begin{cases} \mu_1 = \arctan \dfrac{k_R \sin\varphi}{1 + k_R \cos\varphi} \\ \mu_2 = \arctan \dfrac{k_R \sin 2\varphi}{1 + k_R \cos 2\varphi} \end{cases} \qquad (1.38)$$

The extreme values from the (1.36) formula are of most interest and they can be obtained by canceling the derivative of these formula which leads to an algebraic four degree equation in the following unknown:

$$x = tg\, \frac{\theta_1}{2} \qquad (1.39)$$

and has the same type as the (1.29) equation, such as:

$$mx^4 + nx^3 + px^2 + qx + r = 0 \quad (1.40)$$

with the following coefficients:

$$\begin{cases} m = \zeta_1(1+6\xi_1) \\ n = 2\zeta_2(1-4\xi_2) \\ p = 4\zeta_3 \\ q = 2\zeta_2(1+4\xi_2) \\ r = -\zeta_1(1+2\xi_1) \end{cases} \quad (1.41)$$

for which:

$$\begin{cases} \zeta_1 = R_1\sqrt{a_1^2+b_1^2}\cos\mu_1;\ \zeta_2 = R_1\sqrt{a_1^2+b_1^2}\sin\mu_1 \\ \zeta_3 = R_1\sqrt{a_1^2+b_1^2}\cos\mu_2 \\ \xi_1 = \sqrt{\dfrac{a_2^2+b_2^2}{a_1^2+b_1^2}}\dfrac{\cos\mu_2}{\cos\mu_1};\ \xi_2 = \sqrt{\dfrac{a_2^2+b_2^2}{a_1^2+b_1^2}}\dfrac{\sin\mu_2}{\sin\mu_1} \end{cases} \quad (1.42)$$

For the potential four solutions of the (1.40) equation the maximum value are being obtained for the value in the (1.36) equation, $y_{max\ 1,2}$, as well as the minimum ones $y_{min\ 1,2}$. These values can be also deducted from the kinematic analysis of the gears presented in the 1.8 and 1.9 figures and have approximate values sufficient for a practical calculus as stated in [4] and [5]:

$$\begin{cases} y_{\max_1} = 2R_1 + 2R_2 + y_0 - y_{e_2} \\ y_{\max_2} = 2R_1 + 2R_2 + y_0 - y_{e_1} \\ y_{\min_1} = y_0 + y_{i_2} \\ y_{\min_2} = y_0 + y_{i_1} \end{cases} \quad (1.43)$$

for the first type of gear;

$$\begin{cases} y_{\max_1} = 2R_1 + 2R_2 + y_0 - y_{i_2} \\ y_{\max_2} = 2R_1 + 2R_2 + y_0 - y_{e_1} \\ y_{\min_1} = y_0 + y_{e_2} \\ y_{\min_2} = y_0 + y_{i_1} \end{cases} \quad (1.44)$$

for the second type of gear;

where y_a and y_e are notations for the heights of admission and evacuation chambers.

Identical consideration can be taken into account for the engines with opposite pistons included in the secondary category, with a single crank case. From the kinetic analysis from the 1.9 figure the following equations are resulting:

$$\theta_1 = \theta_2 + \pi + \varphi \quad (1.45)$$

as well as:

$$y = y_{p_1} - y_{p_2} + y_0 + 2R_2 \quad (1.46)$$

These formulas are analogue for the (1.31) and (1.32) equations. The displacement expressed by the (1.33) formula will have a similar expression as the one in the (1.36) formula with the following coefficients:

$$\begin{cases} a_0 = 1 + 3k_R + \dfrac{\lambda_1}{4}\left(1 - k_R k_\lambda\right) + \dfrac{y_0}{R_1} \\ a_1 = -\left(1 - k_R \cos\varphi\right) \\ b_1 = k_R \sin\varphi \\ a_2 = -\dfrac{\lambda_1}{4}\left(1 + k_R k_\lambda \cos 2\varphi\right) \\ b_2 = -\dfrac{\lambda_1}{4} k_R k_\lambda \sin 2\varphi \end{cases} \quad (1.47)$$

with the following values for the auxiliary angles:

$$\begin{cases} \mu_1 = -\arctan\dfrac{\sin\varphi}{1 - k_R \cos\varphi} \\ \mu_2 = \arctan\dfrac{k_R k_\lambda \sin 2\varphi}{1 + k_R k_\lambda \cos 2\varphi} \end{cases} \quad (1.48)$$

For the compression ratios formulas analogue with the ones included in the (1.45) are being deducted.

A particular case in the study of kinetic study of opposite pistons engines is being represented by the lack of angular offset ($\varphi = 0$) and this is a situation in which the b_1 and b_2 coefficients are being canceled, and the displacement of pistons is being expressed by the (1.36) formula, becoming analogue with the one with a normal axis gear.

In the 1.10 figure the general aspect of piston displacement overall variation is being described as in (1.36) keeping in mind the quality of extreme points.

The 1.11 figure is a representation of a DOXFORD 58JS3 marine engine gear with three in-line cylinders, a two stroke functioning cycle, as well as opposite pistons that are driving a single crank shaft, this representing the variation of dynamic dimensions for similar gears.

The main engine noted has the following technical data:

- Rotation speed: n = 222 rpm;
- Piston diameters: D = 580 mm;
- Crank radius for the gear driving the first piston: $R_1 = 440$ mm;
- Crank radius for the gear driving the second piston: $R_2 = 170$ mm;
- The reciprocating rod length at the first piston: $L_1 = 1520$ mm;
- The reciprocating rod length at the second piston: $L_2 = 1100$ mm;
- Angular offset: $\varphi = 0$;
- The minimum distance between pistons: $y_0 = 34$ mm;
- The height of scavenging (admission) chambers: $y_a = 124$ mm;
- The height of evacuation chambers: $y_2 = 102$ mm;

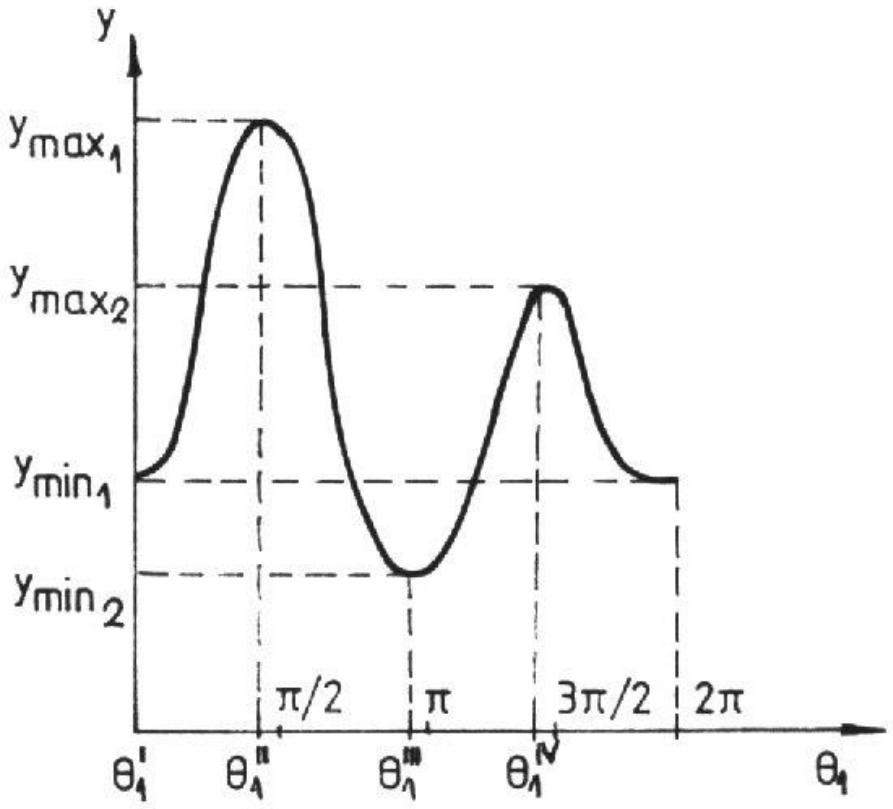

Figure 1.10: The piston overall displacement variation

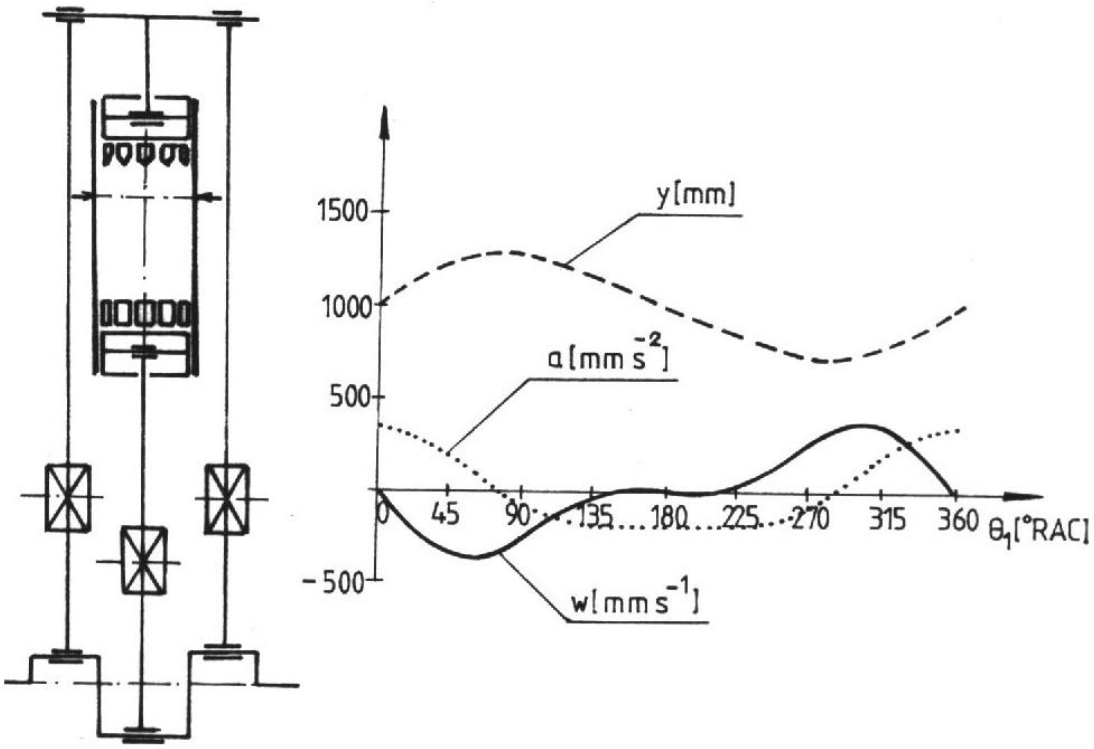

Figure 1.11: The gear diagram for the DOXFORD 58JS3 marine engine and kinematic dimensions for it

1.2 Engine gear dynamics

Following the kinematic analysis of the engine gear the speeds, displacements and accelerations for their components have successively resulted. These values allow the analysis and the calculation for forces and moments that drive these components.

1.2.1. The dynamic model of the engine gear

In order to establish the forces and momentum that drive in the elements and the couples of engine gears we have to adopt a suitable dynamic model for it as it is suggested in the 1.12 figure.

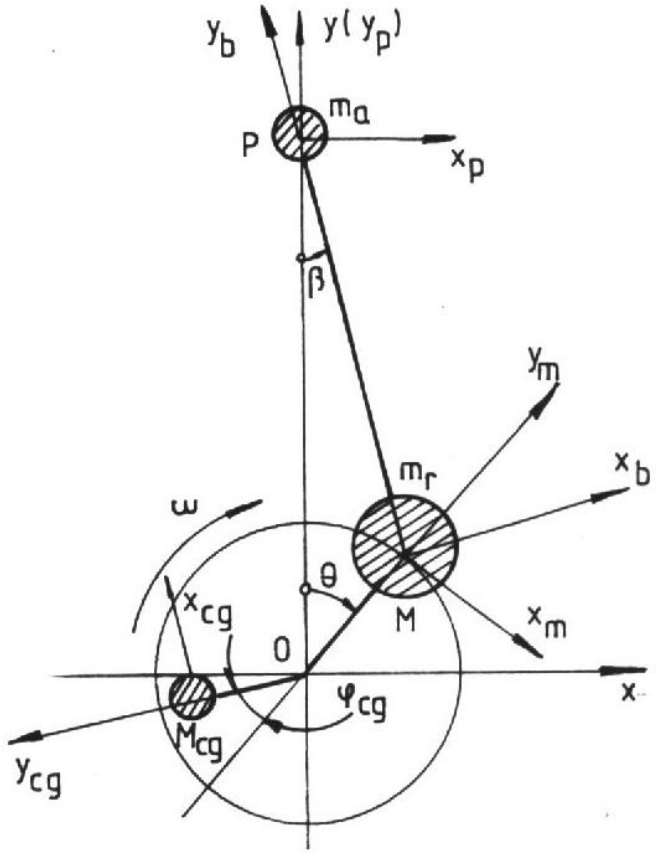

Figure 1.12: Dynamic model for the engine gear

The model is being based on the meshing of included elements in the engine gear and mass concentration of these ones in characteristic points. Thus m_a stands for the sum of masses with an alternative motion, while m_r stand for the sum of masses with a rotation motion and m_{cg} stands for the sum of masses for the counterweights fitted at a φ_{cg} angle facing the corner axis (figure 1.13). the values for these concentrated masses are expressed using the formula:

$$m_a = m_p + m_{ba} \quad (1.50)$$

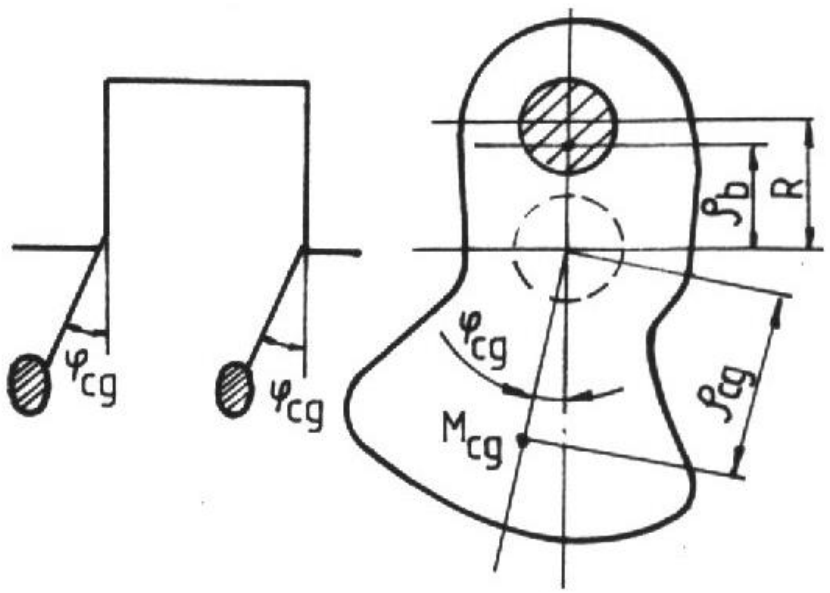

Figure 1.13: The elbow of the crank shaft fitted with counterweights

All this weight is being concentrated in the articulation of the piston fitted with a nut (or in the draw bar of the piston fitted with the nut of the crosshead gear in the case of marine two stroke slow engines), in which m_p is the mass of the piston group that includes the mass of the piston, the mass of piston rings and the mass of the piston nut in the case of four stroke engines, while in the case of two stroke marine engine adds the mass of the crosshead system and piston draw bar, while the m_{ba} is the mass of the reciprocating rod facing the piston which has an alternative motion.

The value of m_r is given by the formula:

$$m_r = m_m + 2m'_{bm} + m_{ba} \quad (1.51)$$

where m_m is the crank mass, while m_{br}, mass of the bracket facing the crankpin given by the following formula:

$$m'_{bm} = m'_b \frac{\rho_b}{R} \quad (1.52)$$

m_b' is the effective mas for the bracket and ρ_b is the ordinate corresponding the weight center of the bracket, while m_b is the reciprocating rod mass facing the crankpin which has a rotation motion as well as the crankpin. In order to mash the reciprocating rod in those two concentrated masses in P and M points the following formulas have been applied:

$$\begin{cases} m_{ba} = \dfrac{L_m}{L} m_b \\ m_{br} = \dfrac{L_p}{L} m_b \end{cases} \quad (1.53)$$

The above formulas are deducted from the conditions of dynamic equivalence [4], [11], [14] and [17] applied for a real reciprocating rod that has a m_b and the meshed in two masses, the distances L_m and L_p are extracted from the 1.1 figure. In the case of the gear fitted with main reciprocating rod and secondary reciprocating rods these masses are reduced and can be calculated by applying the formulas [4]:

$$\begin{cases} m_{ba} = m_b \dfrac{L_m}{L} + \sum\limits_{i\geq 2} (i-1) m_{b_1} \dfrac{l_p}{l} \dfrac{r\cos\left[(i-1)\gamma_1\right]}{L} \\ m_{br} = m_b \dfrac{L_p}{L} + \sum\limits_{i\geq 2} (i-1) m_{b_1} \dfrac{l_p}{l} \dfrac{L - r\cos\left[(i-1)\gamma_1\right]}{L} \end{cases} \quad (1.54)$$

where m_{b1}, l_p and l_m are dimensions corresponding with the secondary reciprocating rods (as shown in the 1.6 figure).

According with the 1.12 figure in the dynamic model proposed we are going to use the following reference systems: Oxyz – the reference Cartesian coordinate system which is straight and fixed, associated with the still positions of the engine; $Px_py_pz_p$ - the Cartesian reference system, straight, mobile, associated with the piston (or crosshead system for slow marine engines); $Mx_by_bz_b$ - the Cartesian reference system, straight, mobile associated with the crank; $M_{cg}x_{cg}y_{cg}z_{cg}$ - the Cartesian reference system, straight, mobile associated with the counterweights.

Keeping in mind the previous observations it has to be mentioned that the forces and moments driving with the engine drive, as well as the specification that the following vectors have been introduced $\vec{\imath}, \vec{j}, \vec{k}$ corresponding with the axes Ox, Oy and Oz:

- Inertia force of masses with a rotation motion:

$$F_r = -m_r a_n \quad (1.55)$$

with a_n being the normal acceleration of the drive (as shown in the 1.1 table):

$$a_n = -R\omega^2 j_m \quad (1.56)$$

while the angular speed can also be written as a vectorial formula:

$$\omega = \omega k \quad (1.57)$$

- Inertia force for counterweights:

$$F_{rcg} = -m_{cg} a_{ncg} \quad (1.58)$$

where the normal acceleration of the counterweights is given by the formula:

$$a_{ncg} = -\rho_{cg}\omega^2 j_{cg} \quad (1.59)$$

- Inertia force of masses in an alternative motion:

$$F_a = -m_a a_p \quad (1.60)$$

with:

$$a_p = -a_p j_p \quad (1.61)$$

in which the piston acceleration noted with a_p, is being given by the third formula from the (1.4) or in harmonic components, as noted in the 1.1 table.

- Inertia correcting moment [11], [14], [17]:

$$\Delta M_{ibt} = (i_b^2 - i_{be}^2) m_b \varepsilon_b = \Delta J_{bGb} \varepsilon_b \quad (1.62)$$

where i_b is the reciprocating rod gyration radius, i_{be} is the gyration radius for a two equivalent mass system calculated facing the reciprocating rod mass center G_b (as shown in the 1.1 figure), ΔJ_{bGb} is the angular correction for the reciprocating rod inertia moment facing the same point; thus the angular acceleration of the reciprocating rod has the formula given in the (1.4) equations, or the following vectorial formula:

$$\varepsilon = \varepsilon_b k_b \quad (1.63)$$

- Mass for components in rotational motion:

$$G_r = (m_r + m_{cg}) g \quad (1.64)$$

- Mass for components in translation motion:

$$G_a = m_a g \quad (1.65)$$

- Gas pressure force acting on the piston head:

$$-F_p = -F_a j_p \quad (1.66)$$

Gas pressure force will be calculated by applying the following formula:

$$F_p = (p - p_{cart}) \frac{\pi D^2}{4} = p_g \frac{\pi D^2}{4} \quad (1.67)$$

Gas pressure inside the cylinder is variable as a function the rotation angle $p = p(\theta)$ (as in [3], chapter [5]) and p_{cart} as the counter-pressure coming from the engine case.

- Gas pressure that acts on the piston head:

$$F_p = F_p j_p = p_g \frac{\pi D^2}{4} j_p \qquad (1.68)$$

- Total force acting on the *P* articulation:

$$F = -F_p + F_a + G_a = F_j = \left(-p_g \frac{\pi D^2}{4} - m_a a_p - m_a g\right) j_p \quad (1.69)$$

- The components of *F* on the axis:

$$F = N + B = Ni + Bj_b \quad (1.70)$$

with the following values:

$$\begin{cases} N = F \tan\beta \\ B = \dfrac{F}{\cos\beta} \end{cases} \qquad (1.71)$$

- Reaction force inside the stay of the reciprocating rod:

$$R_{1pb} = B - (F_{ba} + G_{ba}) = \frac{F j_b}{cos\beta} - \left(- m_{ba} a_p - m_{ba} g\right) j = R_{1pbxb} i_b + R_{1pbyb} j_b = R_{1pbxb} i + R_{1pbyb} j \qquad (1.72)$$

where the following vectorial relations have been used:

$$j = i_b sin\beta + j_b cos\beta$$
$$j_b = - i sin\beta + j cos\beta \qquad (1.73)$$

in the above formulas the Oxyz components are:

$$\begin{cases} R_{l_{pb_x}} = \left(p_g \dfrac{\pi D^2}{4} + m_{ba} a_p + m_{ba} g \right) \tan \beta \\ R_{l_{pb_y}} = -p_g \dfrac{\pi D^2}{4} - m_{ba} a_p - m_{ba} g \end{cases} \quad (1.74)$$

from which the geometrical place for the R_{lpb} peak vector describes a curve called the *polar diagram* for the liner included in the reciprocating rod bracket, expressed in polar coordinates through the module and angular pole:

$$\begin{cases} R_{l_{pb}} = \sqrt{R_{l_{pb_x}}^2 + R_{l_{pb_y}}^2} \\ \varphi_{l_{pb}} = \arctan \dfrac{R_{l_{pb_y}}}{R_{l_{pb_x}}} \end{cases} \quad (1.75)$$

In an analog manner the components facing the $Mx_by_bz_b$ are expressed by:

$$\begin{cases} R_{l_{pbx_b}} = m_{ba} a_p \sin \beta + m_{ba} g \sin \beta \\ R_{l_{pby_b}} = B + m_{ba} a_p \cos \beta + m_{ba} g \cos \beta \end{cases} \quad (1.76)$$

with the possibility of drawing the polar diagram depending on the entire system.

- Crankpin force:

$$R_{lm} = B + F_{br} + G_{br} = Bj_b + m_{br} R\omega^2 j_m - m_{br} gj = R_{mxb} i_b + R_{myb} j_b = R_{lmxm} i_m$$
$$j_m = T i_m + Z j_m \quad (1.77)$$

In the above formula we can apply the following correlation:

$$j_b = -i_m \sin(\theta + \beta) + j_m \cos(\theta + \beta)$$
$$j = -i_m \cos\theta + j_m \sin\theta \quad (1.78)$$
$$j_m = i_b \sin(\theta + \beta) + j_b \cos(\theta + \beta)$$
$$j = i_b \sin\beta + j_b \cos\beta)$$

The values for the components facing the axis are:

$$\begin{cases} R_{lm_{x_m}} = T_M = -F\,\dfrac{\sin(\theta+\beta)}{\cos\theta} + m_{ba} g \sin\theta \\ R_{lm_{y_m}} = Z_M = F\,\dfrac{\cos(\theta+\beta)}{\cos\theta} + m_{br} R\omega^2 - m_{br} g\cos\theta \end{cases} \quad (1.79)$$

Further one the module and the polar angle can be determined:

$$\begin{cases} R_{lm} = \sqrt{R^2_{lm_{x_m}} + R^2_{lm_{y_m}}} \\ \varphi_{lm} = \arctan\dfrac{R_{lm_{y_m}}}{R_{lm_{x_m}}} \end{cases} \quad (1.80)$$

In the reference system attached to the reciprocating rod the coordinated will be:

$$\begin{cases} R_{m_{x_b}} = m_{br} R\omega^2 \sin(\theta+\beta) - m_{br} g \sin\beta \\ R_{m_{y_b}} = B + m_{br} R\omega^2 \cos(\theta+\beta) - m_{br} g\cos\beta \end{cases} \quad (1.81)$$

- The force acting on the crank in the M point is:

$$R_m = R_{lm} + F_{mr} + G_m = T_M i_m + m_m g sin\theta i_m + Z_M j_m - m_m g cos\theta j_m + m_m R\omega^2 j_m = T i_m + Z j_m \quad (1.82)$$

Where F_{mr} and G_m are inertia forces and gravity forces acting on the crank. The components are:

$$\begin{cases} T = \left(p_g \dfrac{\pi D^2}{4} + m_a a_p + m_a g \right) \dfrac{\sin(\theta+\beta)}{\cos\beta} + m_r g \sin\theta + m_{cg} g \sin\varphi_{cg} + m_{cg} \rho_{cg} \omega^2 \sin\varphi_{cg} \\ Z = -\left(p_g \dfrac{\pi D^2}{4} + m_a a_p + m_a g \right) \dfrac{\cos(\theta+\beta)}{\cos\beta} + m_r R\omega^2 - -m_r g \sin\theta + m_{cg} \rho_{cg} \omega^2 \cos\varphi_{cg} - \\ \qquad\qquad - m_{cg} g \cos\varphi_{cg} \end{cases}$$

(1.83)

The above formula is being used to demonstrate the *polar configuration for the crankpin*.

- The force acting in the thrust bearing:

$$R_{lp} = R_{lpx}i + R_{lpy}j = R_{lpx}i_m + R_{lpy}j_m \quad (1.84)$$

having:

$$\begin{cases} R_{lp_x} = \left(p_g \dfrac{\pi D^2}{4} + m_a a_p + m_a g \right) tg\beta + m_r R\omega^2 \sin\theta + m_{cg}\rho_{cg}\omega^2 \sin\left(\theta + \varphi_{cg}\right) \\ R_{lp_y} = -p_g \dfrac{\pi D^2}{4} - m_a a_p + m_r R\omega^2 \cos\theta + m_{cg}\rho_{cg}\omega^2 \cos\left(\theta + \varphi_{cg}\right) - \left(m_a + m_r + m_{cg}\right) g \end{cases}$$

(1.85)

resulting that:

$$R_{l_p} = \sqrt{R_{l_{Px}}^2 + R_{l_{Py}}^2}\,;\ \varphi_{l_p} = \arctan\frac{R_{l_{Py}}}{R_{l_{Px}}} \quad (1.86)$$

and these formulas sit at the base of the *polar configuration of the thrust bearing*.

- The active motor moment is being defined by the formula:

$$M = Mk = TRk \qquad (1.87)$$

- On the fixed parts of the engine the following forces will act:
  - The overturning engine moment (roll)

$$M_{ras} = M_{ras}k \qquad (1.88)$$

in which:

$$M_{răs} = -\left(p_g \frac{\pi D^2}{4} + m_a a_p + m_a g \right) R \frac{\sin\left(\theta + \beta\right)}{\cos\beta} \quad (1.89)$$

- The pressure force of gasses acting on the piston head:

$$F_P' = F_P' j \qquad (1.90)$$

with:

$$F_P' = p_g \frac{\pi D^2}{4} \quad (1.91)$$

- The vertical force acting on the crankpin:

$$R_{lp_y} = -\left(p_g \frac{\pi D^2}{4} + m_a a_p \right) + m_r R\omega^2 \cos\theta + m_{cg} \rho_{cg} \omega^2 \cos(\theta + \varphi_{cg}) - \\ -(m_a + m_r + m_{cg})g + m_r R\omega^2 \cos\theta + m_{cg} \rho_{cg} \omega^2 \cos(\theta + \varphi_{cg}) \qquad (1.92)$$

- The vertical force acting on the engine support:

$$R_{post_y} = F_p + R_{lp_y} \qquad (1.93)$$

- The normal components acting on the cylinder fender (or the crosshead slider, for the two stroke engine):

$$N = -\left(p_g \frac{\pi D^2}{4} + m_a a_p + m_a g \right) \tan\beta \quad (1.94)$$

- The horizontal component acting on the crankpin:

$$R_{lp_x} = \left(p_g \frac{\pi D^2}{4} + m_a a_p + m_a g \right) tg\beta + m_r R\omega^2 \sin\theta + m_{cg} \rho_{cg} \omega^2 \sin(\theta + \varphi_{cg}) \qquad (1.95)$$

- The horizontal component acting on the engine support:

$$R_{post_x} = N + R_{lp_x} = m_r R\omega^2 \sin\theta + m_{cg} \rho_{cg} \omega^2 \sin(\theta + \varphi_{cg}) \qquad (1.96)$$

It has to mentioned the forces and moments previously define are, in fact, periodical functions with general coordinates that can be developed in Fourier series (as in presented in 12.2.3 and 12.2.24 paragraphs).

Thus, the gas pressure from the cylinder hast the following series development depending on the θ coordinate:

$$p = p(\theta) = \bar{p} + \sum_{k=1}^{\infty} \left(a_{p_k} \cos k\theta + b_{p_k} \sin k\theta \right) = \bar{p} + \sum_{k=1}^{\infty} p_k \cos\left(k\theta - \varphi_p\right) \quad (1.97)$$

for the above series the medium value is:

$$\bar{p} = \frac{1}{T_c} \int_0^{T_c} p(\theta) d\theta \quad (1.98)$$

while the harmonic coefficients a_{pk} and b_{pk}, the amplitudes p_k and the initial phases φ_p are given by the following formulas:

$$\begin{cases} a_{p_k} = \dfrac{2}{T_c} \displaystyle\int_0^{T_c} p(\theta) \cos k\theta d\theta \\ b_{p_k} = \dfrac{2}{T_c} \displaystyle\int_0^{T_c} p(\theta) \sin k\theta d\theta \\ p_k = \sqrt{a_{p_k}^2 + b_{p_k}^2} \\ \varphi_{p_k} = \arctan \dfrac{b_{p_k}}{a_{p_k}} \end{cases} \quad (1.99)$$

In these relations T_c represents the periodical for the motor time:

$T_c = \tau\pi = 2\pi$ – for two stroke engines

$T_c = \tau\pi = 4\pi$ – for four stroke engines (1.100)

Thus, by developing all the other forces in series (the ones in 1.97) developed in the engine gear will can be developed in a similar Fourier series.

In the previous considerations the real couples haven't been taken into account, but inside of them friction forces can appear and clearances exist and all of them lead to the so-called *cylinder run-out* and this is generated by the run-out between the couple cylinder-piston, as well as the changes in the reactions occurring in bearings, due to changes in value for the *N* force, as well as the modification of al

chain reactions in bearings and the lubricating mode for these parts. In other words, for a two stroke engine the force acting in the engine gear diagram is being presented, as well as the diagram of forces that are acting on fixed parts of the engine, as shown in the 1.14 figure.

Table 1.2 the list of forces and moments acting on the components of the engine gear are being presented for the normal axis case of marine engines, these being very useful in a practical calculation based on the general formulas previously presented.

Further on the 1.15 figure represents the variations of these forces depending on the reciprocating rod angle, while the 1.16 figure contains the polar diagrams for the crankpins and thrust bearings for a 5K90MC type of marine engine with an overall power equal to 22850 kW and a nominal rotational speed equal to 94 rpm manufactured by the MAN B&W company.

This first chapter is being concluded with a specific observation consisting in the fact that the gear containing a main reciprocating rod and secondary reciprocating rods have tangential forces and total radial forces T_t and Z_t that are being obtained by adding up corresponding forces for the two gears, the main and secondary ones keeping in mind the angular off-set γ and the mass m_{br} from the 1.54 set of formulas.

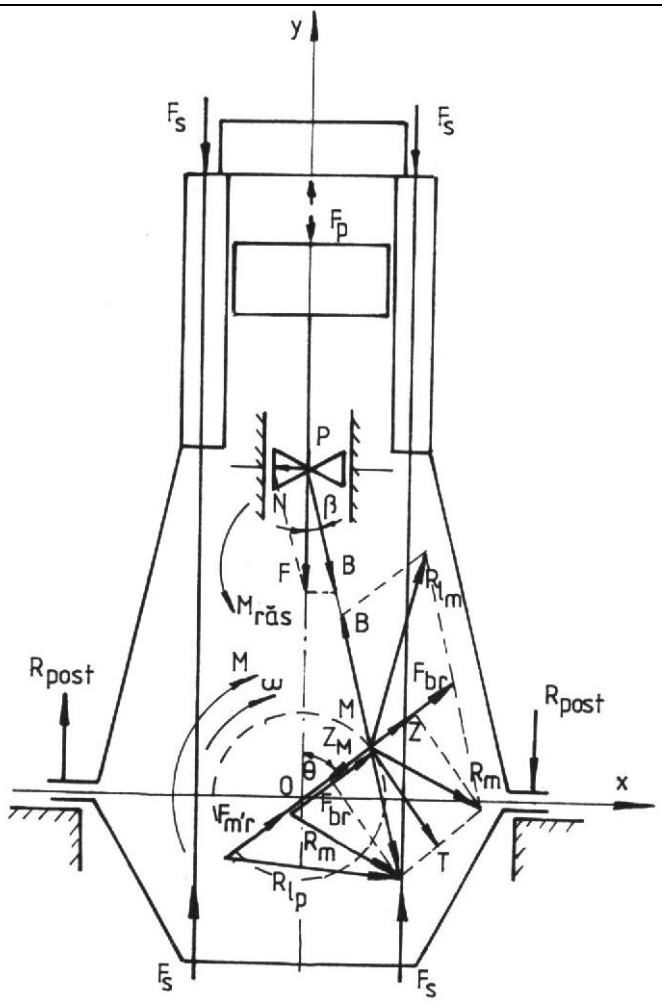

Figure 1.14: The force acting on the engine gear diagram

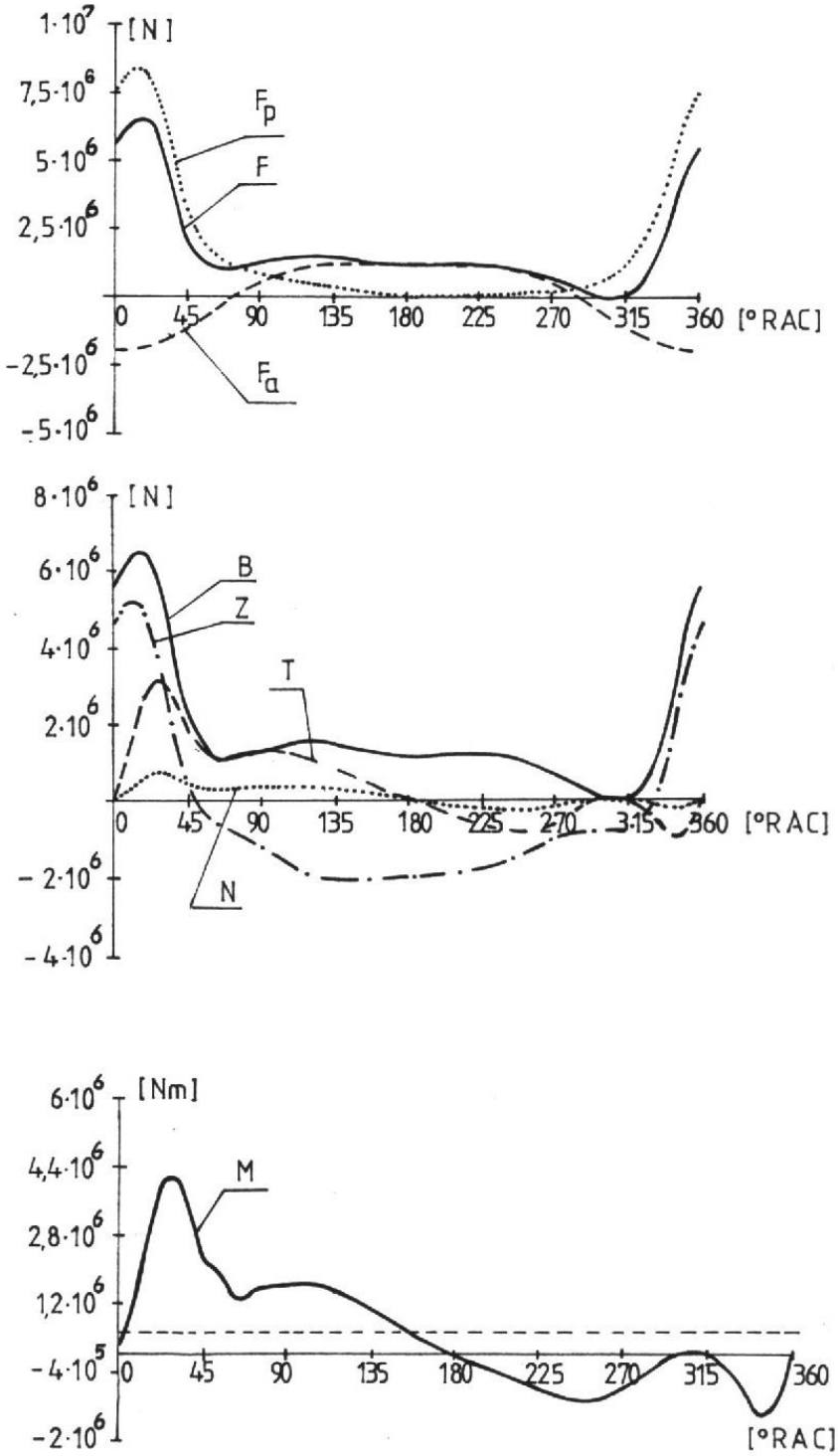

Figure 1.15: The reciprocating rod angular variation and the monocylindrical engine moment for the MAN B&W 5K90MC marine engine

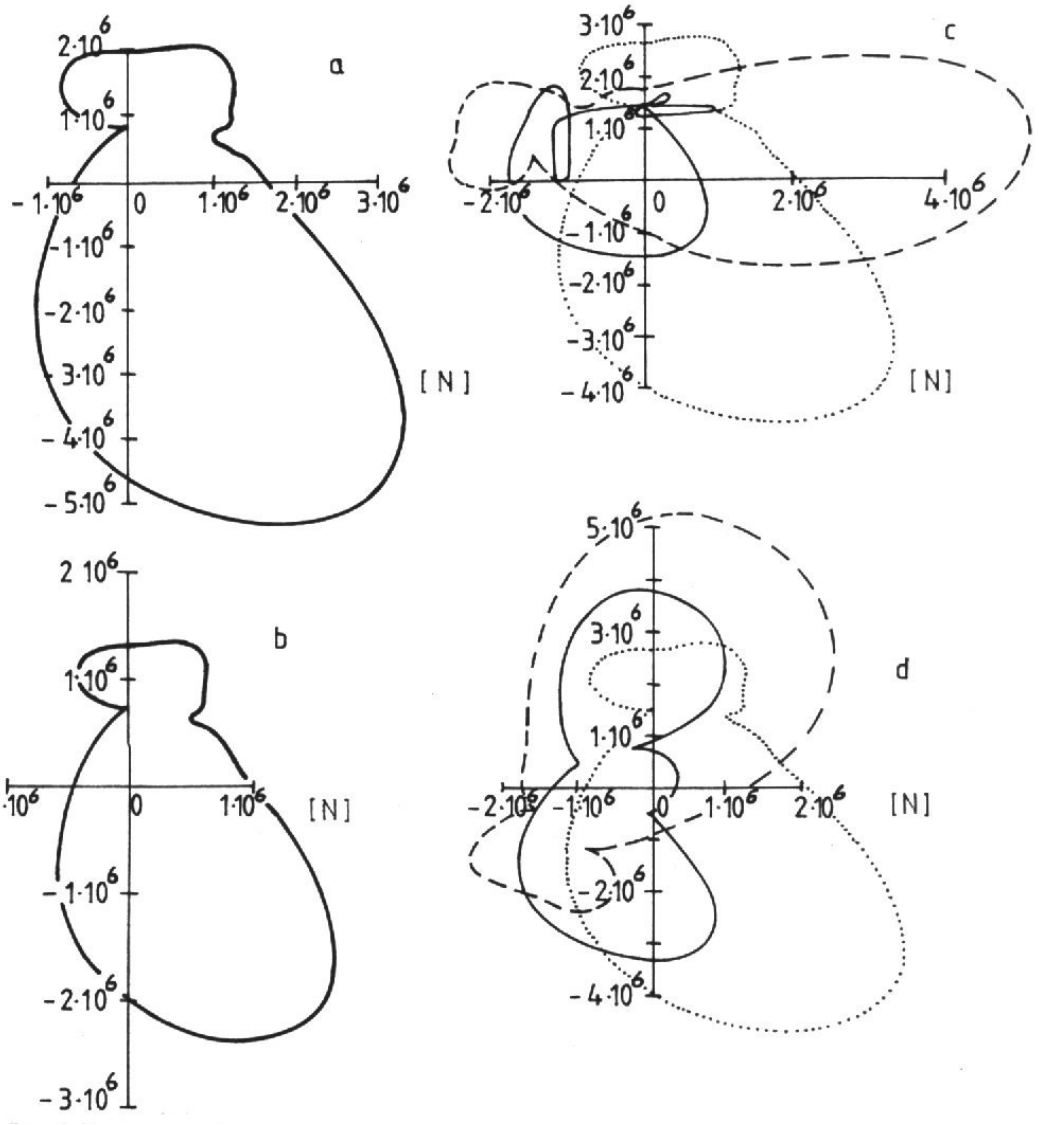

Figure 1.16: Polar diagrams for crankpins of the MAN B&W 5K90MC marine engine: a – for the crankpin, b – for the end thrust bearing, c – for the intermediary crankpins

Table 1.2: Forces and moments acting on marine engine components

No.	Name	Calculus formula
1	Gas pressure forces	$F_p = A_p\left[p(\theta) - p_{cart}\right] \cong \frac{\pi D^2}{4} p(\theta)$
2	Inertia for piston assembly	$F_{p_a} = -m_p a_p$

3	Inertia of reciprocating rod that has an alternative motion	$F_{ba} = m_{ba} a_p$
4	Inertia of reciprocating rod that has a rotation motion	$F_{br} = -m_{br} R\omega^2$
5	Crank inertia	$F_{m'r} = -\left(m_m + 2m'_{bm}\right) R\omega^2$
6	Inertia of masses in an alternative motion	$F_a = -m_a a_p$
7	Inertia of masses in an rotation motion	$F_r = -m_r R\omega^2$
8	The force applied by the articulating piston	$F = F_p + F_a$
9	The normal force applied on the cylinder liner	$N = F \tan\beta$
10	The force acting along the reciprocating rod	$B = F/\cos\beta$
11	Tangential force	$T = F \sin(\alpha + \beta)/\cos\beta$
12	Radial force	$Z_M = F \cos(\alpha + \beta)/\cos\beta$
13	Resulting force of the reciprocating rod acting on the thrust baring	$Z = Z_M + F_{br} = Z_M - m_{bm} R\omega^2$
14	Resulting force acting on the thrust baring	$\vec{R}_m = \vec{B} + \vec{F}_{rb} = \vec{T} + \vec{Z}$
15	The resulting for inside the thurst bearing	$\vec{R}_{lm} = -\vec{B} + \vec{F}_{rb}$
16	Resulting force of the reciprocating rod acting on the crankpin	$\vec{R}_p = \vec{R}_M + \vec{F}_{m'r}$ *
17	The force acting on the engine support	$R_{post} = F_p + R_{pl_y}$
18	Tie piece tightening force	$F_s = F_p$
19	Engine moment	$M = TR = FR \sin(\alpha + \beta)/\cos\beta$
20	Rolling moment	$M_{r\tilde{o}} = N \cdot OP = FR \sin(\alpha + \beta)/\cos\beta = M$

* In a real situation the resulting force acting on the crankpin is calculated by using two forces of such type calculated from the corners of the crankpin, as it has been shown in the 1.16 figure.

1.2.2 Crankshaft revolutionary motion evening

The previous remarks regarding the kinematics and the dynamics of the engine gear have been made on the base hypothesis having in its core the angular speed ω. In reality, due to the alternative motion of the pistons inside the cylinders and the variation of gas pressure, strong tangential forces occur, thus the engine momentum varies as well in a resultant manner (in the case of engines with more than one cylinders), symbolized as M_Σ, its value being obtained by adding all the momentum M for each cylinder. As a consequence big differences can occur in the case of the M_Σ coefficient total value and the one constant for the resistance momentum, noted by $M_{res} = M_{\Sigma,}$ this being opposite by the gear driven by the marine propulsion system (it being a propeller or a generator impeller). Figure 1.17 presents the variation of the poly cylindrical instant momentum for a MAN B&W 5K90MC type of main engine, indicating the medium value of M_Σ in the range defined by the formula:

$$T_{M\Sigma} = \frac{T_M}{i} = \frac{T_c}{i} = \delta \qquad (1.101)$$

It can be noticed that it is similar with the value of the constant angular off-set between two successive launches. It also has to be mentioned that keeping this off-set at a constant value is, in fact, a basic hypothesis, as it will be shown in the following parts.

The mentioned differences imply corresponding variations of the kinetic energy of all moving masses, as well as the ones of the angular speed of the crankshaft. *The unevenness degree of the motion* can be defined as:

$$\delta_\omega = \frac{\omega_{max} - \omega_{min}}{2} \qquad (1.102)$$

when the uneven functioning takes part in the (ω_{max} - ω_{max}) range of the angular speed of the crankshaft. The median speed of ω is calculated with formula:

$$\overline{\omega} = \frac{\omega_{max} - \omega_{min}}{2} = \frac{\pi n}{30} \left[\text{rot} / \text{min}\right] \qquad (1.103)$$

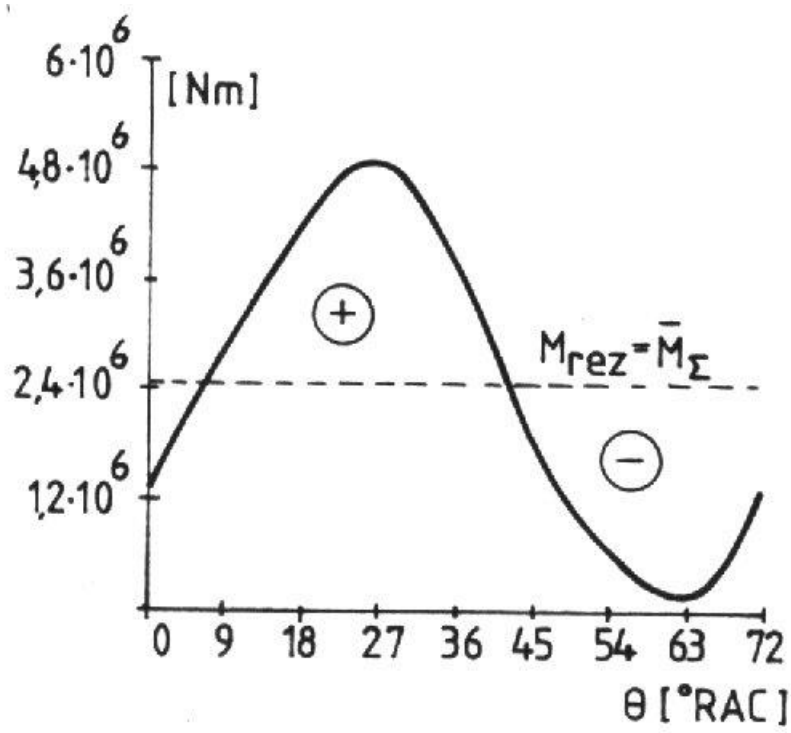

Figure 1.17: The variation of the ploy cylindrical engine momentum depending on the angle of the reciprocating rod for a MAN B&W 5K90MC marine engine

In order to highlight the kinetic energies and the differences mentioned for the momentum we have to rely on the system with a degree of freedom of movement diagramed in the 1.18 figure. The kinetic energy of this kind of mechanism can be calculated with the following formula:

$$E_c = E_{cm\prime} + E_{cb} + E_{cp} = \frac{1}{2}J_{m\prime 0} + \frac{1}{2}m_b\,(x_{Gb}^2 + y_{Gb}^2) + \frac{1}{2}J_{bGb}\omega^2 +$$

$$\frac{1}{2}Jm_p y^2 = \frac{1}{2}\theta^2\,[J_{m0} + m_b\left(c_{1bx}^2 + c_{1by}^2\right) + J_{bGb}c\ \ {}^{2}_{\omega b} + m_p c_{wp}^2\,] \qquad (1.104)$$

in the above formula J_{m0} is the mechanical inertial moment for the crankpin, being reduced to the axis value, the rest of the elements being defined in the previous chapters. Thus, the following moments will be noted as:

$$J(\theta) = J_{m_0^{'}} + m_b\left(c_{1_{b_x}}^2 + c_{1_{b_y}}^2\right) + J_{b_{Gb}} c_{\omega_b}^2 + m_p c_{w_p}^2 \tag{1.105}$$

Practically that is the definition of the *generalized inertia moment*. In the process of developing the motion equation for the entire system with one degree of movement we need to define the *centripetal stiffness moment* as:

$$C(\theta) = \frac{1}{2}\frac{dJ(\theta)}{d\theta} = m_b\left(c_{1_{b_x}} c_{2_{b_x}} + c_{1_{b_y}} c_{2_{b_y}}\right) + J_{b_{Gb}} c_{\omega_b} c_{\varepsilon_b} + m_p c_{w_p} c_{a_p} \tag{1.106}$$

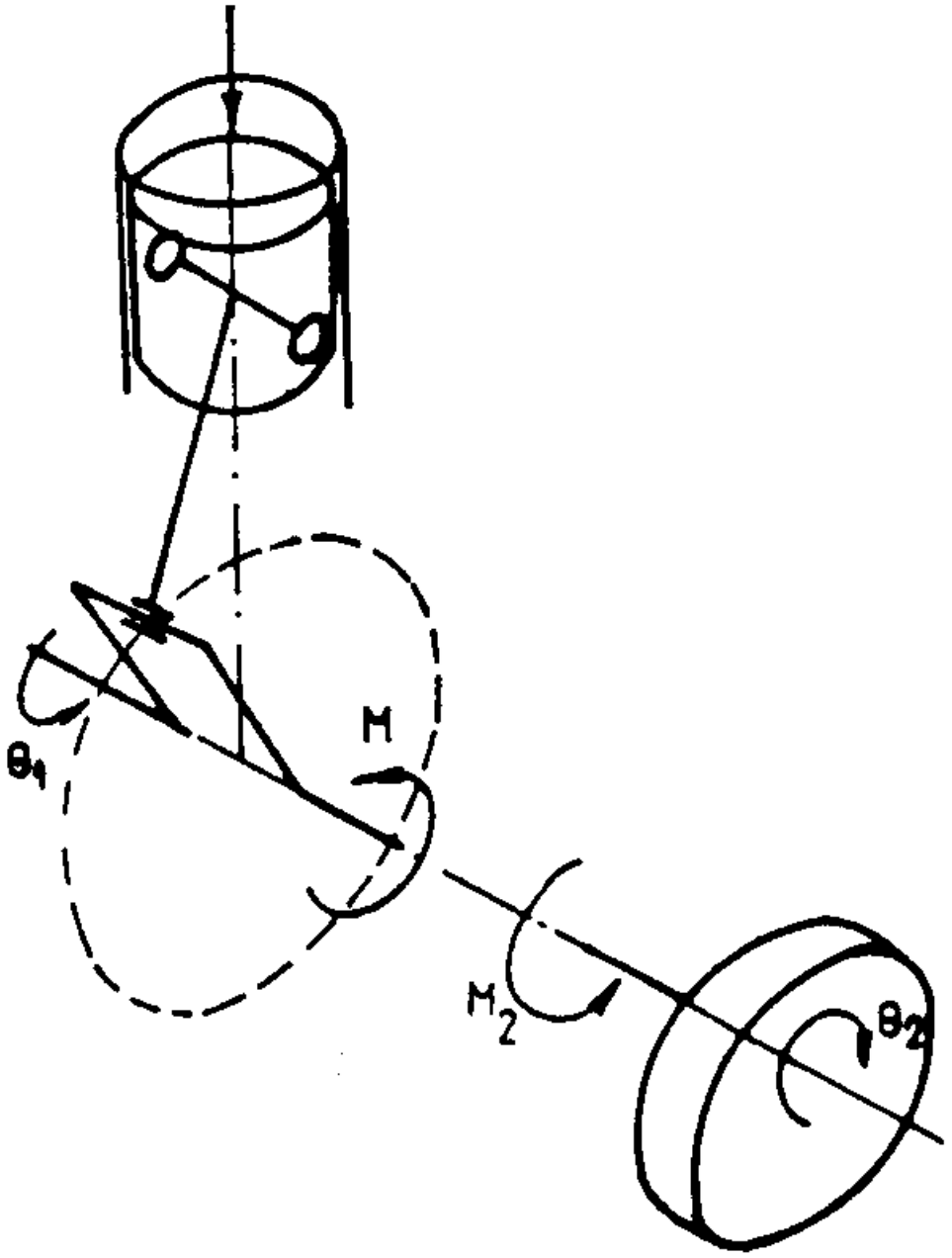

Figure 1.18: One degree of freedom mechanism diagram

Thus the kinetic energy of the entire system can be written as:

$$E_c(\theta) = \frac{1}{2} J(\theta)\theta^2 \qquad (1.107)$$

Thus, the virtual mechanical work will be:

$$\delta L = -p(\theta)A_p\delta y + M\delta\theta = -\left[p(\theta)A_p c_{w_p} + M\right]\delta\theta \quad (1.108)$$

From the above formula we can highlight the general force as:

$$Q = -p(\theta)A_p c_{w_p} + M \quad (1.109)$$

The motion equation for the entire system will be:

$$J(\theta)\theta + C(\theta)\theta = Q \quad (1.110)$$

By trans ponding this equation for the multidimensional system of the shaft line of a marine main engine this will become:

$$J_t\theta = M_\Sigma - M_{rez} \quad (1.111)$$

In the equation above J_t is the total inertia momentum obtained by adding J_0, the inertia momentum of all parts in motion reduced to the rotation axis, as well as J_v, the inertia momentum of the flywheel that uniforms the entire motion the last one being considered, at a first glimpse, as being much higher than the first inertia moment, thus:

$$\frac{1}{2}J_v d\omega^2 \cong \left(M_\Sigma - M_{rez}\right)d\theta \quad (1.112)$$

furthermore, by integration the inertia momentum of the flywheel can be obtained:

$$J_v = \frac{A_\oplus}{\delta_\omega \overline{\omega}^2} \quad (1.113)$$

in the above figure the bellow term is the positive area from the 1.17 figure, this meaning, at a certain scale this is the energetic overlaps towards the main consumer. It can be observed that in the (1.111) equation a unilineal term has been canceled, but it will further developed in the next paragraphs. From the same situation

it can be noticed that the unevenness degree is being registered for the moment of the multi cylindrical engine by introducing the flywheel.

The simplifying procedures previously used can be canceled by using an exact analytic and graphic method [17] and by describing the energy depending on moment inertia diagram. The steps will be described in the following paragraphs:

- *The calculus of the inertia moment for motion masses facing the rotation axis*. The formula for the total inertia moment is:

$$J_t = J_0 + J_v \quad (1.114)$$

where the inertia moment J_0 is:

$$J_0 = i\left(J_{m_0'} + J_{br} + J_a\right) + \sum J_{fl,cg} \quad (1.115)$$

in the above formula J_{br} is the inertia moment for the reciprocating rod mass facing the crankpin (which has a rotation motion):

$$J_{br} = m_{br} R^2 \quad (1.116)$$

J_a is the inertia moment for masses with an alternative motion, being reduced as a inertia moment facing the rotation axis, while $\sum J_{fl,cg}$ is the sum of all inertia moments for coupling flanges in several areas of the crankshaft, of all counterweights and other elements. For J_{m0} the following formula applies:

$$J_{m_0'} = J_{m_0} + J_p + 2J_{b_0'} \quad (1.117)$$

where the inertia moment for the thrust bearing is being reduced to the rotation axis, being:

$$J_{m_0} = J_m + m_m R^2 \quad (1.118)$$

meanwhile J_{b0} is the bracket moment facing the rotation axis, which is being calculated using analytical formulas or by meshing the shape of the bracket in far

more simpler areas [5], [14], [17]. The only unsolved unknown remains the one of J_a; for this the mass m_a kinetic energy preservation condition will be applied as:

$$\frac{1}{2} m_a w_p = \frac{1}{2} J_a \omega^2 \qquad (1.119)$$

In the above formula w_p can be equaled with the formula specified in the 1.1 table, obtaining the following equation:

$$J_a = \frac{1}{2} m_a R^2 \left(b_0 + \sum_{k=1}^{\infty} b_k \cos k\theta \right) = \bar{J}_a + \sum_{k=1}^{\infty} J_{a_k} \qquad (1.120)$$

in the same time the b_k coefficients in the above formula and the harmonic development are given by the (1.119) formula and the harmonic coefficients from the formula for the piston motion mentioned in the (1.14) equation. Thus, the mean value for the inertia moment, as its harmonic order component k will have the value given by the formula:

$$\begin{cases} \bar{J}_a = \frac{1}{2} m_a R^2 b_0 \cong \frac{1}{2} m_a R^2 \left(a_1^2 + 4a_2^2 \right) = \frac{1}{2} m_a R^2 \left(1 + \frac{\lambda^2}{4} \right) \cong \frac{1}{2} m_a R^2 \\ J_{a_k} = \frac{1}{2} m_a R^2 b_k \cos k\theta \end{cases} \qquad (1.121)$$

The first value can be found in [5], [12] and [17]; the las values can be substituted for the values of k that are satisfying the following condition:

$k = \pi$ - for two stroke engines;

$k = \pi/2$ for four stroke engines (1.22);

the values will be multiplied for the i number of cylinders (as shown in the 1.19 figure).

- *Mechanical work variation calculus developed in an engine cycle*. Mechanical work cycle depending on the θ angle is being calculate with the following formula:

$$L(\theta)=\int_0^{\theta} p(\theta)dV=\int_0^{\theta} F_p(\theta)dy_p=\int_0^{\theta} M_p(\theta)d\theta \quad (1.123)$$

having a $M_p(\theta)$ instantaneous moment for the gas pressure:

$$M_p(\theta)=F_p(\theta)R\frac{\sin(\theta+\beta)}{\cos\beta} \quad (1.124)$$

and this equation is analogue with the no. 19 equation from the 1.2 table. In a $\Delta\theta$ calculus rate is being applied and by dividing the period *0* - T_c in a $n_0=T_c/\Delta\theta$ equidistant intervals, the following iterative calculus formula is being obtained:

$$L(\theta_{j+1})=L(\theta_j)+\frac{M_p(\theta_j)+M_p(\theta_{j+1})}{2}\Delta\theta, j=1\div n_0 \quad (1.125)$$

The mechanical work cumulated in a cycle rate is being shown in the 1.20a figure, by placing the variation curve for the mono cylindrical mechanical work (which is linear and resistant, because of the moment is constant); at the ending of a cycle the two values are constant. By summing them up analytical or graphical the same variations can be described in the same manner for the poly cylindrical engine (as shown in the 1.20b figure); with L_s symbolizing the additional mechanical work (excess mechanical work).

- *Generating the inertia energy-moment diagrams*. The 1.9 figure describes the means of generating this diagram, which also presents the mean of the energy is being transferred between the crankshaft and the engine parts having an alternative motion. For this, in an analytical or graphical manner, the value of θ is being eliminated between the mathematical functions $L_{S\Sigma} = L_{S\Sigma}(\theta)$ and $J_a = J_a(\theta)$, this way generating the $L_{S\Sigma} = L_{S\Sigma}(J_a)$ diagram through the x coordinating points.
- The calculus for the flywheel inertia momentum. For this we have to consider that the value of J_v starts from the origin of the reference system described in the 1.19 figure, passes through the Ox secant (the value of x

on the inertia energy-moment diagram), obtaining in this manner the value of the φ_x angle:

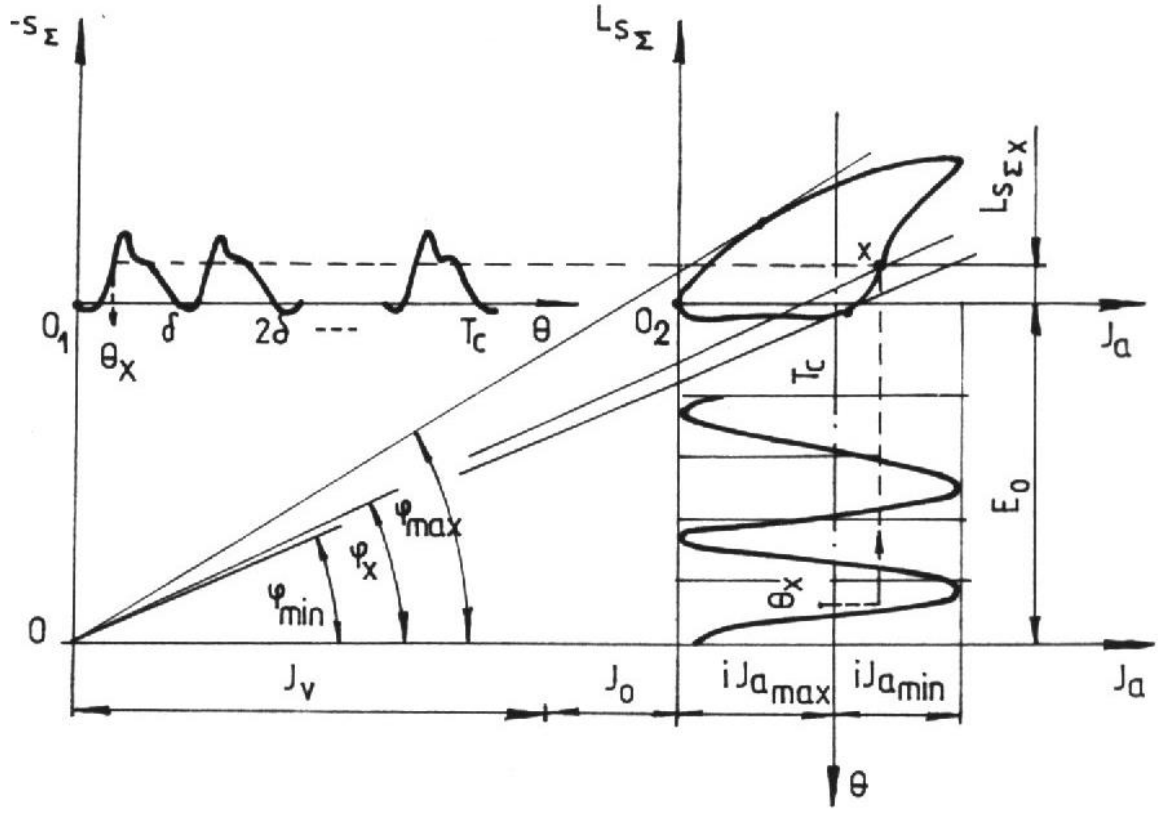

Figure 1.19: Diagrams for the flywheel inertia moment calculus

$$\tan\varphi_x = \frac{L_{s_{\Sigma_x}} + E_0}{J_x} = \frac{E_{c_x}}{J_x} = \frac{\frac{1}{2}J_x\omega_x^2}{J_x} = \frac{1}{2}\omega_x^2 \qquad (1.126)$$

From the above formula the following can be concluded:

$$\omega_x = \sqrt{2\tan\varphi_x} \qquad (1.127)$$

By replacing the values of the angular speeds in the (1.126) formula in the case of the minimum and maximum values corresponding to φ_{min} and φ_{max} generated by the tangent lines generated from the origin 0 to the extreme points of the $L_{S\Sigma} = L_{S\Sigma}(J_a)$

curve with the abscise axis, afterwards by introducing these values in the (1.102) and (1.103) equations the following effective values will be obtained:

$$\begin{cases} \varphi_{max} = \arctan\left[\dfrac{\overline{\omega}}{2}\left(1+\dfrac{\delta_\omega}{2}\right)^2\right] \\ \varphi_{min} = \arctan\left[\dfrac{\overline{\omega}}{2}\left(1-\dfrac{\delta_\omega}{2}\right)^2\right] \end{cases} \quad (1.128)$$

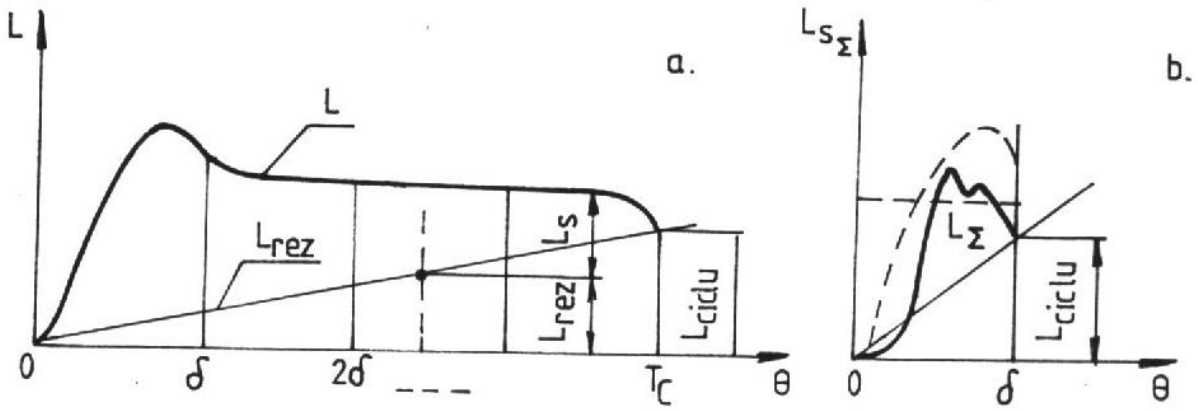

Figure 1.20: Mechanical work variation generated in an engine cycle depending on the crank rod: a – single cylinder engine, b – poly cylinder engine

Knowing the values of these angles the tangents for the previous chapter can be generated and at the intersection between them the 0 origin of the system lays down, used for reading at a certain scale the inertia moment J_v for the flywheel.

By applying on of the methods above we can obtain the value for the flywheel inertia moment, also by applying the calculus diagram presented in the 1.21. figure. These diagrams are also used in order to calculate the diameter of the flywheel with the formula:

$$\overline{D}_v = \sqrt[3]{\frac{4J_v}{\pi\rho bh}} \quad (1.129)$$

In the mentioned figure are also being pointed out the values and dimensions for the Sulzer 6RND90 marine engine.

It has been mentioned at the beginning of the subchapter that the flywheel radius is dropping in value if the number of cylinders raises, and this is also described in a graphical manner in the 1.22 figure. For these, the unevenness degree of the crankshaft rotation motion varies in the range 1/20 – 1/50 for slow speed propulsion engine and 1/100 – 1/300 for auxiliary engines.

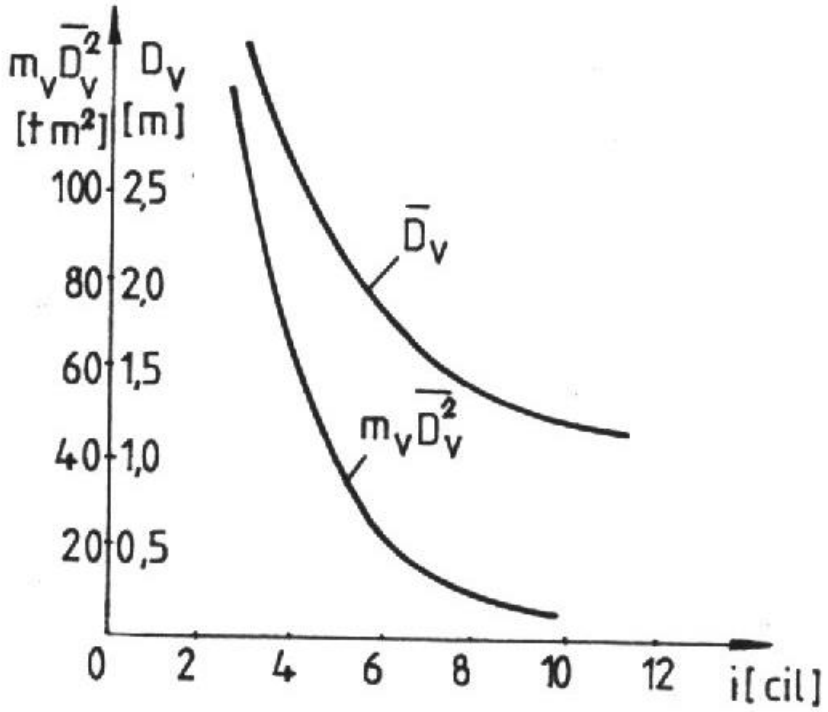

Figure 1.20: The variation range for the diameter and the inertia moment of the flywheel depending upon the number of cylinders

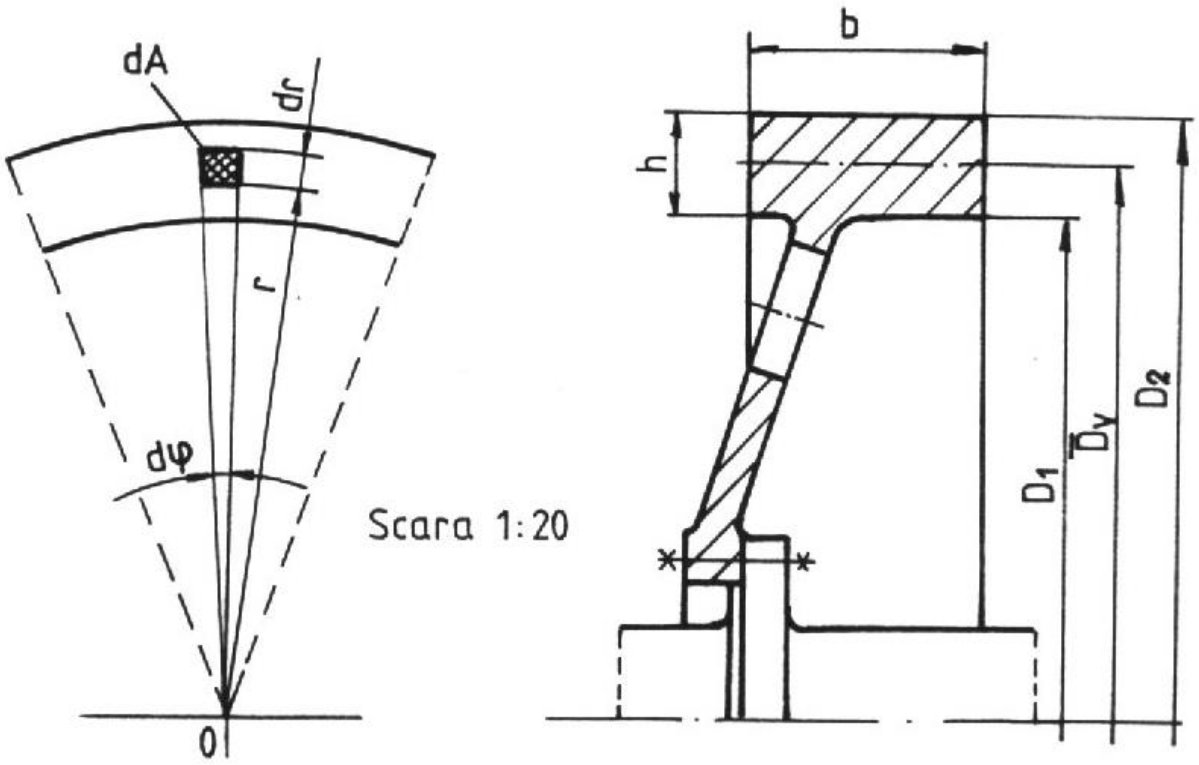

Figure 1.21: The calculus diagram for the flywheel diameter and the fitting solution for the flywheel for a marine main engine Sulzer 6RND90 type

References:

1. Bățaga, N., Burnete, N., Cãzilã, A., Rus, I., Sopa, S., Teberean, I. *Motoare cu ardere internã*, Editura Didacticã și Pedagogicã, București, 1995;

2. Bienzo, C.B., Grammel, R. *Engineering Dynamics*, Van Nostrand, 1954;

3. Buzbuchi, N., Dragalina, Al., Manea, L., Moroianu, C., Dinescu, C. *Motoare navale. Procese și caracteristici*, Editura Didacticã și Pedagogicã, București, 1997;

4. Buzbuchi, N. *Dinamica sistemelor de propulsie navalã*, Tipografia Institutului de Marinã Civilã Constanța, 1998;

5. Buzbuchi, N., Dinescu, C. *Complemente de* d*inamica motoarelor navale*, Editura Alas, Cãlãrași, 1995;

6. Buzbuchi, N., Pruiu, A., Bratu, D. *Determinarea coeficienþilor armonici ai deplasãrii, vitezei și acceleraţiei pistonului*, Volumul "Sesiunea de comunicări Științifice", Universitatea "Ovidius", Constanþa, 1991;

7. Buzbuchi, N., Pruiu, A., Bratu, D. *Metodã de analizã cinematicã a motoarelor diesel cu pistoane opuse*, Volumul "Sesiunea de comunicări Știinþifice", Universitatea "Ovidius", Constanța, 1991;

8. Doughty, S. *Fundamentals of Internal Combustion Engine Torsional Vibration*, ASME Paper 88-ICE6, the Energy-Sourses Technology Conference and Exhibition, New Orleans, Lousiana, 10-14 Jan., 1988;

9. Dughty, S. *Mecahnics of Machines*, John Wiley & Sons Inc., 1988;

10. Dumitru, Gh. ș.a. *Diagnosticarea vibroacusticã a instalaþiilor de propulsie navale cu motoare cu aprindere prin comprimare*, Grant nr. 952/1995, Universitatea "Dunãrea de Jos", Galați, 1995;

11. Gaiginschi, R., Zãtreanu, Gh. *Motoare cu ardere internã*, vol. 1, Editura "Shakti", Iași, 1997;

12. Granwald, B. *Teoria, calculul și construcţia motoarelor pentru autovehicule rutiere*, Editura Didacticã și Pedagogicã, București, 1980;

13. Orbeck, F. *Development Leading to the New DOXFORD 3-Cylinder Engine*, the Institute of Marine Engineering, North West England Branch, 1977;

14. Panã, C., Popa, M.G., Negurescu, N. *Motoare cu ardere internă. Cinematicã, dinamicã, echilibraj*, Editura “Matrix”, București, 1997;

15. Rãdoi, M., Deciu, E. *Mecanica*, Editura Didacticã și Pedagogicã, 1981;

16. Ripianu, A. *Calculul cinematic și dinamic al arborilor cotiți"*, Editura "Dacia", Cluj, 1981;

17. Taraza, D. *Dinamica motoarelor cu ardere internã*, Editura Didacticã și Pedagogicã, București, 1985;

18. Vanșeidt, V.A. *Motoare Diesel*, Editura Tehnicã, București, 1959;

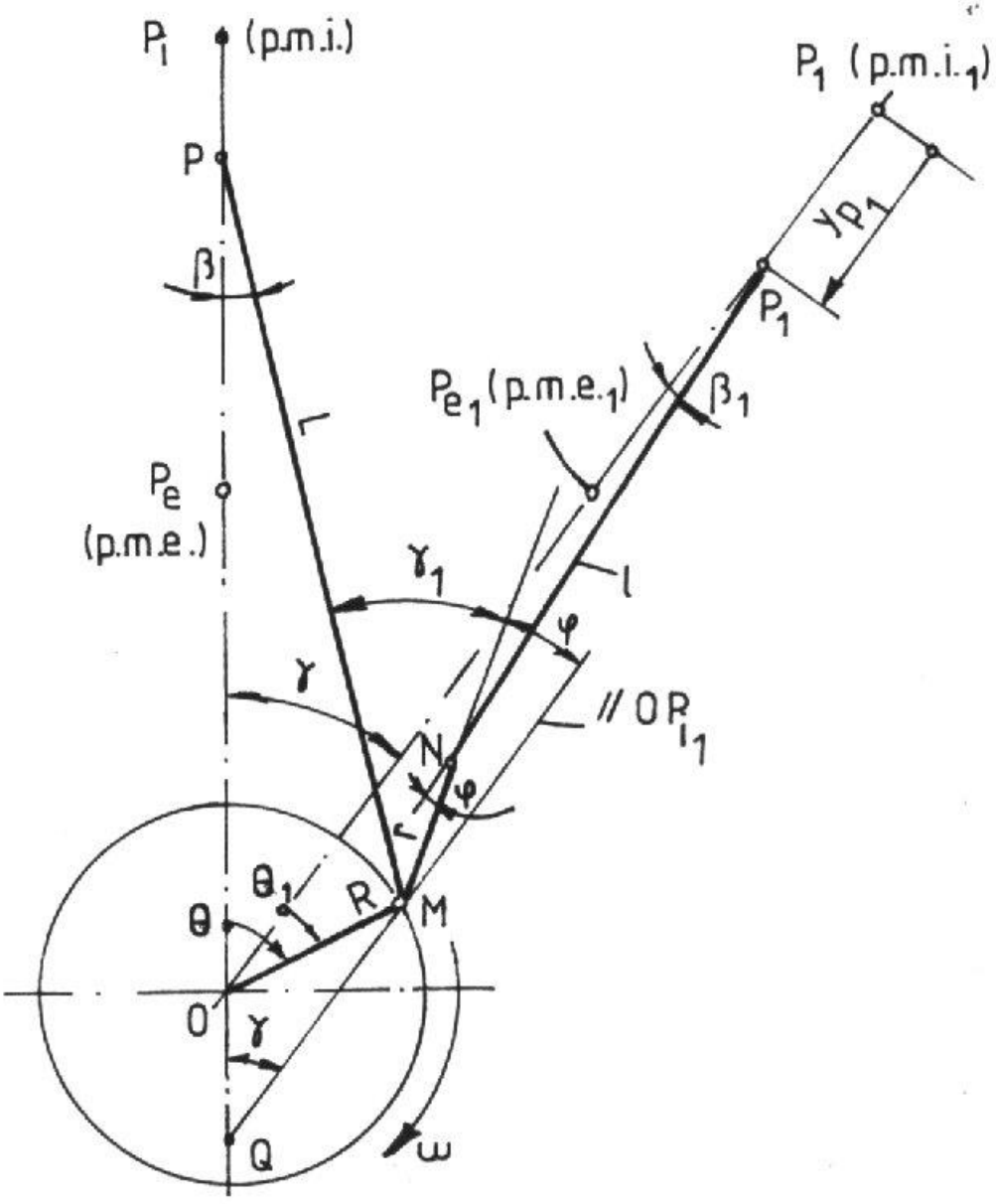

Figure 1.6: Kinematic calculus diagram for the gear fitted with main reciprocating rod and secondary reciprocating rods

2. MARINE ENGINES BALANCING

An internal combustion marine engine is considered balanced when the reactions in its supports are dimensional constant, as well as direction and orientation. Due to the fact that this condition can't be satisfied in the case of a heat engine we will further examine the causes that are generating the lack of balancing in the marine engine.

2.1 Causes generating the lack of balance in marine engines

In order to analyze the way each engine gear force category act on the reactions from the engine supports we will research on the unbalance generated by each and every one of these forces, as shown in the 1.14 figure. the 1.2.1 paragraph showed the action of forces acting on the fixed, as well as the mobile one for a single cylinder engine.

Further on, we will analyze the pressure forces effect as well as the masses inertia effect for the rolling occurrence, for which they are dimensional equal.

Thus, the total rolling momentum M_{ras} is being defined in the 1.2.1 paragraph, being generated by the components $M_{ras\ p}$ and $M_{ras\ a}$, while the total momentum M is being decomposed in the main dimensions M_p and M_a in the following manner:

$$M_{rās} = M_{rās_p} + M_{rās_a} \quad (2.1)$$

and:

$$M = M_p + M_a \quad (2.2)$$

For each component the following equivalents apply:

$$M_{rās_p} = M_p;\ M_{rās_a} = M_a \quad (2.3)$$

having all these in mind, as a general rule, if the engine is considered as being a single cylinder one it will be unbalanced and the main components that generate partial momentum act on different construction engine elements. Regarding the inertia of moving masses in rotation motion symbolized as Fr, even if it has a constant value it is variable in its direction and orientation but it will be transferred to the engine supports and will the generate the so called quiver motion.

If the engine has more than one cylinders than moments will occur that will unbalance the engine and they are generated by the unbalancing forces that act in different plan, spatial speaking. The force diagram and the momentum diagram for the poly cylindrical engine is being presented in the 2.1 figure. The engine is to be considered normal axial, with identical cylinders and displayed at an even distance, this meaning that:

$$a_j - a_{j+1} = a = const.,\ j = \overline{1, n-1} \qquad (2.4)$$

where a_j is the distance between the cylinder j-order axis, being normal on the Oxyz axis and the Oz axis is identical with the rotation axis, while Oy is parallel with the cylinder axis and Ox is perpendicular on the rotation axis. Two neighboring cylinders gears have been taken into consideration: *j* and *j + 1*.

The masses inertia forces in rotation motion for each cylinder $F_{r\mathrm{i}}$ is being decompound in the following elements:

$$\begin{cases} X_{r_j} = F_{r_j} \sin \alpha_j \\ Y_{r_j} = F_{r_j} \cos \alpha_j,\ j = \overline{1, i} \end{cases} \qquad (2.5)$$

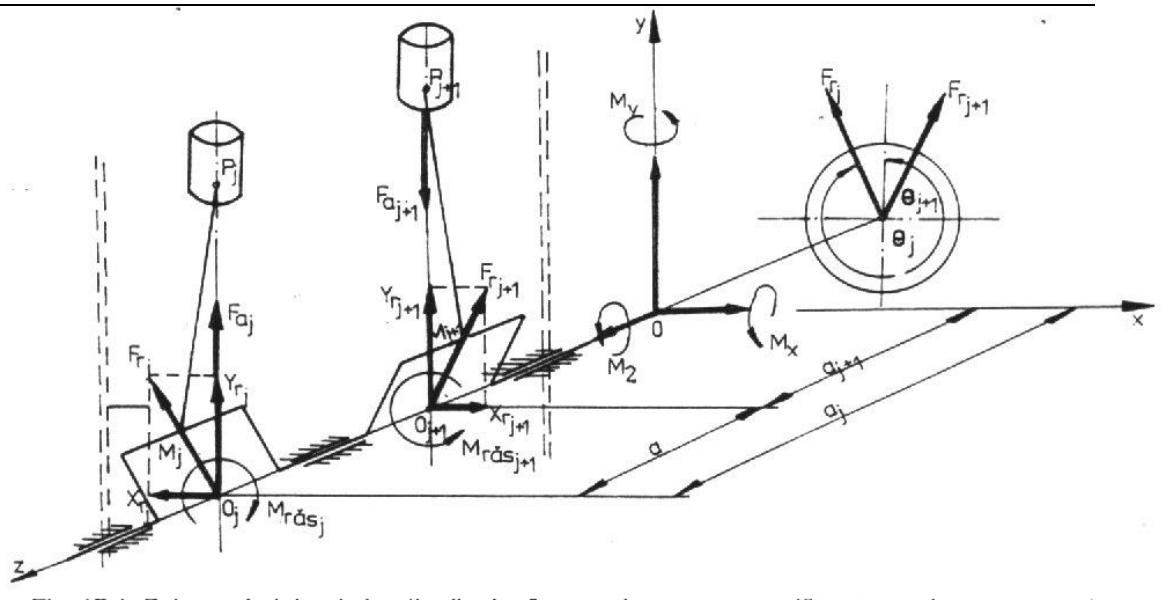

Figure 2.1: Inertia forces diagram with two neighboring engine gears which are projected on the Oxyz axis system

in the above formulas F_{ri} has the following deducted expression (from the formulas 1.55 and 1.56):

$$F_{r_j} = -m_r R\omega^2 = const.,\ j = \overline{1,i} \qquad (2.6)$$

according with the previous specifications.

The mass inertia of forces having a translation motion, Fai are being deducted from the (1.60) equation as well from the 1.1 table and they have the following expressions:

$$F_{a_j} = -m_a a_{p_j},\ j = \overline{1,i} \quad (2.7)$$

in the above formula a_p has the value extracted from the 1.1 table, thus:

$$a_{p_j} = -R\omega^2\left[a_1 \cos\theta_j + \sum_{k=1}^{\infty}(2k)^2 a_{2k} \cos 2k\theta_j\right] \quad (2.8)$$

the coefficients a_1 and a_{2k} are being given by the (1.14) formula.

The Fai force is being projected on the Oxyz axis system and generates the following components:

$$\begin{cases} X_{a_j} = 0 \\ Y_{a_j} = F_{a_j},\ j = \overline{1,i} \end{cases} \quad (2.9)$$

In the above statements it has been assumed that m_a and m_r masses are identical for all mechanisms, this being considered identical.

$$\begin{cases} X = \sum_{j=1}^{i} (X_{r_j} + X_{a_j}) \\ Y = \sum_{j=1}^{i} (Y_{r_j} + Y_{a_j}) \end{cases} \quad (2.10)$$

as for two of the momentum:

$$M_x = \sum_{j=1}^{i} (Y_{r_j} + Y_{a_j}) a_j = \sum_{j=1}^{i} Y_{r_j} a_j + \sum_{j=1}^{i} Y_{a_j} a_j = M_{r_x} + M_{a_x} \quad (2.11)$$

these are being displayed around the Ox axis, and it is called a *gallop momentum (pitch),* that generates a vibration around the Oxy plan and has two main components: M_{rx} *– gallop momentum for inertia of masses with a rotation motion* and M_{ax} *– gallop momentum for inertia if masses with an alternative motion*, as well as the momentum equal with:

$$M_y = \sum_{j=1}^{i} X_{r_j} \cdot a_j = M_{r_j} \quad (2.12)$$

This final moment is called the *serpentine momentum (gyration momentum)* and generated a quivering motion for the engine in the Oxz plan, thus it has an effective gallop component for the inertia forces of masses in rotation motion.

In the same time the rollover moments that act in each plan of the engine carry on. By adding them these moments generate a single total moment acting in the xOy plan called the *rolling momentum*, calculated with following formula:

$$M_z = \sum_{j=1}^{i} M_{r\tilde{a}s_j} = \sum_{j=1}^{i} (M_{r\tilde{a}s_{p_j}} + \sum M_{r\tilde{a}s_{a_j}}), \qquad (2.13)$$

This momentum includes the rolling momentum of all inertia for masses with a alternative motion and all pressure forces generated by gases, according with the (2.1) formula. In the previous formulas *i* represents the total number of cylinders.

It can be concluded that from the (2.10) and (2.11) that the resulting inertia forces and the rolling momentum are not dependent on the distance between cylinders. On the other hand the gallop moments and the serpentine moments are dependent on these distances. That is why the balancing process can be studied on the bases of two type of loads: the inertia forces and the rolling momentum; the inertia forces momentum (the gallop and serpentine momentum).

These moments that generate engine unbalancing are called *external momentum* because these one act on the engine supports. On the other hand the force couple momentum that load the support crankpins are called *internal momentum*. In this manner it will be mentioned that the balancing process consists in the complete cancelation of all variable forces and momentum acting on the engine supports. Above all, there are two means of balancing: using some sort of *balancing masses* (*counterweights*) that have inertia forces that cancel the inertia forces of moving masses, as well as their momentum, or picking an optimal solution consisting in an optimal crankshaft, with the possibility of canceling the forces and momentum of inertia. Generally, an intermediary solution is being chosen that combines the two mentioned previously.

2.2 Balancing the one single cylinder engine

The observations made in the previous paragraph are used as a base to study the unbalancing phenomena that occur in the normal axis single cylinder which is

being generated by the F_r and F_a forces, as well as the rolling momentum M_{ras} with its main components $M_{ras\ p}$ and $M_{ras\ a}$, thus we will be analyzing the means of balancing these components at each turn in the following.

2.2.1 Rotation masses inertia force balancing

The no. 7 formula from the 1.2 table expresses the inertia of masses with a rotation motion; this force is being balanced by using two counterweights with a m_{er} in the elongation of brackets (as shown in the 1.13 figure). Assuming that the force F_r acts on the symmetric plan of the elbow, we will consider that the two counterweight have even masses and that they will develop an inertia force that will balance F_r:

$$2m_{e_r}\rho_{e_r} = F_r \qquad (2.14)$$

In the above formula exists two unknown values: the balancing mass m_{er} and the distance from the mass center to the rotation axis ρ_{er}. If one of the condition is being applied it implies the other one.

2.2.2 Balancing the inertia forces of masses with a translation motion

The formula for the inertia is given by the no. 2 relation from the 1.2 table, while the formula for the piston acceleration is also given in the 1.2 table, thus mass inertia forces in translation motion for the one single cylindrical engine with a normal end axis has the following shape:

$$\begin{aligned} F_a &= m_a R\omega^2\left[a_1\cos\theta + \sum_{k=1}^{\infty}(2k)^2\cdot a_{2k}\cdot\cos 2k\theta\right] = \\ &= m_a R\omega^2 a_1\cos\theta + m_a R\omega^2\sum_{k=1}^{\infty}(2k)^2 a_{2k}\cos 2k\theta = \\ &= -m_a R\omega^2\cos\theta + \sum_{k=1}^{\infty} m_a R(2k)^2 a_{2k}\cos 2k\theta = \\ &= F_{a_1} + \sum_{k=1}^{\infty} F_{a_{2k}} \end{aligned} \qquad (2.15)$$

in the above formula, if we have in mind the value $a_1 = -1$, the following notations have been made:

$$F_{a_1} = -m_a R\omega^2 \cos\theta \qquad (2.16)$$

and:

$$F_{a_{2k}} = m_a R a_{2k} (2k\omega) \cos 2k\theta \qquad (2.17)$$

thus only 1st order harmonic persists as well as the superior even harmonics.

In the initial momentum $\tau_0 = 0$, we will have a angular value $\theta = 0^0$ RAC (the reciprocating rod is at the lower dead center), thus:

$$F_{a_1} = -m_a R\omega^2; \quad F_{a_{2k}} = m_a R a_{2k} (2k\omega)^2 \qquad (2.18)$$

Having in mind the formulas from (1.14) the sign of the a_{2k} coefficients can be set from the harmonic developed out of the piston deployment:

$$sign\, a_{2k} = \begin{cases} 1, & k = 2p \\ -1, & k = 2p-1,\ p \in \mathrm{N} \end{cases} \qquad (2.19)$$

The observation from the (2.17) formula becomes the meaning of a initial phase by introducing an additional angle φ_{2k}:

$$F_{a_{2k}} = m_a R(2k\omega)^2 a_{2k} \cos 2k\theta = -m_a R(2k\omega)^2 |a_{2k}| \cos(2k\theta + \varphi_{2k}) \qquad (2.20)$$

and:

$$\varphi_{2k} = \begin{cases} \pi, & k = 2p \\ 0, & k = 2p-1, \quad p \in \mathrm{N} \end{cases} \qquad (2.21)$$

Further one:

$$|F_{a_{2k}}| = m_a R(2k\omega)^2 |a_{2k}| \qquad (2.22)$$

and this allows to obtain the expression of the superior harmonic with an even order:

$$F_{a_{2k}} = -\left|F_{a_{2k}}\right| \cos\left(2k\theta + \varphi_{2k}\right) \quad (2.23)$$

The last formula is not fixed because it can have the following vectorial meaning: it should be considered an applied vector on the *O* center, with a constant value, equal with $|F_{a2k}|$; this vector will be spinning around the reciprocating rod orientation having an angular speed equal with $2k\omega$; in the $\theta = 0\ ^0RAC$, when the reciprocating rod reaches the lower dead center point this vector will form an φ_{2k} angle with the Oy axis (as in figure 2.2a); keeping in mind the usual sign convention [6], [11] and [17], in strict coordination with the sign of a_{2k}, the module vectors $|F_{a1}|$ and $|F_{a4k-1}|$ will be on the same phase with the reciprocating rod when it is in the lower dead center; and the module vectors $|F_{a4k}|$ will be faced on opposite position towards this; after the τ time period, in which the reciprocating rod generates the $\theta = \omega\pi$ and the vector surpasses a certain angle equal with $2k\theta = 2k\omega\tau$, the vector projection on the Oy axis is $|F_{a2k}|cos(2k\theta + \varphi_{2k})$ representing the actual value of the module harmonic *2k* in any given moment (as shown in the 2.2b figure).

The $|F_{a2k}|$ mentioned vector can be balanced with an equal vector that has an opposite orientation, obtained by using a rotation mass with the same speed as the vector, but at a difference of 180^0, having a mass center placed at a ρ_{ea2k} towards the rotation axis. The balancing mass can be calculated with the following formula:

$$m^*_{e_{a_{2k}}} = m_a \frac{R}{\rho_{e_{a_{2k}}}} \left|a_{2k}\right| \quad (2.24)$$

This value is being obtained by imposing the value of ρ_{ea2k}. The main thing that has to be obtained by balancing the $|F_{a2k}|cos(2k\theta + \varphi_{2k})$ value and that how it is shown that it remains unbalanced by the component $|F_{a2k}|sin(2k\theta + \varphi_{2k})$, this leading to another vectorial interpretation (as shown in the 2.2c figure): thus $|F_{a2k}|$ is the resultant of two vectors with a constant dimension and it is equal with $|F_{a2k}|/2$ and

they spin in opposite directions with an angular speed equal to $2k\omega$ and generate the φ_{2k}, in other words - φ_{2k} in the $\tau_0 = 0$ ($\theta = 0\ ^0RAC$); the two vectors are being balanced using two masses with the following dimension:

$$m_{e_{a_{2k}}} = \frac{1}{2} m^*_{e_{a_{2k}}} \qquad (2.25)$$

the two masses are symmetric towards the cylinder axis and are spinning one depending on the other with an angular speed equal with $2k\omega$; the normal projections on the cylinder axis for centrifugal inertia mass forces m_{ea2k} are canceling each other in a reciprocating manner.

In the case of the a_p acceleration we have to limit ourselves at the first two harmonics by applying the simplified formulas from the 1.1 table, thus we will obtain the order 1 harmonics for the mass inertia force that have an alternative motion (as mentioned in 2.16), or the 2nd order harmonics:

$$F_{a_2} = -\lambda m_a R\omega^2 \cos 2\theta \qquad (2.26)$$

In practice, in the case of the normal single cylindrical engine the balancing process is being limited to the firs two harmonics. The complete balancing diagram for the inertia forces is being drawn out from the [6], [10], [11] and [17] elements of references that will be listed at the end of this chapter.

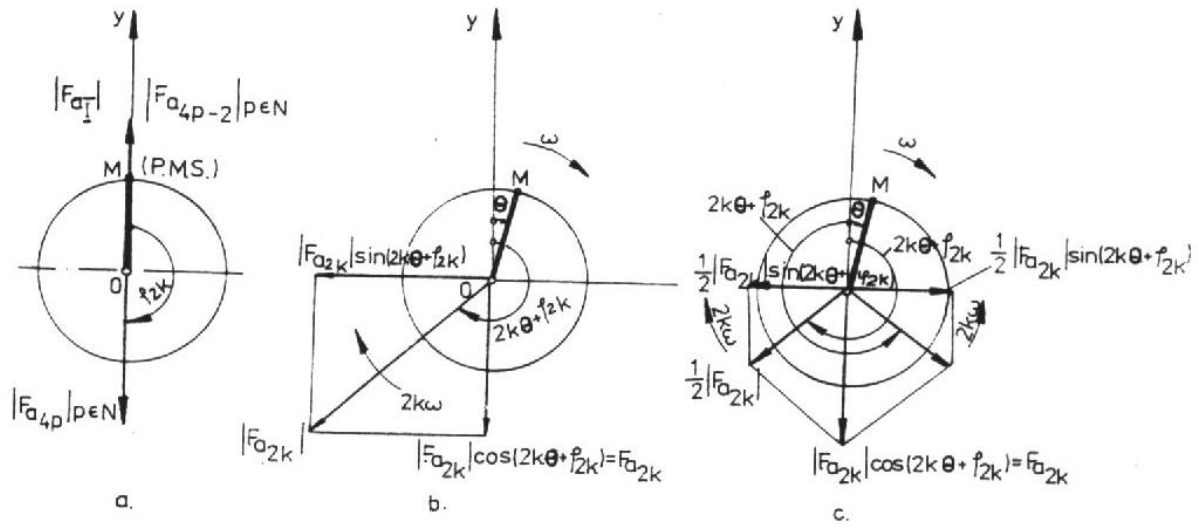

Figure 2.2: The vectorial interpretation of inertia forces generated by the masses with an alternative motion

2.2.3 Rolling momentum balancing of pressure forces generated by gasses and mass inertia forces with a translation motion

The rolling-over momentum generated by the gas pressure has the following formula which has also been mentioned in the 1.2, no. 19 formula:

$$M_{r\check{s}_p} = F_p R \frac{\sin(\theta+\beta)}{\cos\beta} \qquad (2.27)$$

in the above formula F_p is given by the (1.124) formula by applying the (2.3) formula.

The momentum is, in fact, a periodical function that depends on the θ rotation angle, the period being the one of the T_c cycle (as shown in 1.97), thus this hypothesis can be further developed by applying the analogue principles with a harmonic analysis for the gas pressure of the motor fluid (as shown in 1.97) in a Fourier series:

$$M_{r\check{s}_p} = \overline{M}_{r\check{s}_p} + \sum_{k=1}^{\infty} M_{r\check{s}_{pk}} \qquad (2.28)$$

around the median value:

$$\overline{M}_{r\acute{a}s_p} = \frac{1}{T_c}\int_0^{T_c} M_{r\acute{a}s_p}(\theta)d\theta \qquad (2.29)$$

and the harmonic components with a k order have the following values:

$$M_{r\acute{a}s_{p_k}} = \left|M_{r\acute{a}s_{p_k}}\right|\cos\left(k\theta - \varphi_{p_k}\right) \qquad (2.30)$$

having a module and a phase given by the relations (as it will be shown in the 4.2 paragraph):

$$\begin{cases} \left|M_{r\acute{a}s_{p_k}}\right| = \sqrt{X^2_{p_k} + Y^2_{p_k}} \\ \varphi_{p_k} = \arctan\dfrac{X_{p_k}}{Y_{p_k}} \end{cases} \qquad (2.31)$$

In the above formula the harmonic coefficients have the following formula:

$$\begin{cases} X_{p_k} = \dfrac{2}{T_c}\displaystyle\int_0^{T_c} M_{r\hat{a}s_{p_k}}(\theta)\cos k\theta\, d\theta \\ Y_{p_k} = \dfrac{2}{T_c}\displaystyle\int_0^{T_c} M_{r\hat{a}s_{p_k}}(\theta)\sin k\theta\, d\theta \end{cases} \qquad (2.32)$$

From the above formula and the vectorial interpretation applied in the 2.3 figure the projection of a spinning vector that has a module projected on the Oz rotation axis, with a $k\omega$, in the opposite orientation facing the crankshaft and forms an angle φ_{pk} with the rotation axis when the crank is in the lower dead center position.

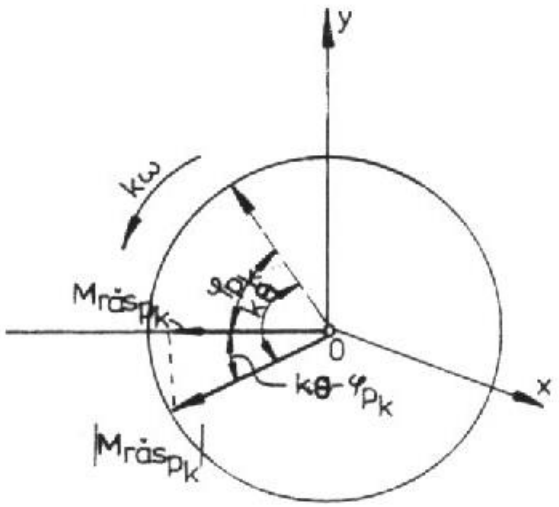

Figure 2.3: Vectorial interpretation of the harmonic component with a k order for the roll moment generated by gas pressure

Analog, by applying the corresponding formulas for the inertia of masses in alternative motion (as presented in 2.15) the formula for the rolling motion is being generated due to this force itself:

$$M_{r\tilde{a}a} = F_a R \frac{\sin(\theta+\beta)}{\cos\beta} = \sum_{k=1}^{\infty} M_{r\tilde{a}a_k} \quad (2.33)$$

For the harmonic component with a *k* order the following formula will apply:

$$M_{r\tilde{a}a_k} = \left| M_{r\tilde{a}a_k} \right| \sin\left(k\theta + \varphi_{a_k}\right) \quad (2.34)$$

with a module and a phase given by de formula bellow:

$$\begin{cases} \left| M_{r\tilde{a}a_k} \right| = m_a R^2 \omega^2 |b_k| \\ \varphi_{a_k} = \begin{cases} 0, \; k = 1,5,6,\ldots \\ \pi, \; k = 2,3,4,\ldots \end{cases} \end{cases} \quad (2.35)$$

the b_k coefficients are being given by the following sets of formulas:

$$\begin{cases} b_1 = \frac{1}{4}\lambda a_1 - 2a_2 \\ b_2 = \frac{1}{2}a_1 - 4\lambda a_4 \\ b_3 = \frac{1}{4}\lambda a_1 + 2a_2 - 8a_4 \\ b_4 = \lambda a_2 - 9\lambda a_6 \\ b_5 = 8a_4 - 18a_6 \\ b_6 = 4\lambda a_4 - 16\lambda a_8, \ldots \end{cases} \quad (2.36)$$

The vectorial interpretation of the rolling moment generated by the inertia of masses with a translation motion is being presented in the 2.4 figure. the rolling momentum generated by the gasses pressure force depends on the engine load (by the means of pressure), practical being invariable towards the rotation speed, thus it can be concluded that it cannot be balanced with counterweights, unlike the momentum generated by the mass inertia force which have a translation motion. According with [4] and [17] the k=2 order harmonic forces of the two effects are in opposite phase, the unbalance being generated by the momentum from the second category and it is being lowered in endurance by the condition:

$$\left|M\right|_{rcs_{p2}} \cong \left|M\right|_{rcs_{a2}} \quad (2.37)$$

In case of an off-set engine gear an additional elements of the rolling momentum occurs which is being generated by the gas pressure.

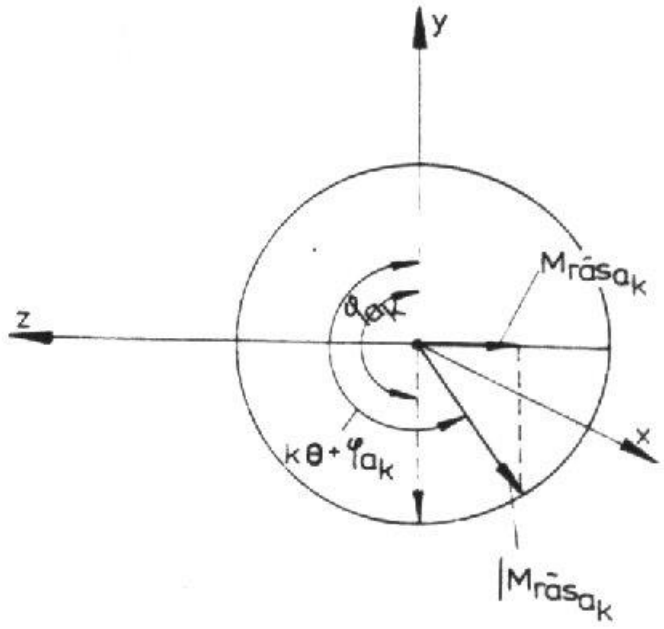

Figure 2.4: Vectorial interpretation of the harmonic interpretation of a k-order for the rolling momentum generated by the inertial phenomena

The total component of the rolling momentum will be obtained by adding up the two vectors which leads to the formula for the momentum generated by the gas pressure force and the inertia, with the following formulas:

$$M_{r\check{a}s_k} = \left|M_{r\check{a}s_k}\right| \sin\left(k\theta + \varphi_k\right) \qquad (2.38)$$

with the following module and phase:

$$\begin{cases} \left|M_{r\check{a}s_k}\right| = \sqrt{\left|M_{r\check{a}s_{pk}}\right|^2 + \left|M_{r\check{a}s_{ak}}\right|^2 + 2\left|M_{r\check{a}s_{pk}}\right|\left|M_{r\check{a}s_{ak}}\right| \sin\left(\varphi_{p_k} + \varphi_{a_k}\right)} \\ \varphi_k = \arctan\dfrac{\left|M_{r\check{a}s_{pk}}\right| \cos\varphi_{p_k} + \left|M_{r\check{a}s_{ak}}\right| \sin\varphi_{a_k}}{\left|M_{r\check{a}s_{pk}}\right| \sin\varphi_{p_k} + \left|M_{r\check{a}s_{ak}}\right| \cos\varphi_{a_k}} \end{cases} \qquad (2.39)$$

and with a vectorial description that reassembles the ones previously applied: the projection on the Oz axis of a spinning vector having a kω speed and an opposite

orientation towards the crankshaft, with a phase angle on the Oy axis at the initial momentum.

2.3 Balancing a poly cylindrical engine with cylinders in a line configuration

The hypothesis around which the following considerations will be developed are: the engine has even distributed combustions, identical cylinders and equal in distance. Further on the two main types of loads are being analyzed: inertia forces and rolling momentum, as well as momentum of these forces.

2.3.1 Inertia force balancing and the rolling momentum

The issue of loading forces ca be solved by applying an unitary approach [9], keeping in mind the vectorial interpretations presented in the following chapters. Thus, on the basis of previous interpretations the vectorial module will be expressed using the following formula:

$$|V_k| \in \left\{ |F_r|, |F_{a_k}|, |M_{r\omega_k}| \right\}_{k \in N} \qquad (2.40)$$

and this is a vector with an angular speed equal to kω and this is being projected on the Oy axis, this vector also describes the inertia force of masses with an alternative motion towards Oy axis and this is happening when the crank in passes through the lower dead center position and it is given by the initial phase symbolized as ψ_k. When $\psi_k = 0$, the vector describes the inertia force of rotation masses, or the 1st order harmonic of the inertia for all masses with a translation motion. Either way the last specification on the unitary interpretation states the fact the rotation orientation of the $|V_i|$ vector is identical with the on applied on the crankshaft when taking into account the inertia forces and opposite in case of the rolling momentum. In the case of the poly cylindrical engine, for the same harmonic order k there a vector for each cylinder $|Vk_i|$, $j = 1 - i$ and this allows the an association can be made between the star of these vectors and the star shape described by the crank which can be obtained by

projecting all the crank corners on a normal plane of the rotation axis (as it is shown in the 2.5 figure and on the same figure the combustion order has been numbered for that crank). In these conditions the angle formed by two consecutive vectors is equal with $k\tau\pi/i$, in which τ is the number of engine strokes and the time needed to achieve an engine cycle. Further on, two different cases can occur:

- $k\frac{\tau\pi}{i} = 2p\pi, p \in N$ (2.41)

and this lead to:

$k = 2pi / \tau$ for:

pi – for two stroke engines;

pi / 2 – for four stroke engines.

and this is the case for which all vectors have a resultant with a value different from 0 which is *i* times higher than the module of the k-order component for one cylinder:

$$\left|V_k\right| = \sum_{j=1}^{i}\left|V_{k_j}\right| = i\left|V_{k_j}\right| = i\left|V_{k1}\right| \neq 0. \qquad (2.42)$$

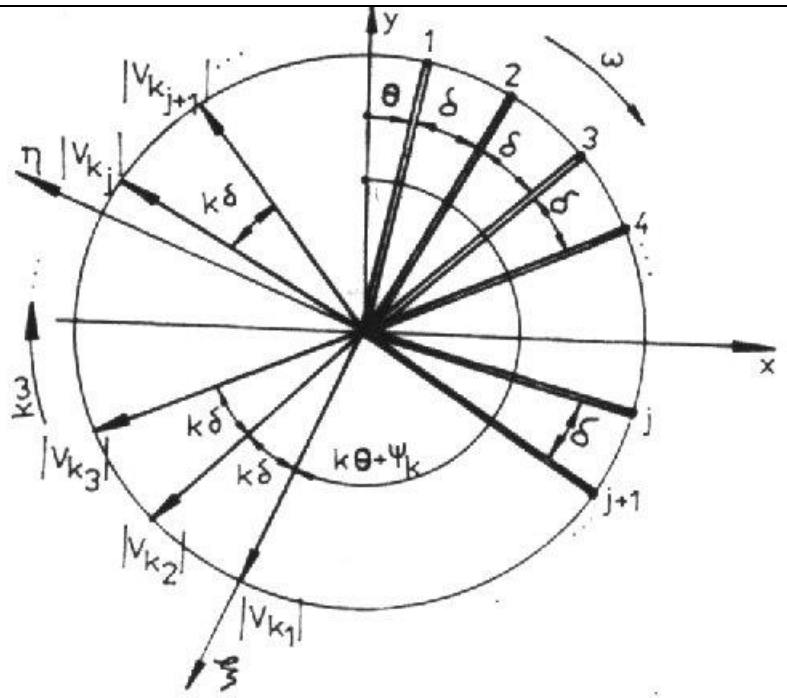

Figure 2.5: The star-shaped diagram described by V_{kj} vectors and the cranks

Because of the fact that all vectors are in the same phase the resulting vector stays all the time in the same perpendicular plan on the crank shaft rotation axis, as well as the specified vectors and as a consequence this vector can be balanced by using the equilibration masses;

- $k\frac{\tau\pi}{i} \neq 2p\pi, p \in N$, a case for which the calculus for the resultant the vectors will be projected on the mobile system symbolized by Oξη, one of these projections being similar with the crank orientation l, and the other one is normal on the axis. The resultant will have the following module:

$$|V_k| = \sqrt{V_{k_\xi}^2 + V_{k_\eta}^2} \qquad (2.43)$$

in the above formula the components have the following values:

$$\begin{cases} V_{k_\xi} = \left|V_{k_1}\right| \sum_{j=1}^{i} \cos(j-1)k\delta = \left|V_{k_1}\right| \dfrac{\sin(i\delta/2)\cos[(i-1)\delta/2]}{\sin(\delta/2)} = 0 \\ V_{k_\eta} = \left|V_{k_1}\right| \sum_{j=1}^{i} \sin(j-1)k\delta = \left|V_{k_1}\right| \dfrac{\sin(i\delta/2)\sin[(i-1)\delta/2]}{\sin(\delta/2)} = 0 \end{cases} \quad (2.44)$$

because:

$$i\delta/2 = i\tau\pi/2i = \tau\pi/2:$$

$$\pi - \textit{for two stroke engines;}$$

$$2\pi - \textit{for four stroke engines.}$$

Thus, for the cases in which:

$$k \neq 2pi/\tau:$$

$$pi - \textit{for two stroke engines;}$$

$$pi/2 - \textit{for four stroke engines.} \quad (2.45)$$

the vectors generate a zero value resultant: $\left|V_k\right| = 0$.

The previous observations are valid for all engines with an even number of cylinders. For the general case it can be seen that the harmonic orders carry on and depend on the stroke number of engine cycle and on the number of cylinders:

k = pi for two stroke engines;

k = pi/2 for four stroke engines and i = 2m and m Ɛ N; (2.46)

k = pi for four stroke engines and i = 2m + 1 and m e N.

It can be noticed that the engines with the cylinders displayed in line have a better balance once the number of cylinders increases because the harmonic order increases as well and this due to the fact that minimum harmonic order does not cancel itself, the amplitude of the superior harmonics constantly decreasing. In the meantime two stroke engines are superior comparing to four stroke engines with the

same number of cylinders, the lowest balancing features being recorded in the case of four stroke engine with an even number of cylinders.

The 2.6 figure presents the balancing solution for mass inertia forces with an alternative motion F_{a2k} (for normal axis set gears, just the even harmonic components remain). In this case two balancing weights are being used symbolized by m_{ea2k} that are spinning in different orientation facing each other with an angular speed equal to $2k\omega$ and that are developing centrifugal inertia forces with a $|F_{ea2k}|$ dimension which have the projections on the Oy axis and that are balancing the inertia force F_{a2k} for the entire engine mass multiplied by i, according to (2.42) formula. From the above stated the formula for the balancing mass can be deducted:

$$m_{e_{a_{2k}}} = \frac{i}{2} m_a \frac{R}{\rho_{e_{a_{2k}}}} |a_{2k}| \qquad (2.47)$$

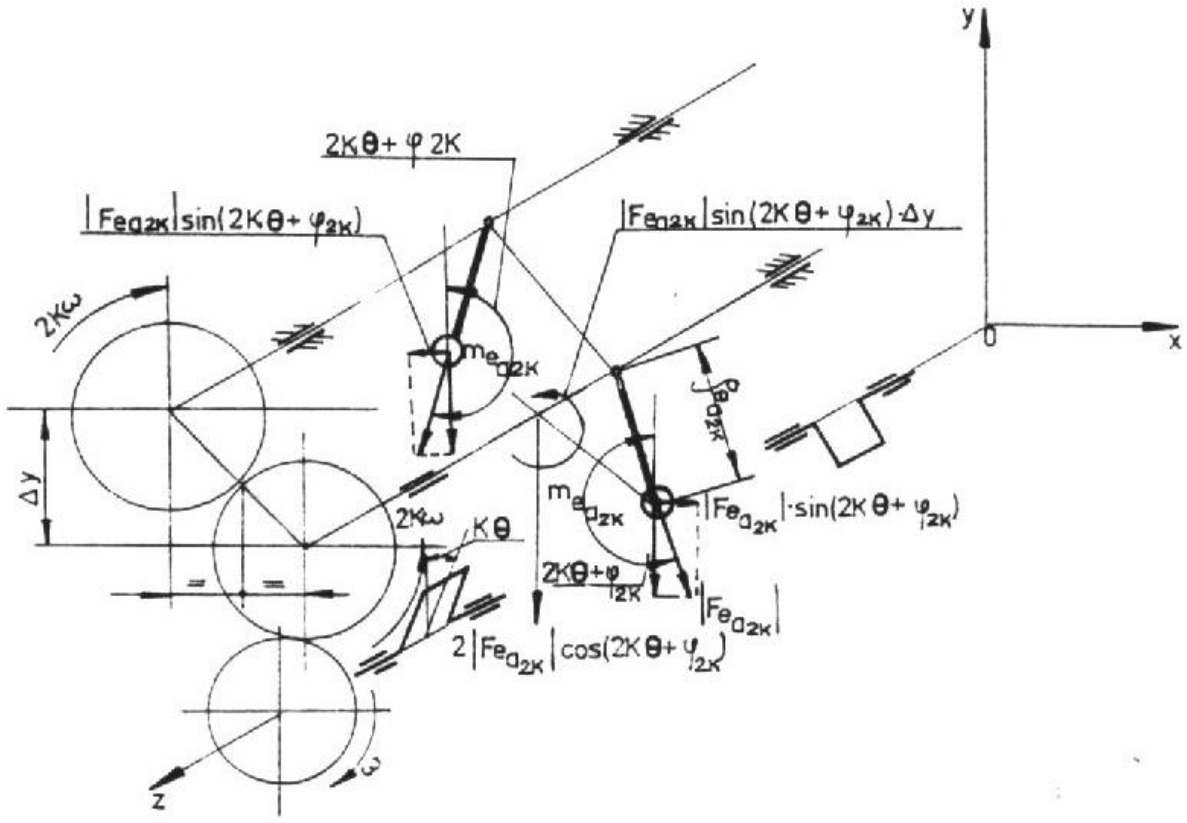

Figure 2.6: Alternative motion inertia forces balancing diagram for a poly cylindrical engine with all cylinders displayed in line

In the above formula ρ_{ea2k} is the distance from the counterweight mass center to the rotation axis of it. Additional, the presented solution also presents the possibility of balancing the rolling moment with an even order which is generated by the forces with an alternation motion by offsetting the balancing masses along the Oy axis with the Δy distance, given by the balancing formula between the additional engine couple of horizontal components of all centrifugal forces generated by the counterweights and the specific rolling momentum multiplied by the number of cylinders by:

$$\Delta y = \frac{2}{(2k)^2} R \left| \frac{b_{2k}}{a_{2k}} \right| \qquad (2.48)$$

having b_1 given by the (2.36) formula. For modern marine engines the solution applied in the case of four stroke engines fitted with four cylinders (such as Mitsubishi and others), for which the 2nd order harmonic remains or for which the previous quantity becomes equal with the crank length L, or more precisely, keeping in mind the formula (2.37), the following results:

$$\Delta y = L(1 - z) \qquad (2.49)$$

with:

$$z = \left| M_{r\omega_{p2}} \right| / \left| M_{r\omega_{a2}} \right|$$

2.3.2 Inertia momentum balancing

Further on the analysis of inertia momentum balancing is being dealt with, this forces being generated by masses with a rotation motion and afterwards by the masses with an alternative motion.

2.3.2.1 Momentum balancing for inertia forces generated by masses with a rotation motion

Even though the inertia forces resultant of masses with a rotation motion is 0 for all engines with even displayed combustions, the star diagram described by these is superposed on the one described by the cranks by the fact that they act on different plans and they will generate an unbalancing moment that acts on the engines supports as it is shown in the 2.7 figure. The gallop and serpentine momentum components that are being projected in the Oyz and Oxz plans are given by the formulas:

$$M_{r_x} = \sum_{j=1}^{i} Y_{r_j} a_j ; M_{ry} = \sum_{j=1}^{i} X_{r_j} a_j \quad (2.50)$$

with the following resultant:

$$M_r = \sqrt{M_{r_x}^2 + M_{r_y}^2} \qquad (2.51)$$

and the angle between it and the Ox axis is:

$$\varphi_r = \arctan \frac{M_{r_y}}{M_{r_x}} \qquad (2.52)$$

This resultant vector has a spinning characteristic and has a speed equal with the one of the crankshaft. It is an external moment that generated the vibration of the engine fitted on the support. Even if it has a constant dimension it is variable as orientation towards the crankshaft. The balancing can be realized by applying a M_{er} vector which is equal but has a different orientation, and this can be done by adding two extra masses m'_{er}, which have the same weight but different rotation speeds symbolized by ω and are placed at a ρ''_{er} distance towards the rotation axis with the following dimensioning equation:

$$m_{e_r}^* \rho_{e_r}^* \omega^2 \left[(i-1) + l_m \right] = M_r \qquad (2.53)$$

and the length of the crankpin is symbolized by l_m.

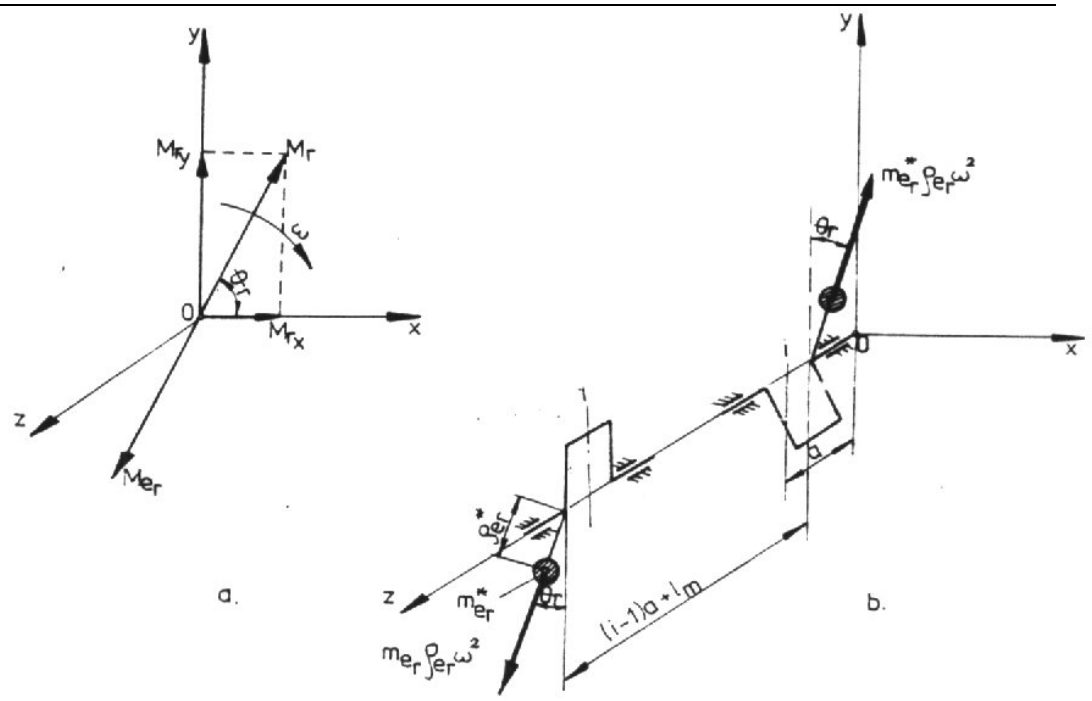

Figure 2.7: Balancing diagram for inertia forces momentum generated by masses with a rotation motion

2.3.2.2 Balancing the inertia forces generated by masses with a translation motion

The inertia forces of masses with an alternative motion occur in parallel vectorial system and are deployed in the same plans (acting in the Oyz plan and have parallel vectorial supports parallel with Oy). The vectorial system is being reduced to a single resultant given by the following formula:

$$R_a = \sum_{j=1}^{i} F_{a_j} ; M_a = M_{a_x} = \sum_{j=1}^{i} Y_{a_j} a_j \quad (2.54)$$

in the last formula the end term includes only the gallop vectorial elements (as shown in the 2.8 figure). The balancing of the first component has been studied in the 2.3.1 paragraph, that is why, in this paragraph only the second component will be dealt with.

According to Varignon's theory the sum of all moments of a vectorial system will be equal to the resulting moment of the entire system towards one point set as C_0, thus:

$$\sum_{j=1}^{i} F_{a_j} a_j = R_a a_{rez} \qquad (2.55)$$

in the above equation a_{rez} in the coordinate of the C_0 center in the system presented in the 2.8 diagram. We can extract the *2k* order harmonic components from the previous equation, thus the following formula will result:

$$a_{rez} = \frac{\sum_{j=1}^{i} a_j \cos\{2k[\theta + (j-1)\delta + \varphi_{2k}]\}}{\sum_{j=1}^{i} \cos\{2k[\theta + (j-1)\delta + \varphi_{2k}]\}} \qquad (2.56)$$

The above formula is valid only if the combustion are distributed in an even manner. If the additional conditions are placed in [1] then the following condition will result:

$$\begin{cases} 2k(j-1)\delta = 2p\pi, p \in N \\ a_j = (i-j+1)a \end{cases} \qquad (2.57)$$

in the above formula *a* is the distance between two consecutive cylinders, the first equation suggesting the fact that the 2k order terms are permanently in phase and that means the resulting force is 0, and the second equation suggests that the cylinder *i* is placed at a distance *a* towards the reference origin system, thus the (2.56) equation will be modified as it is shown below:

$$a_{rez} = \frac{\sum_{j=1}^{i}(i - j + 1)}{i} a = \frac{i(i+1)}{2i} a = \frac{i+1}{2} a \quad (2.58)$$

from the above formula it can be suggested that base of the resultant force is in the middle of the crankcase. Thus, an observation will be made that is rational to calculate the unbalancing moment of the inertia force for all masses with an alternative motion towards the C_0 point, keeping in mind the total inertia forces occurring in the total moment of the crankshaft. Calculated in this manner it will be defined as an external moment and the corresponding moment for only a half of length for the crankshaft is an internal moment by definition. For the harmonic components that have a 0 valued resultant the minimum value of the external moment does not depend on the point used as a reference at the beginning of the calculus; on the other hand for the harmonic components that have a resultant which is not equal to 0, the minimum value for the external moment will be calculated towards the symmetrical central plan that passes through the crankshaft (through the C_0 point), because, in this case the base of the resultant force is *the central axis of the vectorial system*.

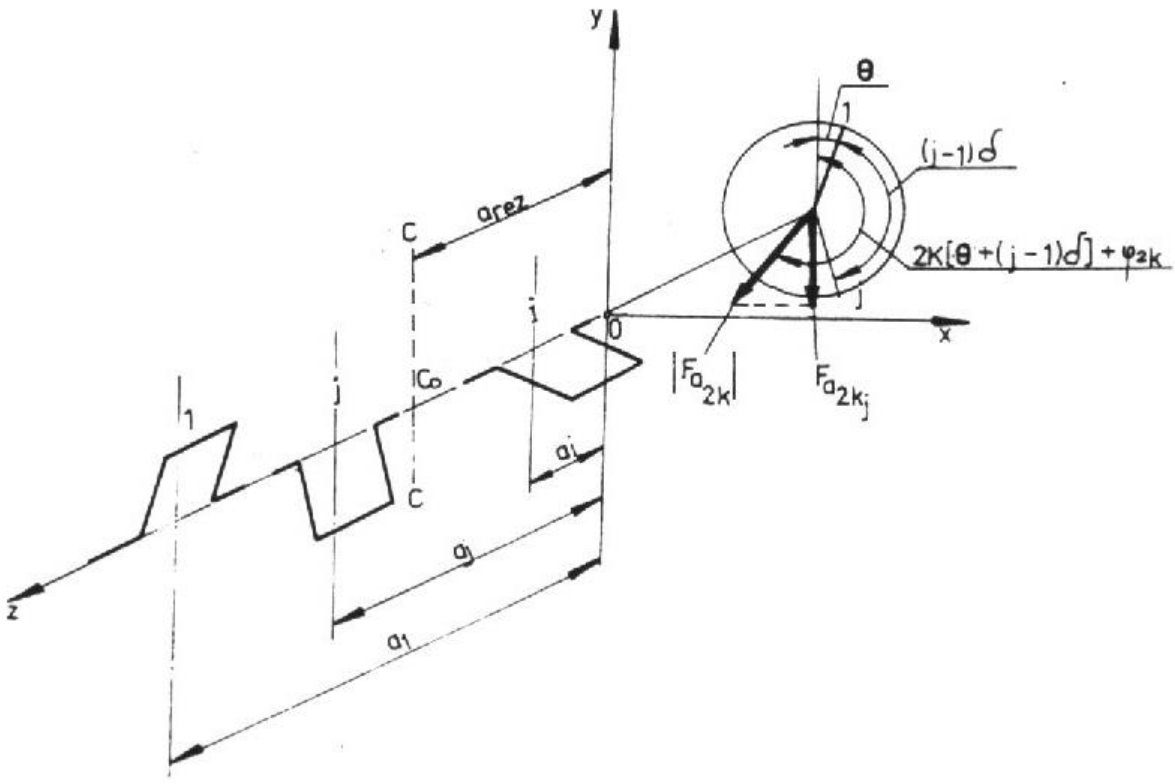

Figure 2.8: The diagram for the calculus of force inertia moments for masses with an alternative motion

Thus, each time this is possible, the preferred solution chosen for a crankshaft is one with a symmetrical center plan and this is valid only for the engines with an even number of cylinders, while this will not four stroke engines, having a crank phase, also not for two stroke engines that have an opposite phase. For the first category, four stroke engines with an crank phase a number of possibilities of achieving a symmetrical number of crankshafts exists, expressed as:

$$\nu = \frac{1}{2}\left(\frac{i}{2}-1\right)! \qquad (2.59)$$

and the bellow formula is valid for all crankshaft configuration:

$$\mu = 2^{\left(\frac{i}{2}-1\right)} \qquad (2.60)$$

For the engine mentioned in the second category, two stroke engines, the number of possibilities of achieving semi-symmetrical crankshafts is being given by the following formula:

$$N = \nu\mu \qquad (2.61)$$

for each configuration the combustion order is easily calculated.

One sort of this solution of crankshaft is being presented in the 2.9 figure, where it can be noticed that two cranks have been taken into account and they are equally distanced towards the symmetrical center plan having the *j* and *i-j+1*, while the distances facing their symmetrical plans to the C_0 point are:

$$a_j - a_{rez} = a_{rez} - a_{i-j+1} = \frac{i-2j+1}{2}a \quad (2.62)$$

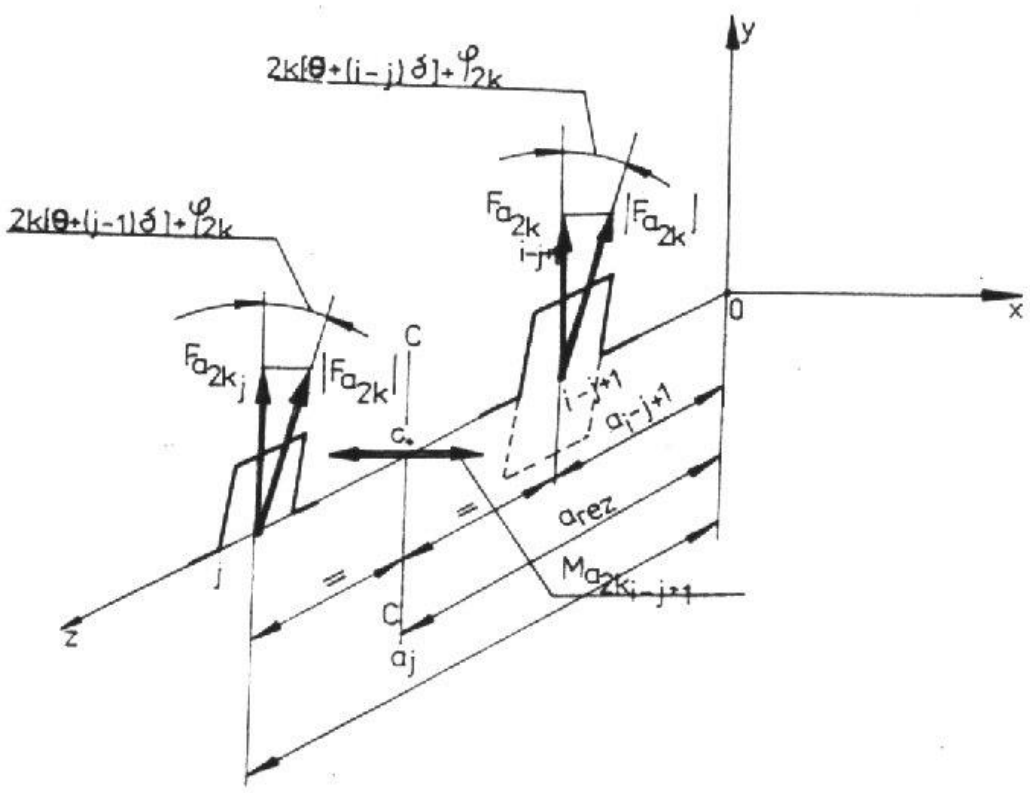

Figure 2.9: Calculus diagram for the gallop moment of inertia forces that have an alternative motion, for a crankshaft with a symmetrical central plan

Inertia moments for masses having an alternative motion associated to the cylinders symbolized by *j* and *i-j+1* towards the C_0 point are calculated with:

$$M_{a_{2k}} = \sum_{j=1}^{i/2}\left(M_{a_{2k_j}} - M_{a_{2k_{i-j+1}}} \right) = \sum_{j=1}^{i/2}\left[F_{a_{2k_j}} \left(a_j - a_{rez} \right) - F_{a_{2k_{i-j+1}}} \left(a_{rez} - a_{i-j+1} \right) \right] =$$

$$= \sum_{j=1}^{i/2} (i-j+1)\, a \left| F_{a_{2k}} \right| \sin\left\{ 2k\left[\theta + \frac{i-1}{2}\delta \right] + \varphi_{2k} \right\} \sin\left[k(i-2j+1)\delta \right] = 0 \quad (2.63)$$

because the angle between the two plans of the crankshafts elbows is:

$$(i-j+1)\delta = 0 - \textit{for a four stroke engine} \quad (2.64)$$

$$(i-j+1)\delta = \pi - \textit{for a four stroke engine}$$

Thus in the case of engines with a symmetrical center plan the gallop moments for the even order components will be equal to 0. Keeping in mind that the engine can have a normal axis only the harmonics of 1st order remain. These harmonics generate a null moment towards the central symmetrical plan in the case of four stroke engines because all the cranks are phased. On the other hand, in the case of two stroke engines 1st order harmonics generate a different moment towards the middle point fixed as a reference on the crankshaft of the marine main engine.

In order to balance the moment M_{ap} a device can be used, this being presented in the 2.10 figure in which p represents the harmonic order that generate a moment different of 0: the first order or the *2k* order occurs when the crankshaft doesn't have a central symmetrical plan, if the engine has an uneven number of cylinders. In this case the number of solutions for the dynamic crankshafts is calculated with:

$$N = \frac{1}{2}(i-1)! \quad (2.65)$$

The balancing condition is:

$$2m^*_{e_{a_{2k}}} \rho^*_{e_{a_{2k}}} (p\omega)^2 \cos\varphi_{a_p} l = M_{a_p} \quad (2.66)$$

in the above formula the overriding angle φ_{ap} and is the angle of all counterweights with a null usual value due to the persistence presented only by the components contributing to the gallop moments.

The analysis of certain types of engines with a certain number of cylinders have been studied in [1], [6], [11] and [17].

For marine diesel engines with a larger number of cylinders balancing solutions are being applied, such not respecting an equal distance between cylinders and the ignoring the set order of combustion [1], [14] and [17].

For practical and technical solutions needed to balance marine engines with inline displayed cylinders the solution proposed in the 3.5 paragraphed must be analyzed.

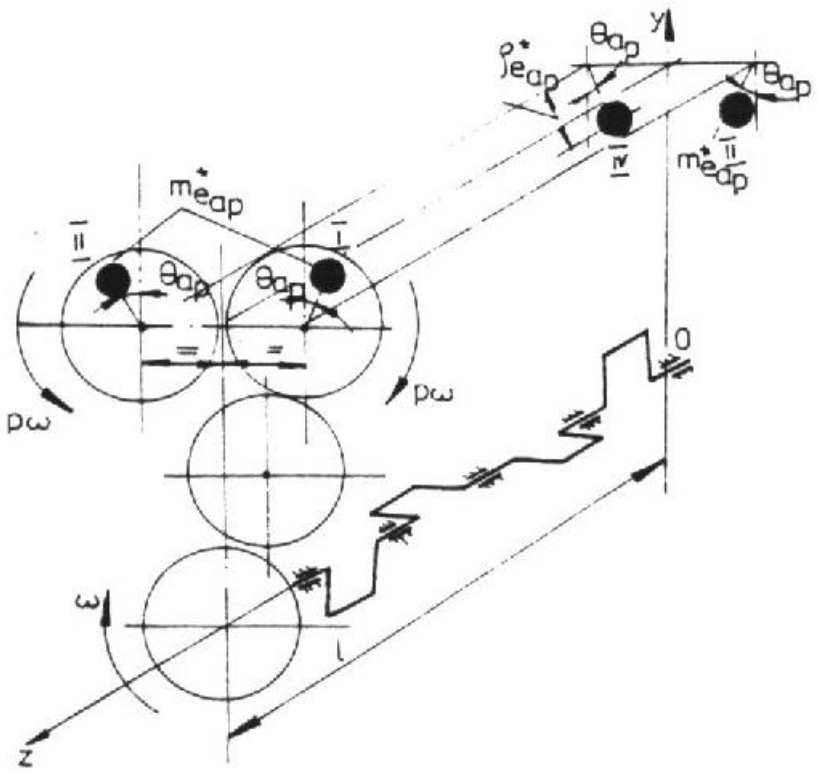

Figure 2.10: Balancing device diagram for the M_{ap} moment

2.4 Balancing a V displayed cylinders engine

As it has been shown in the 1.1.2 paragraph, the crankshaft of a V displayed cylinder engine, having an *i* number of cylinders, has the same configuration as an engine with cylinders displayed inline having an *i/2* number of cylinders and an even combustion. If the number of cylinders for a four stroke engine with cylinders displayed in a V shape is a multiple of four than it's crankshaft can be seen as a crankshaft of a four stroke engine with inline displayed cylinders engine or the one of a two stroke engine with inline displayed cylinders.

According to the 2.11 figure, for a V shape engine with a normal axis, having the construction of reciprocating rods as shown in the bellow figure, all reciprocating rods assembly placed on the same crankpin have the harmonic resultants having a *p* order (*p=1* or *2k* for the normal axis mechanism) from the left line, as well as the right ones are calculated by applying the following formula:

$$\begin{cases} F_{a_{Ps}} = \left|F_{a_p}\right| \cos p(\theta + \gamma/2) \\ F_{a_{Pds}} = \left|F_{a_p}\right| \sin p(\theta + \gamma/2) \end{cases} \quad (2.67)$$

with a given module expressed as:

$$\left|F_{a_p}\right| = m_a R(p\omega)^2 \left|a_p\right| \quad (2.68)$$

these two harmonic components generate the following projections on the system axis as presented in the 2.11 figure:

$$\begin{cases} F_{a_{Px}} = 2\left|F_{a_p}\right| \sin\frac{\gamma}{2} \sin\frac{p\gamma}{2} \sin p\theta = A_p \sin p\theta \\ F_{a_{Py}} = 2\left|F_{a_p}\right| \cos\frac{\gamma}{2} \cos\frac{p\gamma}{2} \cos p\theta = B_p \cos p\theta \end{cases} \quad (2.69)$$

from which:

$$\frac{F_{a_{p_x}}^2}{A_p^2} + \frac{F_{a_{p_y}}^2}{B_p^2} = 1 \qquad (2.70)$$

This allows us to analyze in a vectorial manner the harmonics with a *p* order: a spinning vector with a variable dimension, with an angular speed multiplied by *p*, thus *p* times higher than the speed of the crankshaft, which has an extremity described by an semi sphere with the A_p and B_p semi axis.

From these formulas, knowing the balancing conditions from [7], [11] and [14] we can conclude the following statements:

- If $A_p = B_p$ than the *V* shape configuration is defined by $\gamma = [(2m+1)/(p+1)]\pi$, $p \in N$. For the 1st order harmonic $\gamma = \pi/2$, thus the resulting vector describes a circle and can be balanced by using counterweights;

- If $A_p = B_p$ than the solution is $\gamma = \pi$ and $p = 2k$ and this means that for engines with opposite facing cylinders the inertia forces with an even order are null replacing the 1st order harmonic.

In a particular manner we can calculate the orders of harmonics that generate the null component having one of the axis as a reference.

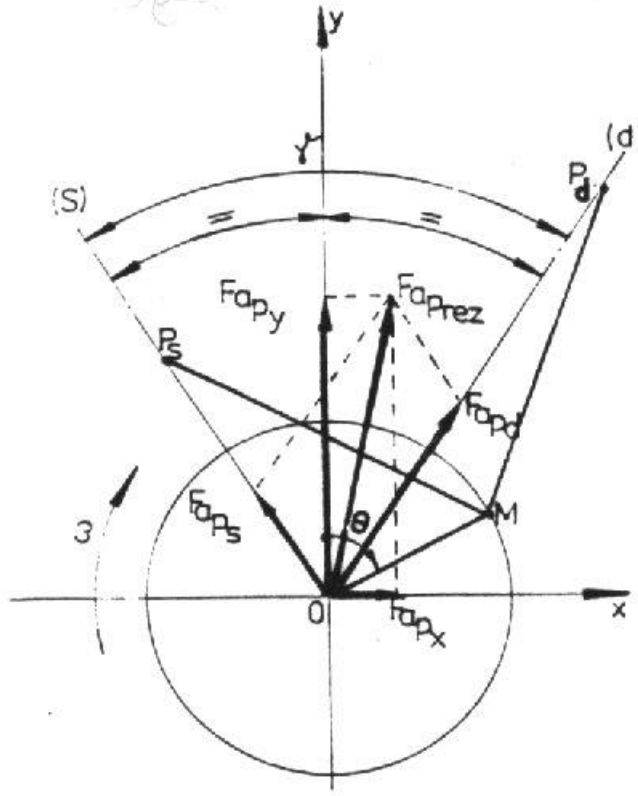

Figure 2.11: The diagram for calculating the harmonic resultant with an *p* order for a V cylinder displayed engine

2.5 Engine balancing with opposite displayed cylinders

In order to analyze this consideration we need to see the engine with opposite displayed cylinders as having two crankshafts, for which the kinetic phenomena has been analyzed in the 1.1.3 paragraph. The diagram used to calculate the unbalancing moments is being presented in the 2.12 figure.

If the two crankshafts would be fixed in the same phase al the harmonic components of the inertia moments would be balanced.

It has been presented that, in order to ensure the distribution forces, the misalignment between the two crankshafts has to be $\varphi = 5 - 7\ ^0RAC$, thus meaning that the vectors that describe the inertia forces don't have to be in fixed opposition and the value of the normal resultant will be insignificant.

Regarding the external moments with a p order, keeping in mind the formula $\theta_1 = \theta_2 + \varphi$ we will have the following formulas:

$$\begin{cases} M_{a_{p_{x_1}}} = \left|F_{a_p}\right|\sum_{j=1}^{i} a_j \cos\left(p\theta_{1_j} + \varphi_p\right) \\ M_{a_{p_{x_2}}} = \left|F_{a_p}\right|\sum_{j=1}^{i} a_j \cos\left[\pi - p\left(\theta_{1_j} - \varphi\right) - \varphi_p\right] \end{cases} \tag{2.71}$$

also:

$$\begin{cases} M_{a_{p_{y_1}}} = \left|F_{a_p}\right|\sum_{j=1}^{i} a_j \sin\left(p\theta_{1_j} + \varphi_p\right) \\ M_{a_{p_{y_2}}} = \left|F_{a_p}\right|\sum_{j=1}^{i} a_j \sin\left[\pi - p\left(\theta_{1_j} - \varphi\right) - \varphi_p\right] \end{cases} \tag{2.72}$$

The resultants on the two axis will then be:

$$\begin{cases} M_{a_{p_x}} = M_{a_{p_{x_1}}} + M_{a_{p_{x2}}} = -2\left|F_{a_p}\right|\sin\frac{p\varphi}{2}\sum_{j=1}^{i} a_j \cos\left(p\theta_{1_j} - \frac{p\varphi}{2} + \varphi_p\right) \\ M_{a_{p_y}} = M_{a_{p_{y_1}}} + M_{a_{p_{y2}}} = 2\left|F_{a_p}\right|\sin\frac{p\varphi}{2}\sum_{j=1}^{i} a_j \sin\left(p\theta_{1_j} - \frac{p\varphi}{2} + \varphi_p\right) \end{cases} \tag{2.73}$$

The mentioned values for the unbalancing momentum generates the fact that these values will be in the range of (0.1 – 0.2) through the factor $2\sin\frac{p\varphi}{2}$ from the value of the momentum generated on a single crankshaft. Generally this can't be applied for this kind of engine, special balancing solutions being needed.

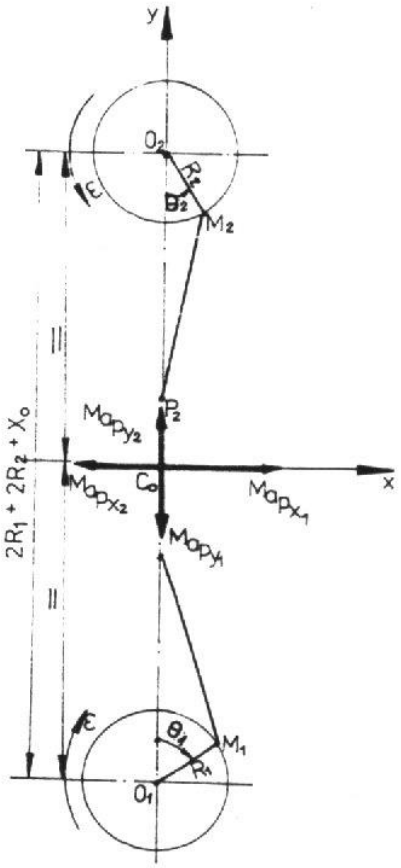

Figure 2.12: Calculus diagram for the unbalancing moments of the engine

References:

1. Bărănescu G.; *Teoria echilibrajului motoarelor cu ardere internă în linie*, Editura Academiei Române, București, 1975;

2. Băþaga, N., Burnete, N., Căzilă, A., Rus, I., Sopa, S., Teberean, I., *Motoare cu ardere internă*, Editura Didactică și Pedagogică, București, 1995;

3. Buzbuchi, N. *Dinamica sistemelor de propulsie navală*, Tipografia Institutului de Marină Civilă Constanța, 1998;

4. Buzbuchi, N., Dragalina, Al., Manea, L., Moroianu, C., Dinescu, C., *Motoare navale. Procese și caracteristici*, Editura Didactică și Pedagogică, București, 1997;

5. Buzbuchi, N., Taraza D., Lyridis, D., *Improvement of Marine Diesel Engine Dynamic Behaviour on Design and Operating Stage*, Institute of Marine Engineering Trans., London, 1995;

6. Buzbuchi, N., Dinescu, C., *Complemente de* d*inamica motoarelor navale*, Editura Alas, Călărași, 1995;

7. Buzbuchi, N., Pruiu, A., *Modificări constructive la arborii cotiþi ai motoarelor navale în doi timpi*, Volumul "Calculul și construcția motoarelor", a V-a Consfătuire națională: "Creativitate în construcþia, fabricarea și repararea automobilelor", Pitești, 1993;

8. Buzbuchi, N., Pruiu, A., Bratu, D., *Echilibrarea momentelor de ruliu ale motoarelor navale*, Volumul "Sesiunea de comunicări științifice", Universitatea "Ovidius", Constanța, 1991;

9. Buzbuchi, N., Pruiu, A., Hreniuc, V., *Metoda de tratare unitară a dezechilibrului motorului naval*, Volumul "Sesiunea de comunicări științifice ", Universitatea "Dunărea de Jos", Galați, 1991,

10. Gaiginschi, R., Zătreanu, Gh., *Motoare cu ardere internă*, vol. 1, Editura "Shakti", Iași, 1997;

11. Greenwald, B., *Teoria, calculul și construcția motoarelor pentru autovehicule rutiere*, Editura Didactică și Pedagogică, București, 1980;

12. Kovach, M., *Motor Vehicle Engines*, Editions Mir, Moscow, 1979;

13. MacCamhoil, M., *Static and Dynamic Balancing of Rigid Rotors*, Brüel & Kjaer, Naerum, Denmark, 1990;

14. Panã, C., Popa, M.G., Negurescu, N., *Motoare cu ardere internã,. Cinematicã, dinamicã, echilibraj*, Editura "Matrix", Bucureşti, 1997;

15. Rãdoi, M., Deciu, E.; *Mecanica*, Editura Didacticã şi Pedagogicã, 1981;

16. Ripianu, A., Crãciun, I. *Osii, arbori drepţi şi cotiţi"*, Editura Tehnicã, Bucureşti, 1977;

17. Ripianu, A., *Calculul cinematic şi dinamic al arborilor cotiţi"*, Editura "Dacia", Cluj, 1981,

18. Taraza, D., *Dinamica motoarelor cu ardere internã*, Editura Didacticã şi Pedagogicã, Bucureşti, 1985,

19. Taraza, D., *Estimation of the Mean Indicated Pressure from Measurement of the Crankshafts Angular Speed Variation*, International Off-Highway & Powerplant Congress & Exposition, Milwaukee, Wisconsin, 1993.

3. DYNAMIC PHENOMENA ONBOARD SHIPS

The present chapter represents a passing from the dynamic study of the marine engine seen as an technical entity to the connection between the propulsion engine-shaft line-hull, this being an dependency without which no study can be undertaken regarding the ships propulsion systems.

3.1 General view over the dynamic phenomena onboard ships

Increasing the dimension of commercial ships, as well as the overall power of propulsion systems in the last decades are features that challenge the engineers, designers and shipbuilders and one of the most important ones is defined by the increasing vibration level onboard ships. The vibration phenomena onboard ships are very important and need to be taken into account because they simultaneous influence:

- The endurance of several structural components in the hull;
- The technical statement of various machines and devices fitted onboard;
- The crew and passengers comfort level.

In order to set the origin of these vibrations we can easily notice that construction elements of ships have an elastic nature being exposed to excitations generated the following sources: main engines and auxiliary engines, propellers and the shear effect of the seas.

In order to achieve a precise study of vibrations onboard ships, as in any case involving vibrations, it is compulsory to keep in mind two complementary features of these phenomena, the excitation sources, as well as the reactions of propulsion installations and apparatus and the way naval structures react on these vibrations. Thus, in order to prevent the generation process of unneeded vibrations, being necessary to use a simultaneous approach from a static and dynamic point of view regarding the way the propulsion system and the hull react. The hydrodynamic functioning of the propeller in the aft region of the ship is, in fact, the origin of

another source of excitation and vibration. In the [7] reference the diagram of all sources of vibrations onboard ships have been presented, including all the coupling systems that can occur in case of several types of vibrations generated by the after mentioned excitations. This is why, reanalyzing the 3.1 diagram we can reestablish the excitation sources for vibrations generated onboard ships, but, more than this, the diagram highlights the main methods applied to limit the effects of these excitation sources that can be generated by the propeller, the engine and the sea induced effects, this being correlated with the above mentioned classification.

3.2 The vibrations generated by the marine main engine

According to the facts previously stated, the main vibrations generated onboard ships is being represented by the main engine included in the overall propulsion system. This is why in the next paragraphs a short presentation of the main types of vibrations generated by the main engine will be studied categorized as: the vibrations of shaft lines and the vibrations of the building blocks of these ones.

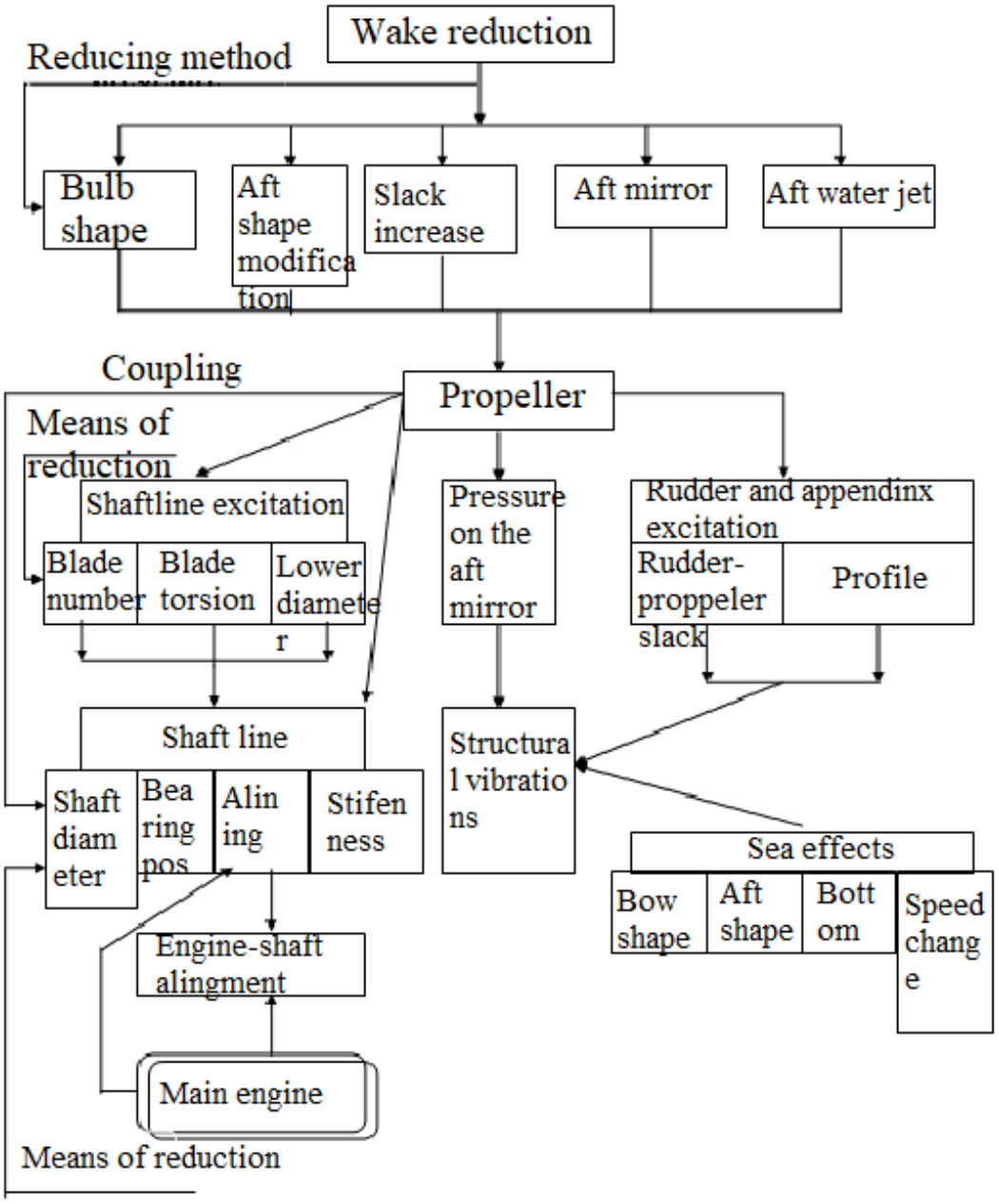

Figure 3.1: Excitation source diagram of vibrations generated onboard ships and main means of preventing and reducing them

3.2.1 Shaft line vibrations generated by marine engines

The propulsion systems fitted with diesel engines are being directly coupled with the main propeller and this represent the two main sources of vibrations generated on the shaft lines, the main sources being the engine itself and the propeller.

The excitation forces of the shaft lines in the case of a slow turning marine engine are being presented in the 3.2 figure, in which F is a total axial force and it being calculated by adding up the gas pressure force, F_p, which, in its own turn can be divided in a normal component, N that acts on the cross-head system and a B component acting along the reciprocating rod. The las component, B, at its own turn can be divided into a tangential force, T and a radial one, Z, both of them acting on the crank nut, as it was mentioned in the 1.2.1 paragraph.

The vibrations acting on the shaft line of a marine engine of this type are being analyzed in this chapter, but a dynamic quasi-stationary behavior is being considered, this meaning, in fact, that the engine is functioning in a stabilized manner (constant values for effective power and rotation speed, as it has been shown in [5], 8th chapter). The changes in balance of the presented system represented by such an engine are low in amplitude and have a periodical occurrence.

The mathematical models for the different vibration shapes lead to differential equation systems. The parameters of these equations can have a constant value, such as the values for masses and stiffness coefficients, or variable, such as rotation speed, power, excitation frequency and duration.

For an example the linear differential equation for forced vibrations for the elastic system that shapes the propulsion marine engine shaft line has the following shape, based on a matrix notation:

$$[M]\{x\} + [D]\{x\} + [R]\{x\} = \{F(t)\}, \qquad (3.1)$$

In the above differential equation the following notations have been used:

- ***[M]*** – mass matrix (or moments with inertia mass);
- ***[D]*** – amortization coefficients matrix;
- ***[R]*** – stiffness matrix;

- ***{F(τ)}*** – column vector for all moments and excitation forces;
- ***{x}*** – column vector for angular and linear elongations;
- ***τ*** – duration (time).

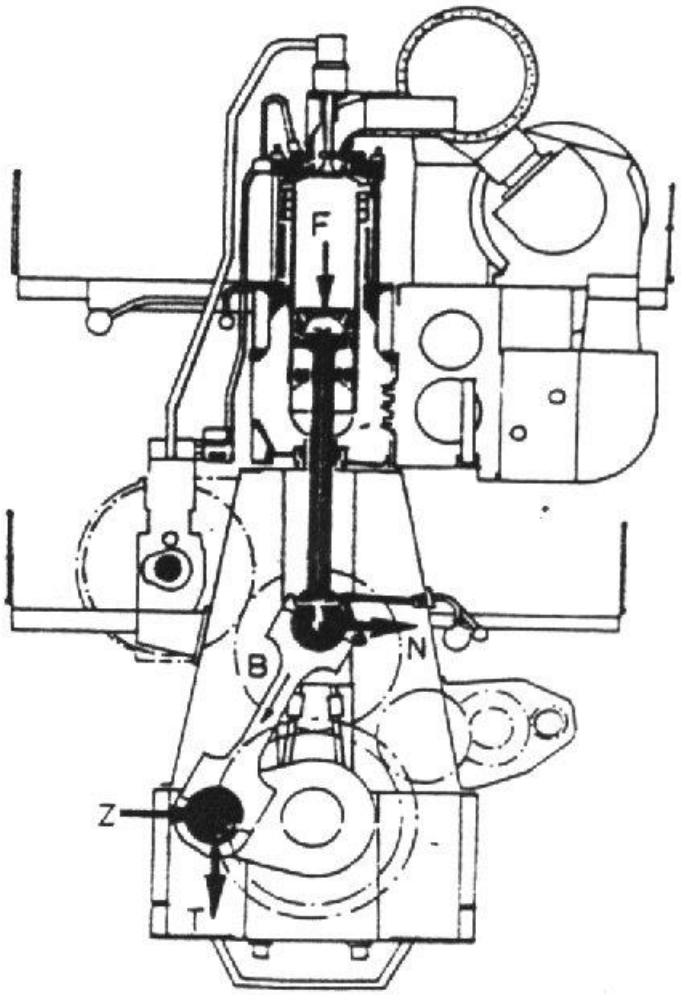

Figure 3.2: Excitation forces on the shaft line for a marine slow engine diagram

In order to find a solution for the issue of *free vibrations* generated on the shaft line the *{F(τ)} = 0*, equation 3.1 has to have a homogeneous characteristic. This equation will allow us to calculate the values for self pulsations depending on the values of *[M]*, *[D]* and *[R]* matrix, in other words the geometry of the equivalent

oscillatory system. Its own pulsation characteristics allow the calculus for the critical rotation speed for the reference engine, this meaning that the rotations for which the resonance phenomena occurs with all the excitations harmonics components. Usually the self pulsations are being calculated without taking into consideration the attenuation from the entire system. Experience has shown that the influence of attenuations are not substantial important the values for its own pulsations, even if in [10] and [11] the torsional attenuations can have a certain influence, especially when these ones are being considered as variable on harmonic orders. Further on they will be taken into account in this manner.

The oscillatory system generates a response equivalent for the shaft line of the marine main engine and during periods when excitations occurs its *forced vibrations* and this means, mathematical speaking, that this is the optimal solution for the homogenous equation. In stationary conditions the excitation is, in fact, a periodical function and can be represented as a Fourier series development. A particular solution can be calculated for each harmonic order.

The resonance occurs when the pulsation excitation has a certain harmonic order which is the same with its own pulsation for the entire system. In the area of this pulsation the dynamic multiplier [2] can lead to the increase of the vibration amplitude, all these being leveled only by the attenuation degree of the entire system. Afterwards it is obvious that this kind of situation must be avoided, being by far to dangerous and for this situation there are two possible solutions:

- the action in an opposite phase having a resonance frequency at the excitation point; this being in fact the active compensation process and this implies that a complex technical solution must be used, such as digital control systems or other advance computers;
- the modifying process for the dynamic behavior of the entire system in such a manner that peak amplitudes are not overriding acceptable values that are compulsory and imposed by the naval classification societies. It’s the same thing as the condition that resonance does not occurs in the area described by the normal engine cycle. This is the most chosen solution and

can be obtain by modifying the geometry of the entire system (as it will be shown in the 6th chapter).

In the process of solving the issues of vibrations acting on the shaft lines in the case of a naval engine the calculus of autopulsation depends essentially on its geometry, as it has been shown. Even if the inertia moments and masses of the entire system can be deducted with a low level of difficulty, in order to obtain the values of the stiffness coefficients is much more difficult. In order to achieve this two reliable methods have been developed:

- the torsional stiffness coefficients for the crankshaft can be calculated by using empirical formulas as mentioned in [13], [14] references. In order to test the exactness of this method experimental validation has to be applied [14];
- the torsional stiffness and the ones generated by different vibrations types can be established by applying a tridimensional model with *finite elements*, as shown in the 3.3 figure.

If the structural elements and the boundary conditions are well chosen, then the values of stiffness coefficients calculated can approach in a very fine manner with the values in recorder in real situations this analysis being applied more often lately since the early stage of engine design. This method allows designers to extract an important amount of precise information in a more rapid manner, thus the results will eventually have to be confirmed by practical measurements methods.

The shaft lines that are driven in a direct way by the propulsion main engines have three specific main types of vibration types:

- shaft line torsional vibrations;
- shaft line bending vibrations;
- shaft line axial vibrations.

It also has to be specified that the propeller gyroscopic effect (also called whirling) specified in [10], [11] hasn’t been taken into consideration in the analysis made in this chapter.

Recent research specified in references [7], [10], [11], [94], [95], [98] and [99] suggests the fact that coupling phenomena between different types of vibrations have to be considered in order to achieve a precise analysis of the shaft line vibrations, which will be detailed in the 4.4 subchapter.

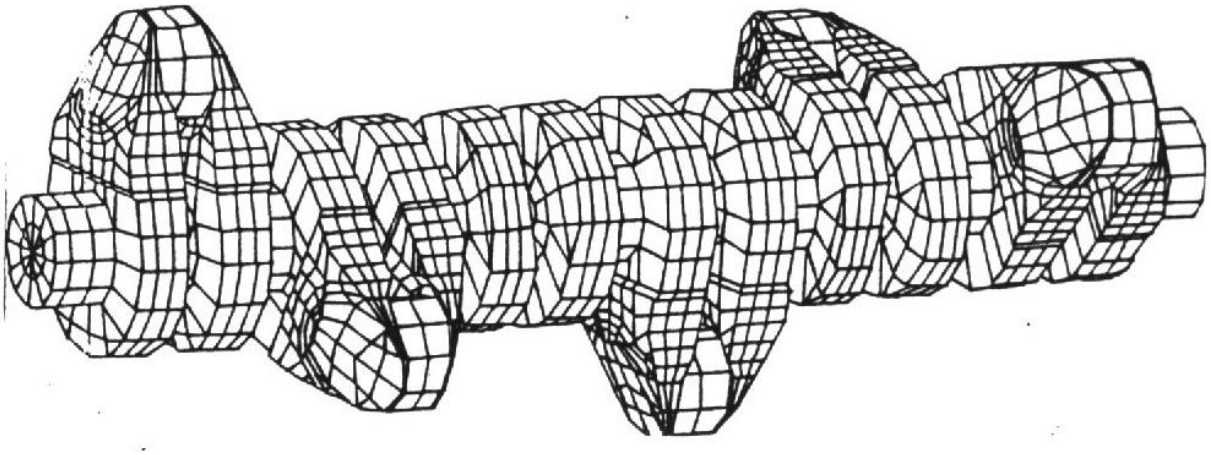

Figure 3.3: Crankshaft meshing for a Sulzer RTA type of marine main engine

3.2.2 Maine engine structural resistance vibrations

The normal force acting in the crosshead system of a slow engine (as presented in the 3.2 figure) generates a rolling moment through its components resulting from the forces generated by gas pressure and also from the inertia forces of alternative motion masses developed in an individual manner in each cylinder and this moment varies depending on the value of the rotation angle of the crankshaft. According to reference [6] and [14] this type of forces are called *lateral forces and moments*, these being developed in Fourier series, as it has been shown in 2.2.3 and 2.3.1 paragraphs. These moments and forces act as excitatory forces on the structural vibrations of main engines components and these vibrations have a very complex feature. This feature depends on the complicated construction of these structures, as well as on the complex characteristic of the load applied on the engine. The excitation degree, as a vectorial sum for the entire engine [13], for a given harmonic order depends on the combustion order, this being valid for the characteristic configurations of the vibration modes for

all structural resistance for a slow marine engine with six cylinders displayed in a line configuration, as presented in the 3.4 figure.

Depending on the number of cylinders and the harmonic order the lateral excitations can generate other structural vibrations that depend the on the resistance of the engine itself, in the so called H and X modes. The major harmonic orders will stimulate, for an example, the engine vibration in a H mode, also known as the rolling force of the engine.

These vibrations can influence the additional systems fitted on the main engine, such as overcharging blowers, auxiliary blowers, etc., being able to generate local vibrations in the engine compartment and the structural elements of the double bottom deck, but most of all, these phenomena have to be dealt with and reduces. The usually remedy for the structural vibrations of the main engine construction elements is represented by the process of fitting traverse stiffeners in the upper part of the main engine.

This requirement is being applied in the case of 4, 8 and 12 cylinder configuration engines. In the case of marine engines with 5 or 6 cylinders this solution has to be applied only when the sea trials confirms their necessity.

The mentioned type of stiffeners acts on the structural stiffness of the entire engine leading to a higher level of system pulsation vibrations. Usually hydraulic traverse stiffeners are preferred because these have a better behavior when small changes occur in the structural configuration slight changes, especially during the loading-unloading operations, as well as in the case when deformations occur during normal ship operation (as shown in the 3.5 figure).

Specified vibration influence that act on the engine can be studied by generating a tridimensional substructure of the entire engine. These can be treated by using the *finite element method* [10], as well as the *modal analysis method*. An assembly like that which combines three main substructures, corresponding, in fact to a single cylinder structure, is being shown in the 3.6 figure. This example is being extracted from the simulations made on a slow marine engine Sulzer RTA type.

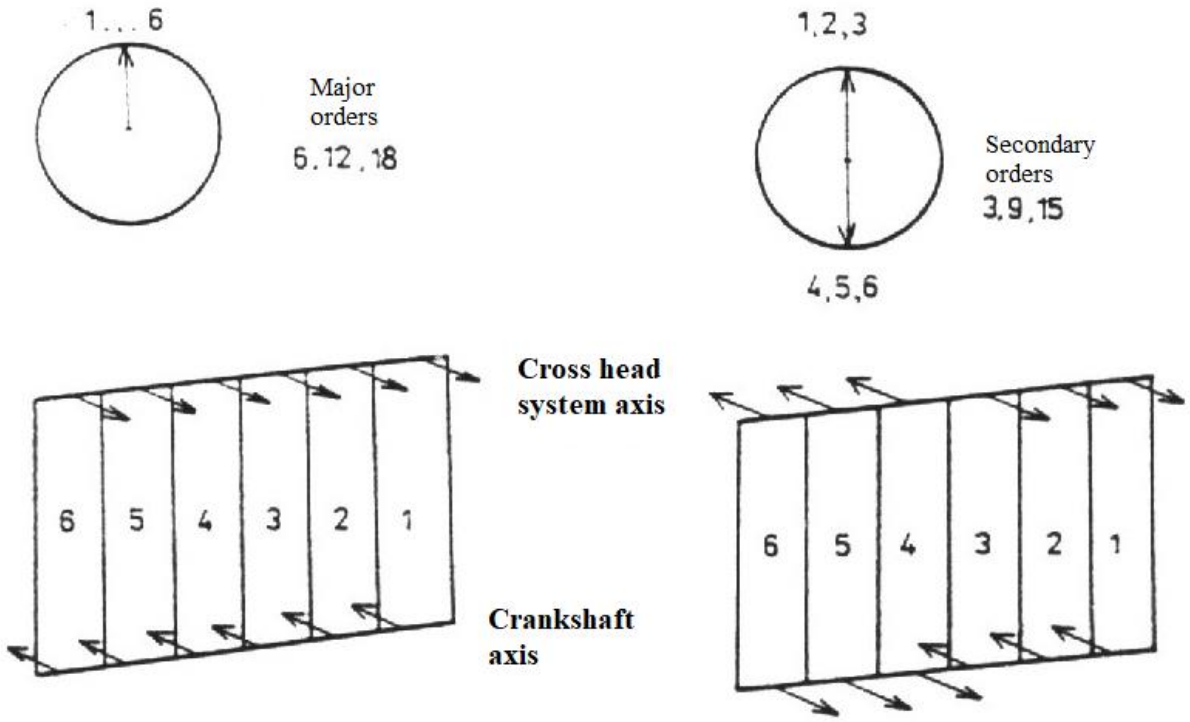

Figure 3.4: H and X vibration modes for the structural resistance for a marine main engine

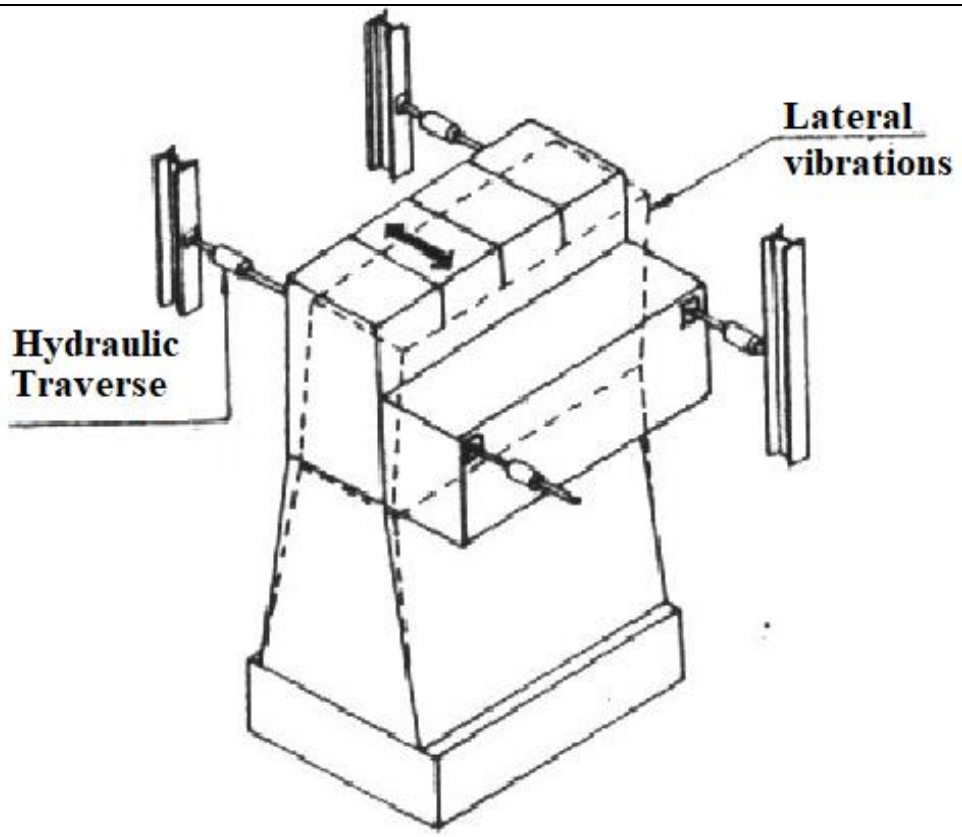

Figure 3.5: Stiffening diagram for the structural resistance of a marine main engine

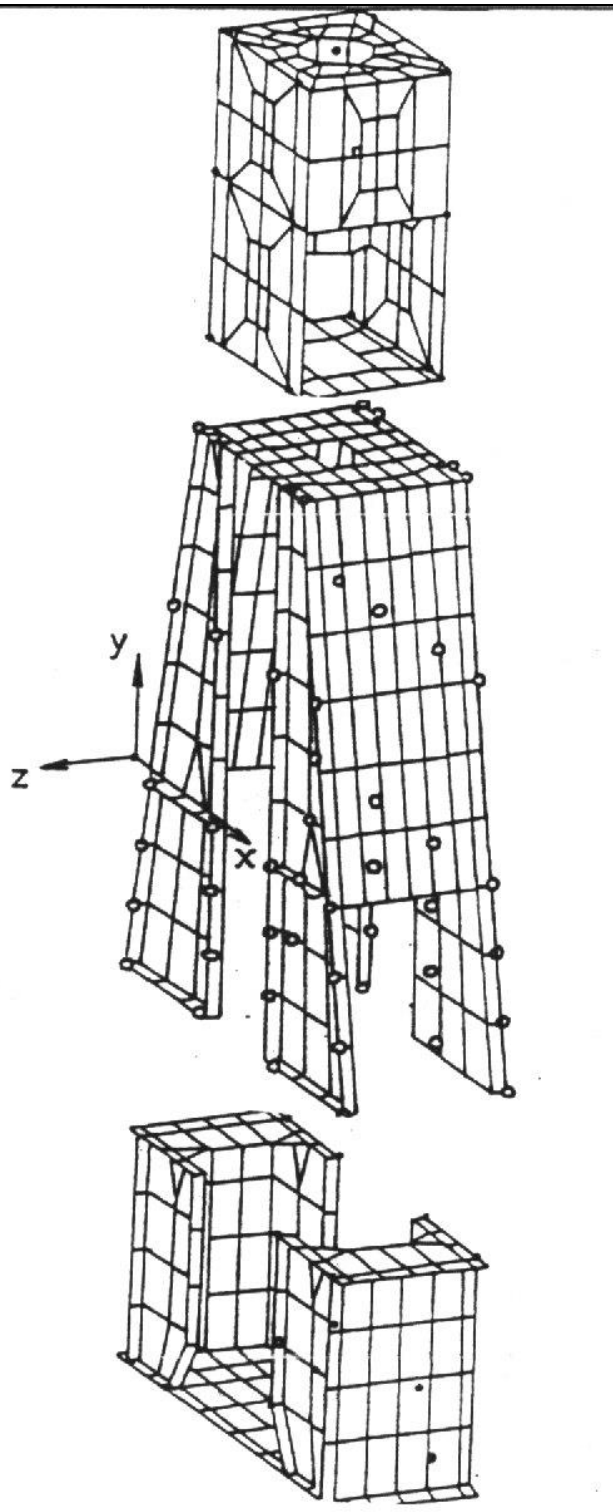

Figure 3.6: Structural messing for the marine main engine Sulzer RTA type

3.3 Propeller induced vibrations

In the previous paragraph the mechanical generated excitations have been presented (generated by the engine itself), further on the hydrodynamic generated excitations will be presented (the ones generated by the propeller).

The propeller can generate excitation vibrations to the ship's hull through:

- momentum and forces transferred to the ship body through the shaft line;
- pressure variations sent through the aft mirror while it's submerged;
- forces and momentum acting on the rudder and bearings of the shaft line.

The most important ones are, for the present study, are the excitations sent to the shaft line. At the base of force variations and transferred momentum by the propeller to the shaft line the *wake* can be considered, this being the environment specific to the propeller. This phenomenon, as the cavitation one, leads to increased variations in pressure amplitude on the aft mirror of the ship hull.

The propeller sends variations of these three forces to the shaft line, as well momentum along it, around the axis system presented in the 3.7 figure. From all of these, according to the type of vibrations specific considered shaft lines in the 3.2.1 paragraph, only the thrust force variations and for the torsion momentum will be taken into account for this study, thus, only the forces along the Oz axis. The calculus methodology of these forces will be presented in a detailed manner in the 4.3.3 chapter. That is why certain considerations on the main parameters that have an influence on the level of vibrations induced by the propeller to the shaft line of the main propulsion engine:

- *disc ratio* – this influence depends on the propeller blade number; the chosen number of blades will be done upon an wake analysis and an analysis of the level of risk regarding the occurrence of several types of vibrations of the shaft line;
- *propeller blade torsion* – a very efficient method used to reduce the level of excitation sent to the shaft line;

- *propeller blade number* – this has to be done depending on the main engine number of cylinders and in order to prevent the resonance effect the blade number will not be a divisor of the number of cylinders;
- *the wake* – the total number of shapes on the water surface from the aft area, in this manner the multiple harmonics of the wake phenomena depends on the shapes of the aft region, more aviated forms leading to a reduced level in unevenness of the wake generate by the ship;
- *cavitation* – as long as this phenomena does not reach a forbidden level that can lead to propulsive efficiency decrease it can be affirmed that it has a low influence on the excitations sent by the propeller to the shaft line.

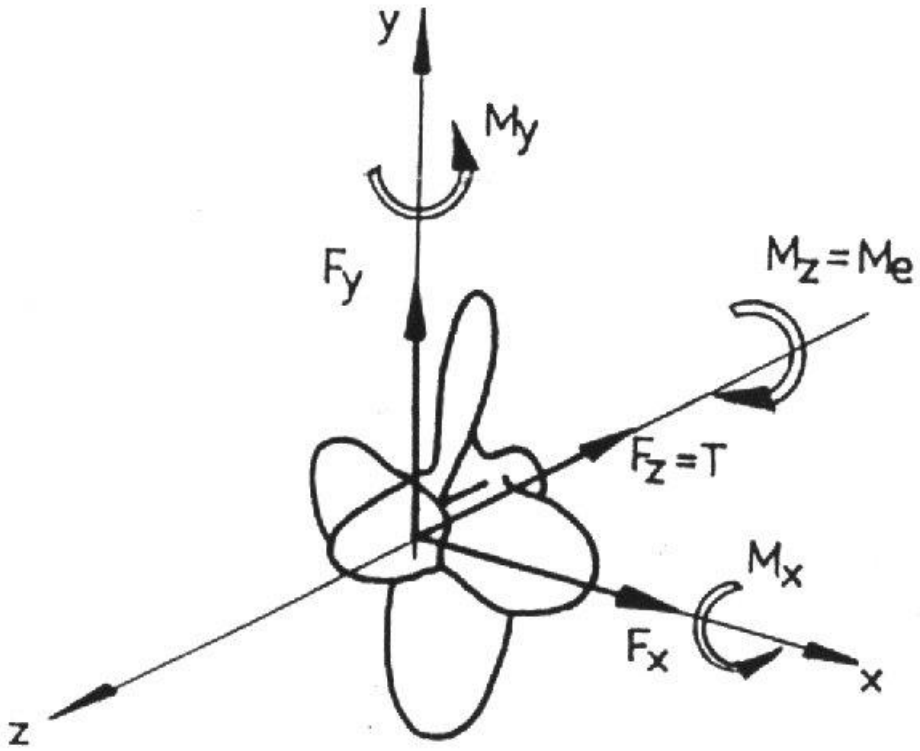

Figure 3.7: Forces and momentum diagram generated by the propeller on the shaft line

3.4 Sea effects induced vibrations

If we consider the action of the hull on the body (hull) of the ship as a source of continuous excitation that can generate vibration phenomena of its structure, it can be stated that the main focus might be set on background vertical vibrations of the ship.

According to the actual orientation in ship design two types of this kind of excitations can be defined: the *whipping excitations* and the *springing excitation*.

The whipping phenomenon, which is the most studied one, is the result of the impact generated by the hydrodynamic shocks applied on the bottom of the ship in the bow area. The occurrence of this phenomena is owed to the navigation process in hydro-meteorological conditions which allow the relative motion of the bow being sufficient in size to generate the mentioned impacts. Out of them the most important ones will be defined as above:

- *slamming* – when the shock is occurs in the plan area of the bottom of the ship, especially when the bow of the ship emerges and submerges (as shown in the 3.8a figure);
- *slapping* – when the shock is generated above the bow area, without submerging back in the water.

Approximating the effects of *slamming and slapping* can be done in an analytical manner or by using measurements in the test basin, but both the methods have a certain amount of doubt. That is why it is impossible to consider the influence of these forces in the design stage.

The springing is the second main type of excitation mentioned and it is generated by the hydrodynamic forces generated by the hull and corresponds with a phenomenon that assemblies the vibrating stage of any ship (as shown in the 3.8b figure). This is generated when its own hull frequency, vibrating according with the first method of vibration (out of the two existing ones), is being placed in the frequency range occurring at the junction between hull/ship ratio if the energy spectral density for the hull is high enough.

Dimensional approximation for the developed mechanical loads can be done in an analytical manner. In this way the spectral method of linearizing equations must be remembered because this shapes the phenomenon, allowing the usage of transfer functions, as well as realizing the spectral calculus with the same reserves regarding their own excitations, also mentioned in the case of the *whipping* phenomenon.

The lowered rate of the preciseness in the case of approximation methods of excitation forces along with the lower level of information regarding the hull shape influence on the level of these excitations don not allow a precise formulation of some sort of recommendations on means of preventing *whipping* and *springing* effects.

Even if the influence of sailing conditions on the whipping effect is very important, a way to prevent it in the design process can be made in an approximation manner based on the following considerations:

- generating *slamming* or slapping through the over-dimensioned plate or "U" shape from the projection stage for the bottom shape of the shape and over-dimensioned steeps for the hull;

- keeping a constant value for the draft in any sailing conditions at a recommended level;

- as much as possible the avoidance of using a bulbous bows.

The phenomenon depends as well on ships length and, in some particular cases, on the ships speed.

Regarding the springing effect there is no possibility of reducing its effects because this phenomenon depends on the length of the ship as well as cargo distribution onboard and the amount of the ballast used.

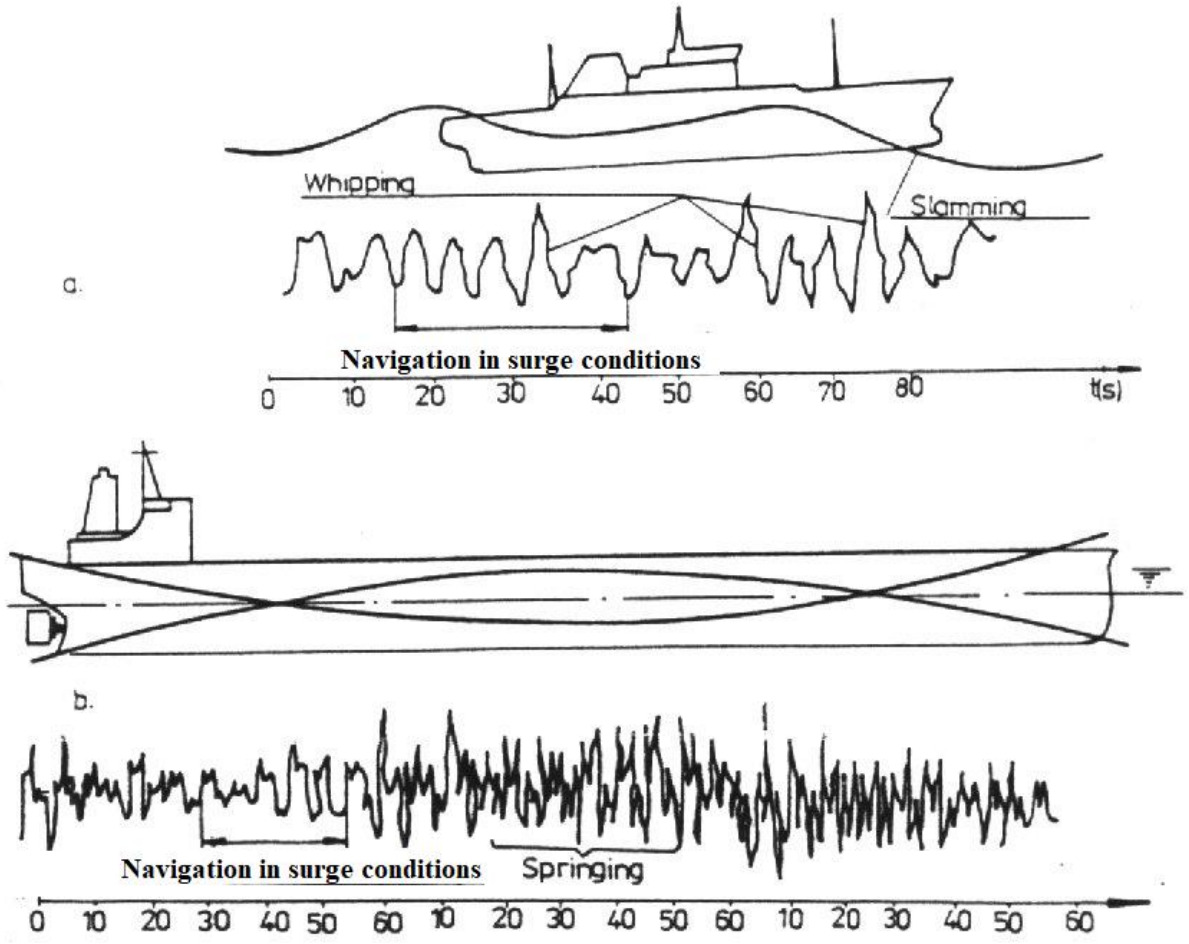

Figure 3.8: Highlighting the vibrations excitations induced in the ship's hull

Generally these phenomena are correlated with the relation between value level of the first frequency of vertical variations and one of the major components from the hull spectral range. Thus it is obvious in the 3.9 figure and on its basis the highlights the influence of the ship's length between perpendiculars, *Lpp*, on the *whipping* or *springing* occurrence. It can be noticed that for ships with a lower overall level in comparison with the hull length the submerge risks are much higher, that is why the importance of the bow's shape influences the occurrence pf the whipping phenomenon. The springing phenomenon exists at any level but is more obvious when its own first frequency is much similar with the major component of the hull's spectral values.

By reducing the value of speed these effects can have a lower occurrence chance and by modifying the course of the ship has the same effect on these phenomena.

For whipping, by using the appropriate quantity of ballast water the draft in the bow part increases and the risk of whipping reduces. For springing, by modifying the cargo distribution onboard the occurrence chances can be dramatically reduced. A vibration analysis on the generated bodies by the excitation sources previously mentioned leads to the categorizing the vibrations as it follows:

- local vibrations;
- assembly vibrations;
- hull vibrations.

In the first category vibrations exciting a structural element (such as frames, panels, plates, transverses, bulkheads) are included having a dynamic behavior with a reduced influence on the additional elements.

The second category includes vibrations with an important effect on main parts of ships structure such as: deck structures, aft part, the hull itself etc. All these structural elements form an assembly. In the 3.10 figure vertical and longitudinal vibrations are being presented for deck structures.

The last category includes a series of vibrations acting on the hull itself, this being the most important category:

- vertical bending vibrations;
- transverse bending vibrations;
- torsional vibrations coupled with bending vibrations;
- longitudinal vibrations.

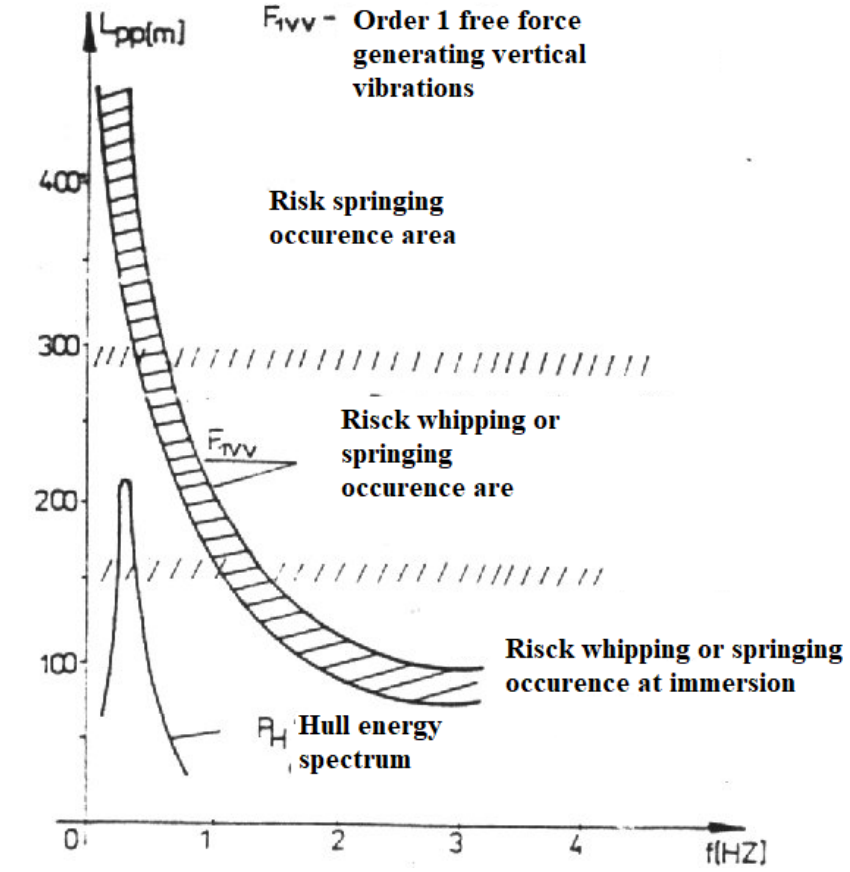

Figure 3.9: Ship length influence on the whipping and springing occurrence

Generally the hull's vibrations are increasing in the moment it is obvious that the resonance between the frequency of the hull and the frequency of the excitation really exists.

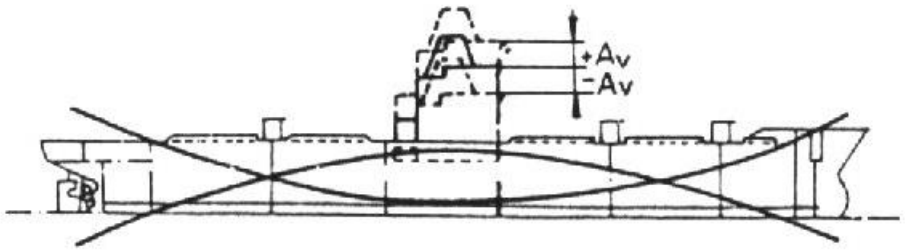

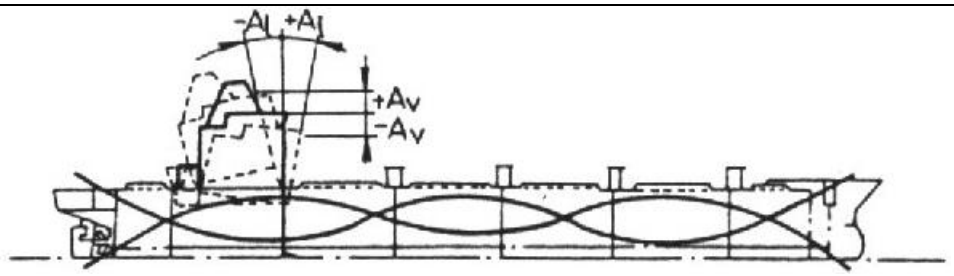

Figure 3.10: Vertical and perpendicular vibration occurrence diagram on deck structures

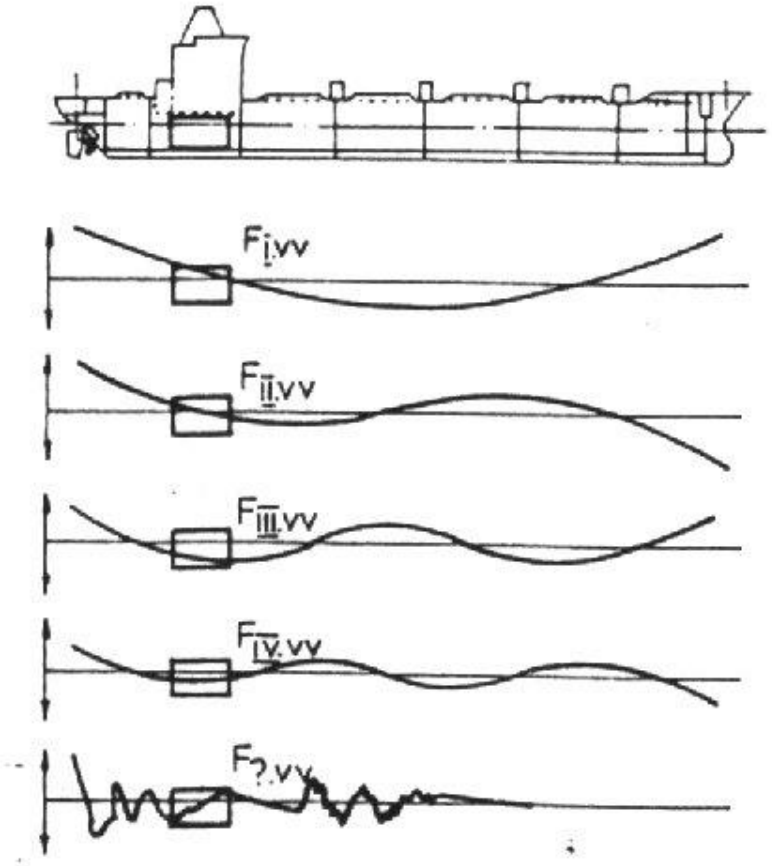

Figure 3.11: Vibration modes in the case of the ship's hull

In the above figure, 3.11, five ways of generating vibrations on the ship's hull are being described, the last mode being influenced by the vibration modes for all over

deck structures, on decks, on the double bottom deck, on the propulsion system and on the cargo.

3.5 Hull-main engine dynamic interaction

Alternative and rotation motion masses for each engine mechanism generate periodical forces with 1st and 2nd order in each individual cylinder. For all engines with an usual number of cylinders the vectorial resultant of these forces is zero (as presented in the 2.3.1 paragraph).

These forces are called free forces even if they have a zero resultant value and they generate some unbalancing moments called free moments. Mainly, for a marine engine only 1st order and horizontal moments are taken into consideration, M_w and M_{1H}, as well as 2nd order moments M_{2V} (as presented in the bellow figure).

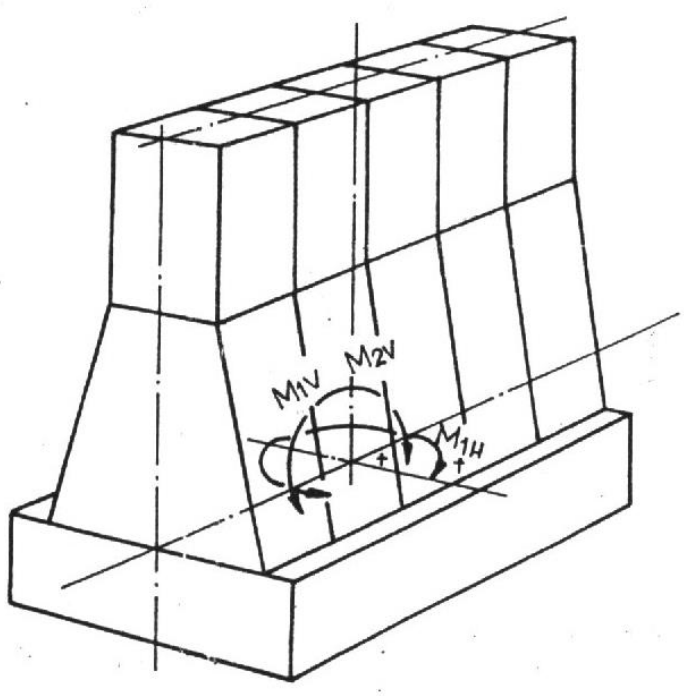

Figure 3.12: Free moments diagram acting on the marine engine

Free moments can be reduced by selecting an optimal combustion order, but even this is achieved, these free moments will still have an influence on the torsional and axial vibrations, in the same manner as the internal an lateral moments. For all

engines with a large number of cylinders only the free vertical momentum is taken into account, while for propulsion system with only four cylinders the 1st order free moment will also be taken into consideration in an additional manner.

These free moments can generate vibrations on the hull when one or more from the following conditions are reached:

- excitatory harmonic frequency is close in value with the one of the ship (resonance). This condition depends on the structural feature of the hull and the way the cargo is being distributed onboard;

- free momentum act near a cluster of the own hull vibration (as seen in the 3.14 figure). This condition depends on the position where the main engine has been installed onboard;

- the amplitude of free unbalancing momentum overrides the influence of the hull's structural amortization and this amplitude depends on the bore size and the combustion order;

In case of engines with a short shaft line and with a small number of cylinders the engine has to be placed near the first aft cluster of its own vibration mode generated towards the hull. If the excitation frequency and the hull self-excitation frequency are close in value balancing measures have to be taken. The solution can be the generation of an additional free moment in every mentioned case, but this moment has to be the same in frequency as the engine's free moment, but with a different phase.

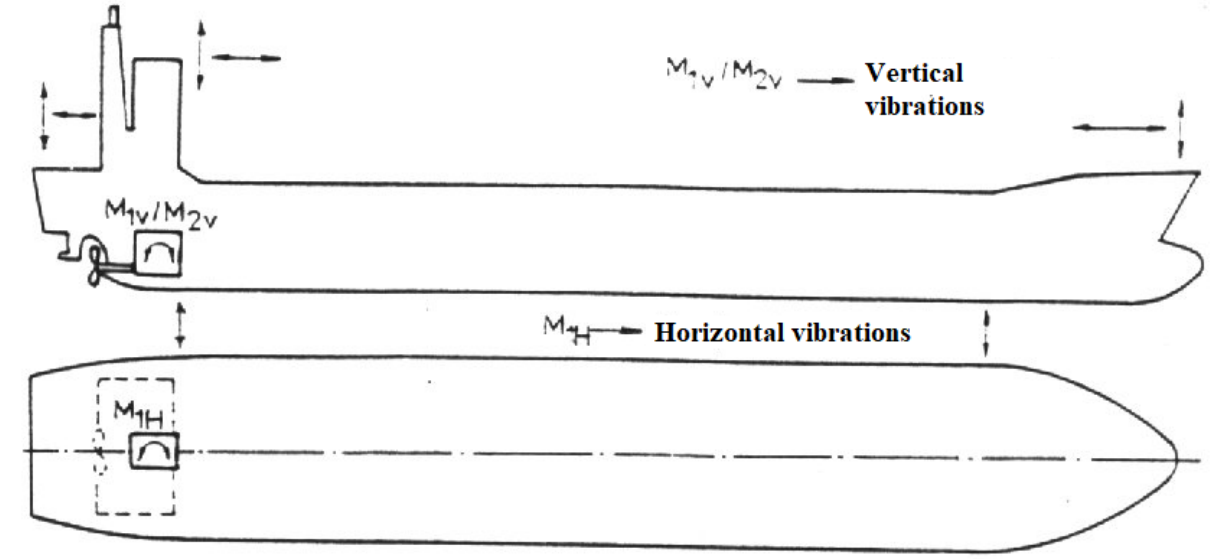

Figure 3.13: Vertical and horizontal unbalancing moments diagram for a marine engine fitted onboard a ship, moments generating vibrations related to the hull

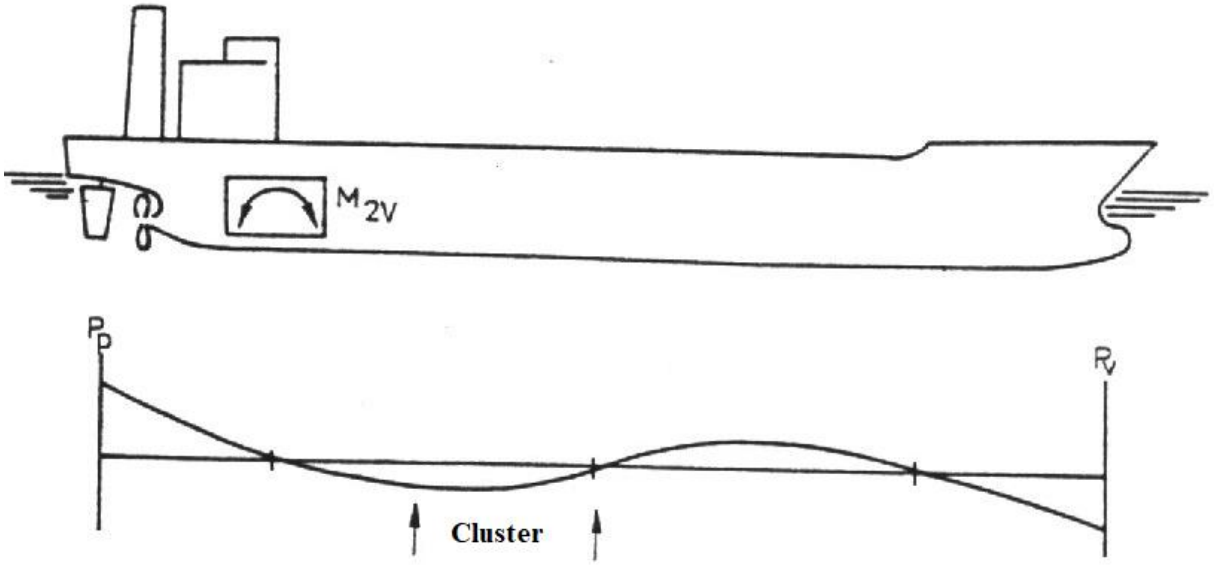

Figure 3.14: Unbalancing moment acting diagram, vertical and with a 2nd order towards the hull vibration behavior

Free moment with a 2nd order is being lowered in an usual manner for all modern main engines and this is being achieved by fitting equalizers with balancing masses (or counterweights) and the most common type is the *Lanchester* type, at each end of the engine. This counterweights actually spin at a double speed of the crankshaft. If the cluster of the own vibration mode is the same with the one of a counterweight then it is enough and safe to use one single counterweight (as shown in the 3.15 and 3.16 figures). The devices have certain advantages and the main one is the fact that the excitatory unbalancing is being dealt with straight at its source.

The generating solution of an equal moment, but with an opposite phase can be realized by using an electrical driven 2nd order equalizer which can be fitted in the rudder control room (as it can be seen in the 3.17 figure). The electrical engine rotational speed an phasing the compensatory moment have to be set on direct correspondence with the rotational speed of the main engine and have to be control with their evolution. The advantage of this sort of electrical equalizer is that it is always available for controlling and setting, but the main advantage is represented by the high price. It can't be used to compensate free moments, a specific feature for marine slow turning engines.

1st order free moments, M_{1H} and M_{1V} are generated by the same vectorial sum of free forces of masses having a rotation motion and of those with an alternative motion. These moments and forces act having an equal frequency with the one of the crankshaft. The highest values is being recorded in the case of four cylinder engines, in comparison with the engine with a higher number of cylinders.

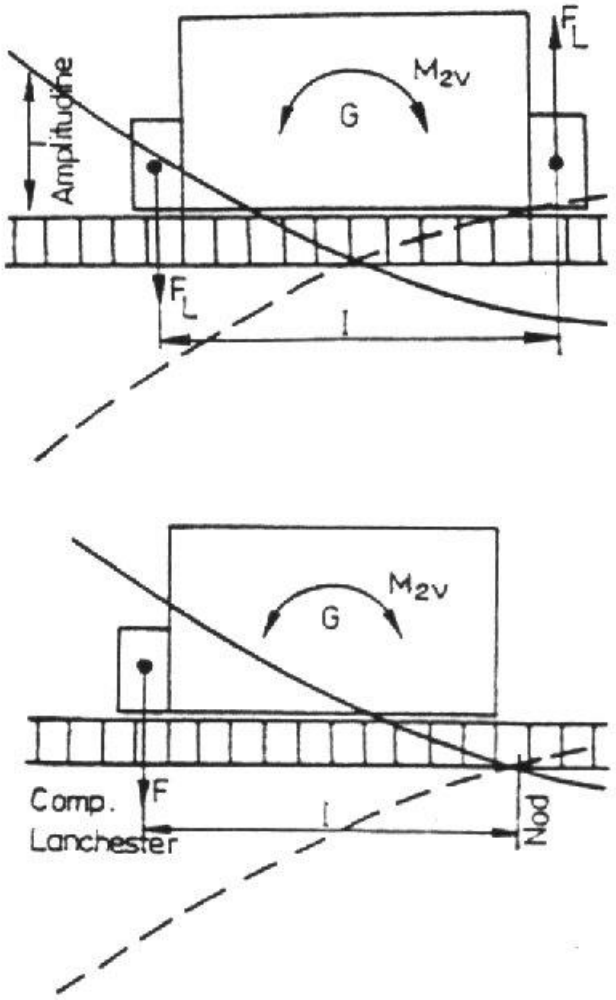

Figure 3.16: 2nd order vertical moment balancing through a compensatory device

For most ships the frequency of the own horizontal vibrations is higher than the one of vertical vibrations.

That's why the situation of hull simultaneous resonating vibrations generated by M_{1H} and M_{1W} momentum is extremely rare. If this situation, in fact, occurs the specific component of the 1st order free moment can be totally compensated in the plan it acts and this can be done by fitting some counterweights with the purpose of not totally reducing the effective amplitude of this free moment, but it modifies its phase, thus the unbalance in the other plan can be reduced and this technical feature

can be accepted if the unbalance stage is not critical. In these rare cases in which the resonance is generated in both components of the free moment with an 1st order the unique mass using balancing solution is not suitable.

On the other hand effective counterweights are being combined with other counterweights that have an opposite rotation direction, at the same rotational speed, the 1st order unbalancing compensation will be cumulated.

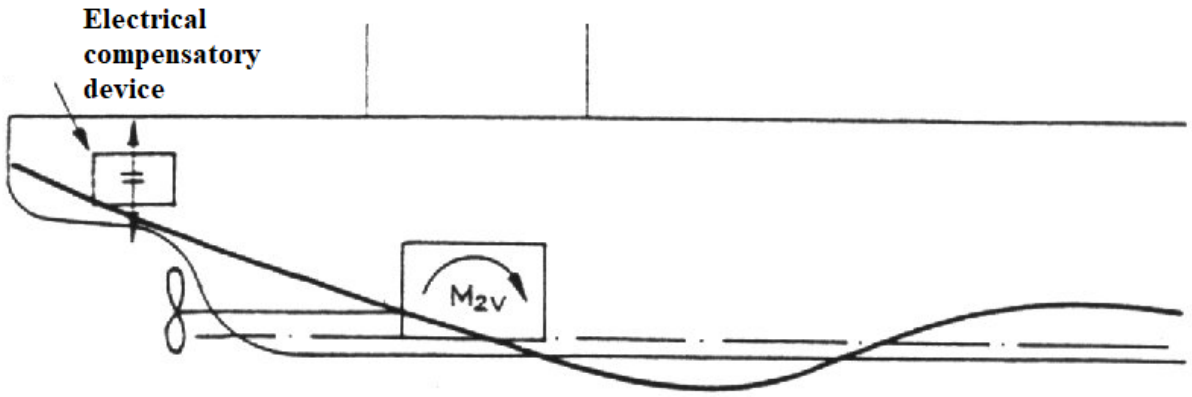

Figure 3.17: Electrical compensatory device operation

In the figure 3.18 the balancing solution is being presented for all free moments with 1st and 2nd order obtained by including additional *Lanchester* counterweights at a compensatory device. In this manner even marine engines with major disadvantages, mainly the ones with four cylinders, can be perfectly balanced, thus the risk of exciting vibrations on the ship's hull by free moments can completely avoided.

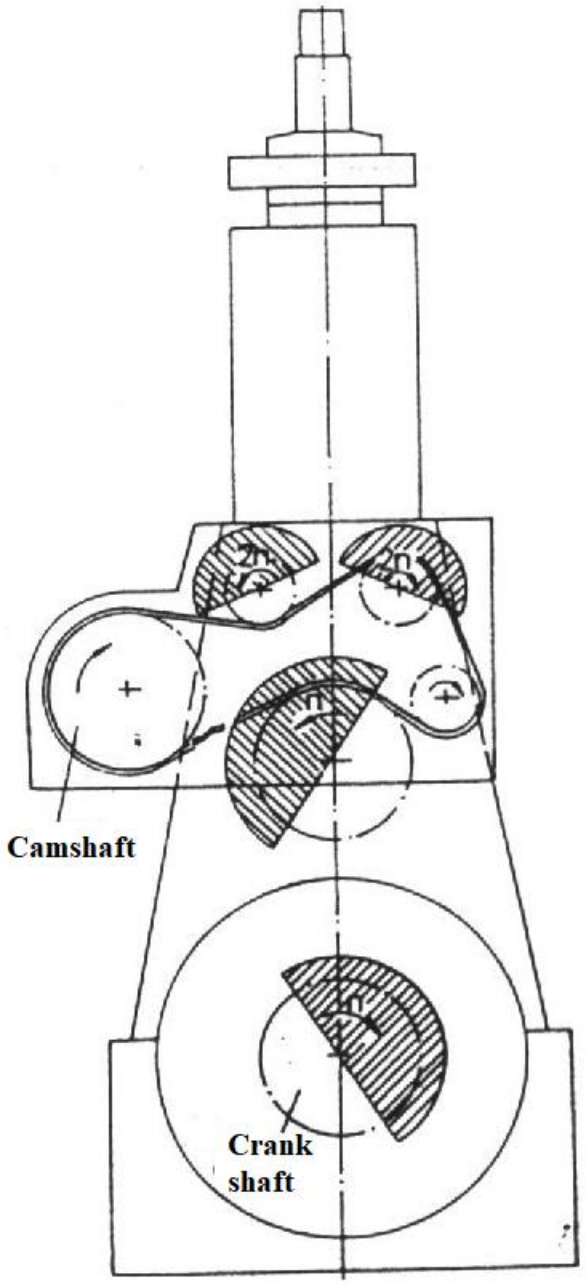

Figure 3.18: Simultaneous balancing diagram of free moments with a 1st order and a 2nd order for marine engines

References:

1. Bărănescu, G. *Teoria echilibrajului motoarelor cu ardere internã în linie*, Editura Academiei Române, București, 1975;

2. Brayard, J. *Avant projet de l'hélice standard, sillage et suction*, ENSTA, Paris, 1975;

3. Brayard, J., Chataignier, P. *Efforts subis par le navire à la mer*, ENSTA, Paris, 1974;

4. Bryndum, L., Jakobsen, S.B. *Vibration Characteristics of Two-Stroke Low Speed Diesel Engines*, MAN B&W, Copenhagen, 1987;

5. Buzbuchi, N., Dragalina, Al., Manea, L., Moroianu, C., Dinescu, C. *Motoare navale. Procese și caracteristici*, Editura Didacticã și Pedagogicã, București, 1997;

6. Buzbuchi, N. *Dinamica sistemelor de propulsie navalã*, Tipografia Institutului de Marinã Civilã Constanța, 1998;

7. Buzbuchi, N., Dinescu, C. *Vibrațiile motoarelor navale*, Tipografia Institutului de Marinã Civilã, Constanța, 1993;

8. Buzbuchi, N., Dinescu, C. *Complemente de dinamica motoarelor navale*, Editura Alas, Cãlãrași, 1995;

9. Buzbuchi, N., Taraza, D. *On Vibration Analysis in Ship Installations with Two-Stroke Diesel Engines*, the Transaction Volume of the Motor and Motor Vehicle Engines, Izmir, 1993;

10. Jenzer, J. *Vibration Analysis for Modern Ship Machinery*, New Sulzer Diesel, Winterthur, Switzerland, 1991;

11. Jenzer, J., Frossard de Saugny, H. *On the Dynamics of Diesel Power Plant*, New Sulzer Diesel, Winterthur, Switzerland, 1991;

12. Taraza, D., Buzbuchi, N. *Considerații asupra vibrațiilor complexe ale motoarelor navale*, Volumul celei de-a VII-a Conferințe naþionale de vibrații mecanice, Timișoara, 1993;

13.*** *Reccomandations en vue de limiter les effets des vibrations à bord des navires*, Bureau Veritas, N.I., Juin, 1979;

14.*** *An Intoduction to Vibration Aspects of Two-Stroke Diesel Engines in Ships*, MAN B&W a/s, Copenhagen, Denmark.

4. SHAFT LINE DRIVEN BY MAIN ENGINES VIBRATIONS

From the category of dynamic phenomena generically presented in the previous chapter, the outmost important dynamic phenomenon will be presented in the actual chapter, this being about the complexity of vibrations in shaft lines driven by marine engines

4.1 Free vibrations of marine engines shaft lines

The study of individual vibrations acting on engine shat lines is absolutely necessary to be done before doing any kind of study that has the subject represented by the real phenomenon itself, this being represented by the coupled vibrations that occur in the shaft line. Current study methodologies of the three types of basic free vibrations, torsional, bending and axial can be seen as an analysis for the excitations sources for these vibrations in order to establish the value of true forced vibrations. This aspects will be studied in this fourth chapter included in the present study.

4.1.1 Free torsional vibrations

The first stage in the study process of torsional free vibrations is represented by the calculus of own pulsation regime and the vibration modes. In order to solve the complex issues generated in such a study for this type of vibrations we have to start from the 1.18 figure and the motion equation itself noted as 1.10, aimed at the entire system including an engine drive and a disc driven by the crank. The motion equation for this type of system is:

$$\theta_2 = \; -M - \; M_2 \qquad (4.1)$$

in the above equation θ_2 is the rotation angle of the disc, having an mechanical inertia moment J_2, while M_2 is the stationary moment that acts on the opposite rotational direction (the opposite moment from the previous mentioned diagram). It

can be assumed that the mono-cylindrical and the mentioned disc are connected through an flexible area without torsional rigid mass *C*. In this case the engine momentum *M* is:

$$M = C(\theta_2 - \theta_1), \qquad (4.2)$$

where θ_1 represents the torsional motion of the crank. By introducing this last value in the last value of 1.110 equation the following equations systems are obtained:

$$\begin{cases} J(\theta_1)\theta_1 + C(\theta_1)\theta_1^2 + C\theta_1 - C\theta_2 = -p(\theta_1)A_p c_{wp}(\theta_1) \\ J(\theta_2)\theta_2 - C\theta_1 + C\theta_2 = -M \end{cases} \qquad (4.3)$$

The first equation in the system above is not a linear equation with variable terms, while the second one is a linear equation with constant coefficients. The means of solving this equation system is by approximating the previous motion equations for which the usual calculus technics can be applied relatively easy as it results from [70] and [91]. In this purpose two main stages have to be passed through:

- The annulation of the variable coefficients;
- The annulation of all non-linear terms.

The first variable coefficient is $J(\theta_1)$, representing the general inertia moment (1.106), for which the medium value applied per cycle will be used and this being defined as:

$$J_1 = \left[\frac{1}{2\pi} \int_0^{2\pi} \frac{d\theta_1}{J(\theta_1)} \right]^{-1} \cdot \qquad (4.4)$$

This mathematical integral has a numerical solution. The second variable coefficient is the centripetal stiffness (1.106) which is a part of the non-linear term along with the part of the analysis carried on. For an engine operating at a constant rotational speed the speed of the vibrating movement is, in fact, a small part of the angular speed, thus the coefficient of the centripetal coefficient θ_1 can be replaced

with the square value of the angular speed, ω^2. Thus, the first term, the centripetal coefficient becomes a function of the rotational angle θ_1. In the previous hypothesis, regarding the constant motion, this variable can be replaced with the first relation mentioned in the 1.1 formula table: $\omega\tau = \theta$. Thus, the centripetal coefficient can be transferred in the right member of the motion equation and, by doing this, it becomes a time function. The same considerations can be done for the inertia pressure force, thus the entire right term of the equation is only a time function, this modified equation becoming:

$$\begin{cases} J\,(\theta_1)\theta_1 + C\,(\theta_1) - C\theta_2 = -p(\omega\tau)A_p c_{wp}(\theta_1) - C(\omega\tau)\omega^2 \\ J\,\theta_2 - C\theta_1 + C\theta_2 = -M \end{cases} \qquad (4.5)$$

It has to mentioned that the linearized motion equations contain in the right member the formula for the applied equation in the case of the crank, this being represented by the gas pressure force multiplied by the piston speed coefficient (1.3), as well as the variable inertia force (as shown in the 1.120 equations) which can be applied for the entire mechanism through the centripetal coefficient.

The equation system has a set of solutions that are, in fact, the answer for the free torsional vibrations solutions, thus the solution for these vibrations will be homogeneous as the one presented below:

$$\left(\begin{bmatrix} J_1 & 0 \\ 0 & J_2 \end{bmatrix} \begin{Bmatrix} \theta_1^2 \\ \theta_2^2 \end{Bmatrix} + \begin{bmatrix} C & -C \\ -C & C \end{bmatrix} \begin{Bmatrix} \theta_1 \\ \theta_1 \end{Bmatrix} \right) = \begin{Bmatrix} 0 \\ 0 \end{Bmatrix} \qquad (4.6)$$

the solutions for the above equation can be rewritten as:

$$\begin{Bmatrix} \theta_1 \\ \theta \end{Bmatrix} = \begin{Bmatrix} \Theta_1 \\ \Theta_2 \end{Bmatrix} e^{I^* \omega\tau}, \quad (4.7)$$

in the above equations ω is the own vibrating frequency, $i^* = \sqrt{-1}$, while Θ_1 and Θ_2 are the values for vibratory motion values for the two mentioned discs. These solutions are introduced in the (4.6) equation system and lead to the following solution:

$$\left(\begin{bmatrix} C & -C \\ -C & C \end{bmatrix} - \omega^2 \begin{bmatrix} J_1 & 0 \\ 0 & J_2 \end{bmatrix}\right)\begin{Bmatrix} \Theta_1 \\ \Theta_2 \end{Bmatrix} = \begin{Bmatrix} 0 \\ 0 \end{Bmatrix}, \qquad (4.8)$$

and this represents a two equation system which are linear and homogeneous, with the following different solutions, but only and only if this calculated determinant has a null value:

$$\begin{vmatrix} C - \omega^2 J_1 & -C \\ -C & C - \omega^2 J_1 \end{vmatrix} = 0 \qquad (4.9)$$

or:

$$\omega^2 \left[\omega^2 J_1 J_2 - C\left(J_1 + J_2\right)\right] = 0. \qquad (4.10)$$

Further on the values of the won frequency regime will be:

$$\omega_1 = 0$$
$$\omega_2 = \sqrt{\frac{C\left(J_1 + J_2\right)}{J_1 J_2}} \qquad (4.11)$$

The first equation corresponds to a rigid system. If these values are replaced in the equation of motion homogenous system and if the amplitude of the first disc gets an arbitrary value (usually unitary) the vibration mode is being obtained with and 1st order attribute (with a single cluster):

$$\begin{Bmatrix} \Theta_1 \\ \Theta_2 \end{Bmatrix} = \begin{Bmatrix} 1.0 \\ -J_1/J_2 \end{Bmatrix} \qquad (4.12)$$

After presenting this simplified bidimensional model the next stage is to calculate free vibrations of a n-dimensional system, which simulates the shaft line which is being driven by the marine engine. The crankshaft has a complicated shape that is why it will be replace with a simpler model, a straight fine one, which is an

equivalent of the real shaped one. In this manner an oscillatory equivalent system will be obtained and it is being formed from flexible elements without mass which are being bound by a series of discs and, on them, mechanical inertia momentum are being focused, that are being reduced at the rotation axis of the bends along with the other engine elements that have a certain type of motion (such as reciprocating rods, flywheel used to even the rotation motion of the crankshaft and the propeller) that can be calculated by keeping in mind the water adherent masses [7], [14] and [43]. In the same manner this elements can be calculated by applying an experimental method.

For this, the equivalent oscillatory system of the shaft line driven by the marine engine (as shown in figure 4.1a) has been calculated by applying the reduction equation called BICERI [89], with its representation in the 4.1b figure. By symbolizing the vibration angular amplitude with Θ_j for an *j* order disc, with *J [Nms^2]* the mechanical inertia moment for this disc, with *C [Nm]* the torsional stiffness for the flexible area between order *j* and *j+1* which is considered massless, the dynamic balancing equation will become:

$$J_j \phi_j + C_j(\phi_j - \phi_{j+1}) - C_{j-1}(\phi_{j-1} - \phi_j) = 0. \quad (4.13)$$

If we include the *J* index in the *1 – n* variation domain, keeping in mind the fact that we have *n-1* flexible areas between the n discs we can specify the fact that (4.13) equation represents, in fact, the motion equation system for all discs included in the system. If we consider all system solutions have a harmonic form, by introducing them in the (4.13) equation a homogenous n equation system is obtained with *n* unknown solutions, Θ_j being a system with a compatibility that represents an algebraic equation with a *2n* order in the ω_0 solution. This the own pulsation regime can be calculated. In order to solve this equation, in this stage, the Holzer – Tolle method has been applied [67], [91] and this is consisting in the iterative minimization of the residual momentum in order to verify the condition of generating free torsional vibrations:

$$\sum_{j=1}^{n} J_j \omega_0^2 \phi_j = 0. \qquad (4.14)$$

The tables below, 4.1 and 4.2 represent the calculus for the above stated and at their bases the vibrations modes have been represented having I and II order for the exemplification of a Sulzer RND80 main engine with six cylinder in a line configuration with a 17400 HP and a nominal rotation speed equal to 122 rpm.

Table 4.1: The calculus of the 1st order torsional vibration

Disc number	J_j [Nms^2]	Θ_j [rad]	C_j [10^9 Nm]	$\sum_{j=1}^{n} J_j \omega_0^2 \Theta_j$ [10^5 Nm]
1	8290.0	1.0000000	1.156870	178.107
2	8046.2	0.9846043	1.156870	384.316
3	8046.2	0.9544958	1.156870	513.319
4	8046.2	0.9101243	1.156870	670.653
5	8046.2	0.8521530	1.156870	817.964
6	8290.0	0.7814480	0.723536	957.146
7	4293.9	0.6491606	0.078441	1017.033
8	73120.0	-0.6473968	-	0.000

Table 4.2: The calculus of the 2nd order torsional vibration

Disc number	J_j [Nms^2]	Θ_j [rad]	C_j [10^9 Nm]	$\sum_{j=1}^{n} J_j \omega_0^2 \Theta_j$ [10^5 Nm]
1	8290.0	1.0000000	1.156870	2909.840
2	8046.2	0.7484730	1.156870	5023.726
3	8046.2	0.3142214	1.156870	5911.170
4	8046.2	-0.1967409	1.156870	535.552
5	8046.2	-0.6596730	1.156870	3492.430
6	8290.0	-0.9615592	0.723536	694.447
7	4293.9	-1.0575388	0.078441	-899.459
8	73120.0	0.0891297	-	0.000

The obtained results for the self-pulsation regime are ω_{0I} =46.351 s^{-1} and ω_{0II} =187.351 s^{-1}. Based on these results the first two vibrations modes have been calculated, as shown in the 4.1c figure. Analyzing the vibrations modes it can be observed that the first mode has the first cluster with an O_I order at the middle of the shaft line, while the second one has the first cluster O_{II1} at the middle area of the crankshaft and this, in fact means that the two halves of the crankshaft have and opposite phase vibration regime, but second order also generates vibrations on the screw shaft, near the propeller.

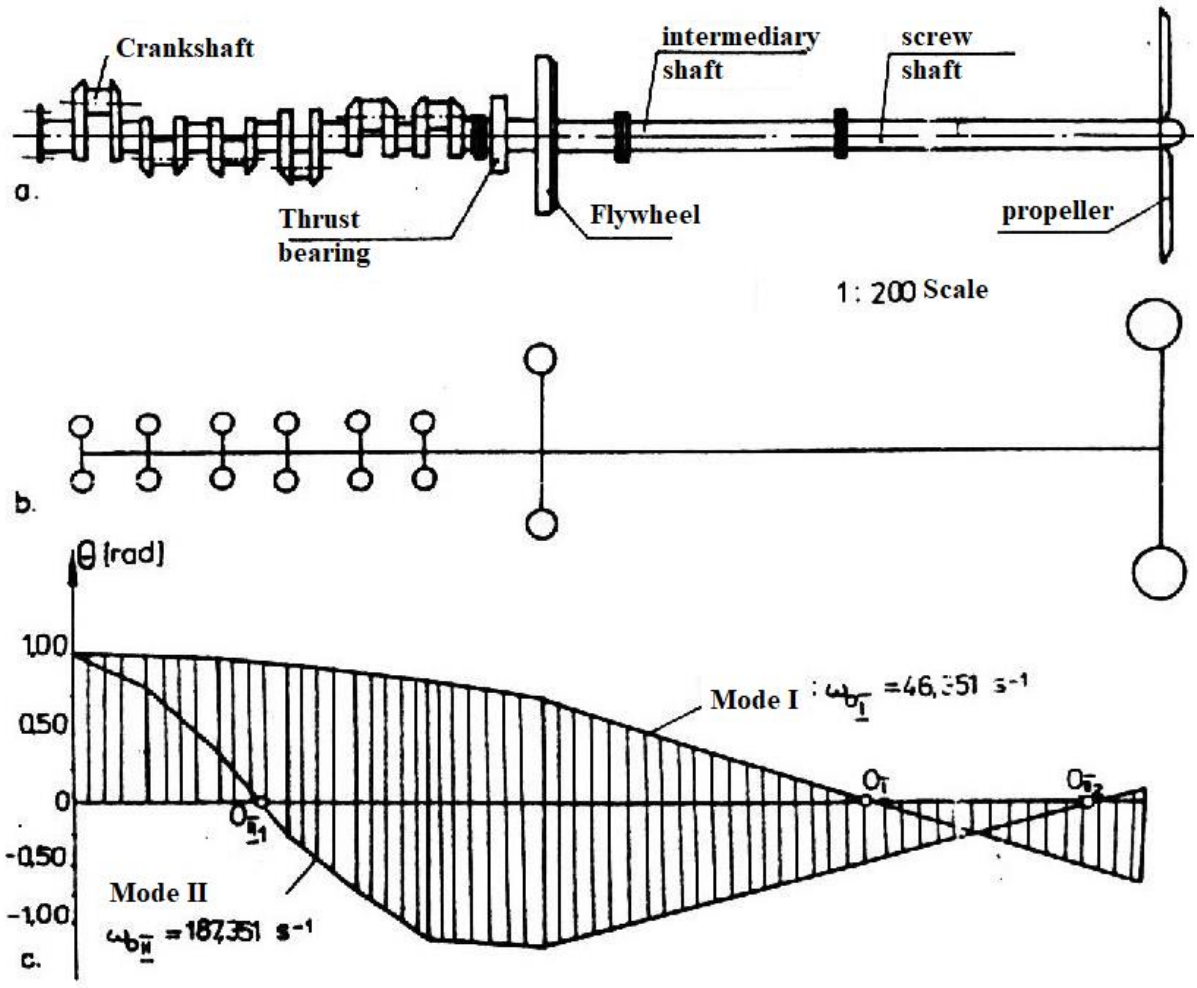

Figure 4.1: Free torsional vibrations for the shaft line driven by de Sulzer 6RND90 main engine: a – shaft line; b – equivalent oscillatory system; c – self induced 1st order vibrations

The calculus for the forced torsional vibrations, including the attenuated ones, the torsional vibrations amplitude spectrum, the additional tensions diagram passing through the shaft line and the comparison with the restrictions imposed by the naval classification societies, as well as the critical rotation diagrams for the previously mentioned engine have been presented in the no. [17] reference. All these have been done by applying the Holzer method (as specified in the 4.3.1 paragraph).

That is why this paragraph will be ended by calculating just the self induced torsional vibrations for the shaft line driven by the main engine, and after, an unitary presentation of the excitation source analysis for each individual type of vibration will be done in the second part of this fourth chapter, a rigorous calculus being done, based on the matrix methods.

4.1.2 Free bending vibrations

According to reference no. [91], due to the complicated construction of the crankshaft, the real mass is being replaced with a reduced mass, m_r, which can be calculated by applying the kinetic energy equality condition:

$$m_r = \frac{\sum_{j=1}^{n} m_j Y_j^2}{Y_r^2}, \qquad (4.15)$$

in the above equation the following notations have been made:

- m_j is the mass of all elements for which a meshing has been done;
- Y_j is vibrating motion amplitude corresponding to all m_j masses;
- Y_r is bending vibration amplitude.

The calculus for the y_j deformations is possible by applying the 4.2 diagram in which a crank is being loaded in its median plan with a F force and is being leaned on its extremities. It can be noticed that the situation is identical with the one in which the crank would be fixed and imbedded at the level of its median plan and the deformation towards the force are identical with the force acting on the reaction of these one, thus $F_1 = F/2$.

The needed value of y_r in order to proceed with the calculus can be determined by applying the Castigliano theorem [26], [91], [89], which states that M_1, M_2 and M_3 are bending momentum applied on the three constructive elements of the crank, while

I_1, I_2 and I_3 are their inertia momentum, while E is the elasticity mode for the material from which the crankshaft is being made of:

$$Y_r = Y_{F_1} = \int_0^{l_1} \frac{M_1}{EI_1} \frac{\partial M_1}{\partial F_1} dz + \int_0^{l_2} \frac{M_2}{EI_2} \frac{\partial M_2}{\partial F_1} + \int_0^{l_3} \frac{M_3}{EI_3} \frac{\partial M_3}{\partial F_1}, \qquad (4.16)$$

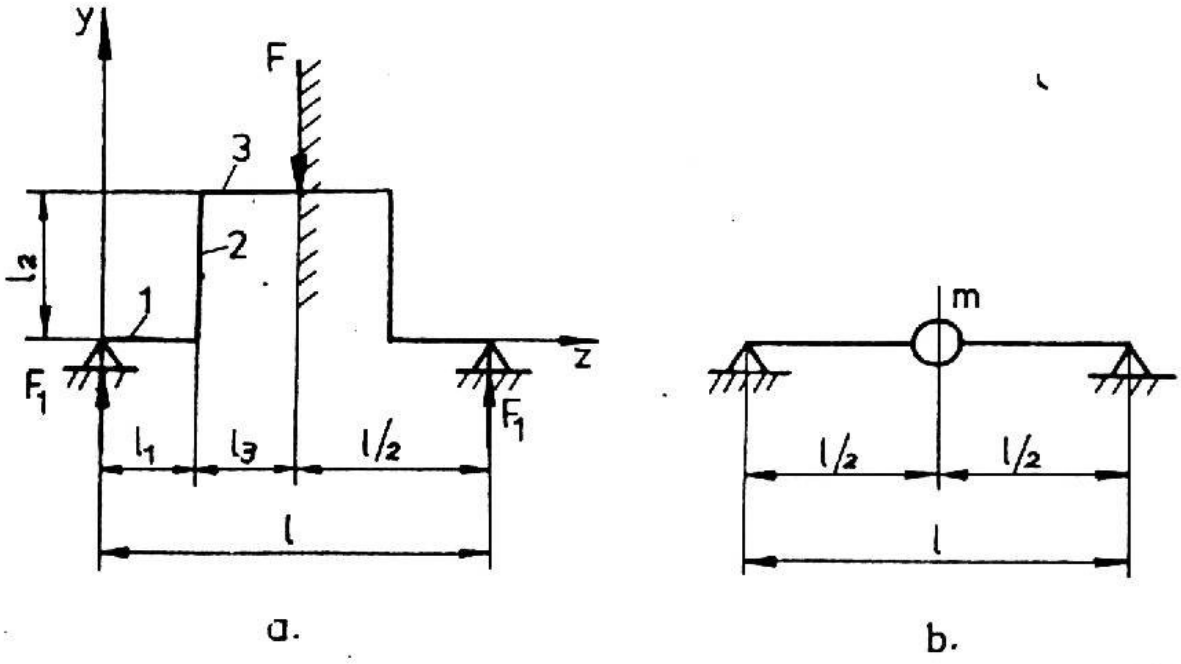

Figure 4.2: Equivalent oscillating system diagram for one crank

The bending momentum that act on the elements in the components of the crank, along with their derivatives are generated by the following expression:

$$M_1 = zF_1, \frac{\partial M_1}{\partial F_1}; M_2 = l_1 F_1, \frac{\partial M_2}{\partial F_1} = l_1; M_3 = (l_1 + z) F_1, \frac{\partial M_3}{\partial F_1} = l_1 + z, \qquad (4.17)$$

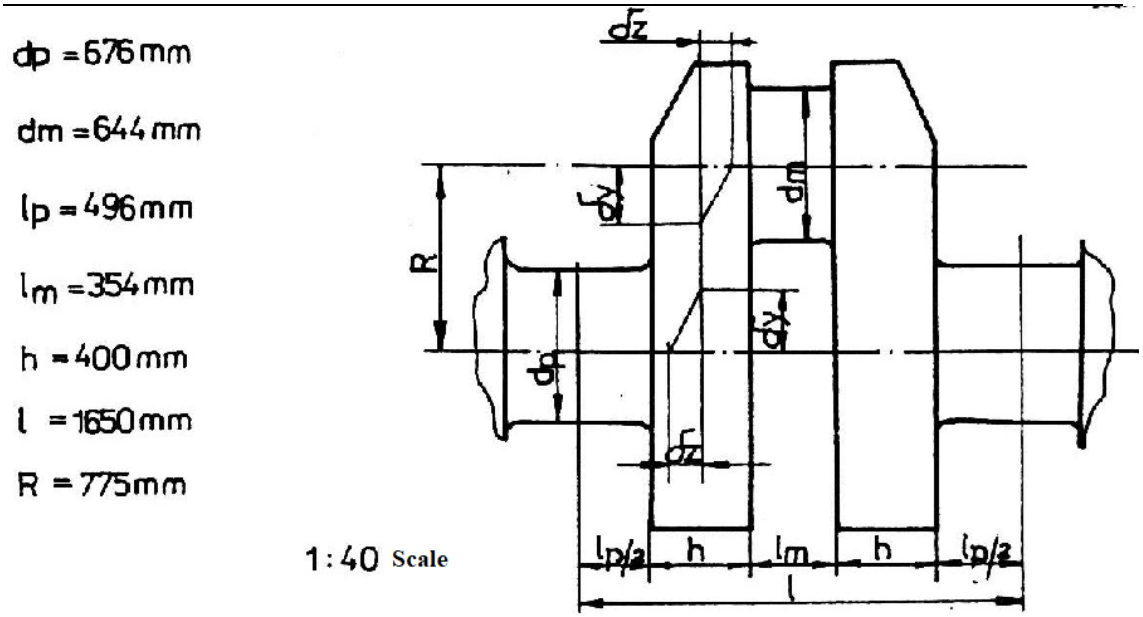

Figure 4.3: Dimensions for a crank fitted on the Sulzer 6RND90 main engine

The inertia moments of these elements are calculated on basis of the dimensions presented in the 4.3 figure.

Taking into account the increase stiffness for a crank in the joining area between bearings and arms [91] is being done by reducing the quotas of the bearing's length, the same thing being applied for the crankpins with the following dimensional values:

$$\delta_z = h/3; \delta_y = d_p/2, \quad (4.18)$$

The values are in the same note as the above presented figure.

Thus, the (4.16) equation then becomes:

$$Y_r = \frac{F_1}{E}\{\frac{(L_1 - \delta_z)^3}{3I_1} + \frac{l_1^2(l_2 - 2\delta_y)}{I_2} + \frac{l_3 - \delta_z}{I_3}[l_1^2 + l_1(l_3 - \delta_z) + \frac{(l_3 - \delta_z)^2}{3}]\}, \quad (4.19)$$

Numerical speaking:

- $Y_r = 7.30735 \times 10^{-11} F_1$ *and* $Y_1 = 0.4840243 \times 10^{-11} F_1$;

- $Y_2 = 2.283857 \times 10^{-11} F_1$ şi $Y_3 = 4.53947 \times 10^{-11} F_1$.

Having these values introduced in the (4.19) equation the reduced value of the crank mass will be $m_r = 817\ kg$. Keeping in mind the dimensions of the shaft line presented in the 4.3 figure the oscillating equivalent system can be obtained, being the same with the one presented in the 4.4b figure.

The masses presented in this figure are:

- $m_1 = \wedge = m_6 = m_r$ *and* $m_7 = m_v + m'_{a'}$ - the mass of the flywheel and the mass of the shaft that supports the flywheel, concentrated in the mass of the first element;

- m_8 - the mass of the intermediary shaft;

- $m_9 = m_{el} + m'_{a'}$ - the mass of the propeller and the screw shaft, concentrated in the center of gravity of the entire system formed by these two masses, being placed at a *21* distance toward the last crankshaft support.

These masses have corresponding gravity forces expressed as:

$$F_j = m_j g,\ j = \overline{1,9}. \qquad (4.20)$$

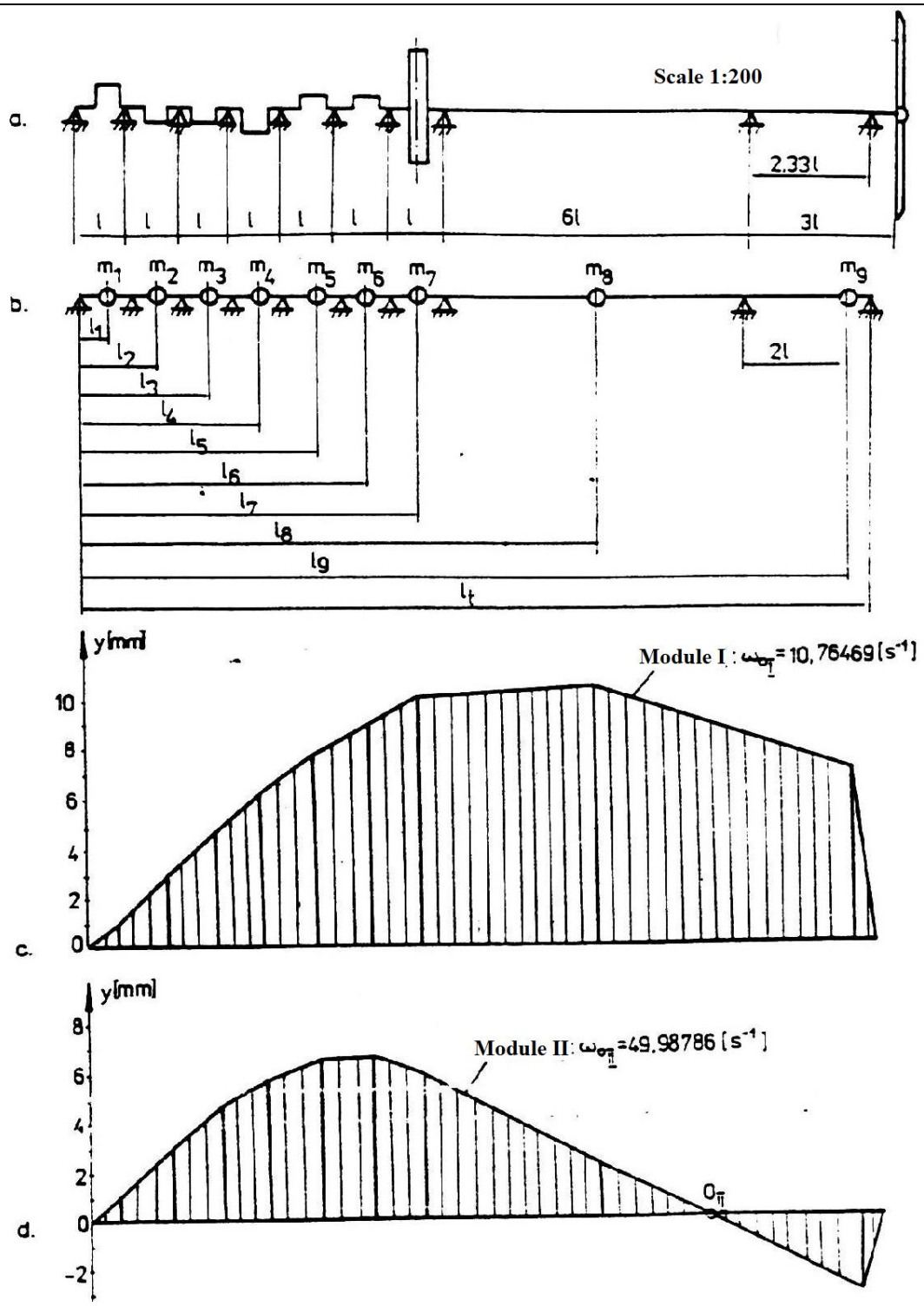

Figure 4.4: Equivalent oscillatory system and the own modes for bending vibrations in the case of a Sulzer 6RND90 main engine

For the previous system, being formed out of nine masses all focused on one single flexible framework with a neglectable mass, it can be considered that the crankpins are not opposing the deformation forces acting on the bending side, while the shaft line vibrates only supported on the ending bearings and that means that mass elongations $Y_j(\tau)$, with $j = 1 - 9$ are generated by the framework's bending feature which occurs in a perpendicular orientation on the axis of the unchanged crossbar. The influence coefficients for the entire system are symbolized by dij, with $i, j = 1 - 9$ and representing the elongation of the framework in the i cross section and it is generated by a force equal with the unity applied in the j cross section.

Using the Mohr-Maxwell method and the Veresceaghin method for the calculus of the elongations, according with the 4.5 figure, we will have the following calculus formula for the influence coefficients:

$$\delta_{ij} = \sum_{i=1}^{3} \frac{m_i m_j}{EI} dz = (S_1 q_1 + S_2 q_2 + S_3 q_3) \frac{1}{EI}, \qquad (4.21)$$

For the dimensions previously indicated the following expressions will be obtained:

$$S_{ij} = \sum_{i=1}^{3} S_i q_i = \frac{l_i (L - l_j)(2L l_j - l_i^2 - l_j^2)}{6L}, \qquad (4.22)$$

Thus, the same applies for the influence coefficients:

$$\delta_{ij} = \frac{l_i (L - l_j)(2L l_j - l_i^2 - l_j^2)}{6EIL} \; for \; i < j$$

$$\delta_{ij} = \frac{l_j (L - l_i)(2L l_i - l_j^2 - l_i^2)}{6EIL} \; for \; i > j \qquad (4.23)$$

$$\frac{l_i^2 (L - l_i)^2}{3EIL} \; for \; i = j$$

Further on, by applying the *effect overlapping principle*, the elongations of the two masses will be expressed by the following formula:

$$Y_j = \sum_{i=1}^{9} F_j \delta_{ij},\ j = \overline{1,9}. \qquad (4.24)$$

Noting the inertia forces acting on the motion masses with F_j, these will have the following calculus formula:

$$F_{ij} = - m_j y_j, \qquad (4.25)$$

from the above formula, introducing it in the (4.27) it would lead to:

$$\sum_{j=1}^{n} m_j \delta_{ij} y_j + y_i = 0, i = \overline{1,9}. \qquad (4.26)$$

Written under a matrix formula, the system (4.26) can be written as:

$$\{[b] = \{y_j\} + \{y\} = \{0\} \qquad (4.27)$$

for which:

$$[b] = [\delta_{ij} m_i]_{i,j=\overline{1,9}} = [\delta][m]. \qquad (4.28)$$

Using the notations for the mass matrix and the influence coefficients will have the following equivalent:

$$[\delta] = \begin{pmatrix} \delta_{11} & \delta_{12} & \cdots & \delta_{19} \\ \delta_{21} & \delta_{22} & \cdots & \delta_{29} \\ \cdots & \cdots & \cdots & \cdots \\ \delta_{91} & \delta_{92} & \cdots & \delta_{99} \end{pmatrix}; \ [m] = \begin{pmatrix} m_1 & 0 & \cdots & 0 \\ 0 & m_2 & \cdots & 0 \\ \cdots & \cdots & \cdots & \cdots \\ 0 & 0 & \cdots & m_9 \end{pmatrix}, \qquad (4.29)$$

Thus, the (4.27) matrix system becomes:

$$\{y_j\} + d\{y\} = \{0\} \qquad (4.30)$$

in which *[d]* is, in fact the following matrix:

$$[d]=[b]^{-1}=[m]^{-1}[\delta]^{-1} \qquad (4.31)$$

Considering that the vibrating motions for mi harmonic masses the compatibility condition for the entire system will be obtained, having the 4.30 formula as a reference:

$$\det([d]-\omega_0^2)=0, \qquad (4.32)$$

this becomes a equation of value and vectors for a square matrix that can be decomposed into a multiplier of triangle matrix, that is why, this equation can be solved by applying the *matrix iteration method*.

Considerable vibrations in its own modes, these having the 1st and 2nd order have been presented in the 4.4c and 4.4d figures, these being calculated on the basis of the values of the results presented in the 4.3 table.

Table 4.3: The calculus of I and II bending vibrations modes

Mass number	m_j [kg]	z_j [m]	$Y_{I\,j}$ [-]	$Y_{II\,j}$ [-]
1	817	0.825	1.0000000	1.0000000
2	817	2.475	2.9677254	2.9123939
3	817	4.125	4.8365882	4.5661747
4	817	5.775	6.5434115	5.8025441
5	817	7.425	8.0240385	6.4818916
6	817	9.075	9.2161028	6.4889013
7	9796	10.725	10.0587390	5.7353914
8	27888	14.025	10.4904310	2.0815935
9	42144	19.800	6.9697096	-4.5020608

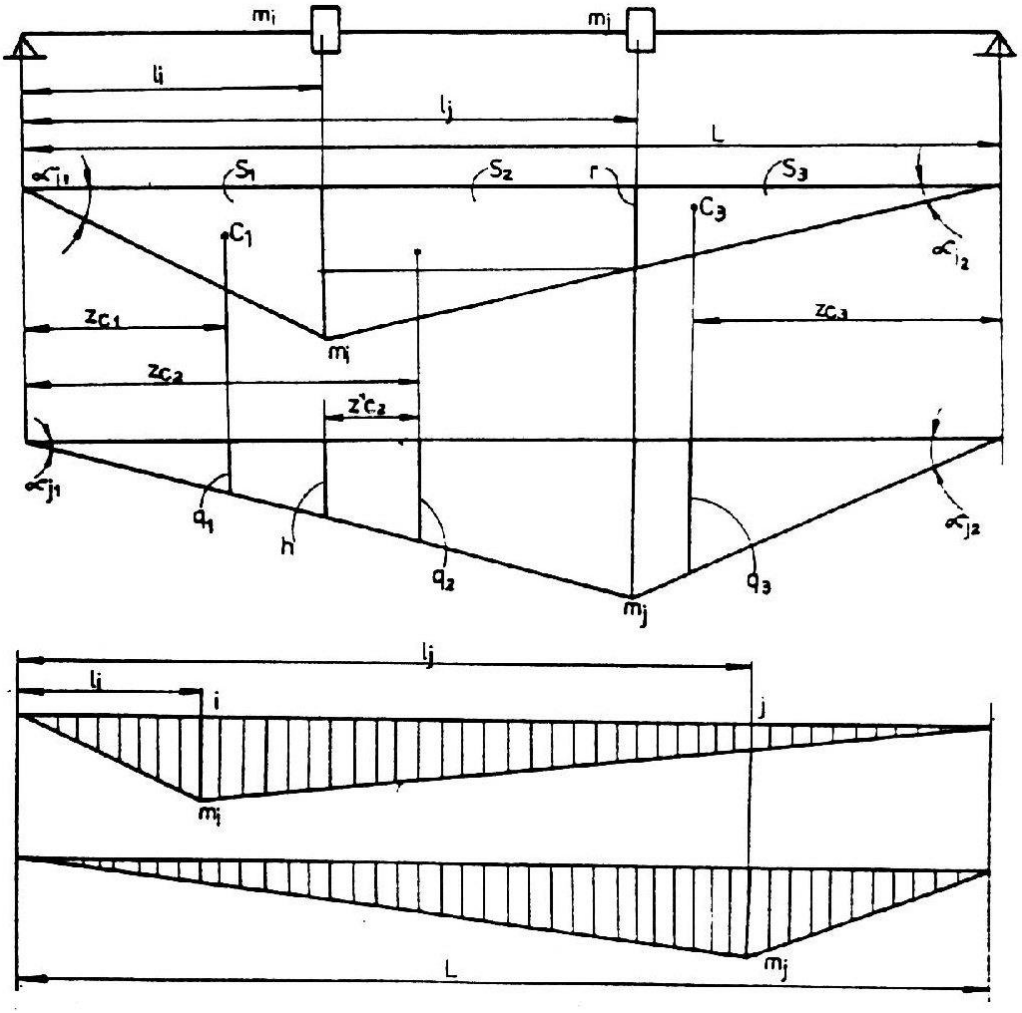

Figure 4.5: Influence coefficients calculus diagram

z_j represents the distances from the m_j masses to the first support from the left side, while Y_{Ij} and Y_{IIj} are the relative amplitudes towards the amplitude of the first mass, for all I and II modes of vibrations. The self-pulsation obtaining by applying these formulas are ω_{0I}=10.76469 s^{-1} and ω_{0II}=49.98786 s^{-1}.

The process of calculating bending deformations for the crankshaft, being a supported in multiple points on the bearings from the crankcase, is being influenced by an approximation degree, that is why a calculus of the forced vibrations is not usually undertaken. In order to avoid dangerous situations that can be generated by

bending vibrations it is needed to seek to avoid resonance generation with strong radial excitation forces. In this purpose the construction of the crankshaft is being stiffened as well as in order to highlight these resonances outside the range of rotation speed in which the engine is functioning.

Critical rotation speeds have been analyzed on the basis of torsional vibrations as it was shown in reference no. [17].

4.1.3 Free axial vibrations

Axial vibrations of shaft lines have an origin in the axial vibrations of the crankshaft and the variations of these forces generated by the propeller thrust, as in the case of torsional vibrations through the so-called *coupling phenomenon*, this one being presented in a detailed manner in the 4.4 chapter of this study.

In order to study the free axial vibrations using an analytical manner the shaft line of the propulsion system can be replaced with an equivalent oscillatory system which is formed by flexible masses and elements with dynamic features that allow us to approximate the real system as stated in references no. [16], [56] and [103]. The masses that interfere are the propellers weight, axial bearing and shafts. All these masses are coupled by using flexible shafts, as presented in the 4.6b figure.

It has to be mentioned that the study of axial vibrations on shaft lines driven by marine engines is an issue that started to seem interesting for more and more marine users due to the excessive vibration level that can be achieved. The most recent problematic aspects haven’t been an target for most naval classification societies and the level of this category of vibrations is being seen as a superficial issue [103], the data being incomplete, but every now and then the data is studied and delivered on request to the final users for a certain type of engine or for a known shaft line geometry.

If for the meshing of the shaft line in mass elements coupled using flexible areas a similar method is being used as in the case of bending vibrations study, the suggested meshing method in the no. [58] and [103] references, tell us that the method

applied for the calculating the specified axial areas doesn't not contain any relevant information.

That is why, for the study of axial vibrations the starting point is represented by the study of crank deformation, this being analyzed in the same manner as the situation in the 4.2 figure, but this time the crank has a load applied consisting of a two axial force system *F*, applied at its ends.

To this purpose, the crank is being considered as an element of the crankshaft being supported by the two neighboring crankpins (as shown in the 4.7a figure), that is why is being replace with to reduced masses $m_1 = m/2$, *m* being the real mass of the crank, but these two masses are connected through a flexible area with the same length (as shown in the 4.7b figure), this element being massless and having an unknown axial stiffness.

The generated deformation by this force system in the cross sections in which this fact is being applied can be calculated by applying the Castigliano theorem, sustaining the idea that the bending deformation has to be calculated. The crank is being fitted at the level of its median plan due to the symmetry of the load applied. This time the fact that certain elements of the crank are influenced by compression (element 1), others to bending (element 2) or simultaneous to both types of loads (element 3).

In this manner the needed deformation is being calculated by applying the Casigliano formula for each one of the three elements in the composition of the crank:

$$z_r = \sum_{s=1}^{3} z_s \text{ , } \quad (4.33)$$

for which *z* is the axial vibration amplitude for the crank in the precise point of the replacing mass and an arbitrary term has a generic formula:

$$z_s = \int_0^{l_s - \delta_s} \frac{M_s}{EI_s} \frac{\delta M_s}{\delta F} ds + \int_0^{l_s - \delta_s} \frac{N_s}{EA_s} \frac{\delta N_s}{\delta F} ds, \quad (4.34)$$

where M symbolizes the bending moment that acts on the chosen arbitrary element mentioned above.

Further on N – represents the compression force, while I_s and A_s is the axial inertia momentum, also the area of the transversal cross section for that certain element, E being the longitudinal flexibility module for that type of material. In the (4.34) formula it has been kept in mind that in the case of the bending phenomenon the crank increased stiffness occurs in the region of crankpins fittings, by reducing the length quota for the crankpin, for the bearing and for the arm with δ_z and δ_v values, according to the (4.18) formula and the 4.3 figure.

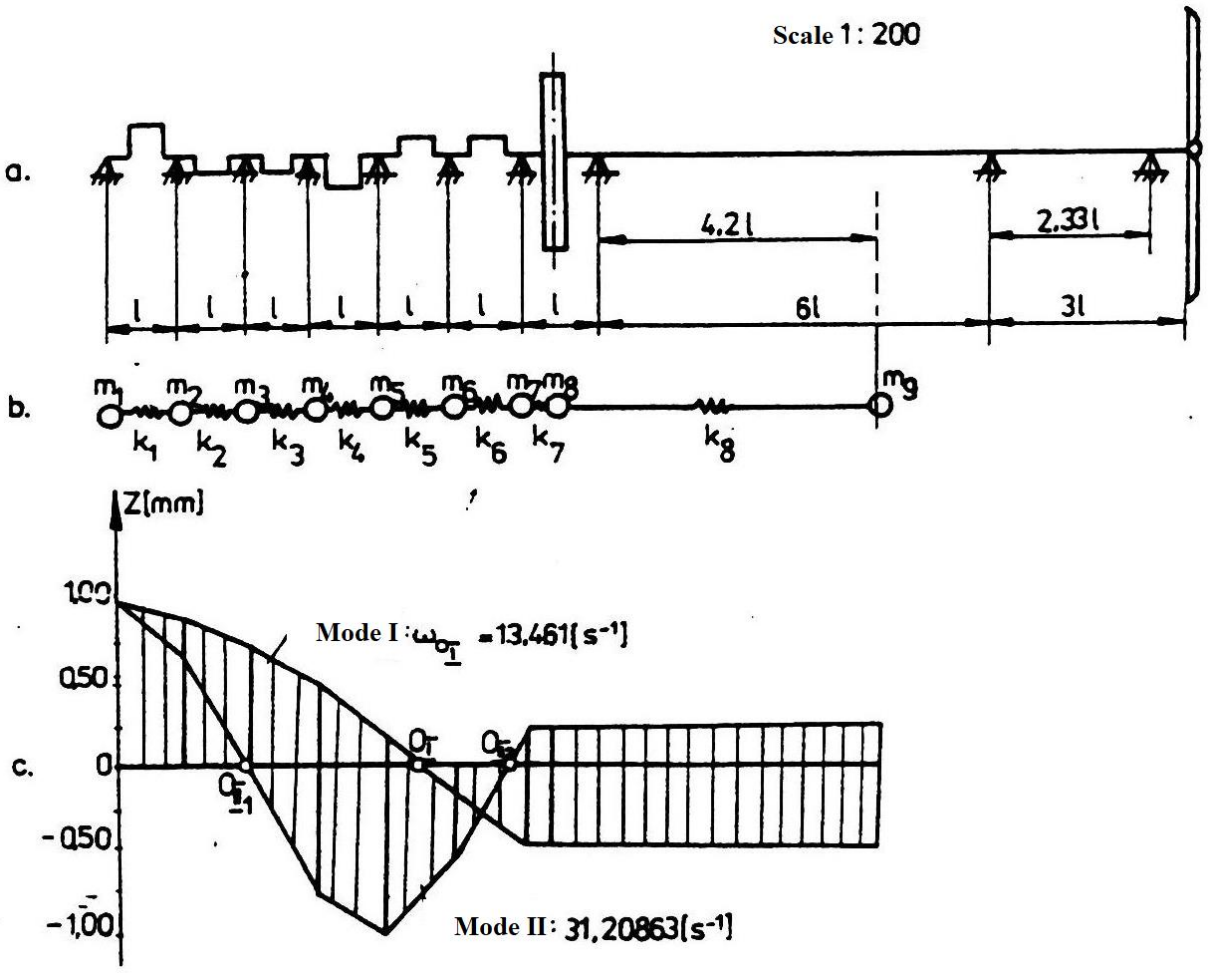

Figure 4.6: Equivalent oscillatory system and its own axial vibrations modes for the Sulzer 6RND90 main engine

Further on, it must be said that the values for the normal forces and for the bending moments that load the three crank elements, as well as the formulas for their corresponding partial derivatives are expressed as it follows:

$$\text{Element 1: } N_1 = F;\ \frac{\partial N_1}{\partial F} = 1 \qquad (4.35)$$

$$\text{Element 2: } M_2 = Fy;\ \frac{\partial M_2}{\partial F} = y \qquad (4.36)$$

$$\text{Element 3: } M_3 = Fl_2;\ \frac{\partial M_3}{\partial F} = l_2 \qquad (4.37)$$

$$N_3 = F;\ \frac{\partial N_3}{\partial F} = l$$

The axial inertia moments, as well as the areas of the cross sections which are being taken into account while performing the calculus are given by the following formulas:

$$I_2 = \frac{bh^3}{12};\ I_3 = \frac{\pi d_m^4}{64};\ A_1 = \frac{\pi d_p^2}{4};\ A_3 = \frac{\pi d_m^2}{4}, \qquad (4.38)$$

where *b* is the average width of the arm [89]. In all the previous formulas, the notations and dimensions for the crank arm are the same used in the 4.3 figure.

Keeping in mind the 2.22, 2.23, 2.24 and 2.25 formulas the 3.4 formula will become:

$$z_r = \int_0^{l_1-\delta_z} \frac{F}{EA_1}dz + \int_0^{l_2-2\delta_y} \frac{Fy}{EI_2}ydy + \int_{0 l_3-\delta_z} \left(\frac{Fl_2}{EI_3}l_2 + \frac{F}{EA_3}\right)dz = \qquad (4.39)$$

$$= \frac{F}{E}\left[\int_0^{l_1-\delta_z} \frac{1}{A_1}dz + \int_0^{l_2-2\delta_y} \frac{y^2}{I_2}dy + \int_0^{l_3-\delta_z} \left(\frac{l_2^2}{I_3} + \frac{1}{A_3}\right)dz\right] =$$

$$= \frac{F}{E}\left[\frac{l_1-\delta_z}{A_1} + \frac{(l_2-2\delta_y)^3}{3I_2} + \frac{l_2^2(l_3-\delta_z)}{I_3} + \frac{l_3-\delta_z}{A_3}\right].$$

The same deformation has been symbolized with z_v and has to take place under the load of the same force system *F* from the equivalent system presented in the 4.7b

figure. by expressing this deformation depending on the axial stiffness K for the massless flexible element from the equivalent oscillatory system will be obtained as:

$$z_r = \frac{F}{K}. \qquad (4.40)$$

By equalizing the 4.39 and 4.40 formulas the analytical expression for the axial stiffness for a crank fitted on the crankshaft of the engine will be obtained:

$$K = \frac{E}{2[\frac{l_1 - \delta_z}{A_1} + \frac{(l_2 - 2\delta_y)^3}{3I_2} + \frac{l_2^2(l_3 - \delta_z)}{I_3} + \frac{l_3 - \delta_z}{A_3}]}, \qquad (4.41)$$

where the factor 2 from the lower part of fraction has been introduced due to the symmetry of the diagram configuration of the crank and the type of support taken into account for this consideration, that is why the total elongation for the entire system on the axial direction will have a double value as the one given by the 4.39 formula.

On the base of previous considerations we can calculate the stiffness of the flexible area between the two equivalent masses, this being the point where the bent has been meshed: $K = 4.33552*10^7$ N/m. In this manner the oscillatory system from the 4.6 b figure has been generated, for which the masses are: $m_1 = m_7 = m/2$, while $m_2 = ... = m_6 = m$; while m_8 has the same meaning as m_7 from the previous paragraph, while m_9 is given by adding the masses of intermediary shafts and screw shafts plus the propeller mass, the las mass being focused in the mass center of the system containing all these masses placed at a 4.21 distance towards the last support. m symbolizes the mass of a crankshaft bent.

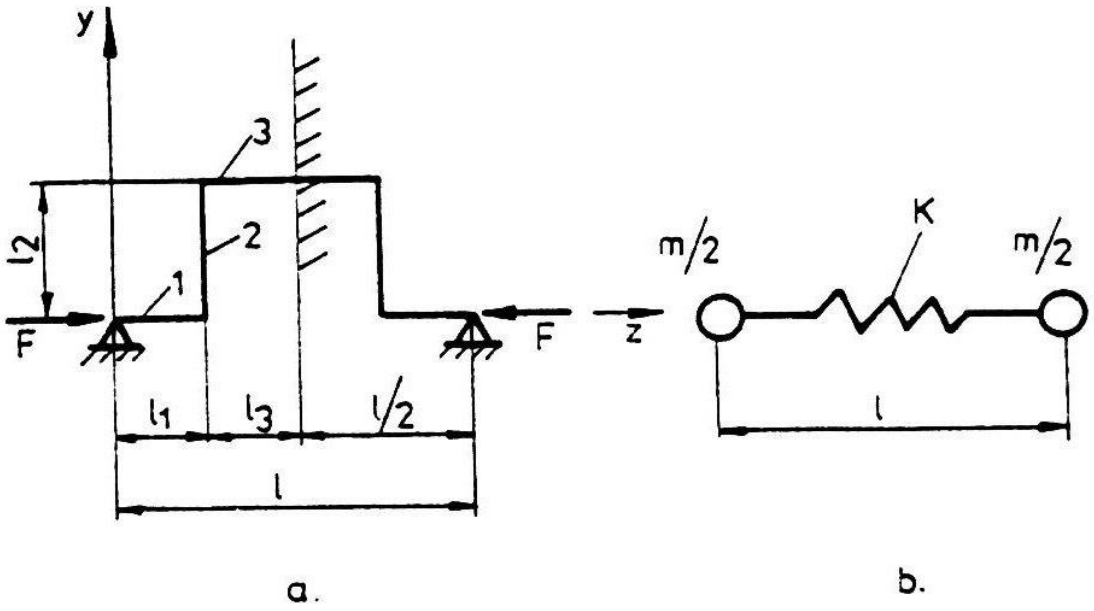

Figure 4.7: Axial oscillatory system diagram for on crank

K_7 and K_8 stiffness are being given by the following formula:

$$k = \frac{EA}{l}, \qquad (4.42)$$

in the above formula A is the cross area surface for the intermediary shaft, as well for the area of the cross section of the screw shaft, while E is the elasticity module in the longitudinal orientation. The l_7 and l_8 lengths are deducted from the 4.62 figure keeping in mind the existent perfect analogy between the torsional vibrations and the axial ones. For the calculus of the later ones doesn't exist a special mathematical tool that is why the one presented in the 4.1.1 paragraph has been applied. In this manner the mechanical inertia moments have been replaced with mass values, while the torsional stiffness have been replace with the stiffness of two areas between two consecutive masses. In the 4.4 and 4.5 tables the calculus results have been presented for the free axial vibrations, according to the first two vibration modes. The relative amplitude has been symbolized by z_j this being done for the axial relative vibrations in the considered masses.

The self-generated pulsations for the shaft line axial vibrations are: ω_{0_I} =18.167 s^{-1} and, respectively $\omega_{0_{II}}$ =42.103 s^{-1}. The self-generated modes are given in the 4.6c figure. it can be noticed the axial vibration shapes resemble with the torsional ones, as the nearest value of 1st degree self-generated torsional pulsations with the same one of 2nd degree axial vibrations.

Table 4.4: The calculus for the I mode of axial vibration

Mass number	m_j [kg]	Z_j [-]	k_j [10^7N/m]	$\sum m_j\omega_0^2 Z_j$ [10^7N]
1	7803	1.0000000	4.33552	0.25753
2	15606	0.9405988	4.33552	0.74201
3	15606	0.7694522	4.33552	1.13833
4	15606	0.5068929	4.33552	1.39941
5	15606	0.1841135	4.33552	1.49424
6	15606	-0.1608390	4.33552	1.41155
7	7803	-0.4861192	9124.78200	1.28636
8	9796	-0.4862602	971.89780	1.12915
9	700032	-0.4874220	-	0.00000

Table 4.5: The calculus for the II mode of axial vibration

Mass number	m_j [kg]	Z_j [-]	k_j [10^7N/m]	$\sum m_j\omega_0^2 Z_j$ [10^7N]
1	7803	1.0000000	2.380953	1.38321
2	15606	0.6809568	2.380953	3.26704
3	15606	-0.0072595	2.380953	3.06621
4	15606	-0.7798258	2.380953	0.90887
5	15606	-0.9894598	2.380953	-1.82840
6	15606	-0.5677331	2.380953	-3.39900
7	7803	0.2162563	9124.78200	-3.09987
8	9796	0.2162563	971.89780	-2.72375
9	700032	0.2139986	-	0.00000

4.2 Excitations sources analysis for shaft line vibrations

The issue of correct analysis of all excitation sources for complex shaft line vibrations is more and more requested, at least in the last years, once on the market a

new generation of marine engines has emerged, and from here arises the opportunity of undertaking this kind of study with the main focus on the force vibrations.

In the actual paragraph, in the first stage, an analysis is being done on the classical source of shaft line vibrations which are driven by internal combustion engines, these being in fact the tangential and radial components of gas pressure forces, as well as the inertia mass forces which have a translation motion.

Marine slow turning engines have a propulsion particularity and this will be presented in a special manner, especially when vibrations induced by the propeller in the shaft line coupled in a direct manner with the marine engine.

4.2.1 Torsional vibrations excitation sources

Tangential forces acting on the crankshaft bent (as it has been shown in the 1.14 and 3.2 figures) are considered as being conventionally applied in the middle of the shaft bearing and it is acting in a tangential manner, being multiplied by the value of the crank radius *R*, this being the main excitation source for torsional vibrations of the shaft line.

That is why, in the next paragraphs just the analytical formulas of tangential excitation forces will be presented, understanding that for the torsional excitatory momentum will obtain the same formulas multiplied by a constant dimension (in this case the crank radius *R*). In this manner we could use the direct values of all tangential forces in the process of complex vibrations acting on the shaft lines of marine engines.

The mathematical formula of this excitation force is:

$$T = T(\alpha) = (F_p + F_a)\frac{\sin(\alpha + \beta)}{\cos\beta} = T_p + T_a, \qquad (4.43)$$

in the above formula F_p symbolizes the gas pressure force developed in the cylinder, Fa is the mass inertia forces with an alternative motion, while θ and β are crank angles, or the bending of the crank.

The component generated by the gas pressure force T_p can be developed in the following Fourier series

$$T_p = T_{p_0} + \sum_{k=1}^{\infty} T_{p_k} \qquad (4.44)$$

In the following formula the mean value of Tp0 is given by the following formula:

$$T_{p_0} = \frac{1}{T_c} \int_o^{T_c} T_p(\alpha) d\alpha, \qquad (4.45)$$

its harmonic components with an *k* order are:

$$T_{p_k} = A_{p_k} \cos k\alpha + B_{p_k} \sin k\alpha, \qquad (4.46)$$

the developing applied coefficients are:

$$A_{p_k} = \frac{2}{T_c} \int_0^{T_c} T_p(\alpha) \cos k\alpha d\alpha, \qquad (4.47)$$

In the previous formulas T_c symbolizes the engine cycle period, being given in the (1.100) formula.

The component given by the mass inertia forces with a translation motion has the following formula:

$$T_{a_k} = m_a R \omega^2 b_k \sin k\alpha = B_{a_k} \sin k\alpha \qquad (4.48)$$

in the above formula ω is the crankshaft angular speed, m_a is the sum of all masses with a translation motion, while b_k (as well as B_k) are harmonic coefficients for tangential excitation generated by the inertial elements [91].

For a single engine cylinder with an random *j* order the tangential excitation force will have the following resulting formula:

$$T_{k_j} = A_{p_{k_j}} \cos k(\alpha - n_j \delta) + (B_{p_{k_j}} + B_{a_k}) \sin k(\alpha - n_j \delta). \qquad (4.49)$$

with the module value given by:

$$|T_{k_j}| = \sqrt{A_{p_{k_j}}^{\ 2} + (B_{p_{k_j}} + B_{a_k})^2}, \qquad (4.50)$$

and the initial phase expressed as follows:

$$\theta_{k_j} = \arctan\frac{A_{p_{k_j}}}{B_{p_{k_j}} + B_{a_k}} - kn_j\delta, \qquad (4.51)$$

In the above formula δ symbolizes the off-setting between two consecutive combustions, while n_j is the number of angular off-settings which separates the combustions between *1* and *j* numbered cylinders, keeping in mind the combustion order (for an example: the Sulzer 6RND main engine has the following combustion order: 1-6-2-4-3-5-1).

In the 4.6 table the developing coefficients for a series has been presented, the first 12 harmonic components for the tangential excitation components , while in the 4.8 figure and 4.9 these variations have been presented towards the crank angle according with the gas pressure components and the inertia of masses with a translation motion.

Table 4.6: Harmonic coefficients for excitation tangential forces for a Sulzer 6RND90 main engine

k	***A_{pk}* [kN]**	***B_{pk}* [kN]**	***B_{ak}* [kN]**
1	301.2	753.4	48.9
2	8.2	657.2	-470.1
3	-54.0	374.9	-145.9
4	-69.2	216.5	-9.8
5	-83.6	116.2	0.9
6	-71.7	69.1	0.0
7	-68.3	56.5	0.0
8	-63.5	49.9	0.0
9	-55.1	42.5	0.0
10	-45.3	24.6	0.0
11	-27.4	7.5	0.0
12	-11.0	-11.4	0.0

4.2.2 Excitation sources for bending vibrations

The radial excitatory force is given by the following formula:

$$Z = Z(\alpha) = (F_p + F_a)\frac{\cos(\alpha+\beta)}{\cos\beta} = Z_p + Z_a. \qquad (4.53)$$

Gas pressure component has the following formula:

$$Z_p = Z_{p_0} + \sum_{k=1}^{\infty} Z_{p_k}, \qquad (4.54)$$

in the above formula the average value Z_{p0} can be calculated in a similar manner by applying (4.45) formula, thus the harmonic components will be calculated by the following formula:

$$Z_{p_k} = A_{p_k}' \cos k\alpha + B_{p_k}' \sin k\alpha, \qquad (4.55)$$

having the harmonic components A'_{pk} and B'_{pk} are similar with the ones expressed in the (4.56) formula.

For the inertial component the following formula is being applied:

$$Z_a = \sum_{k=0}^{\infty} Z_{a_k}, \quad (4.56)$$

for which the harmonic components are:

$$Z_{a_k} = m_a R \omega^2 b_k' \cos k\alpha = B_a' \cos k\alpha, \qquad (4.57)$$

in the above formula the harmonic coefficients are calculated using reference No. [17], but these are not specified at all in the technical literature regarding similar studies.

In the same manner as the analysis of excitations previously presented, the excitatory radial force with an *k* harmonic order applied for the *j* cylinder will be:

$$Z_{k_j} = (A_{p_{k_j}}' + B_{a_k}')\cos k(\alpha - n_j\delta) + B_{p_{k_j}}' \sin k(\alpha - n_j\delta), \qquad (4.58)$$

or, put in a more concentrated form:

$$Z_{k_j} = \left|Z_{k_j}\right| \sin\left(k\theta + \varphi'_{k_j}\right) \qquad (4.59)$$

with the following module:

$$|Z_{k_j}| = \sqrt{(A_{p_{k_j}}' + B_{a_k}')^2 + B_{p_{k_j}}'^2}, \qquad (4.60)$$

and with the following initial phase:

$$\theta_{k_j}' = \arctan \frac{A_{p_{k_j}}' + B_{a_k}'}{B_{p_{k_j}}'} - kn_j\delta. \qquad (4.61)$$

In the 4.7 table the values for the harmonic coefficients corresponding to radial excitatory forces are being presented for the first 12 harmonic components, used as a basis in the process of drawing the crank angle variation curves, as shown figures 4.10 and 4.11.

The radial force has a harmonic structure with the one previously presented that mainly means that the crankshaft bending are the ones applied for the shaft line of the engine.

It has to be mentioned that the harmonic analysis of tangential excitations, as well as radial ones have been presented in the 4.2.1 and 4.2.2 paragraphs and this presentation has been based on the indicated diagram lifted on the operating engine functioning at a normal level, as well as the exact knowledge of all geometrical and mass features for engine drives.

Table 4.7: Harmonic coefficients for excitatory radial force applied in the case of a Sulzer 6RND90 main engine

k	A_{pk} [kN]	B_{pk} [kN]	B_{ak} [kN]
1	1572.3	203.9	138.1
2	1156.1	428.7	450.3
3	672.3	457.2	143.9
4	404.2	387.4	10.1
5	252.4	342.6	1.0
6	156.1	275.6	0.1
7	55.2	143.5	0.0
8	1.5	116.2	0.0
9	-33.4	85.6	0.0
10	-49.0	62.4	0.0
11	-49.8	42.9	0.0
12	-42.7	25.2	0.0

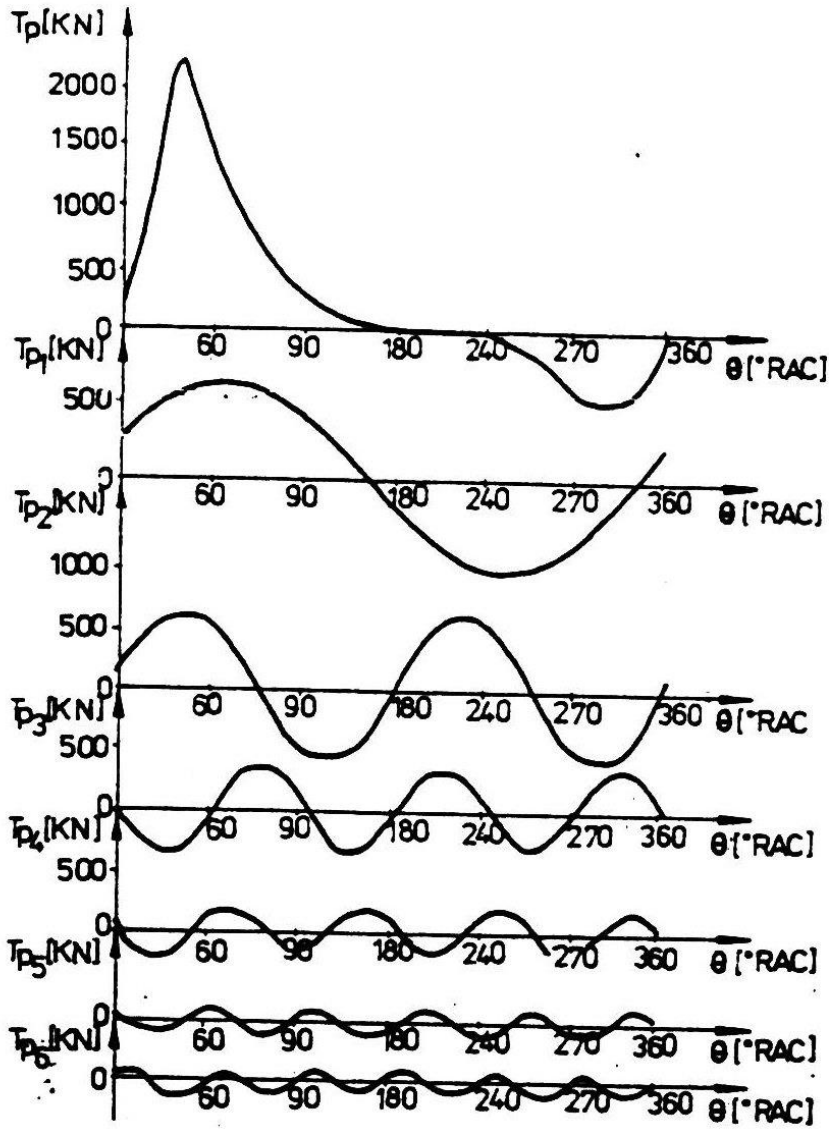

Figure 4.8: Rotational angle variation for the first 6 harmonic components of the tangential harmonics generated by gas pressure forces for a Sulzer 6RND90 main engine

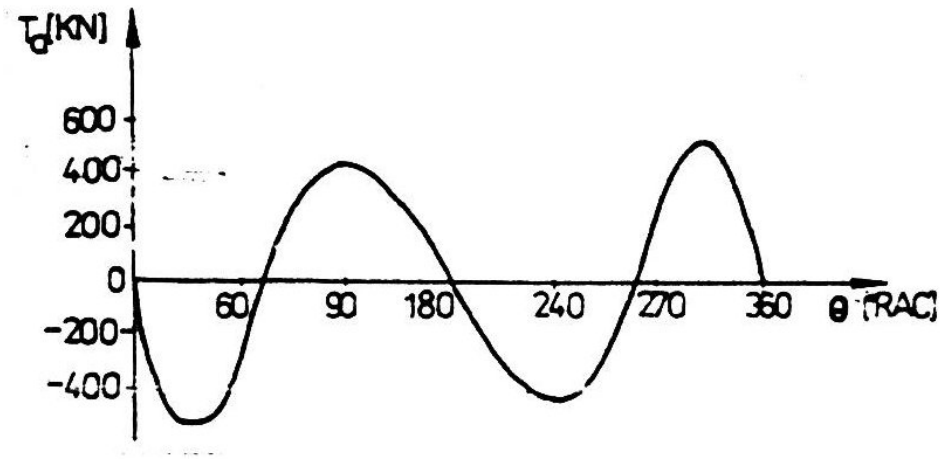

Figure 4.9: Rotational angle variation for tangential excitation generated by mass inertia for a Sulzer 6RND90 main engine

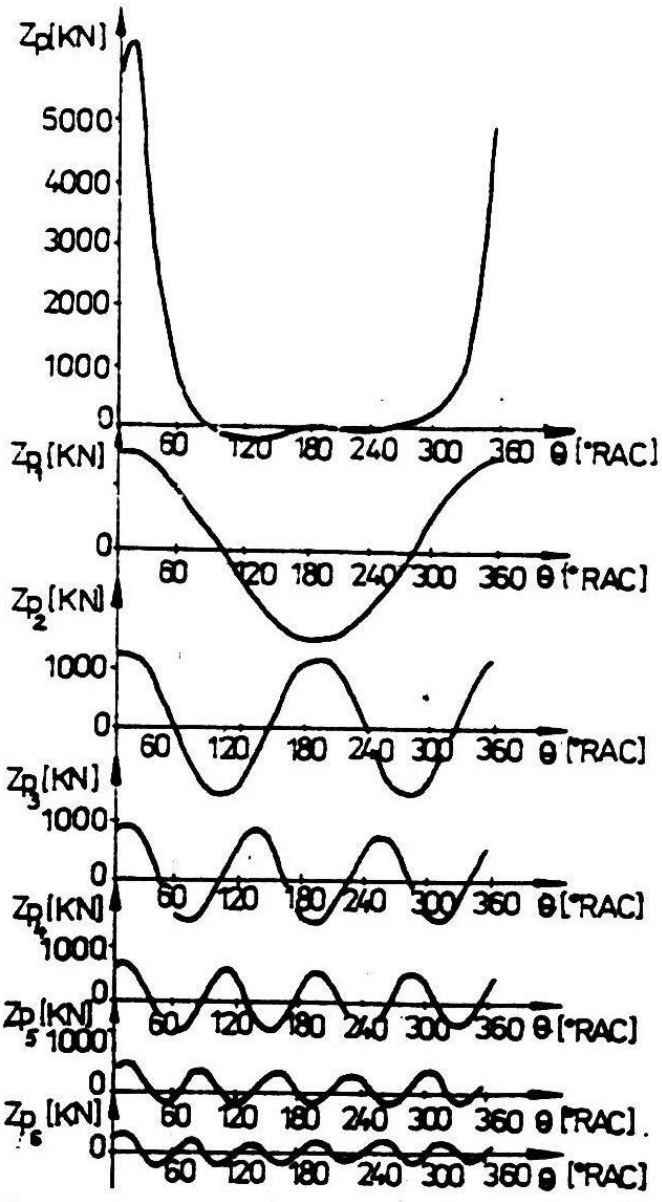

Figure 4.10: The rotational angle variation for the first 6 harmonic components of radial excitations generated by gas pressure

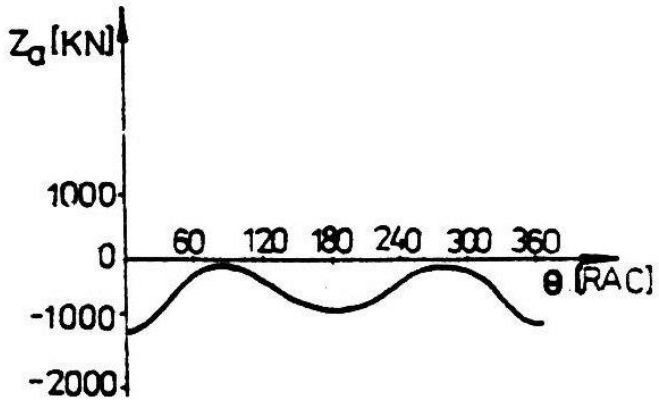

Figure 4.11: Rotational variation angle for the radial excitation generated by inertia forces

4.2.3 Axial vibrations excitations sources

Naval propeller induced excitations analysis, shaft line main source of axial vibrations, generated by the thrust bearing force variation, as it was previously shown, represents an important stage the present study, being a particular features for slow turning main engines.

The issue has been dealt with by applying the *propeller swirling model* due to the complexity level of it, that is why a higher amount of attention has been given to it.

The calculus of induce propeller excitations in the shaft line of a main engine that drives it is being based on the swirling horse shows models from which Prandtl has created the bearing line theory, this consisting in the idea of reduction of each individual profile of an finite hydrofoil to a single throw point, so, by replacing the hydrofoil with a single tied swirling, which is being placed on the point line equal with ¼ of the local string *c* of the mentioned hydrofoil, on the throw segment [-b/2, b/2], as it is presented in the 4.12 figure. According with the elements presented in the figure the swirling surface will be reduced, in this certain model, at a plane surface that contains all the free swirls being considered reciprocating, as well as parallel, but having an infinite upstream speed V and these elements are being deduced straight from the value of the throw segment and stretches to infinite downstream. The study of propulsive operation is based on the hydrofoil theory, thus, on the flow with a profile round circulation.

According to this model a system consisting of a finite number of propeller blades will be considered, each propeller blade could be considered as a resultant of the spinning around the Oz axis for the finite hydrofoil, as shown in the 4.12 figure. Thus, the propeller blade is being replaced with a tied swirls line, symbolized by Ω_p, interfering in reciprocal manner with the free swirls that are elapsed form the freeboard, this being of two types: free transversal swirls, Ω_{lt} and these have a perpendicular axis on the throw swirl and free longitudinal swirls, symbolized by Ω_p,

with an axis parallel with the axis of tied swirls. Those two types of swirls are generated by the propeller rotational force.

For the calculus of disc propeller induced speeds a propeller with a z_p number of propulsive blades will be considered and this system rotates with a ω angular speed towards the Oxyz Cartesian axis system, the origin being the same with the propeller center, while the Oxz axis has the propeller axis, according to the 4.13 figure. Thus a *P(x,y,z)* random space point is being considered in which the value for the swirling induced speed is being calculated using the Biot-Savart formula, mentioning the fact that the propeller operates in free waters, the current being uninterrupted. *I* symbolizes a random point on a d_{r1} element included on infinite thin line of free swirls. The cylindrical coordinates for the *I* point are $s,\ \psi tan\theta_j,\ \zeta,$ and the Cartesian ones are defined by $\xi,\ \eta$ and ζ. A corresponding point $J(s,\ \theta_j,\ 0)$ on the infinite element d_{rp} which is thin infinite for the tied swirls around the *j* propeller blade. The Cartesian coordinates of this point are: $s\ sin\theta_j,\ s\ cos\theta_j,\ 0$.

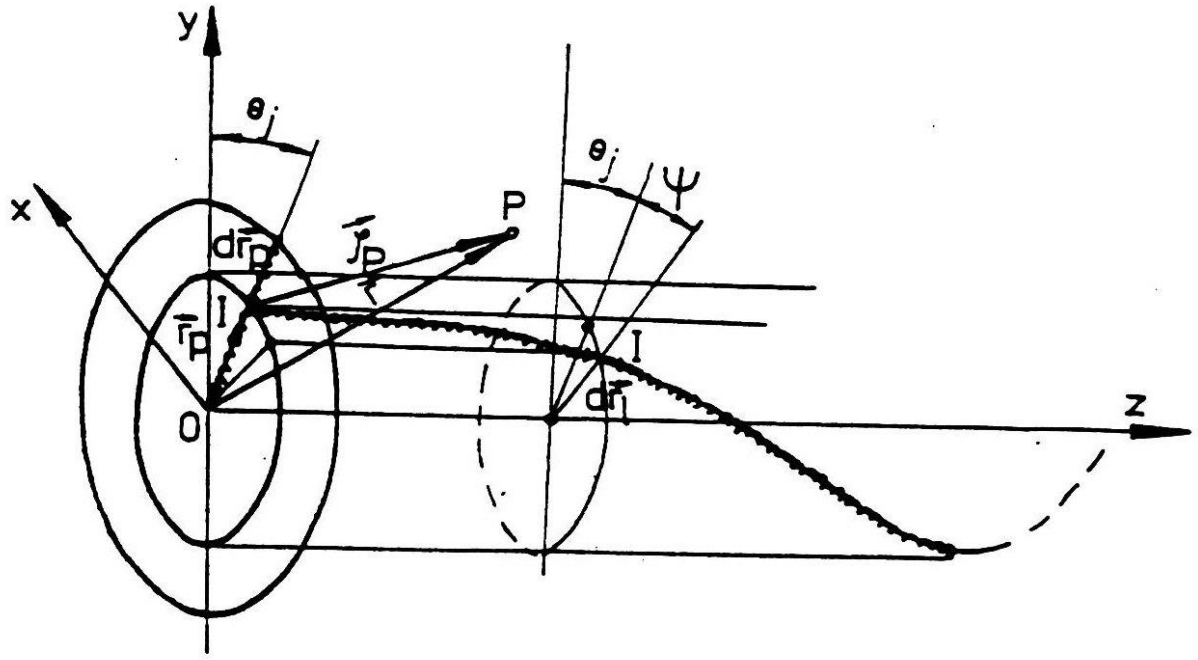

Figure 4.12: Rotational model for the propulsive propeller

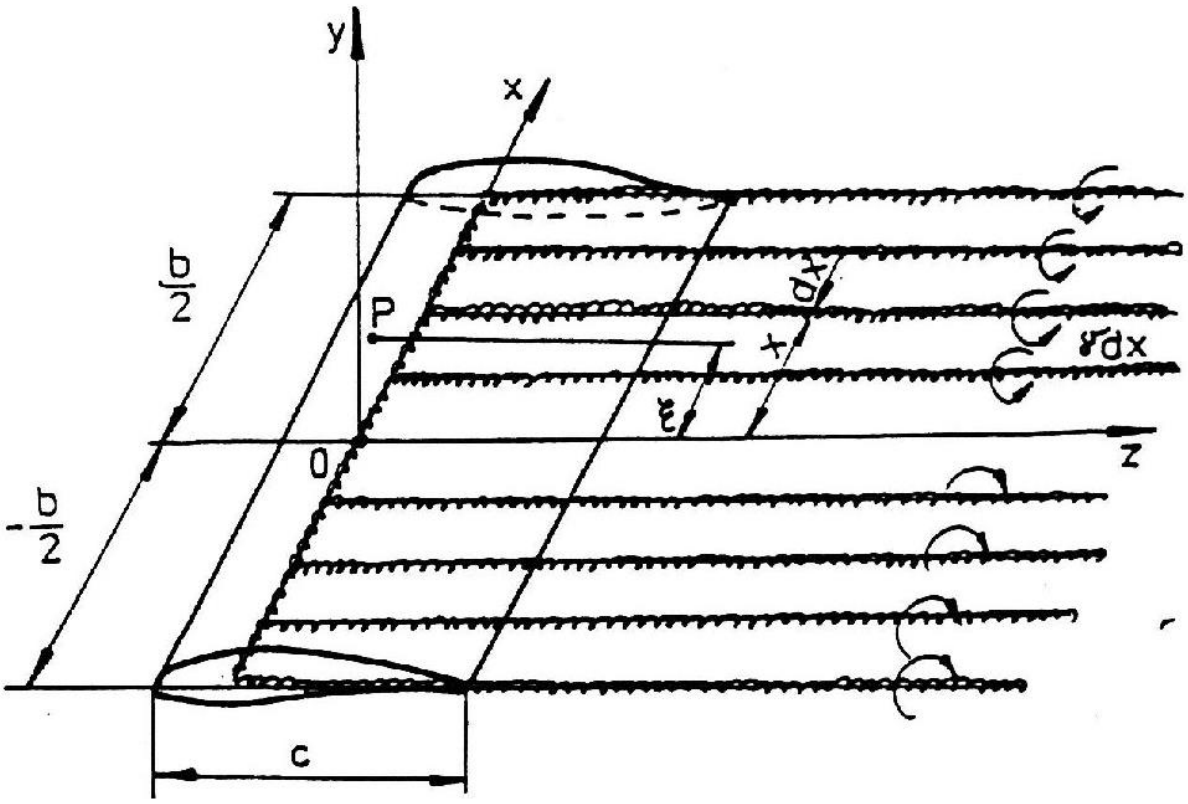

Figure 4.13: Rotational model for the finite hydrofoil

The real functioning process for the propeller on the hull aft part takes place in an ununiformed environment influenced by the hull itself. The propeller is being fitted in the aft part of the shape, the ship's body trace acts on it, and this was mentioned as wake in the 3.3 paragraph. This phenomenon hasn't been studied that much because it always has a random complex characteristic for its motion. In the study of marine propellers an important part is played by the starting phase of the wake, which acts on the immediate vicinity of the hull, the area where the propeller is being fitted. Thus the average flow speed in the propeller disc, symbolized by V' will be much smaller than the V speed of the ship toward the infinite upstream point (as shown in the above figure).

If we consider the swirling system as being connected to the propeller blade given by the motion function $\Gamma(r,\theta)$, r being the current radius and θ the rotational angle for the propeller functioning in an effective wake environment. The main

components for the induced speeds are symbolized by u_a and u_t. The angles highlighted in the 4.14 figure are:

- β – ideal speed V_0 angle with the plan of the disc propeller (*pitch angle*);
- β_{ind} – absolute speed V_R angle with the same plan (*induced angle*);
- i – resulting speed angle with the profile span (*incidence angle*);
- i_0 – null lift axis angle with profile span;
- δ – stall angle (*profile positioning angle*);
- δ_0 – null lift axis angle with the disc propeller plan;

In these conditions the resulting absolute force will be calculating applying the following formula:

$$V_R = V + \omega \, x \, r + u_t \quad (4.62)$$

The connecting formula between the modules of these speed values and angles, in the case of a propeller blade element at the current radius r, will be obtained at the junction between a coaxial cylinder with the propeller rotation axis and its own disc, given in the following formula:

$$\frac{u_a}{V^*} + \frac{u_t}{V^*} \tan\beta_{ind} = \frac{\tan\beta_{ind}}{\tan\beta} - 1 \qquad (4.63)$$

in the above formula w symbolizes the average wake coefficient which is calculated with the experimental methods mentioned in reference No. [10], depending on the global characteristic of a bulk-carrier ship with a 55000 tdw capacity, a common ship for the Romanian Commercial Navy fleet. These ships are usually fitted with a Sulzer main engine mentioned in the previous paragraphs, for which the thrust force is kept in mind while the ship is in operation through water with its speed V being reduced and this phenomenon is created by the wake effect. The basic issue consists in finding a model as real as possible. Thus, for the propeller operating in an uneven flow, a circulation fluctuation has to be taken into account, as it has been shown, defined by r radius as well as θ, known as the rotational angle, by generalizing the dependency formula on a single variable, linear for the Glauret proposed

circulation form, as mentioned in reference No. [43]. This allows us to generate the following formulas for the induced speeds:

$$u_a = \frac{1}{4\pi}\int_{R_b}^{R_e} \frac{\partial \Gamma(r,\alpha)}{\partial s}\frac{i_a}{r-s}ds, \qquad (4.65)$$

in the above formula i_a and i_t are axial and tangential integrating factors, which are approximated by applying Bessel functions using asymptotic functions, as noted in the No. [6] reference:

$$i_t = \begin{cases} z_p\left(\frac{s}{r}-1\right)B_2, for\ s > r \\ -z_p\left(\frac{s}{r}-1\right)(1-B_1) for\ s < r \end{cases}$$

as well as:

$$i_t = \begin{cases} z_p\left(\frac{s}{r}-1\right)B_2, for\ s > r \\ -z_p\left(\frac{s}{r}-1\right)(1+B_1) for\ s < r \end{cases} \qquad (4.67)$$

In the previous formulas the following notations have been made:

$$\mu = \frac{r}{s\tan\beta}; \mu_0 = \frac{1}{\tan\beta}. \qquad (4.68)$$

The resulting B1,2 coefficients from the previous developments have the following formulas:

$$B_{1,2} = \sqrt[4]{\frac{1+\mu_0^2}{1+\mu^2}}\left[\frac{1}{e^{z_p A_{1,2}} - } + \frac{1}{2z_p}\frac{\mu_0^2}{1+\mu_0^2}\ln\left(1+\frac{1}{e^{z_p A_{1,2}}-1}\right)\right], \qquad (4.70)$$

with:

$$A_{1,2} = +\_\left(\sqrt{1+\mu^2}-\sqrt{1+\mu_0^2}\right)\_ + \frac{1}{2}\ln\frac{\left(\sqrt{1+\mu_0^2}-1\right)\left(\sqrt{1+\mu^2}+1\right)}{\left(\sqrt{1+\mu_0^2}+1\right)\left(\sqrt{1+\mu^2}-1\right)}, \qquad (4.71)$$

The limitations conditions that have to be satisfied by the circulations are:

$$\Gamma\left(R_e, \theta_j\right) = \Gamma\left(R_b, \theta_j\right) = 0 \qquad (4.71)$$

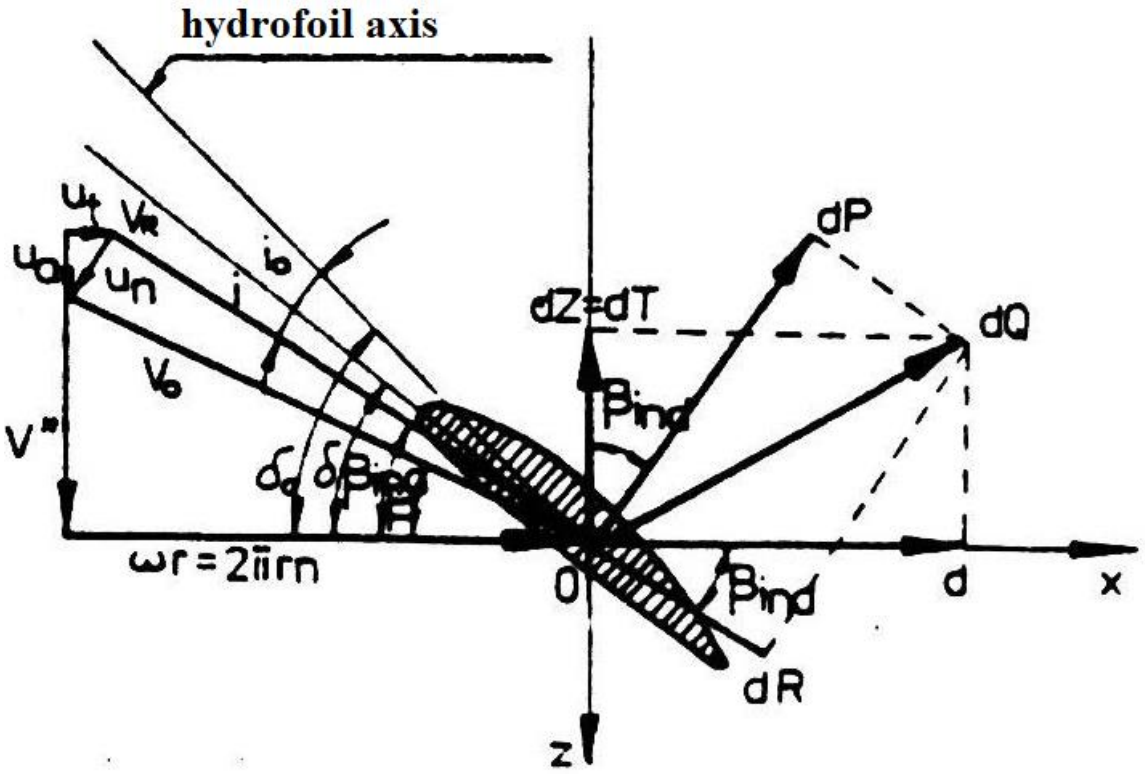

Figure 4.14: Elementary forces acting on the propeller

thus, for the integrating factors:

$$i_a = \begin{cases} 0\,, \quad for\ \frac{s}{r} \to 0 \\ \frac{z_p}{\tan\beta'}, \frac{s}{r} \to \infty \\ 1, for\ \frac{s}{r} \to 1 \end{cases} \qquad (4.72)$$

and:

$$i_a = \begin{cases} z_p, & for \frac{s}{r} \to 0 \\ 0, & \frac{s}{r} \to \infty \\ 1, & for \frac{s}{r} \to 1 \end{cases} \quad (4.73)$$

Further on the variable exchange will be taken place:

$$\begin{cases} r = \frac{1}{2}(R_e + R_B) - \frac{1}{2}(R_e - R_b)\cos\tau \\ s = \frac{1}{2}(R_e + R_b) - \frac{1}{2}(R_e - R_b)\cos\sigma, \end{cases} \quad (4.74)$$

Thus the variation domain for *r* and *s* being *[R_b, R_e]*, the new coordinates τ and σ will be in the domain *[0, π]*, the first variable is defining the radius position for the point for which the induced speed value is being calculated, while the two position for the point for which the free swirl is being generated. R_e and R_b are the radius values for the propeller disc, as well for the radius of the propeller hub. In order to ease the calculus the dimensionless values will be introduced:

$$G(s,\theta) = \frac{\Gamma(s,\theta)}{2\pi R_e V^*}; \bar{r}_b = \frac{R_b}{r_e}; a = \frac{\pi}{2(1-\bar{r}_b)} \quad (4.75)$$

the first notation in the above formula denotes the dimensionless circulation, while the second one the dimensionless radius of the propeller hub. For the first dimension the following variation law will be proposed, based on the previous presented features:

$$G(r,\alpha) = G(\sigma,\alpha) = \sum_{k=1}^{\infty} G_k(\alpha)\cos k\alpha, \quad (4.76)$$

for the $G_k(\theta)$ coefficients the following trigonometrical sums will be proposed:

$$G_k(\alpha) = \sum_{j=1}^{k} g_j \sin j\alpha. \quad (4.77)$$

The integrating factors can also be developed in a Fourier set through the new variable values introduced by the (4.74) formula:

$$i_{a,t}(\tau,\sigma)=\sum_{i=1}^{\infty} I_{a,t_i}(\tau)\sin i\sigma. \quad (4.78)$$

By limiting the radius domain value, as well as the sectioning ones for the propeller blades taken into the calculus, r_k and s_i, due to practical reasons, at a *2n* number, as well by introducing the variable change from the (4.74) in the (4.66) and (4.67) formulas we can say that the (4.78) formula is a linear system with a *2n* number of equations for the *2n* values generated for *2i*, having an equation system with *2n* unknowns, $I_{a,t}$ for each value of $k = 1–n$.

By introducing the integrating factors previously obtained in the (4.65) formula, as the dimensionless circulation (4.75) and the new variables the formulas for the induced speeds in the disc propeller will be obtained:

$$\frac{u_{a,t}(\tau,\alpha)}{V^*}=a\sum_{i=1}^{n}\sum_{k=1}^{n} u_{a,t_{k,i}}\sin k\alpha\frac{\sin i\tau}{\sin\tau}. \quad (4.79)$$

for which the $u_{a,t}$ coefficients are given by the following formula:

$$u_{a,t_{k,i}}=(S_n-S_{k-1})\,g_k\,h_{a,t_i}(\tau), S_k=\sum_{j=1}^{k} j=\frac{k(k+1)}{2}, k=\overline{1,n}. \quad (4.80)$$

with the values calculated in the (4.79) formula and the induced speeds, as well as the h_{at} coefficients given by:

$$h_{a,t_i}(\tau)=\begin{cases} I_{a,t_{n+i}}(\tau)-I_{a,t_{n-i}}(\tau), i=\overline{1,n-1} \\ I_{a,t_{2n}}(\tau), i=n. \end{cases} \quad (4.81)$$

thus, the (4.63) has the following form:

$$\sum_{i=1}^{n}[h_{a_i}(\tau)+\tan\beta_{ind}\,h_{t_i}(\tau)]\sin i\tau\bullet\sum_{k=1}^{n}(S_n-S_{k-1})\,g_k\sin k\alpha=\frac{\sin\tau}{a}\left(\frac{\tan\beta_{ind}}{\tan\beta}-1\right), \quad (4.82)$$

the above formula is a *n* unknown equation, with g_k and $k = 1 - n$. In order to solve it the θ coefficient takes the following value: $\theta = \theta_0$ and the τ angle takes *n* values (thus for the *r* radius), for which the β (pass ratio) angle values are calculated in an according manner, as well as the values for the β_{ind} angles (using the inductive efficiency values η_{ind}):

$$\tan\beta_{ind} = \frac{V^*}{\omega r_k};\tan\beta_{ind_k} = \left(\frac{\tan\beta}{\eta_{ind}}\right)_k;\eta_{ind_k} = \eta_H \eta_{0_k} \qquad (4.83)$$

in the above formula η_E is the influence coefficient induced by the hull and can be calculated by applying the experimental formulas from the reference No. [43], while η_0 is the propeller efficiency in free waters (with interrupted flow), which is calculated using the set of diagrams for the studied propeller.

In the same time the calculated coefficients for dimensionless circulation can be calculated by applying the (4.79) formula, as well as the induced speed field, thus the radius circulation distribution and the rotation angle can be calculated by applying the propeller momentum formula:

$$M_e = z_p \rho \int_{R_b}^{R_e} \Gamma(r,\theta)(V^* + u_a) r dr = \frac{\pi}{2} z_p \rho V^{*2} R_e \left(R_e^2 - R_b^2\right) I_1 - \frac{\pi}{4} z_p \rho V^{*2} R_e \left(R_e - R_b\right)^2 I_2$$

(4.84)

for which the integrative values have the following formulas:

$$I_1 = \int_0^{\pi} G(\tau,\theta)\left[1 + \frac{u_a(\tau,\theta)}{V^*}\right]\sin\tau d\tau = m_0 + \sum_{k=1}^{n} m_k \sin\left(k\theta + \varphi_{m_k}\right) \qquad (4.85)$$

and:

$$I_1 = \int_0^{\pi} G(\tau,\theta)\left[1 + \frac{u_a(\tau,\theta)}{V^*}\right]\sin\tau d\tau = m_0 + \sum_{k=1}^{n} m_k \sin\left(k\theta + \varphi_{m_k}\right) \qquad (4.86)$$

m_k and n_k coefficients, as well as $k = 0 - n$ are calculated by applying the principle of dimensionless circulation coefficients and induced speeds by effective solving the integrating equations above.

For this, we use the following notations:

$$\begin{cases} \zeta_0 = 2(1+\bar{r}_b)m_0 - (1-\bar{r}_b)n_0 \\ \mu_k = 2(1+\bar{r}_b)m_k \\ \nu_k = (1-\bar{r})_b)n_k, k = \overline{1,n}, \end{cases} \quad (4.87)$$

$$\begin{cases} \gamma_k = \mu_k \cos\theta_{m_k} - \nu_k \cos\theta_{n_k} \\ \delta_k = \mu_k \sin\theta_{m_k} - \nu_k \sin\theta_{n_k}, k = \overline{1,n}, \end{cases} \quad (4.88)$$

and:

$$\begin{cases} \zeta_k = \sqrt{\gamma_k^2 + \delta_k^2} \\ \theta_{e_k} = \arctan\dfrac{\delta_k}{\gamma_k}. \end{cases} \quad (4.89)$$

as well as the additional notations:

$$\begin{cases} M_{e0} = \dfrac{\pi}{4} z_p \rho V^{*2} R_e^3 (1-\bar{r}_b)\zeta_0 \\ \_M_{e_k}\_ = \dfrac{\pi}{4} z_p \rho V^{*2} R_e^3 (1-\bar{r}_b)\zeta_k, k = \overline{1,n}. \end{cases} \quad (4.90)$$

Finally the resistant momentum formula will be obtained for the studied propeller, as a Fourier development set. If we limit this only at the first n terms, this will be expressed as:

$$M_e = M_e(\alpha) = M_{e0} + \sum_{k=1}^{n} \_M_{e_k}\_ \sin(k\alpha + \theta_{e_k}) = M_{e0} + \sum_{k=1}^{n} M_{e_k}. \quad (4.91)$$

In a similar manner we can calculate the force variation for the thrust force developed by the propeller:

$$T = z_p \rho \int_{R_b}^{R_e} \Gamma(r,\theta)(\omega \ r - u_t) dr \qquad (4.92)$$

or by applying the following development set:

$$T = \frac{\pi}{2} z_p \rho V^* \omega R_e \left(R_e^2 - R_b^2\right) I_3 - \frac{\pi}{4} z_p \rho V^* \omega R_e \left(R_e - R_b\right)^2 I_4 - \pi z_p \rho V^{*2} R_e \left(R_e - R_b\right) I_5 \qquad (4.93)$$

The above integrative equations are solved in separate manner, this generating the following formulas:

$$\begin{cases} I_3 = \int_0^{\pi} G(\tau,\theta) \sin \tau d\tau = \sum_{k=1}^{n} a_k \sin k\theta \\ I_4 = \int_0^{\pi} G(\tau,\theta) \sin 2\tau d\tau = \sum_{k=1}^{n} e_k \sin k\theta \\ I_5 = -\frac{d}{2}\left(w_0 + \sum_{k=1}^{n} w_k \sin k\theta\right) \end{cases} \qquad (4.94)$$

for which the harmonic coefficients are calculating by applying the indicated procedure for the ones specific to the momentum.

With the additional notations:

$$\begin{cases} T_0 = \frac{\pi^2}{4} z_p \rho V^{*2} R_e^2 w_0 \\ \eta_k = \frac{\pi}{2} z_p \rho V^* \omega R_e^3 \left(1 - \bar{r}_b^{\,2}\right) a_k \\ \sigma_k = \frac{\pi}{4} z_p \rho V^* \omega R_e^3 \left(1 - \bar{r}_b\right)^2 e_k \\ \vartheta_k = \frac{\pi^2}{4} z_p \rho V^{*2} R_e^2 w_k, k = \overline{1,n}. \end{cases} \qquad (4.95)$$

and with the resultant expressions for the module and the initial phase expressed as:

$$\begin{cases} |T_k| = \sqrt{(\eta_k - \sigma_k)^2 + \vartheta_k^{\,2}} \\ \varphi'_{e_k} = \operatorname{atan}\dfrac{\vartheta_k}{\eta_k - \sigma_k}, k = \overline{1,n} \end{cases} \qquad (4.96)$$

The harmonic analysis for excitations generated by the thrust force of the propeller will be:

$$T = T(\theta) = T_0 + \sum_{k=1}^{n} |T_k| \sin(k\theta + \varphi'_{e_k}) = T_0 + \sum_{k=1}^{n} T_k \qquad (4.97)$$

In the previous formulas ρ symbolizes the water density, while the harmonic order k is a reference at the propeller rotation period:

$$T_e = \frac{2\pi}{z_p} \qquad (4.98)$$

For the presented propeller being driven by the Sulzer RND90 main engine for which the free vibrations calculations have been presented in the for 4.1 paragraph, having the propeller diameter equal to 6,4 meters and being fitted with 4 propeller blades, tests have been carried out on the ship model at a 1:30 scale, in the cavitation tunnel. The measurement section had a 3 meters length, water speed was 6 m/s. The ship hull model has been made out form fiber glass enforced polyester and the propeller model has been made out of aluminum. In this manned the distribution of speeds in the propeller disc, starting from which the thrust force and the momentum have been calculated by integrating these distributions. This method is purely theoretical-experimental. The measurements also continued by calculating the propeller induced excitations on the exact model by using a complex installation and its diagram has been presented in the 4.15 figure.

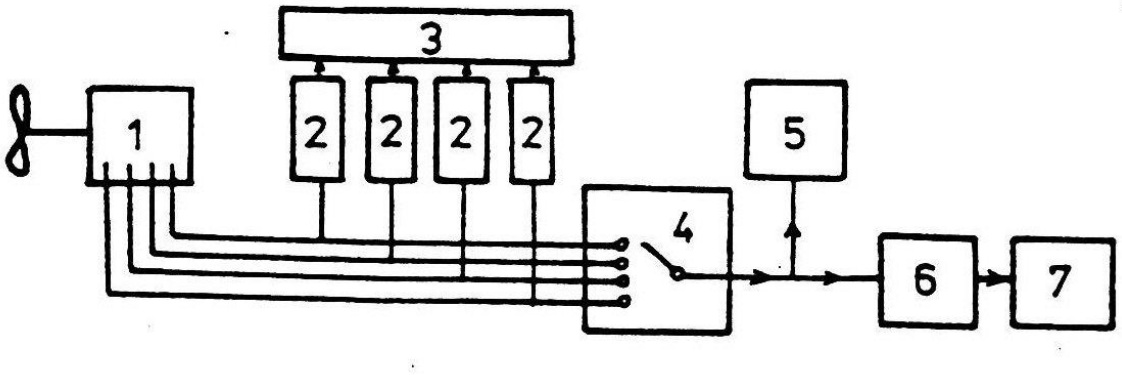

Figure 4.15: Measurement chain diagram for induced excitations by the propeller in the shaft line

The components presented in the above figure are listed below:

1 – H-44 dynamometer;

2 – DA 3414 HBM amplifier;

3 – D 300 Kienzle printer;

4 – Switcher;

5 – HP-1220 oscilloscope;

6 – Dynamic analyzer for 2120 B&K specter;

7 – 2307 B&K recorder;

In the below tables, 4.8 and 4.9 the results of calculations made in the basis of this analytical method have been presented, as well as the ones made on the model, while the 4.16 and 4.17 figures present the variations of crank angle for shaft line excitations induced by the propeller for the above mentioned engine, in comparison with the measurements made on the model.

Table 4.8: Shaft line calculated excitations modules and phases induced by the propeller

k	$\lvert M_{e_k} \rvert$ **[kNm]**	φ_{e_k} **[rad]**	$\lvert T_k \rvert$ **[kN]**	φ'_{e_k} **[rad]**
1	21.52976	0.35145	31.42708	0.43692

2	4.00369	0.72219	7.37728	-1.11682
3	3.75362	-1.19870	5.44444	-0.14334
4	1.47499	-1.12340	2.71710	-0.96497
5	0.92748	1.37264	2.34912	-1.33242
6	0.59780	-0.09851	1.21430	1.28976

Table 4.9: Shaft line measured excitations modules and phases induced by the propeller

k	$\lvert M_{e_k} \rvert$ **[kNm]**	φ_{e_k} **[rad]**	$\lvert T_k \rvert$ **[kN]**	φ'_{e_k} **[rad]**
1	24.20741	0.83240	32.26122	0.47213
2	3.50012	0.80263	6.00541	-1.46412
3	2.98531	-1.10824	4.97780	-0.25139
4	1.10025	-1.15824	2.63916	1.05412
5	0.81088	1.15824	1.98251	-1.05412
6	0.25452	-0.10624	1.20045	1.29467

The comparison between the measured and calculated variations for excitations induced by the propeller in the shaft line of the considered main engine towards the average value of effective dimensions is given in the 4.10 table.

The notations made in the 4.10 table are $\Delta T = T_{\max} - T_{\min}$ and $\Delta T = T_{\max} - T_{\min}$.

Table 4.10: Comparison between calculated values and measured ones for the propeller induced excitations

Load type	**Realized**	**Recommended**	
		Bureau Veritas	ITTC*81
$(\Delta T)_{calc} / T_0$	5.22 %	2÷12 %	1÷..5 %
$(\Delta M_e)_{calc} / M_{e0}$	5.20 %	3÷12 %	1÷5 %
$(\Delta T)_{măs} / T_0$	5.80 %	2÷12 %	1÷5 %
$(\Delta M_e)_{m\_s} / M_{e0}$	7.65 %	3÷12 %	1÷5 %

* The 16th International Towing Tank Conference

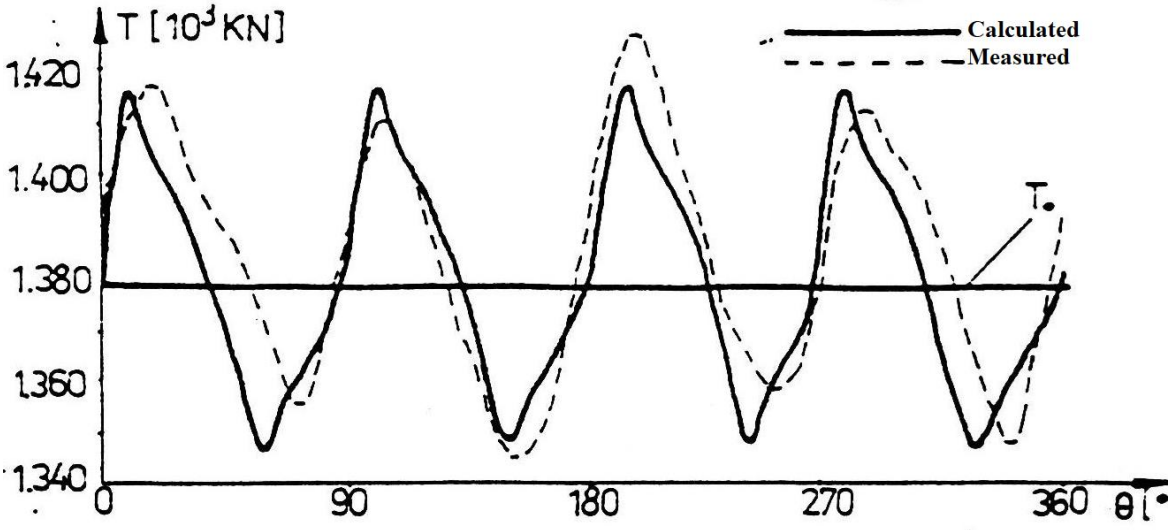

Figure 4.16: Graphic variation of thrust force depending on the rotation angle

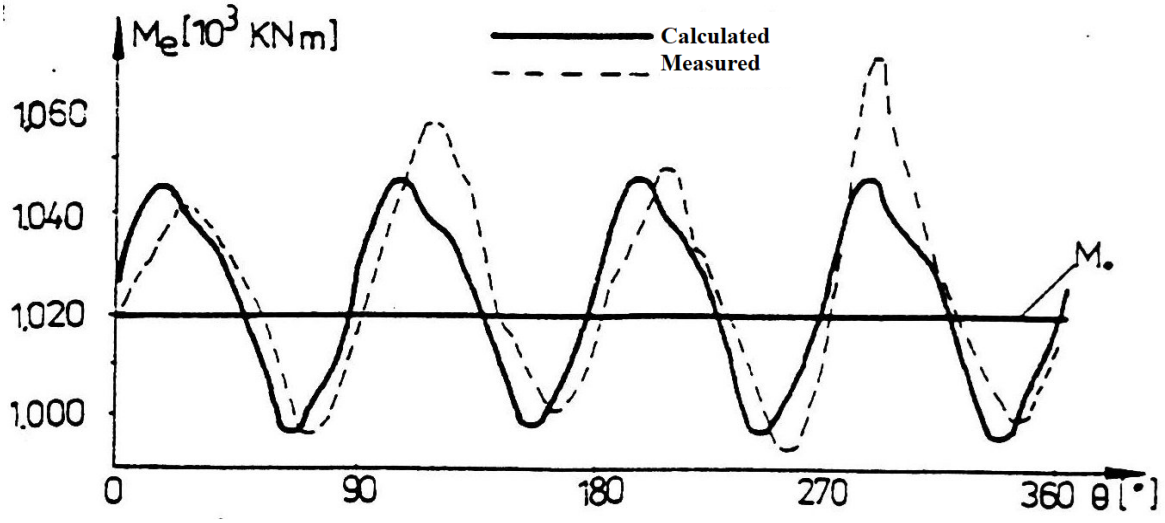

Figure 4.17: Graphical variations for the propeller momentum depending on the rotation angle

Variations have been recorded for harmonic amplitudes with predominant orders, *k = 1* and *k = 2*, these representing 2.11% and 0.0004 % for propeller

momentum, as well as 2.28% and 0.0005% for the thrust force towards the average values of these dimensions, in comparison with the average values equal to 3.16% and 0.005% and 5.80% and 0.005% for the same measured dimensions.

It can be noticed that variations are very close in value for the results obtained after the analytical calculus and the measured values, all values being in the range recommended by the *Bureau Veritas* naval register [103]. This is a classification society that owns one of the most important data base regarding the vibration field onboard merchant ships.

Thus, the obtained results applying the analytical calculus can be considered a basis for the next undertaken study.

4.3 Shaft line forced vibrations for marine main engines

The analysis of shaft line excitations for marine main engines previously made allows the calculus of forced vibrations for these ones. Thus, tangential forces stimulate torsional vibrations, while the radial ones stimulate the bending vibrations, while the ones induced by the propeller mainly stimulate axial vibrations of shaft lines.

The first two excitation types are generated in the hypothesis of geometrical and mass identity of engine drives which are characteristic for each engine cylinder and this hypothesis is currently being accepted because there are any significant difference in real cases. Additional, presented methodologies take into account the individual evolution of fluid engine in every cylinder.

The 3rd excitation category, the ones induced by the propeller in the shaft line, have been calculated applying an analytical method with the condition of knowing the geometrical and functional characteristics of the certain propeller. The main working hypothesis applies the ideal flow characteristic taking into account that all swirling nets are free and are helicoidally perfect in an upstream infinite domain, because they override only the first area, where the propeller is being fitted. Using the shape considered for the speed distribution and the flow model the fact that propeller is fitted in the aft part of the hull is taken into account.

In the following paragraphs, in the first phase the calculus of individual vibrations will be studied, according with the one made in the 4.1 paragraph.

The undertaken study presents and important interest for the calculus, numerical methods being applied for coupled vibrations of shaft lines, while in the 4.4 paragraph all excitation types will be applied for the propulsion system model.

4.3.1 Forced torsional vibrations for marine main engine shaft lines

For a start, the example of the mono-cylindrical engine presented in the 1.2.2 and 4.1.1 paragraphs, as well as the one presented in the 1.18 figure, will be used. The system response at forced torsional vibrations are a practical solution for the entire motion equation system as presented in the (4.3) and (4.5) formulas, obtained by including the excitation term from the right part. If the 2nd excitation term is constant, in the first one two excitation sources will be included and these ones are generated by the gas pressure effect and the inertial effects through the centripetal coefficient.

Thus, the first term will be expressed by the following formula:

$$p(\omega\tau)A_p c_{w_p}(\omega\tau) = RT_p = R\left(T_{p_0} + \sum_{k=1}^{\infty} T_{p_k}\right) \qquad (4.99)$$

in the above formula T_{p0} is given by the (4.45) formula and T_{pk} is given by the 4.46 formula. It has to be mentioned that $p(\theta) = p(\omega\tau)$ factor is being developed in a Fourier set as in (1.97) formula and it depends on the specific rotational speed and the load applied on the engine. Thus, for a complete analysis of torsional vibrations the harmonic coefficients presented in 4.2.1 and are variable depending on the operation conditions.

As it has been shown in the 4.1.1 paragraph, the centripetal stiffness coefficient has been linearized, being obtained by the right member of the first motion equation:

$$C(\omega\tau)\omega^2 = R\sum_{k=1}^{\infty} T_{a_k} \qquad (4.100)$$

while T_{ak} is given by the (4.48) formula, still with a harmonic sum. R remains the crank radius.

Having in mind all these notations, the vibrating motion of those two discs that are simulating the real oscillatory system will be given by the formula given in the references No. [15], [25] and [94]:

$$\theta_j = \sum_{k=1}^{\infty} \left(C_{k_j} \cos k\omega + D_{k_j} \sin k\omega\tau \right) \quad (4.101)$$

The complete study of torsional vibrations on the shaft line is being presented in a diagram manner as in the 4.1.1 chapter, by means of a multidimensional flexible system which contains equivalent discs for engine drives, flywheel and propeller having the purpose of calculating the own pulsation regime and own vibrations shapes into the system. Keeping in mind the excitations generated by the engine and the propeller, on the bases of the model presented in 4.18 we can calculate forced torsional amplitude vibrations which can occur at different operational regimes.

The first stage, the one in which own vibrations modes acting on the shaft lines are calculated, is being accomplished by applying the *Holzer-Tolle method*, that allows us the calculate the excitation degree for certain harmonic elements for engine momentum by expressing their capacity of generating torsional vibrations on shaft lines. In this manner the own pulsation with a 1st degree has been calculated as ω_{OI} = *46,351* s^{-1}, which is very close to the valued measured during sea trials, as ω_{OI} = *48,380* s^{-1}. The mentioned values are available for the same type of main engine kept under surveillance, being the same one as in the case of free vibrations, a Sulzer 6RND90 marine main engine.

Θ_{kj} symbolizes the relative amplitude of own torsional vibrations for all discs simulating engine drives and θ_{kj} is the off-set between the excitatory momentum with an k harmonic order acting on the j order disc and the torsional vibration for the first disc, tied up in between by the following formula:

$$\theta_{k_j} = k\,\theta_j \quad (4.102)$$

in the above formula θ_j symbolizes the angle between the crank with a j order and the cylinder axis facing it. In this way the excitation degree seen as a dimension of k order harmonic component for the engine moment will stimulate forced torsional vibrations on the shaft line of the above mentioned engine as:

$$E_k = \sqrt{\left(\sum_{j=1}^{i}\Theta_{k_j}\sin\theta_{k_j}\right)^2 + \left(\sum_{j=1}^{i}\Theta_{k_j}\cos\theta_{k_j}\right)^2} \qquad (4.103)$$

this having a graphic representation in the 4.20 figure. In the previous formulas, *I* symbolizes the cylinder number, while *n* symbolizes the total discs number from the equivalent oscillatory system of the shaft line. On this basis forced torsional vibrations for the free end calculus using the approximate energetic method [91] will lead, in the first phase, to the angular static deformation given by the (4.104) formula, in which $\omega_{0\gamma}$ represents the own pulsation with an γ degree, while J_j are the mechanical inertia momentum for all oscillating equivalent system discs shown in the 4.18 figure:

$$\Theta_{s_{k1}} = \frac{|M_k|E_k}{\omega_{0_\gamma}^{\ 2}\sum_{k=1}^{n}J_j\Theta_{k_j}^{\ 2}} \qquad (4.104)$$

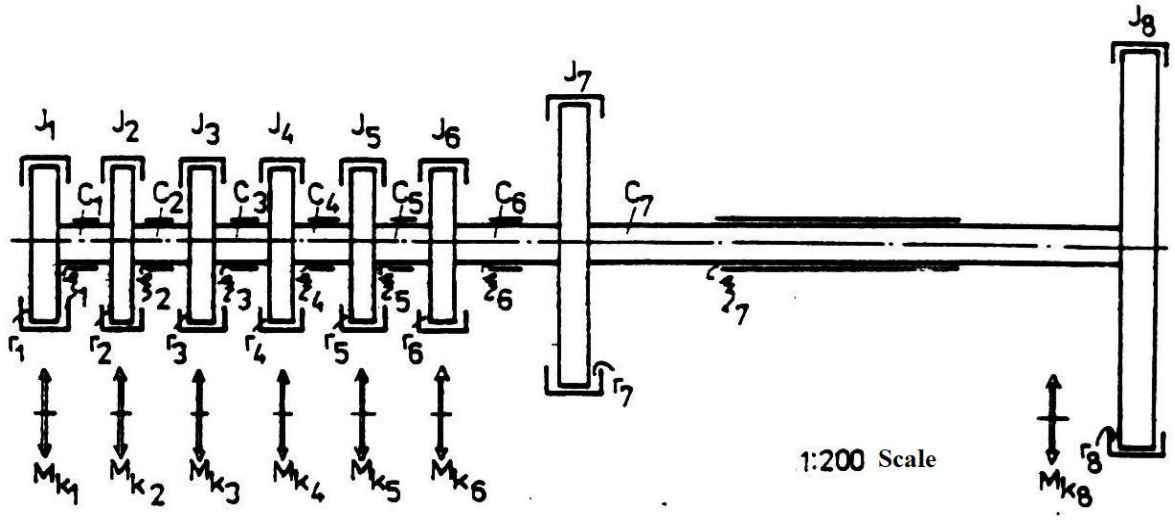

Figure 4.18: Equivalent oscillating system for Sulzer 6RND90 main engine with the diagram of excitation momentum and all the compensations

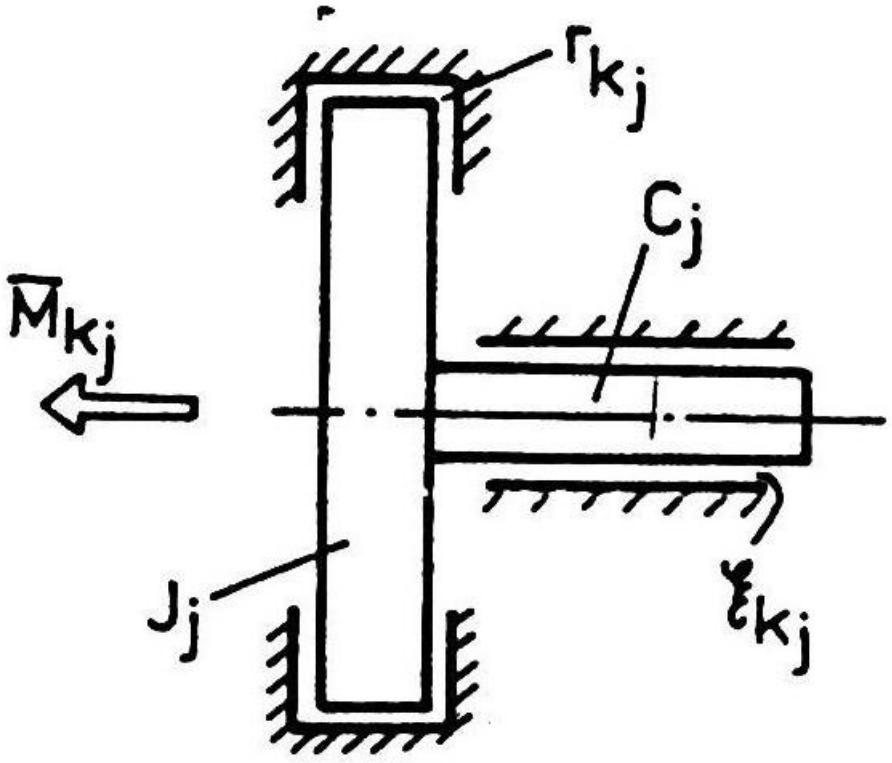

Figure 4.19: Flexible disc-section element diagram from a flexible equivalent oscillating system

From this representation, vibration amplitude at shaft line free end has been calculated by applying the dynamic amplifier A_k mentioned in different methodologies [91] with the following formula:

$$\Theta_{k_1} = A_k \Theta_{s_{k_1}} \qquad (4.105)$$

the calculus formula being valid only for the harmonic component of the engine momentum that can generate resonance in the operation regime range close to

the normal engine functioning regime: $k = \left[\frac{30}{\pi\omega_{01}}\right] \Big/ n_n \cong 4$, n_n being the nominal rotation speed (122 rpm). For all harmonic components of the engine momentum that don't act in the rotation range of the engine, the compensation effect can be neglected, thus allowing the calculus for torsional amplitude vibrations to be done by applying the Holzer methodology, as mentioned in the No. [89]. That is why the theoretical bases and the calculus results for amplitude torsional vibrations which are forced compensated will be presented by applying fast calculus methods, such as the *transfer matrix method [MMT]*.

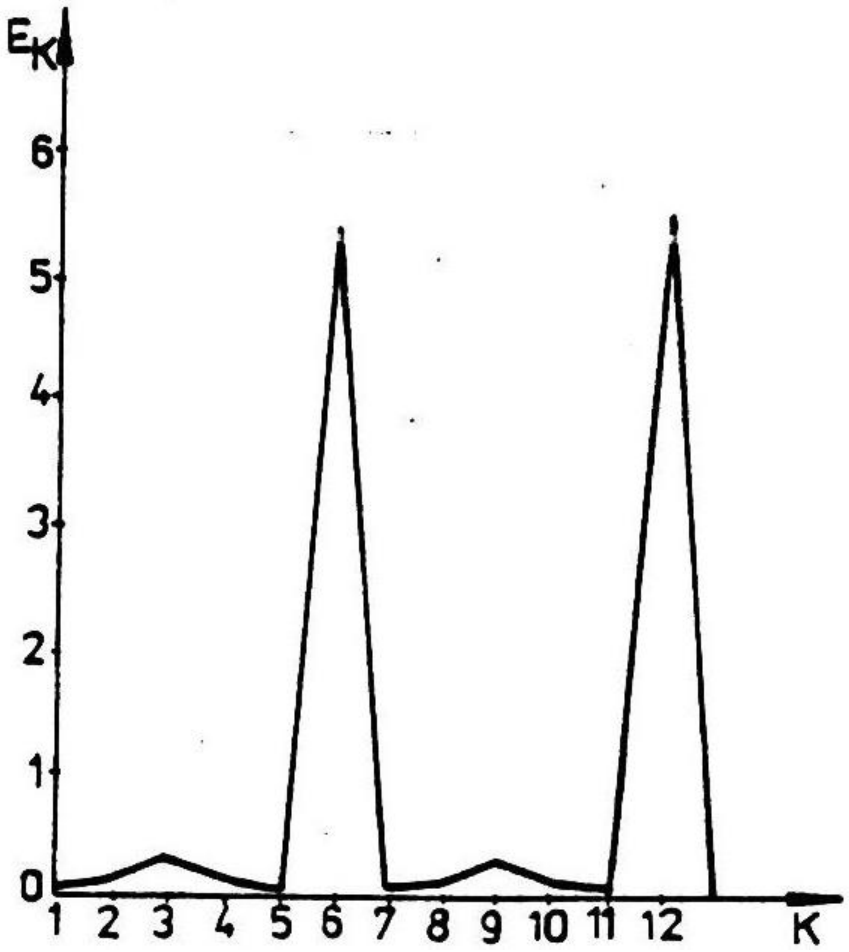

Figure 4.20: Harmonic order excitation variation degree

The general motion for the entire equivalent system from the 4.18 figure can be written as a matrix:

$$[J]\{\theta\} + [\xi]\{\theta\} + [C]\{\theta\} = \{M\} \qquad (4.106)$$

according with the general equation (3.1) applied on the torsional vibrating phenomenon. *[J]* is the diagonal matrix of mechanical inertia momentum which are being reduced at the rotational axis, *[ξ]* is the band matrix of all compensating coefficients in the shaft lines, *[C]* is the torsional stiffness matrix for all sections between two discs, *{M}* and *{θ}* are the column vectors for excitation moments and the ones for the torsional deformations.

If we isolate a random disc with a J order along with the flexible section without a mass as shown in the (4.19) figure we will take into account the compensation in the piston-cylinder group, in the crankpins of a single crank, as well as the compensation on the flywheel and on the propeller disc and by applying the experimental formulas form reference No. [91], the following formula will be obtained:

$$r_{cil_j} = 0.01\omega_{0_1} J_{cil_j}; \xi_{lag_k} = \frac{0.2k + 0.6}{100}\omega_{0_1} J_{cil}; r_{vol_k} = \frac{0.001}{k}\omega_{0_1} J_{vol}; r_e = 30\frac{M_{e_0}}{n} \qquad (4.107)$$

where J_{cilj} can take any value in the range *1 – 6*, $J_{vol} = J_1$, M_{e0} is the average momentum developed by the propeller and *k* is harmonic order, while *n* is the propeller rotation (equal with the one of the engine). The values calculated are being concentrated in the 4.11 and 4.12 table.

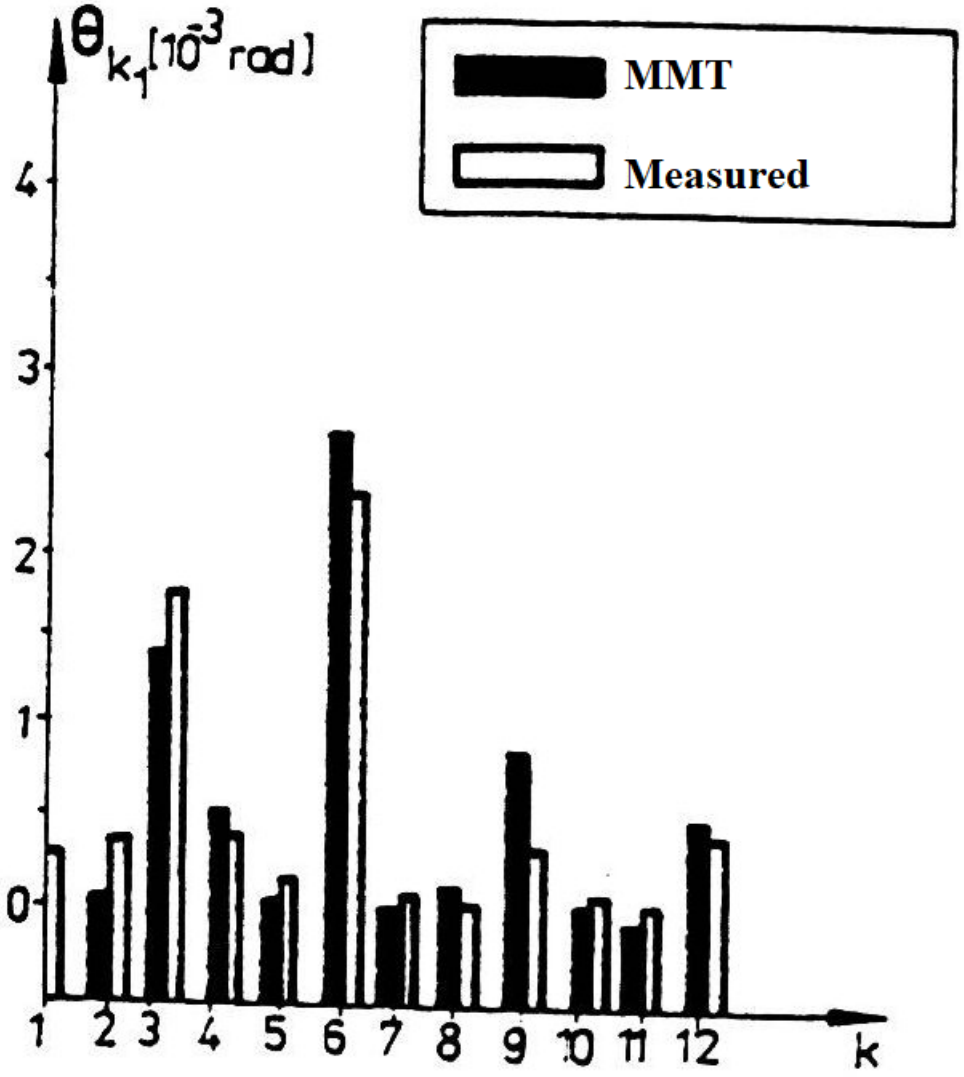

Figure 4.21: Free end torsional vibration amplitude variation at a free end for the engine with a harmonic order

The excitation momentum with a *k* order acting on the *j* disc has a similar force equal with the one given in the (4.50) formula, multiplied by the value of the crank radius *R*.

Table 4.11: Mass and torsional stiffness characteristics for the equivalent oscillating system

Disc number	J_j [Nms^2]	C_j [10^{9}Nm]	r_j [Nms]		
1	8290.0	1.1568	3842.5437		
2	8046.2	1.1568	3729.5387		
3	8046.2	1.1568	3729.5387		
4	8046.2	1.1568	3729.5387		
5	8046.2	1.1568	3729.5387		
6	8290.0	0.7235	3842.5437		
7	4293.9	0.0784	k	1	1990.2
				2	99.5
				3	66.3
				4	49.7
				5	39.8
				6	33.1
				7	28.4
				8	24.8
				9	22.1
				10	19.9
				11	18.0
				12	16.5
8	73120	-	243909.84		

By introducing the term with the 1st order derivative in the matrix equation (4.106) the calculus leads in an automatic manner to the extension of the Holzer procedure in the complex plan, which can be algorithmised in an elegant and compact way, by applying the transfer matrix procedure. The extension in the complex plan also imposes the complex shape of simulating components for engine momentum, as they are given in the above (4.19) figure, as it follows:

$$\overline{M_{k_j}} = M_{k_j}^{Re} + i\, M_{k_j}^{Im}, i = \sqrt{-1}, \qquad (4.108)$$

for which the real and imaginary parts obtained by equation identification (4.50) is written for a stimulating momentum by multiplying each member with the crank radius, with the following formula:

$$M_{k_j} = Re(\overline{M_{k_j}} e^{i\alpha}), \quad (4.109)$$

and they will have the following expressions:

$$M_{k_j}^{Re} = A_{p_{k_j}} \cos kn_j \delta - (B_{p_{k_j}} + B_{a_k}) \sin kn_j \delta, \quad (4.110)$$

as well as:

$$M_{k_j}^{Im} = - A_{p_{k_j}} \sin kn_j \delta - \left(B_{p_{k_j}} + B_{a_k}\right) \cos kn_j \delta. \quad (4.111)$$

Table 4.12: Compensating coefficients in the crankpins for engines depending on the harmonic order

k	**1**	**2**	**3**	**4**	**5**	**6**
ξ_{kj} [Nms]	1491.8	1864.7	2237.7	2610.6	2983.6	3356.5
k	7	8	9	10	11	12
ξ_{kj} [Nms]	3729.5	4102.4	4475.4	4848.4	5221.3	5594.3

It has to be restated that in the previous formulas the harmonic coefficients are proportional with the ones from the (4.47), (4.48) formulas and the ones from the (4.6) table and that means that the proportionality constant is *R*, while δ and n_j have the same meaning as the terms specified in the 4.1.1 table.

For the calculus of forced torsional vibrations acting on the shaft line using the transfer matrix method we shall highlight the *point matrix* and the *field matrix* for each element individually according with the No. [15], [25] and [70] reference, as stated in the following form:

$$[P_k]_j = \begin{pmatrix} 1 & 0 & 0 & 0 & 0 \\ -J(k\omega)^2 & 1 & -r_k(k\omega) & 0 & -M_k^{\mathrm{Re}} \\ 0 & 0 & 1 & 0 & 0 \\ r_k(k\omega) & 0 & -J(k\omega)^2 & 1 & -M_k^{\mathrm{Im}} \\ 0 & 0 & 0 & 0 & 1 \end{pmatrix}_j \quad (4.112)$$

and:

$$[F_k]_j = \begin{pmatrix} 1 & \frac{C}{C^2+(\xi_k k\omega)^2} & 0 & \frac{\xi_k(k\omega)}{C^2+(\xi_k k\omega)^2} & 0 \\ 0 & 1 & 0 & 0 & 0 \\ 0 & -\frac{\xi_k(k\omega)}{C^2+(\xi_k k\omega)^2} & 1 & \frac{C}{C^2+(\xi_k k\omega)^2} & 0 \\ 0 & 0 & 0 & 1 & 0 \\ 0 & 0 & 0 & 0 & 1 \end{pmatrix}_j \quad (4.113)$$

Thus, the following formula will be generated:

$$[Z_k]_j^D = [F_k]_j \cdot [P_k]_j \cdot [Z_k]^D{}_{j-1} \quad (4.114)$$

for which $[Z_k]^D_j$ is the status vector posted at the right side of the *j* order element from the 4.20 figure, depending on the one of the previous element, with the following formula:

$$[Z_k] = \{\Theta_k^{Re}\ M_k^{Re}\ \Theta_k^{Im}\ M_k^{Im}\ 1\}_j^T \quad (4.115)$$

for which *T* is, in fact, the matrix trans ponding operation.

If the (4.114) is being applied in a complex form, as being marked by the above bars, the entire system specified in the 4.18 figure will have the following formula:

$$[Z_k]_n^D = [P_k]_n \left(\prod_{j=1}^{n-1} [F_k]_j [P_k]_j \right) [Z_k]_1^S = [B_k][Z_k]_1^S \quad (4.116)$$

The torsion momentum from the left side has to be null (the superior S order):

$$\overline{M_{1_k}}^{S} = 0$$

or (4.117)

$$\left(M_{1_k}^{\mathrm{Re}}\right)^{S} = \left(M_{1_k}^{\mathrm{Im}}\right)^{S} = 0$$

the mathematical operations indicated in the (4.116) formula are considerably reduced generating the calculus reduction for the second and fourth matrix column from the $[Pk]_1$ matrix.

In order to explain *n* order point matrix we will have to write the harmonic component with a *k* order for the torsional momentum presented in the (4.91) formula under the following form:

$$M_{e_k} = \left|M_{e_k}\right| \sin\left(z_p k\theta + \varphi_{e_k}\right) \quad (4.118)$$

in which z_p is the number of propeller blades, while $|M_{ek}|$ module and the initial phase φ_{ek} are given by the second relation form the (4.89) and (4.90) sets of formulas, having the numerical values presented previously in the 4.7 table. In the (4.118) formula, the harmonic order has been reported at the rotation period of the propeller according with the (4.98) formula. This moment can be rewritten under a complex form, similar with the complex formula of engine momentum (formula 4.108) and by identifying the (4.118) formula we can obtain the real and imaginary parts of the harmonic component for the featuring propeller momentum:

$$\begin{cases} M_{e_k}^{Re} = \left|M_{e_k}\right| \sin\varphi_{e_k} \\ M_{e_k}^{Im} = -\left|M_{e_k}\right| \cos\varphi_{e_k} \end{cases}. \quad (4.119)$$

having this knowledge the n order point matrix has the following form:

$$[P_k]_n = \begin{pmatrix} 1 & 0 & 0 & 0 & 0 \\ -J(k\omega)^2 & 1 & -r_k(k\omega) & 0 & -M_{e_k}^{\mathrm{Re}} \\ 0 & 0 & 1 & 0 & 0 \\ r_k(k\omega) & 0 & -J(k\omega)^2 & 1 & -M_{e_k}^{\mathrm{Im}} \\ 0 & 0 & 0 & 0 & 1 \end{pmatrix}_n \qquad (4.120)$$

The [Bk] matrix from the (4.116) formula can be rewritten as:

$$[B_k] = \begin{pmatrix} b_{1_k} & -b_{3_k} & b_{3_k} \\ b_{2_k} & -b_{4_k} & b_{6_k} \\ b_{3_k} & b_{1_k} & b_{7_k} \\ b_{4_k} & b_{2_k} & b_{8_k} \\ 0 & 0 & 1 \end{pmatrix}. \qquad (4.121)$$

The right limiting conditions will be imposed (with a superior *D* index), analogue as the ones from the (4.117) formula:

$$\overline{M_{n_k}}^D = 0$$

or (4.122)

$$\left(M_{n_k}^{Re}\right)^D = \left(M_{n_k}^{Im}\right)^D$$

and these lead to a linear equation system with two unknown values:

$$\begin{cases} \Theta_{1_k}^{Re} = -\dfrac{b_{2_k} b_{6_k} + b_{4_k} b_{8_k}}{b_{2_k}^2 + b_{4_k}^2} \\ \Theta_{1_k}^{Im} = \dfrac{-b_{2_k} b_{8_k} + b_{4_k} b_{6_k}}{b_{2_k}^2 + b_{4_k}^2} \end{cases}. \qquad (4.123)$$

Thus the Θ_1^{Re} and Θ_1^{Im} components for the status vector $[Z_1]^s$, as well as the total value of the torsional vibration amplitude for the first disc:

$$\Theta_{1_k} = \sqrt{\left(\Theta_{11_k}^{Re}\right)^2 + \left(\Theta_{11_k}^{\mathrm{Im}}\right)^2}. \qquad (4.124)$$

The results for the 12 harmonics are being presented in the 4.21 figure, which, in fact, shows the amplitude variations calculated through the MMT global method, in comparison with the measured values during sea trials onboard as mention in the reference No. [112].

The time variation mode can be calculated for the amplitudes by composition after the following formula:

$$\Theta_j = \sum_{k=1}^{12} \left(\Theta_{j_k}^{\mathrm{Re}} \cos k\omega\tau - \Theta_{j_k}^{\mathrm{Im}} \cos k\omega\tau\right) \qquad (4.125)$$

with the graphical representations in the No. [15] and [25] references, as in the following figures.

The difference between 4.1 and 4.23 figures is represented by the spatial feature, which is tridimensional for the last mentioned one: sections are being obtained in which vibration amplitude has a minimal value. The calculus by applying the matrix method avoids all simplifying hypothesis from the approximation amplitude calculus generally used for practical applications, as mentioned in the No. [67] reference.

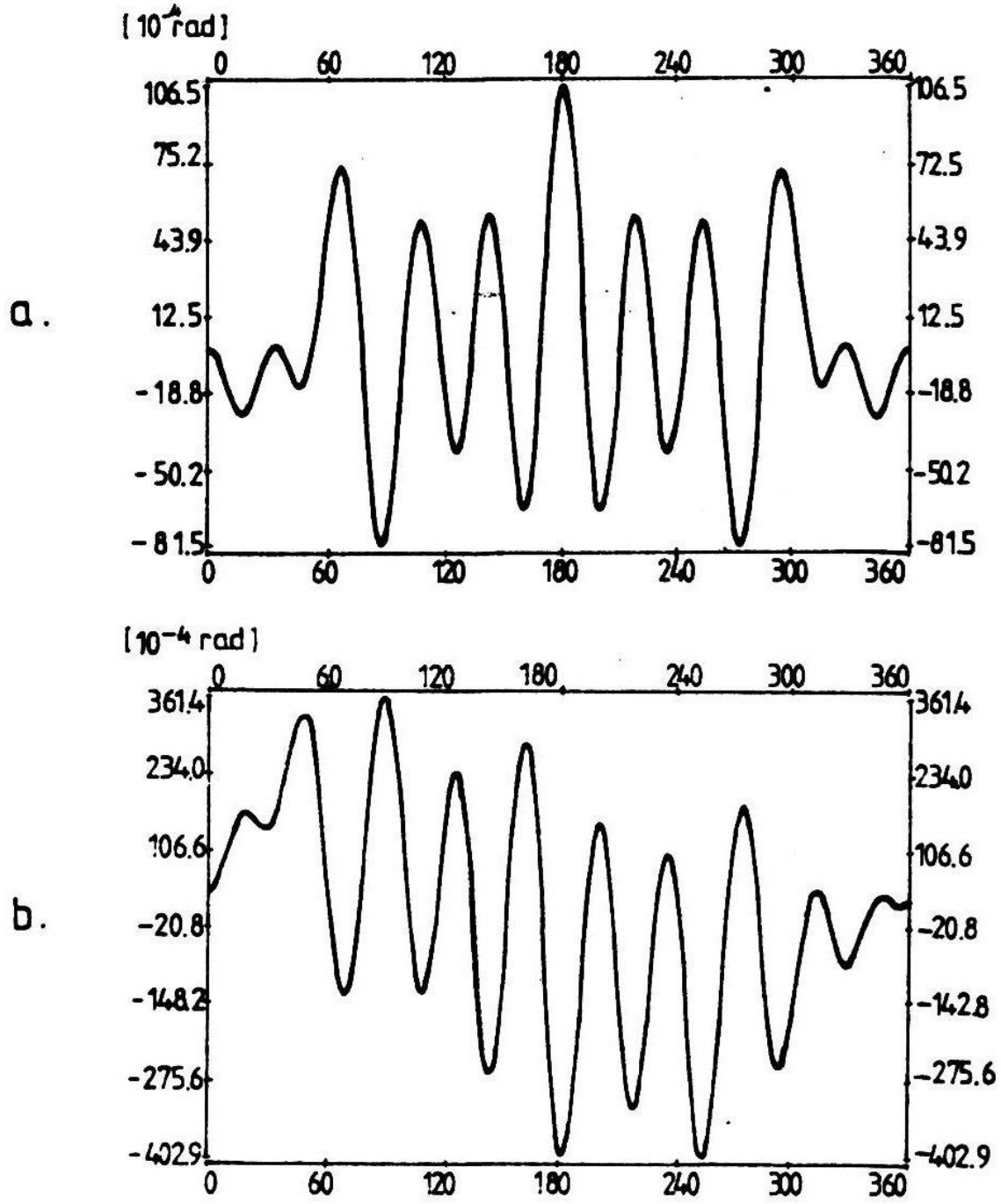

Figure 4.22: Amplitude time variation for torsional vibration: a – for the first disc, b – for the last disc (the propeller); in the case of a shaft line fitted on a marine main engine Sulzer 6RND90

The presentation calculation refers to shaft lines directly fitted to the engine that drives them. These are situations for which the propulsion system contains a semi-fast engine directly fitted with a rotation reduction gear needed to reduce angular speed needed to drive the propeller. Figure 4.24 extracted from reference No. [59] shows the oscillatory equivalent system and the first six own vibration modes for a marine propulsion system with two Sulzer 8ZA engines, with a four stroke functioning, developing a 4500 kW (6120 HP) power at a 510 rpm nominal speed. These engines fit an icebreaker type of ship with a propeller with a rotation speed equal to 138,7 rpm, thus the transmission ration for the reduction system is 3.67.

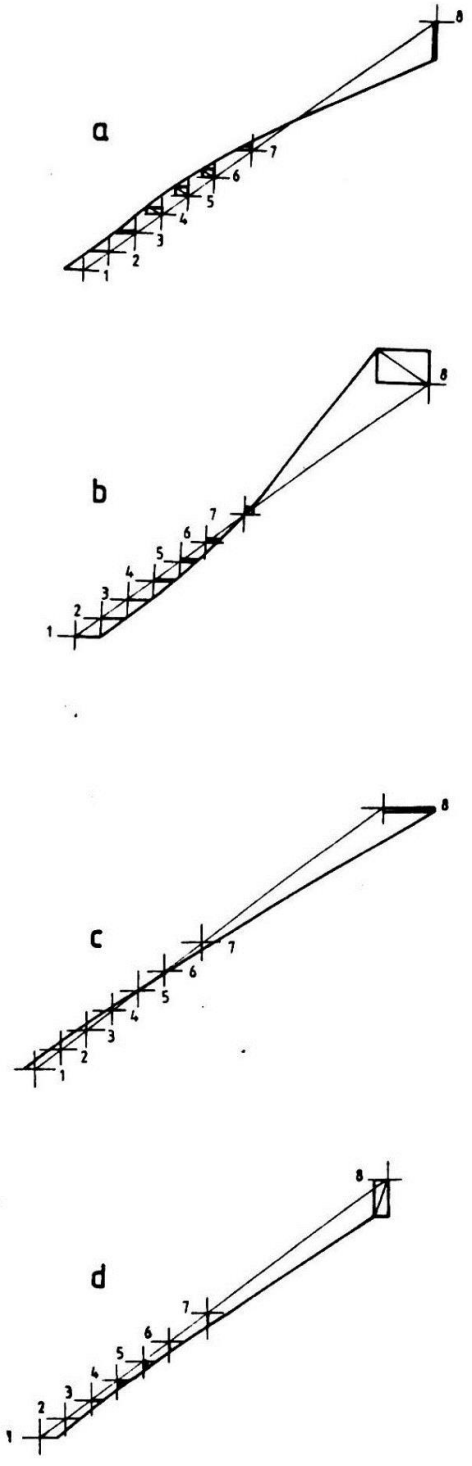

Figure 4.23: Torsional vibrations variations for shaft lines of a Sulzer 6RND90 main engine on harmonic orders equal to: a) k = 3; b) k = 6; c) k = 9; d) k = 12

Reference literature such as [67] and [91] show an even more rigorous calculus procedure for this kind of shaft lines coupled to internal combustion engines using mechanical transmission systems or simple or ramification shaft lines. In the same time it is possible to use mixt solutions such as using a propulsion slow turning engine cu a PTO-generator fitted on the shaft. The 4.25 figure presents this practical situation, as in the case of the first three own vibration ways for a Sulzer 7RTA62 main engine with a 11106 kW power at a nominal rotation speed equal to 88 rpm, as stated in the No. [59] reference.

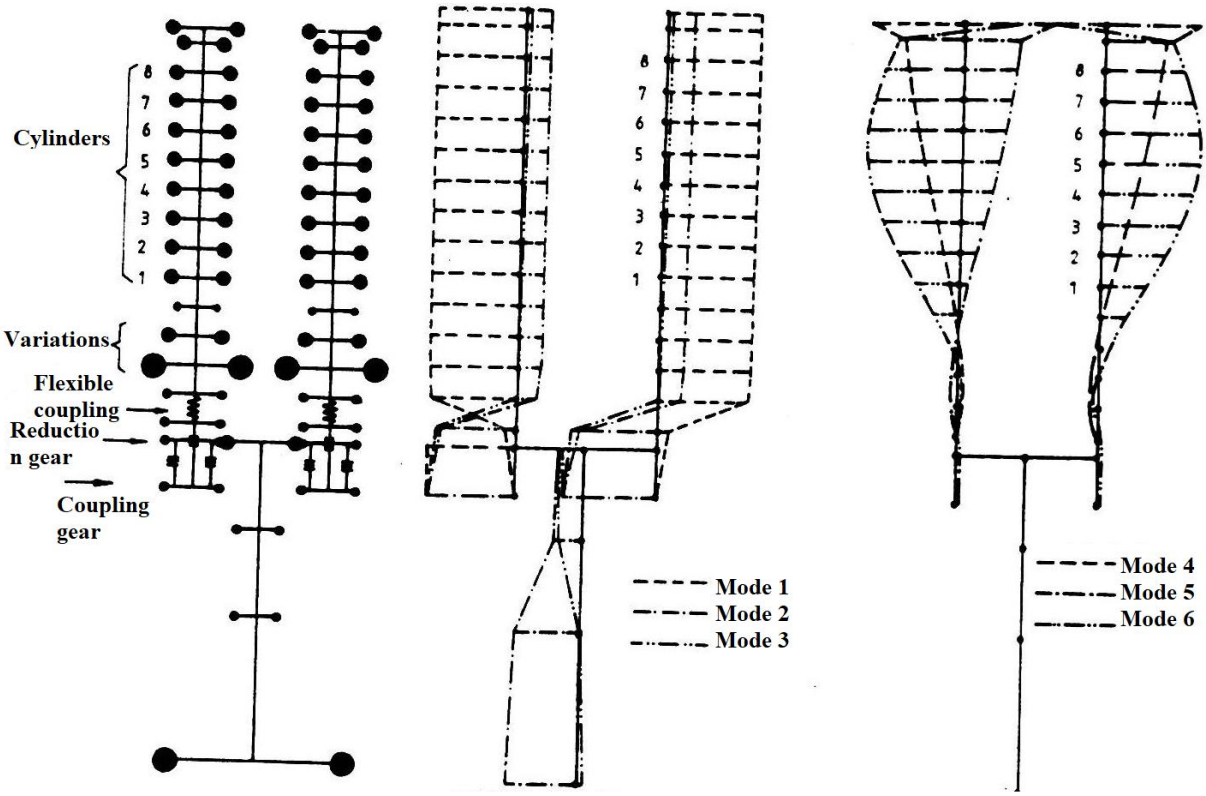

Figure 4.24: Double ramification system fitted with a reduction gear and the Sulzer 8ZA40S main engines as well as the first six own vibration modes diagram

4.3.2 Forced bending vibrations for marine engine shaft lines

In this phase, as in the previous paragraph, we will only study the individual type of vibration, followed up by the analysis of all coupled vibrations, out of which, by particularizing we can pick out the dynamic behavior of the shaft line at these certain individual loads.

Real bending vibrations, as it has been shown in the 4.4 paragraph, are being generated in two plans, Oyz and Oxz, that is why, in the specific literature they are also being called *lateral vibrations of shaft lines*. This type of vibrations can be neglected in the case of shaft lines driven by marine main engines due to the enlarged stiffness of engine bearings. The phenomenon is mostly studied in the case of long shaft lines taking into account the *swirling phenomenon*, as explained in the reference No. [100] and [103] for the propeller, as stated in the 3.2.1 paragraph. In these cases the bending vibrations can stimulate structural load vibrations on the hull and the main engine.

Between the calculus stages of torsional forced vibrations and the bending ones a set of difference occur, such as:

- The system's response to bending excitation vibrations which are the solution for an equation system with a four degree, due to the fact that two degrees of freedom occur, instead of one degree of freedom;
- Dynamic model for the crankshaft which corresponds to a continuous environment and not to a discreet one;
- The shaft line can be considered embedded, such as the propeller shaft in the aft post tube;
- The limiting conditions at the consumer end of the shaft line can correspond to the free articulation, to the support and to the embedment.

The main difficulty in the calculus of forced bending vibrations is not the establishment of a calculation model, but the calculus for a set of parameters, such as bearings stiffness. The calculus methodology specified in the No. [59] reference leads to the calculations of bending forced amplitude vibrations, keeping in mind the after

mentioned sources presented in the 4.2.2 paragraph, as well as the lateral forces variations developed into the propeller (as observed in the 4.15 figure), acting according with the fundamental frequency given by the propeller blade number (as mentioned in the 4.98 formula). When resonance occurs, the only possible measure that can be taken is the one consisting in the processing of supporting bearings stiffness by means of constructive solutions. These considerations are illustrated in the 4.26 figure presenting the bending forced vibrations amplitudes for the shaft line, in case of a ferry-boat which is being propelled by 3 Sulzer 14ZAS40S main engines, with 7723 kW (10500 HP)power each. Calculation processes have lead at a critical bending frequency with a value of 6.8 s^{-1} for the central crankshaft, having a 43 meters length, this being a value that can be allowed for this type of ship because the propeller blade frequency is in the 0 – 11.6 s^{-1} range at a rotational speed equal to 174 rpm. In order to avoid any resonance risks in the entire rotational speed working range values two additional bearings have been installed. This lead to an increased own frequency equal to 13.6 s^{-1} and this is how the propeller rotational speed has increased to 205 rpm, this being the nominal speed for this type of boat, as shown in the 4.27 figure.

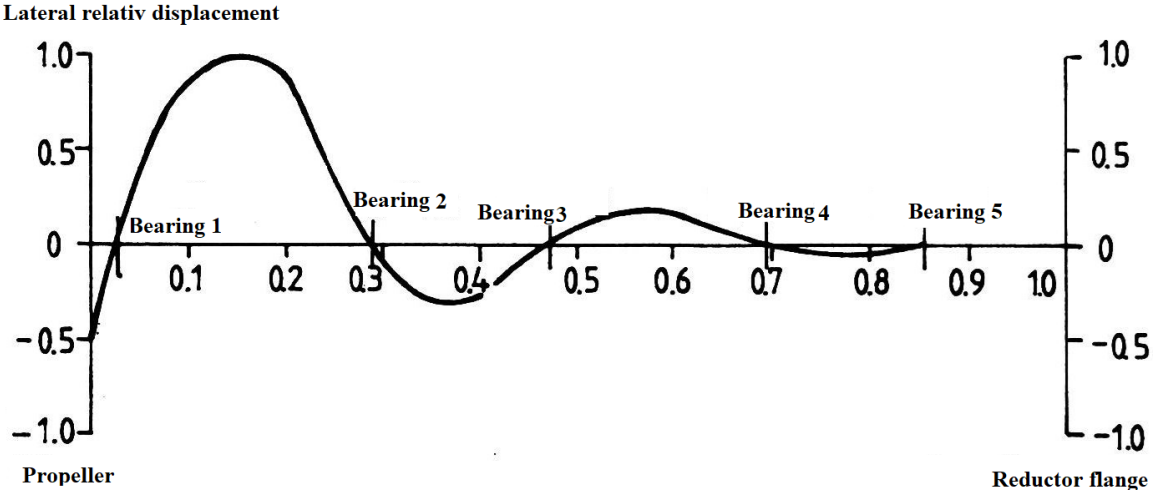

Figure 4.26: Bending vibration amplitude variation for an intermediary shaft line for a marine propulsion system fitted with three Sulzer 14ZA40S engines

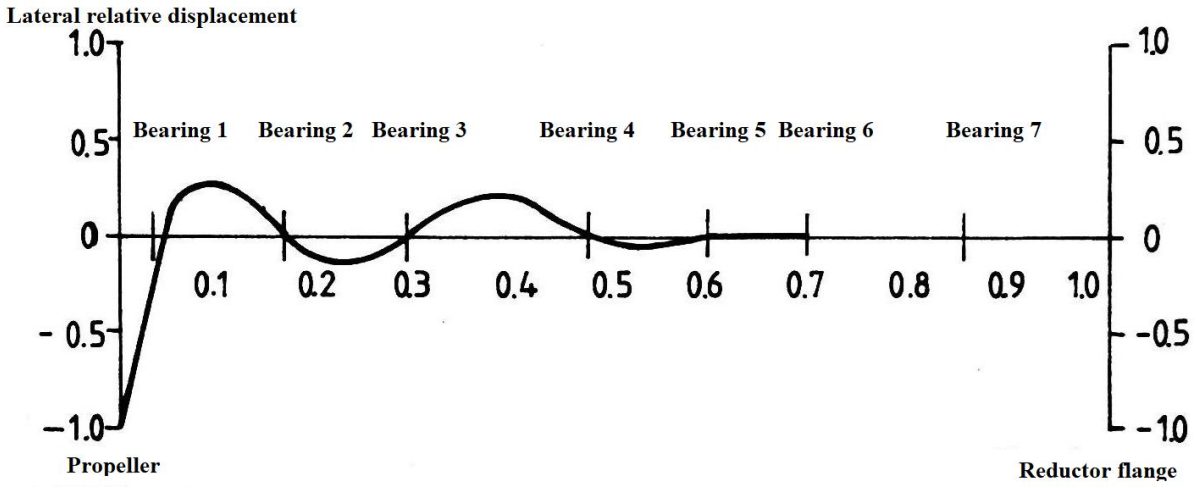

Figure 4.27: Bending vibration amplitude variation for an modified intermediary shaft line for a marine propulsion system fitted with three Sulzer 14ZA40S engines

4.3.3 Forced axial vibrations of marine main engines shaft lines

Forced axial vibrations study can be limited, unlike the torsional one, just at the stage of the study of the subsystem formed from the engine crankshaft, the intermediary one and the propeller shaft. This is due by the fact that the excitations of this type of vibrations are not transferred by PTO ramifications in the complex systems. The vibrations calculus is based on the generic equation expressed in (3.1), having the same nature as the calculus of torsional vibrations due to the analogy between the two types of vibrations. The occurring specific issues that can occur are tied upon the exact calculus of axial stiffness and this has an analytical solution (as seen in the 4.1.3 paragraph), as well as a numerical solution (as expressed in the 4.1.3 paragraph) and an experimental one. This is also a valid calculus compensation coefficients, this thing being usually done in an experimental manner. Regarding the force vectors of axial stimulating vibrations this is given by the thrust force of the propeller (4.97), as well as the axial gas pressure components and the mass inertia having an alternative motion, these last categories being excitation forces that can be

highlighted in the case of a study of the coupling phenomenon for all vibration types generated on shaft lines driven by marine main engines. Thus, in the same manner as in the case forced bending vibrations, we can extract the individual type of vibration representing a major study subject for marine propulsion systems, most of them complex or coupled and this study is being presented in the next paragraph.

4.4 Marine engine shaft lines coupled vibrations

Due to complicated geometrical shapes of the crankshaft it's deformations can have a complex characteristic this leading to the coupling of certain vibration types that can be performed by the main engine.

4.4.1 Mathematical model of shaft lines driven by marine main engines

Considering the crank in the No. [91] reference a part of the crankshaft upon which a torsion momentum M_z acts (as shown in the 4.28a figure), it can be observed that this element has the tendency to generate torsional vibrations, as well as bending vibrations in Oxz parallel plans, these two types of vibrations forming a set of coupled vibrations.

Acting on the crankpin with a variable F_y force placed in the crank plan (as shown in the 4.28b figure) it can be noticed that it has the tendency to generate bending vibrations in the Oyz plan, as well as axial vibrations along the Oz axis.

Thus, the crankshaft geometrical configuration generates the occurrence of complex vibrations on it representing coupled modes for simpler vibrations. Thus, torsional vibrations stimulate bending vibrations as well axial vibrations.

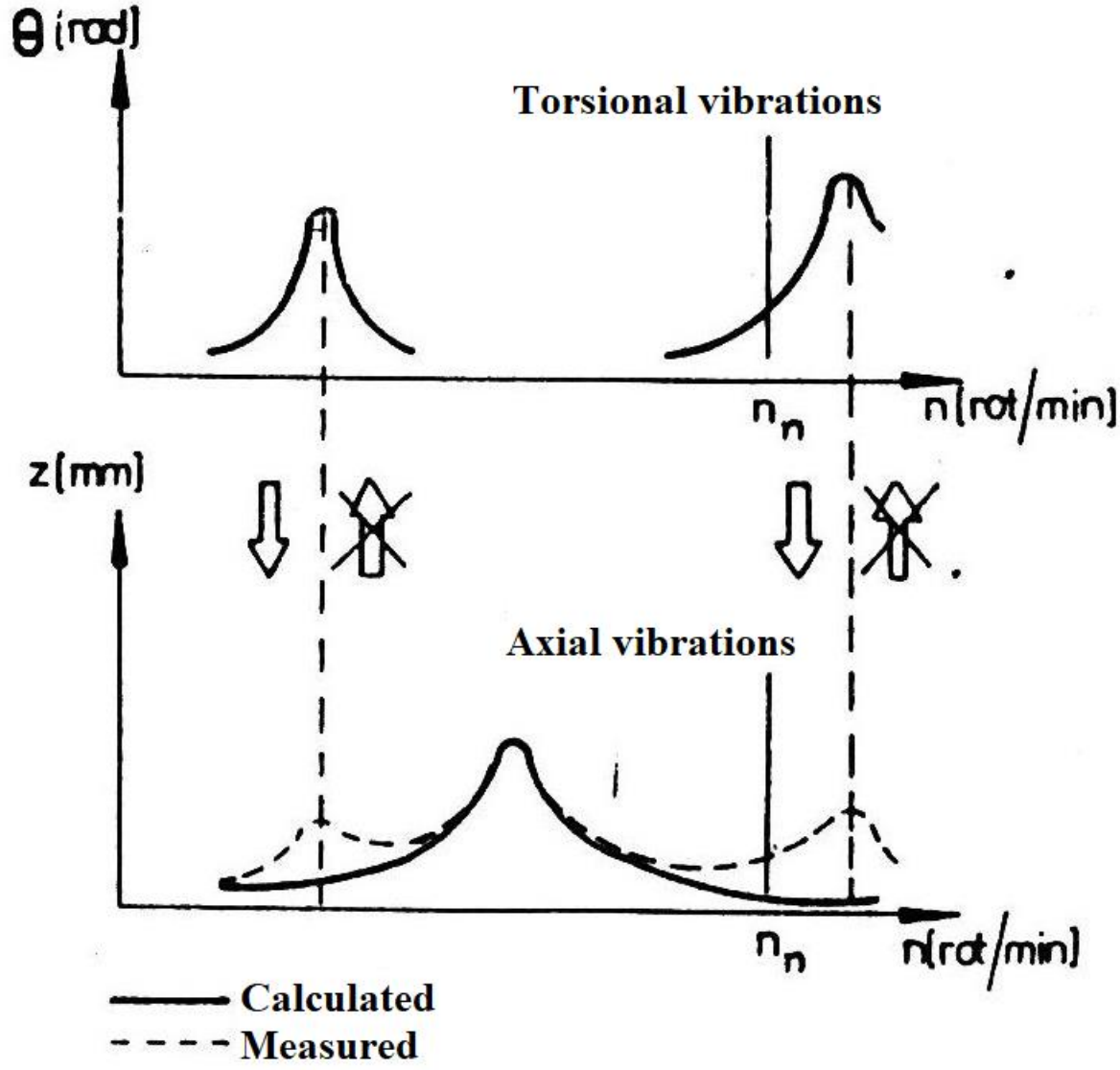

Figure 4.29: Effect of coupling torsional and axial vibrations

In the particular case of marine main engines coupled in a direct manner with the propeller the comparisons made between the calculations and the measured for vibrations type previously specified lead to the following observations, according to the No. [58] reference:

- Axial displacements are influenced by the torsional vibrations: it can be noticed that the axial displacement increases for engine rotations in the area of critical torsional rotations;

- Torsional vibrations amplitude is not influenced by the axial vibrations;
- The effect of vibrations coupling is even more highlighted if the torsional critical rotations and the axial ones are close enough in dimension, and this phenomenon is being presented in the 4.29 figure.

The overall vibration coupling phenomenon onboard ships has been presented in the 3.1 figure.

From the information stated in the previous chapters it can be concluded with the fact that one of the most important issues which has to be solved is that of finding the propulsion system for which the vibration effect can generate excessive vibration levels that can't be used in calculation procedures, these being the so-called standard methods presented in the 4.2 and 4.3 paragraphs. The implicit solution implies the modification of the calculus model for the entire shaft line taking into account the entire range of relevant freedom degrees.

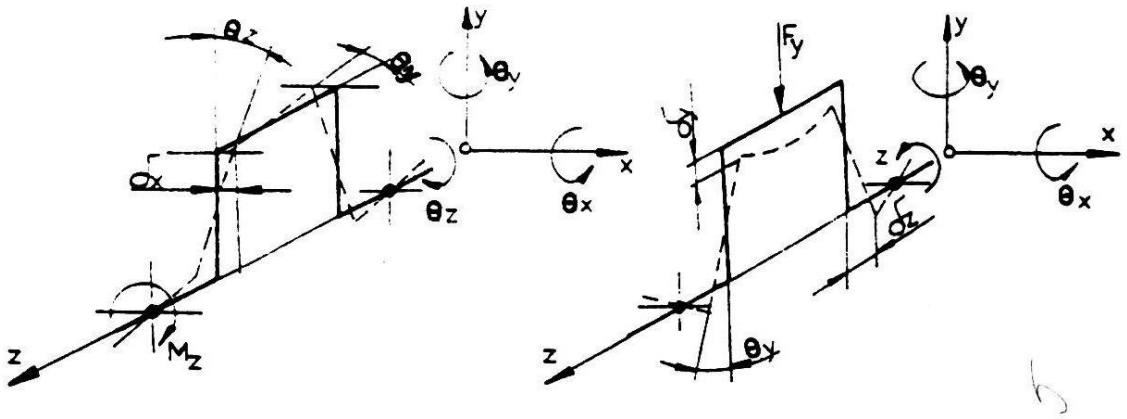

Figure 4.28: Torsional, bending and axial vibration coupling phenomenon graphic model

The creation of a more complex model is being imposed by the fact that the crankshaft is being supported on more than two supports, this being a static undefined system. In the same time the supports modeling process has to take into account the existence of certain slacks in the bearings, these depending on the execution tolerances, as well as the usage level generated during operation.

In the below figure a shaft line of the engine under observation (Sulzer 6RND90 main engine) is being presented, the crankshaft being presented in a graphic manner by straight bar elements.

A much simpler calculus model proposes taking into consideration of a single section of the crankshaft which has a crankpin limited by two arms and the adjacent bearings, which are simply supported. In this case the influence of geometrical parameters on the values of internal efforts is being reduced. This model turns out to be much simpler and acceptable in order to do the calculus for pre-dimensiong, but it doesn't allow the study of influence on different factors influencing the crankshaft resistance. A calculus model that has to analyze the entire crankshaft by using finite elements, as it has been shown in the 3.3 figure is not rational due to the great number of finite elements in the meshing process, especially if tension cluster would be taken into account. This kind of spatial model does a better approximation on the real situation, but also contains lesser elements on each section, thus, offers less information regarding deformation and tension dimensions.

Keeping all these in mind the spatial structural model chosen contains straight structural bars, as shown in the 4.29 figure, the shaft line being considered as a bar system with even distributed masses, this being similar with the arms lengths, as well as masses and inertia momentum focused in certain tension clusters. Through this model, which simplifies the entire issue in a reasonable manner, we can obtain information regarding the dynamic behavior of the shaft line.

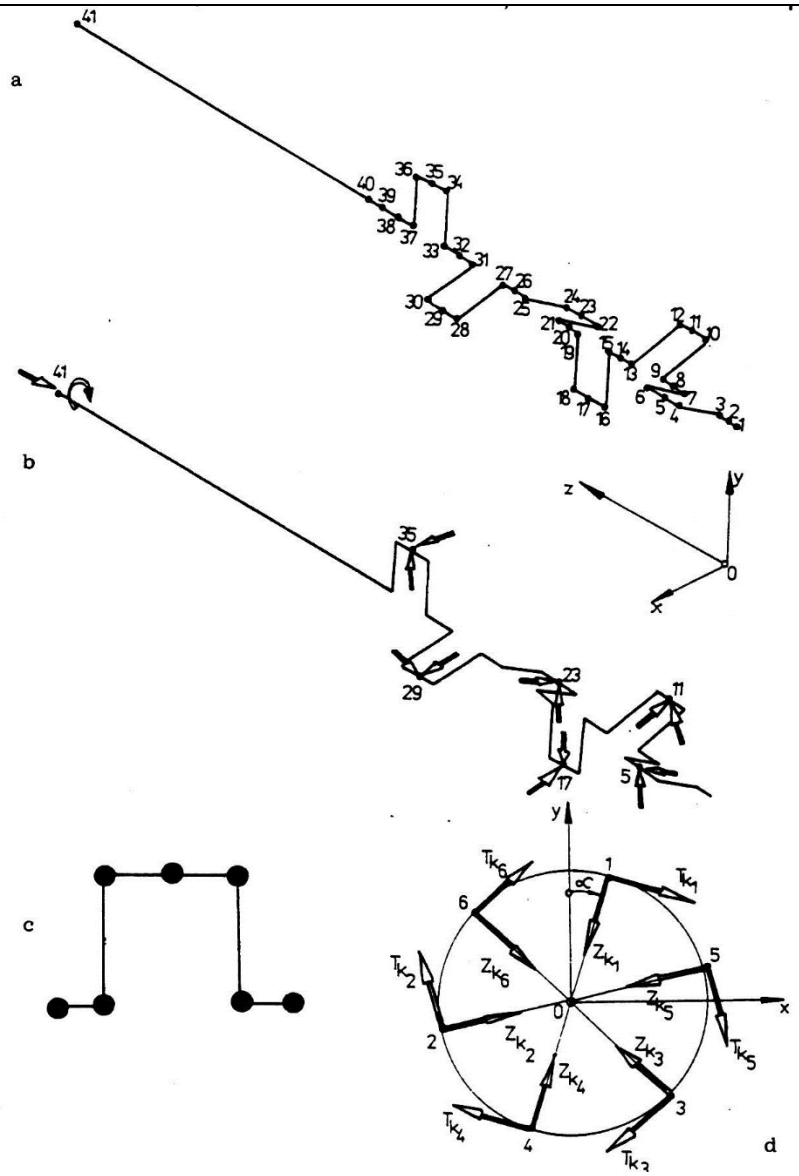

Figure 4.30: Shaft line model for a Sulzer 6RND90 main engine

By supporting the entire structure can be studied by taking into account two ways: embedded crankpins, these allowing the rotation motion only around the Oz axis; supported bearings , these allowing the rotation motion only around Ox, Oy and Oz axis stopped only by the translation motions around Ox and Oy. The real situation is somewhere in between the two cases, a new engine being closer to the first situation in real operation, but after the first slaks occurs in the crankpins, the real situation

tends to be closer to the second case. Thus, the structure is being considered meshed for a real case implying the real case of the shaft line for the Sulzer 6RND90 main engine, for this using a number of 40 finite elements and 41 nods. In 1, 39, 40 and 41 nods, as well as in 5, 11, 17, 23, 29 and 35 masses and moments are being concentrated. For the first mentioned nods series the concentrated inertia masses and moments correspond to the ones of the axial bearing flange, of the flywheel and of the propeller, while the masses and moments focused in the nods of the second category are generated by engine drives reduction corresponding to the cranks. The loading situation of the structure has been done by applying two forces in the middle of the crankpins, thus the nods 5, 11, 17, 23, 29 and 35 are on a tangential and radial direction, being given by the (4.50) and (4.59) formulas. Their components are resulting by decomposing the elements on the axis of the global system from the 4.30 figure, given by the following formulas:

$$\begin{cases} T_{k_{j_x}} = T_{k_j} \cdot \cos\left[k\theta + (i - n_j)\delta\right]; T_{k_{j_y}} = T_{k_j} \cdot \sin\left[k\theta + (i - n_j)\delta\right] \\ Z_{k_{j_x}} = Z_{k_j} \cdot \sin\left[k\theta + (i - n_j)\delta\right]; Z_{k_{j_y}} = Z_{k_j} \cdot \cos\left[k\theta + (i - n_j)\delta\right] \end{cases} \quad (4.126)$$

the dimensions occurring in the above formula have the same meaning as the ones mentioned in the 4.2 paragraph.

The load applied on the last node of the proposed structure is being given by the harmonic formula for the momentum and for the propeller thrust that have been calculated in the 4.3.3 chapter with the (4.91) and (4.97) formulas.

4.4.2 Free coupled vibrations for marine main engine shaft lines

The shaft line coupled vibrations calculus in the case of a marine main engine can be meshed as a spatial structure made out of simple bars and this can be done towards the general reference system known as *the global reference system* and noted with Oxyz, this being a straight system with its origin in the 1st order node.

For reasons regarding the improvement of processing data and for the flexibility of the calculus software we can consider a *local reference system* which is

being attached to every single bar. The local reference system has to fulfill the following elementary conditions in order to allow a better numerical processing stage:

- Its origin is the *I* node with $I < J$;
- The Ox axis for the entire system is the same with the longitudinal axis of the mentioned bar;
- Oxy plan is defined by the Ox axis and a random *K* number placed in the middle of the first quadrant;
- The Oz axis is being chosen as straight on the Oxy plan, thus, the reference system is straight and has the axis orientation identical with the one of the global system.

The stiffness matrix are calculated towards the local reference system and the bar mass coefficients and data regarding the load acting on the bars is being introduced in the software.

Along the entire calculus procedure the positive direction for all forces, momentum, arrows and rotations is being given by the positive axis direction.

On single straight bar displacements in space, *I* – *J*, is being considered as positive, just like in the 4.31a figure and this is how the vector is being composed on the column direction:

$$\overline{\Delta}_{ij} = \left[\overline{\Delta}_i \; \overline{\Delta}_j\right]^T = \left[u_i \quad v_i \quad w_i \quad \theta_{ix} \quad \theta_{iy} \quad \theta_{iz} \quad u_j \quad v_j \quad w_j \quad \theta_{jx} \quad \theta_{jy} \quad \theta_{jz}\right]^T \tag{4.127}$$

in the above formula the line above the symbols mark the local axis system, while the superior index *T* marks the matrix trans ponding operation. In a similar manner the efforts at the elements end are all positive, just like in the 4.31b figure, together being composed in the following column vector:

$$\overline{\Theta}_{ij} = \left[\overline{\Theta}_i \; \overline{\Theta}_j\right]^T = \left[F_{i_x} F_{i_y} F_{i_z} M_{i_x} M_{i_y} M_{i_z} F_{j_x} F_{j_y} F_{j_z} M_{j_x} M_{j_y} M_{j_z}\right]^T \tag{4.128}$$

Applying the usual formulas mentioned in the No. [68] and [75] reference for a single point current displacements *z*, depending on the ending displacements, thus, from this point forward we can calculate the corresponding efforts, by individualizing the obtained results for *z = 0* and *z = 1* (*finite element length*), allowing us to calculate the value of $\overline{\Theta}_i$ and $\overline{\Theta}_j$ vectors. Finally the matrix formula between efforts and end bar displacements *I – J* can be written in a concentrated manner:

$$\overline{\Theta}^{(e)} = \bar{r}^{(e)} \cdot \overline{\Delta}^{(e)} \qquad (4.129)$$

in the above formula $\bar{r}^{(e)}$ is the stiffness matrix for the *I – J* bar, which, in general, is being considered the finite element (e), according to the No. [17] reference.

By applying the virtual mechanical work principle to the finite element *(e)* we can generate the formula for equivalent nodes forces and momentum:

$$\overline{\Theta^{(c)\prime}} = \bar{m}^{(c)}\overline{\Delta}^{(e)} + \bar{r}^{(c)}\overline{\Delta}^{(c)} \qquad (4.130)$$

where $\bar{m}^{(e)}$ is the element masses matrix:

$$\bar{m}^{(e)} = \begin{pmatrix} \bar{m}_{ii} & \bar{m}_{ij} \\ \bar{m}_{ji} & \bar{m}_{jj} \end{pmatrix} \qquad (4.131)$$

for which all internal elements $\bar{m}_{pq}$, p and q have the *i* and *j* successive values. Here on we can generate the following general formula, that takes into account all types of individual vibrations types (torsional, bending and axial):

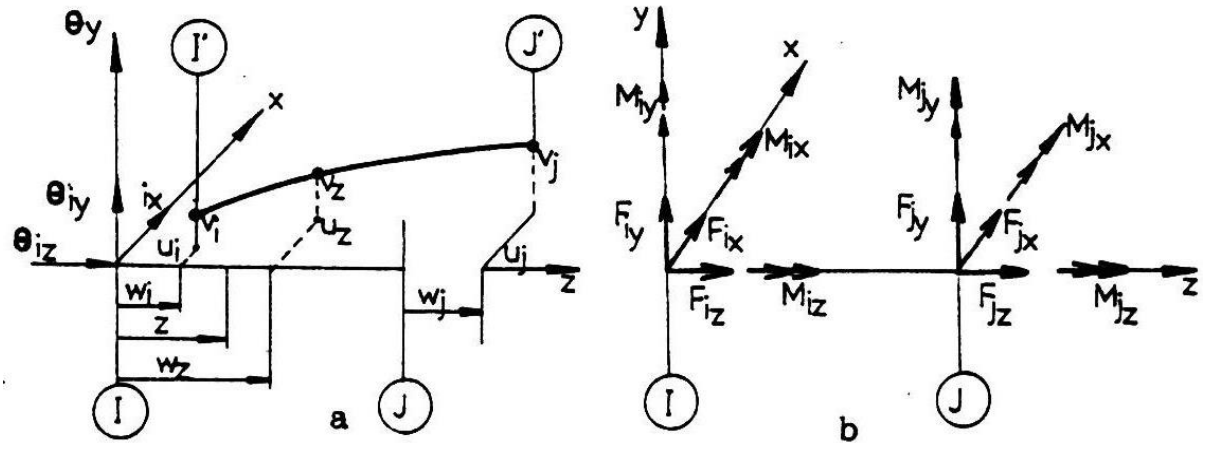

Figure 4.31: Angular and linear displacements diagram for a finite element and the load process with different loads

$$\overline{m}_{pq} = \frac{\rho A l}{420} \cdot \begin{pmatrix} a_{11_{pq}} & 0 & 0 & 0 & 0 & 0 \\ 0 & a_{22_{pq}} & 0 & 0 & 0 & a_{26_{pq}} \\ 0 & 0 & a_{33_{pq}} & 0 & a_{35_{pq}} & 0 \\ 0 & 0 & 0 & a_{44_{pq}} & 0 & 0 \\ 0 & 0 & a_{53_{pq}} & 0 & a_{55_{pq}} & 0 \\ 0 & a_{62_{pq}} & 0 & 0 & 0 & a_{66_{pq}} \end{pmatrix} \qquad (4.132)$$

in the above matrix ρ symbolizes the density, A the bar transversal area, l the length and I_p the polar inertia momentum for it. The coefficients value are given in the 4.13 table.

Table 4.13: Mass matrix coefficients values for the finite element

Index (p,q)	a_{11pq}	a_{22pq}	a_{26pq}	a_{33pq}	a_{35pq}	a_{44pq}	a_{53pq}	a_{55pq}	a_{62pq}	a_{66pq}
(i,i)	140	156	22 l	156	22 l	I_p/A	-22 l	4 l^2	22 l	4 l^2
(i,j)	70	54	-13 l	54	13 l	$I_p/2A$	-13 l	-3 l^2	13 l	-3 l^2
(j,j)	140	156	-22 l	156	22 l	I_p/A	22 l	4 l^2	-22 l	4 l^2
(j,i)	70	54	-13 l	54	13 l	$I_p/2A$	-13 l	-3 l^2	13 l	-3 l^2

The following stage is represented by the reference local system rotation until its axis will have the same direction and the same orientation as the axis of the global reference system. This thing has been done by applying an original methods specified in the No. [19] and [65] references taking into account the conditions that have to be satisfied by the local reference system, as they have been shown in the first part of the paragraph. In this manner, the rotational matrix *L* containing directional cosines, has been generated. As a consequence the local reference system translation will be done in automatic manner and the two system will be identical when the mass and stiffness matrix will be assembled for the entire structure. Thus, out of (4.130) formula will become:

$$\Theta^{(c)'} = \overline{m}^{(c)}\overline{\Delta}^{(e)} + \overline{r}^{(c)}\overline{\Delta}^{(c)} \qquad (4.133)$$

this is also valid for the *(e)* element in the global system context, having:

$$\begin{aligned} r^{(c)} &= \left(L^T \overline{r} L\right)^{(e)} \\ m^{(c)} &= \left(L^T \overline{m} L\right)^{(e)} \end{aligned} \qquad (4.134)$$

The mass and stiffness matrix have a 12X12 dimension for each elements and *12n X 12n* for the entire structure. Some of the nodes (as shown in the 4.30a figure) are representing masses and concentrated efforts. Keeping in mind the rotation inertia for concentrated masses in a random *g* node, the corresponding vector for all displacements will be:

$$\Delta_g = \begin{bmatrix} u & v & w & \theta_x & \theta_y & \theta_z \end{bmatrix}^T \qquad (4.135)$$

That is the nodal mass matrix will have the following form:

$$m_g = \begin{pmatrix} m & 0 & 0 & 0 & 0 & 0 \\ 0 & m & 0 & 0 & 0 & 0 \\ 0 & 0 & m & 0 & 0 & 0 \\ 0 & 0 & 0 & J_x & 0 & 0 \\ 0 & 0 & 0 & 0 & J_y & 0 \\ 0 & 0 & 0 & 0 & 0 & J_z \end{pmatrix} \quad (4.136)$$

In the above matrix J_x, J_y and J_z are the inertia moments for the m mass, from the g node, being reduced at the reference global system axis.

The disrupting external forces from the g node can be either way, forces or couples, thus, these can be grouped into the following column vector:

$$F_g = \begin{bmatrix} F_{g_x} & F_{g_y} & F_{g_z} & M_{g_x} & M_{g_y} & M_{g_z} \end{bmatrix}^T \quad (4.137)$$

Applying the *d'Alembert principle*, from the dynamic equilibrium condition for the g node the following matrix equation will be obtained:

$$F_g - m_g \Delta_g - \sum_{e_h} \Theta_g^{(e)*} = 0 \quad (4.138)$$

By writing the motion equations for all meshing structural nodes the differential equation system that describes the dynamic behavior for the entire structure will be generated, which has the following matrix shape:

$$M\ddot{\Delta} + R\Delta = F \quad (4.139)$$

In the above formula the Δ vector is seen as an unknown value for all displacements:

$$\Delta = \begin{bmatrix} \Delta_1 & \Delta_2 & \cdots & \Delta_g & \cdots & \Delta_n \end{bmatrix}^T \quad (4.140)$$

M is the mass matrix expressed as:

$$\begin{cases} M_{gg} = m_g + \sum\limits_{e_g^I} m_{ii}^{(e_g^I)} + \sum\limits_{e_g^{II}} m_{JJ}^{(e_{JJ}^{II})} \\ M_{gh} = m_{ij}^{(e_g^I)}, g < h \\ M_{gh} = m_{ji}^{(e_g^{II})}, h > g \end{cases} \qquad (4.141)$$

R, the stiffness matrix expressed as:

$$\begin{cases} R_{gg} = \sum\limits_{e_g^I} r_{ii}^{(e_g^I)} + \sum\limits_{e_g^{II}} r_{JJ}^{(e_{JJ}^{II})} \\ R_{gh} = \sum\limits_{e_g^I} r_{ij}^{(e_g^I)}, g < h \\ R_{gh} = \sum\limits_{e_g^{II}} r_{ji}^{(e_g^{II})}, h > g \end{cases} \qquad (4.142)$$

while *F* is the disrupting forces vector with an external influence, having the formula expressed in (4.137).

In the (4.141) and (4.142) formulas the following notations have been used:

$$e_g = e_g^I + e_g^{II} \qquad (4.143)$$

in the above formula e_g' are all the elements from the *g* node that have the opposite end $h>g$ and e_g'' are all the elements from the *g* node that an opposite end $h < g$. In this manner, the matrix assembling for mass and stiffness leads, at the strip form, in a more subtle way.

The modes and own frequencies of coupled vibrations are complex and can be calculated by developing the homogenous matrix equations specific to (4.139) equation. By supposing that the harmonic shaped displacements can lead to a linear solution system the calculus condition for a certain usual solution is:

$$D|\Delta| = \omega^2 |\Delta| \qquad (4.144)$$

for which D = M-1 R is the dynamic matrix for the entire structure, the strip matrix having a strip width equal to 12. The (4.146) equation represents a vector and own value issue and it can be solved by applying the *matrix iteration method*.

4.4.3 Forced coupled vibrations for shaft lines of marine main engines

In order to calculate the forced coupled amplitude vibrations for the suggested structure we have to assume that the answer at the harmonic stimulation has the same pulsation as the vibration, equal to $k\omega$. The calculus has been done by applying harmonic orders with an k order. Thus, the harmonic component of a column vector with a random order for the nodal displacements has the following formula:

$$\Delta_k = \left[R - \left(k \cdot \omega\right)^2 M\right]^{-1} F_k \qquad (4.145)$$

this formula is being generated by applying the *Gauss elimination method*. Specific linear system dimension for the presented structure has an 246 order. Thus, finally we can calculate the average deformed fiber for the shaft line, by adding up all the relevant harmonic components:

$$\Delta = \sum_k \Delta_k \qquad (4.146)$$

In the final part of this theoretical part we also have to mention the fact the presented calculus method based on MEF is valid only for the stationary regime. In the same time, at the nominal calculus regime the compensation coefficients matrix could be ignored as mentioned in No. [58] and [91] references.

4.4.4 Numerical calculus results based on the mathematical model with finite elements

For the calculus of coupled vibrations of the shaft line a calculus program has been generated and its structure is being presented in the 4.32 figure.

MATR_TRANSF
Calculates directional cosines matrix for the crossing from the local reference systems to the global reference system

FORTE_D
Decomposes the thrust force and the propeller momentum in a harmonic set

DATE_GLOB1

INC_NOD
Loads all the nodes with tangential and axial forces decomposed on the global reference system

INC_PROPELLER
Loads the nod that represents the propeller

COND_LIM
Applies the limit conditions for the nodal displacements: axial displacement bounded by the node that represents the thrust bearing and the radial displacements bounded by the nodes representing the middle of the crankpins

Defines the entering data:

- Structure nodes number: 41;
- The finite element number: 40;
- Stiffness and mass assembled matrix dimension: 246;
- Strip width for these matrix: 12;
- Finite elements material density;
- Transversal elements cross section;
- Transversal and longitudinal flexibility module;
- Inertia moments of finite elements towards the global reference system axis;
- Global system coordinates for finite elements nodes, as well as for the points needed in order to define the local reference systems.

DATE_GLOB3

MRSL
Calculates the stiffness matrix for an element in the local reference system

MMSL
Calculates the mass matrix for an element in the local reference system

MRSG
Calculates the stiffness matrix for each element in the global reference system using **MATR_TRANSF**

MMSG
Calculates the mass matrix for each element in the global reference system using **MATR_TRANSF**

MR_STR
Calculates the stiffness matrix for the entire structure (assembly)

MM_STR
Calculates the mass matrix for the entire structure (assembly)

PULS

MATR_DIN
Calculates the dynamic matrix for the entire structure

PULSATIONS
Calculates own values in an increasing manner for the dynamic matrix by using the matrix iteration method with an 10^{-3} error

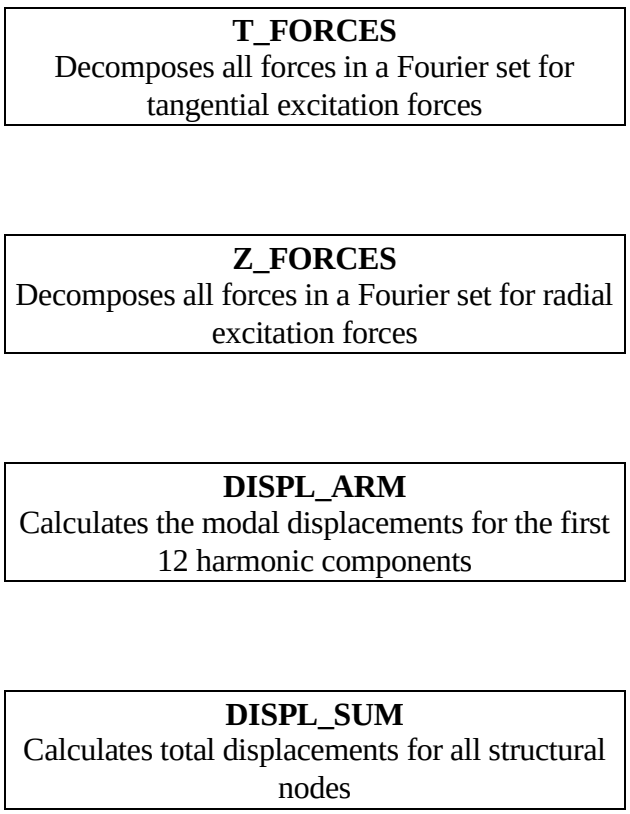

Figure 3.2: Logical diagram for the calculus program of coupled vibrations of shaft lines driven by marine main engines, based in the finite elements method

The results of own values (vibration own frequencies) are also given in the 4.14 table and a comparison of these values is being done, between a Sulzer 6RND90 main engine and a MAN K6SZ 52/105 main engine, fitted onboard a container ship with a 12500 tdw capacity, these ships being specific for the Romanian commercial fleet. The MAN engine develops a 4500 kW power at a rotation speed of 140 rpm, having the same configuration for the crankshaft and the same combustion order as the Sulzer main engine, but driving a four blade propeller with a 4.2 meter diameter (the one driven by the Sulzer main engine having a 6.4 m diameter). The comparison

from the table below is being done between the own frequencies values for individual vibrations types and the coupled ones.

Table 4.14: A comparison between own pulsations of individual vibration types and the coupled ones for two types of marine main engines

Engine type	Pulsation degree	Torsio [s^{-1}]	Bending [s^{-1}]	Axial [s^{-1}]	Coupling [s^{-1}]
6RND90	I	46.351	10.764	18.167	28.274
	II	187.351	49.987	42.103	70.071
K6SZ 52/ 105 Cle	I	83.287	20.054	31.559	36.014
	II	201.405	68.426	77.892	79.238

The results of individual and coupled free vibrations presented in the previous table lead to the following conclusions:

- Own pulsation values of the K6SZ 52/105 are higher than the ones corresponding to the Sulzer 6RND90 engine. This is explained by the fact that the inertia masses and moments are much lower for the first type of engine comparing it to the second one;
- 1st degree own torsional pulsation is pretty close to the 2nd degree one, this phenomenon being more noticeable for the 6RND90 main engine. This suggests that there is a possibility of a coupling phenomenon occurrence between the 1st torsional vibration mode and the 2nd axial one, in the sense of its stimulation by the first one;
- Own pulsations generated by torsional vibrations, for both types of engines have low values comparing them with the individual torsional ones, but they are higher in comparison with the bending and axil ones, indicating the fact that the coupling phenomena occurs between all individual vibration types;
- Own pulsations of individual bending vibrating modes have the lowest values, the influence on the coupling phenomena being much lower in comparison to other individual vibration types, both axial and torsional;

- Own pulsations of coupled vibrations for the K6SZ 52/205 engine are very close in value with the own individual axial vibration modes. This leads to the conclusion that axial vibrations have a bigger influence in the coupling phenomena. For the same engine 2nd degree own pulsation of coupled vibrations is very close to the 1st degree of torsional individual vibrations and this fact confirms the occurrence of a hardened coupling phenomena between the respective vibration modes.

On the basis of free coupled vibrations calculus, in the 4.33 and 4.34 figures the first modes of own complex vibrations have been presented, through torsional and axial bending components in two plans, for the 6RND90 and K6SZ 52/105 main engines. The representations of own modes have been made possible by retaining displacement values corresponding to the middle length of the crankpins.

From the analysis of the own modes of coupled vibrations the following conclusions can be drawn:

- Variation waves of own vibration modes for the two engines are very resembling, due to geometrical and operational characteristics very close to these ones;
- For the 6RND90 main engine own individual vibration modes are alike the coupled vibrations, especially for torsional and bending vibrations (as shown in 4.1, 4.7 and 4.33 figures): for the torsional type the node corresponding to the 1st degree is generated on the propeller shaft, this being valid for the individual case, as well as for the coupled one, while for the 2nd degree mode, on the crankshaft engine. For the bending vibrations own vibration modes are identical in both cases;
- Variation waves of own bending vibration modes are similar with the individual ones and the coupled ones, but the coupled vibration relative amplitude is lower and that marks a lower contribution of this type of vibration in the coupling phenomenon;
- The influence of the axial vibration phenomenon in the coupling of shaft line vibrations for both engines is much more highlighted for the 2nd

vibration mode, in the 1st mode sign changes doesn't occur, the amplitude variation being relatively lower;

- The torsional coupled mode for the 1st degree vibration is very similar with the axial coupled one with a 2nd degree, which is, in fact, a single mode for bot type of engines and this confirms the previous suggestion regarding the coupling process between two vibration modes.

In the 4.35 figure the average deformed fiber for a Sulzer 6RND90 main engine crankshaft is being presented and this is generated for the nominal functioning regime for which a frequency analysis has been done, which will be presented further on in the 4.36 figure.

It has been highlighted that harmonics generate visible resonances. It can be concluded that the critical resonance occurs in the same time with the k = 6 order harmonic, while the influence of the k = 4 order harmonic (the first order harmonic at the propeller frequency) of axial induced excitations in the shaft line by the propeller is being lower enough, contrary with the expectations. Thus, the predominant influence on the axial vibrations is generated by the torsional vibrations, according with the coupling phenomenon described above.

From the facts stated above, synchronized with the global presentation made in the 4.3.3 paragraph, it can be concluded that there is an importance for a certain special type of vibration generated by the nature and the dimensions of the amplitude and the specific excitations for marine propulsion engines and this is the axial one, being generated after the coupling phenomenon of shaft line vibrations. This issue has started lately to be tackled by engine designers and naval constructors, thus, special studies had not yet been done and this highlights even more the after mentioned phenomenon.

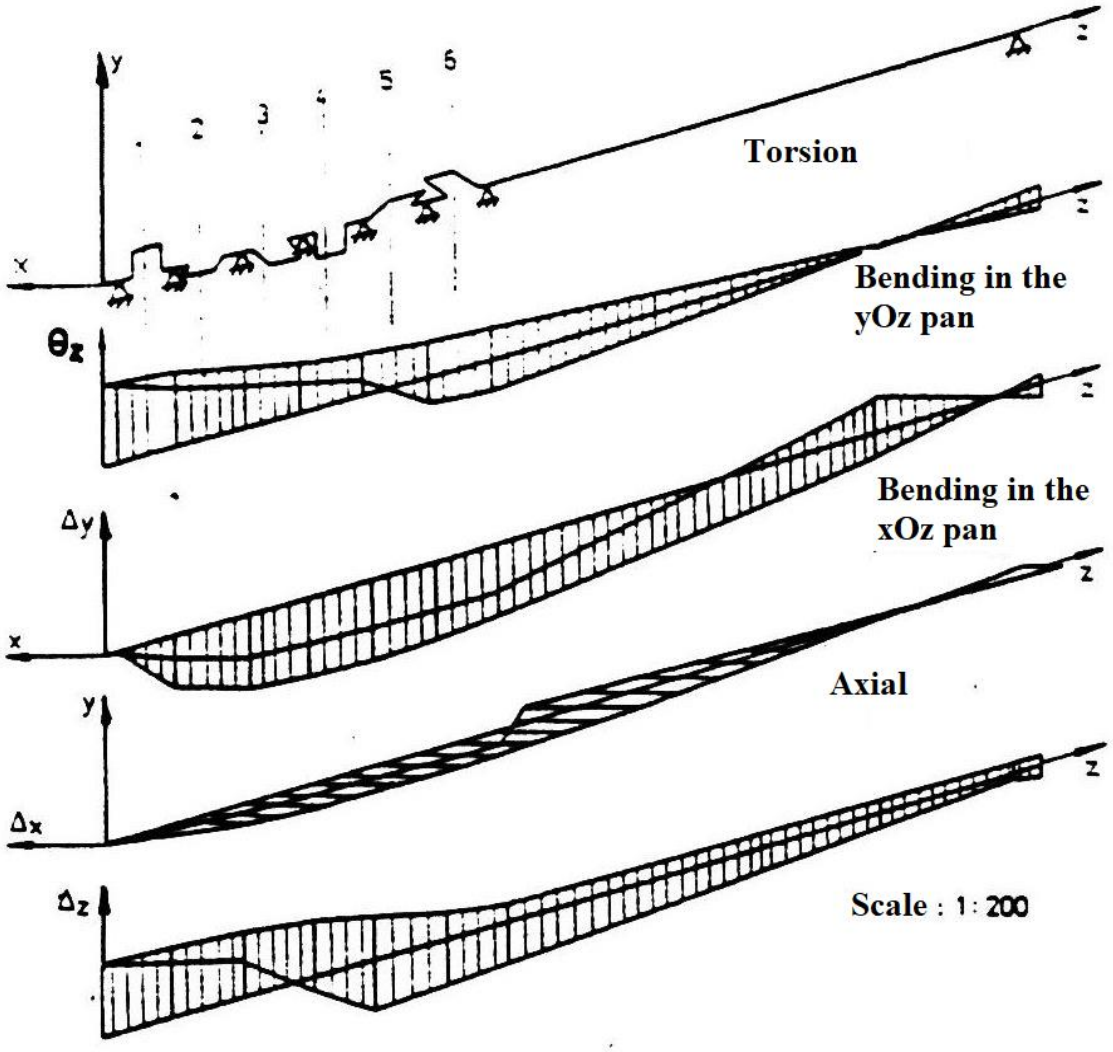

Figure 4.33: Own coupled vibration modes for the Sulzer 6RND90 main engine

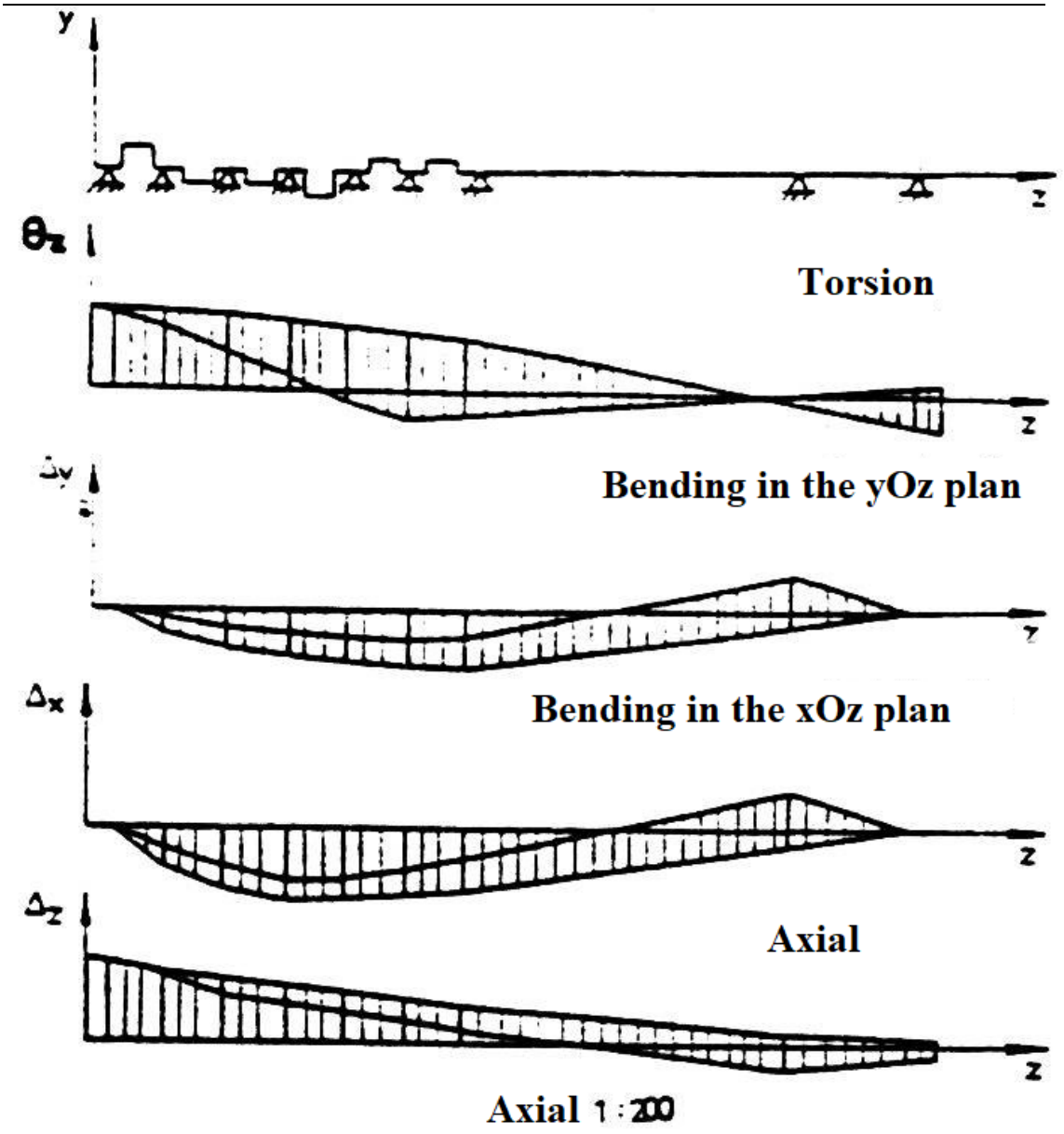

Figure 4.34: Own coupled vibration modes for the MAN K6SZ 52/105 main engine

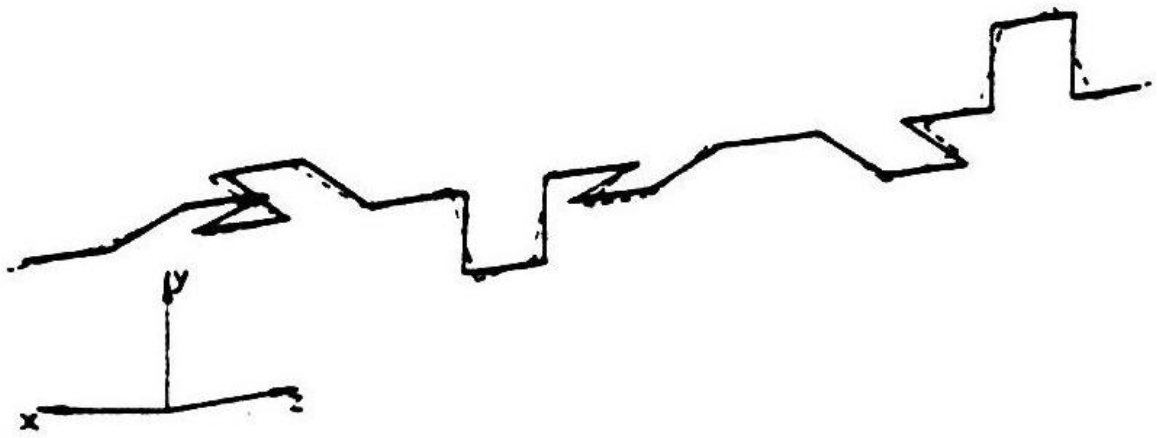

Figure 3.35: Deformed average fiber for a Sulzer 6RND90 marine main engine

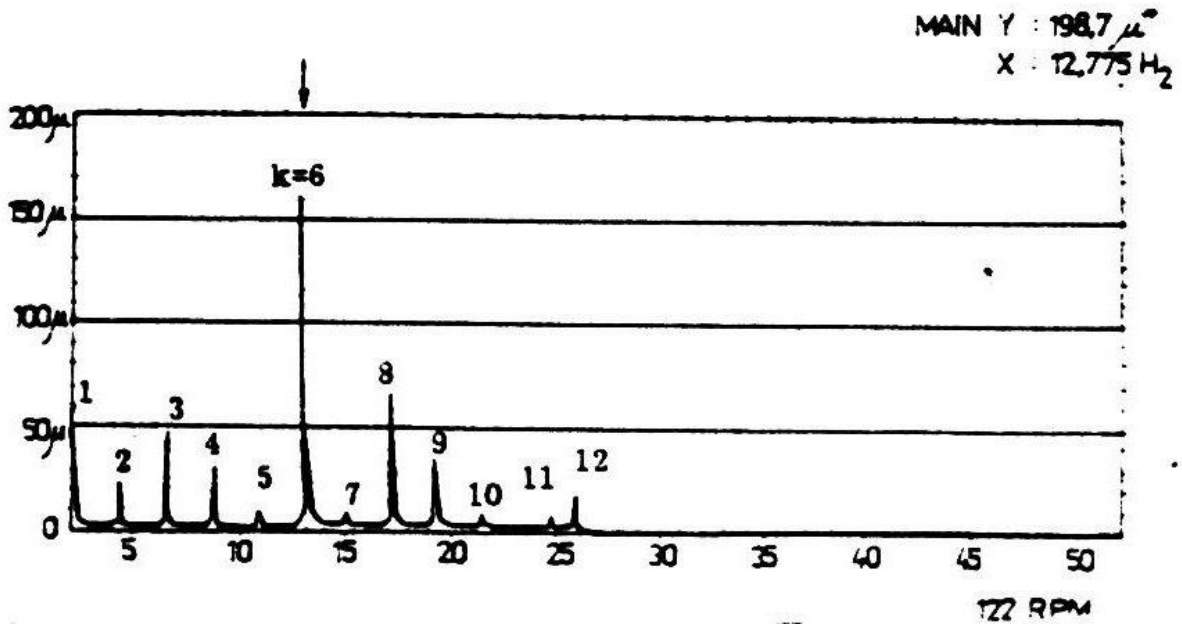

Figure 4.36: Axial vibration amplitude analysis in frequency for a free end in the case of a marine Sulzer 6RND90 main engine

In the reference No. [59] the individual own modes for axial vibrations are presented, with and without vibration compensators for a Sulzer 7RTA62 main engine, shown in the 4.37 and 4.38 figures, as well as the forced axial vibration

amplitudes at the engine free end. This engines develops a 9340 kW effective power at a 78 rpm nominal speed.

It can be noticed on this example that the axial vibration 1st mode has a form very close towards the one calculated for the 6RND90 and K6SZ main engines, as shown in the 4.33 and 4.34 figures and in all cases there is no sign change and that on its entire length, in the range of the axial bearing and the propeller, the relative amplitude is constant, this result being in resonance with the main purpose of this bearing. In exchange the second vibration mode records a single node and its position is placed, as a general rule, on the crankshaft. Own pulsation values for the Sulzer 7RTA62 are: $\omega_{0I} = 9.45\ s^{-1}$ and $\omega_{0II} = 24.6\ s^{-1}$ for the situation of functioning with no axial vibrations compensator, and $\omega_{0I} = 15.78\ s^{-1}$ and $\omega_{0II} = 26.22\ s^{-1}$ when the vibration compensator is fitted.

In the same time, it can be noticed the main engine 6RND90 axial individual vibration of own pulsation are placed in the same range of corresponding values for the two mentioned situations, with and without a vibration compensator, values mentioned in the case of the Sulzer 7RTA62 main engine. In the same time we can observe a reduction of axial vibration amplitude proportion of at least 1/10, as well a reduction from 150 kN to 80 kN for the force from the thrust bearing. In the same time, for the same specified engine, the comparison between measured values and calculus of individual axial vibrations is less favorable than the one specific for the individual torsional vibrations that have been checked in the previous paragraphs for the initial 6RND90 main engine. When the calculated own axial pulsations are very close in value to those measured (recording a 1 – 3 % difference) the axial amplitude vibrations can be different in the operational rotation range and this phenomenon is being explained by the occurrence of the coupling phenomenon of axial and torsional vibrations.

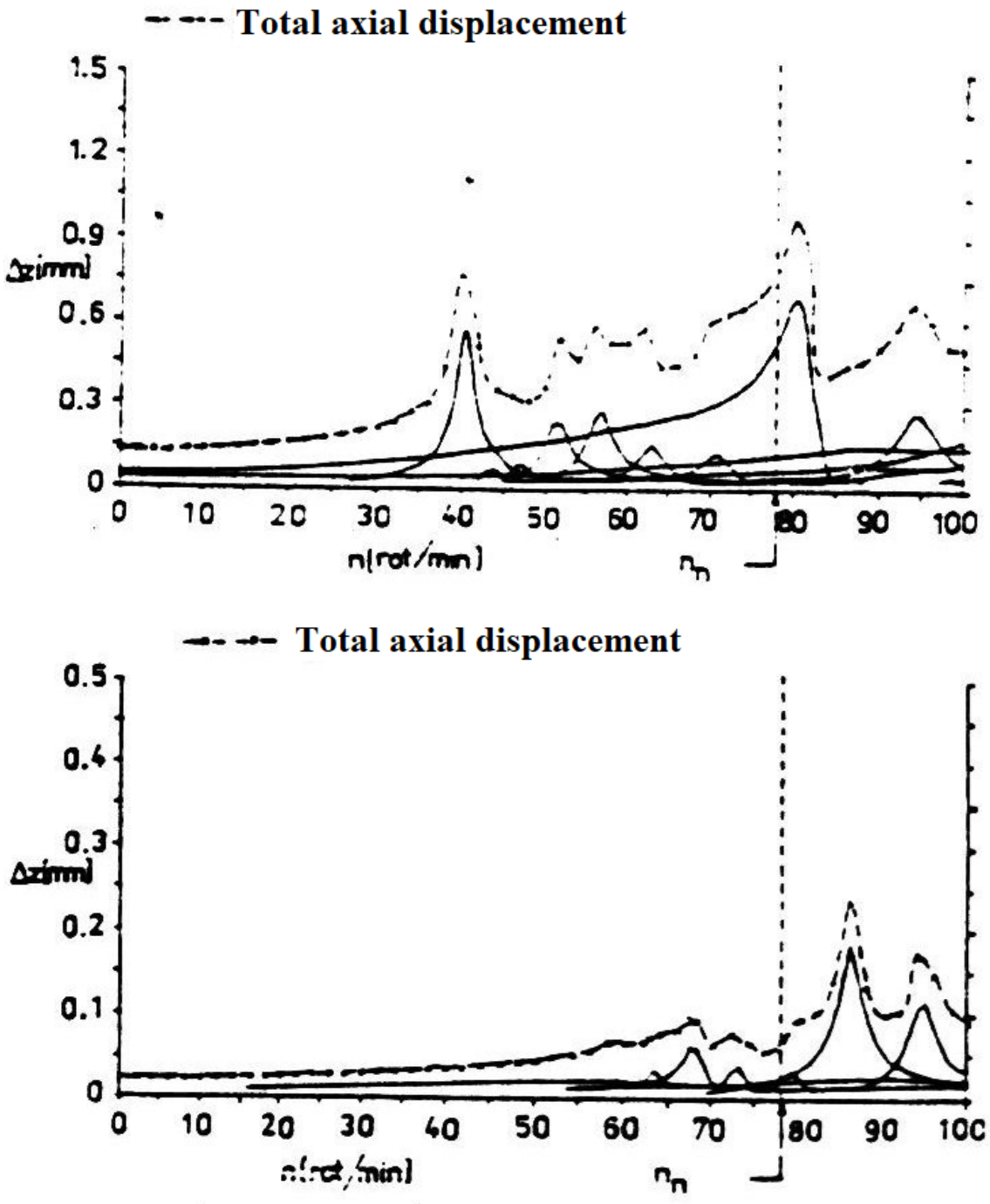

Figure 4.38: Individual axial vibration variation amplitude at the free end for the 7RTA62 main engine: a – without a compensator, b – with a compensator

The issue of shaft line individual vibrations coupling phenomenon started, in this manner to be treated with a maximum degree of attention by the marine engine

designers, as it has been cited in the reference No. [58], in which the subject is being developed by using the finite element method. By using the NASTRAN software the comparative result have been obtained between the amplitude of torsional and axial vibrations with the values measured for a 6RTA58 main engine, with or without an axial vibration compensator, as presented in the 4.39 and 4.40 figures. In this figure the following notations have been used:

- TT – torsional vibrations amplitude generated by the pure tangential excitation;
- AT – axial vibration amplitude, generated by pure radial excitation;
- TT + AT – total torsional vibration amplitude generated by both excitation types;
- TA – axial vibration amplitude generated by the pure tangential excitation;
- AA – axial vibration amplitude generated by the pure radial excitation;
- AA + TA – total axial vibrations amplitude generated by both excitation types, followed by the comparison with the measured values.

The analysis of these diagrams lead to the following conclusions:

- There are no significant differences between TT and AA calculated using NASTRAN software and the ones calculated using standard calculations;
- As it was expected, radial stimulation influence on torsional vibrations (AT) is not significant, in exchange it can be noticed that it plays an important influence of pure torsional excitation by harmonic order $k = 6$ on the axial vibrations, this phenomenon can be registered during operation at a rotation equal to 100 rpm.

We can notice the fact that critical rotation with a $k = 6$ order is very close to the value of nominal rotational speed (this being 122 rpm for the 6RND90 main engine), thus the engine can't operate at a nominal rotational speed unless an axial vibration compensator is fitted at the free end of the crankshaft. If the calculus is being redone in this new scenario it can be noticed that own torsional calculus (these being the critical torsional rotation). In exchange the own pulsation for the second axial mode changes in a significant manner, while the first axial mode remains constant and

this one is not being influenced by the axial compensator. This will, in effect influence, the own pulsation axial mode from 12 s^{-1} at 21 s^{-1}, the mentioned resonance in the case the of no compensator fitted will be avoided by applying this principle.

Even it has a certain influence on the torsional critical rotation with an I/6 order the amplitude of axial vibrations at the crankshaft bow extremity at the nominal rotational speed is much lower: 0.8 mm and not 7 mm for the $k = 6$ order harmonic, while the amplitudes of the other harmonic orders will also be much lower. In this way, figure 4.39b presents the comparison between torsional vibration amplitude calculus with a I/6 order and the axial ones with a II/6 order, by applying the principle of the NASTRAN software, these being compared with the measured values. We can also highlight the fact that a coupling effect between the vibrations modes and types previously mentioned for 6RND90 and K6SZ main engines has been carried out, according with the 4.33 and 4.34 figure, by using the presented software. This program presents the advantage of a meshing for a crankshaft bent in a realistic manner, superior to the one presented in the No. [58] reference, as well as the disadvantage of not taking into consideration the compensations, but this does not mean that this has an influence on the calculus accuracy around the nominal operation regime.

In the No. [99] reference a model based on the MEF method is also being used, being very similar with the proposed one, the calculus being done by using the ANSYS software but also including the compensations. This study has been done for an engine cu $i = 8$ cylinders, with a V configuration, four stroke functioning, with a crankshaft identical with a crankshaft for a $i = 4$ cylinder engine with an inline configuration and a four stroke functioning and having phase cranks. In the 4.41 figure is being presented, as a comparison, the first four coupled vibration modes, for a spatial structure formed by bars obtained in a similar manner with the one form the present paragraph and one that has the same shape as the bent (as presented for Sulzer RTA main engines in the 3.3 figure).

The observed differences on these two last models are insignificant. That is why the complex MEF based model can be checked for the calculus of coupled vibrations which is not plausible in this case.

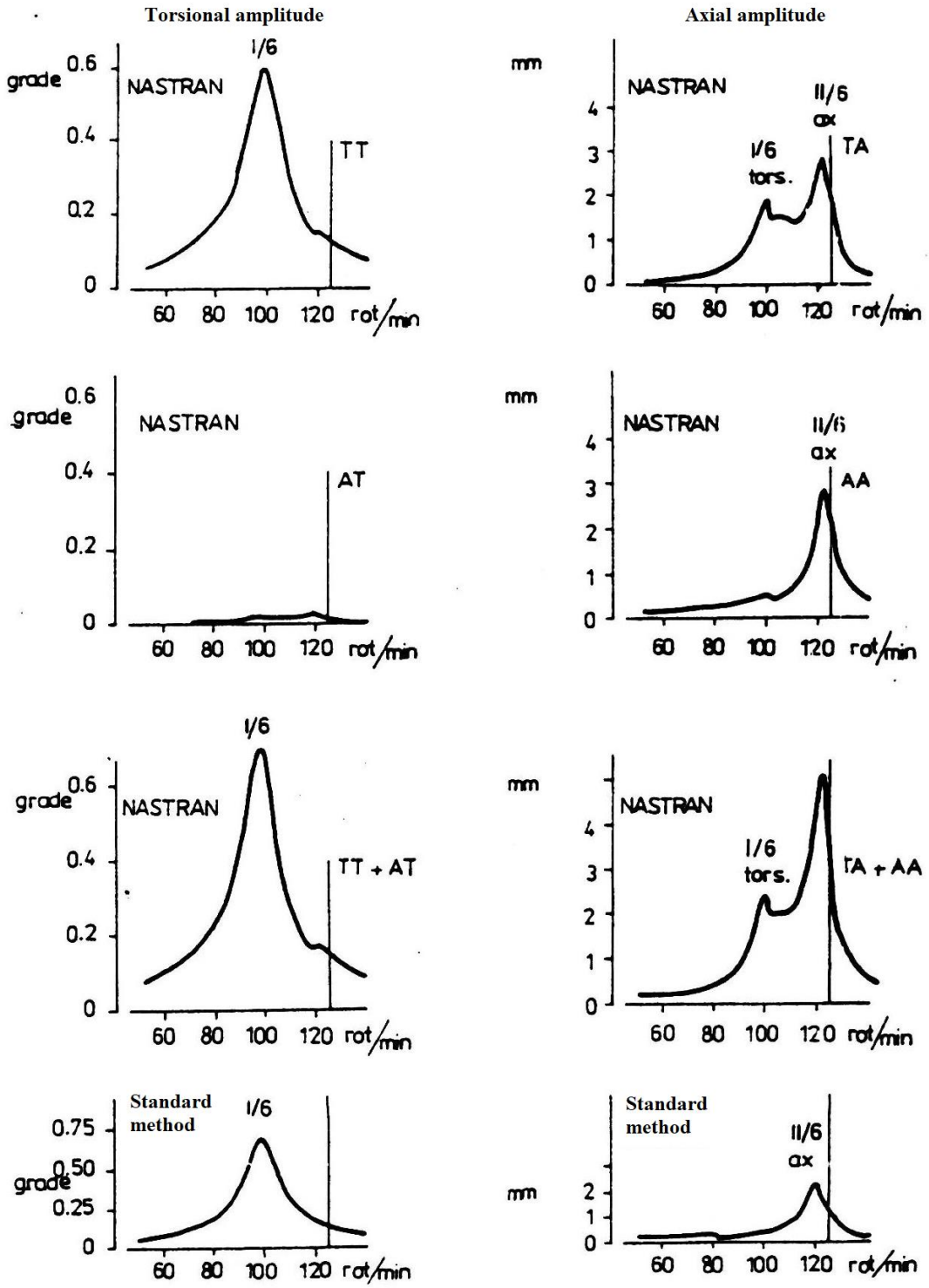

Figure 4.39: Axial and torsional vibrations amplitudes comparison for a Sulzer 6RTA58 main engine without axial vibration compensator

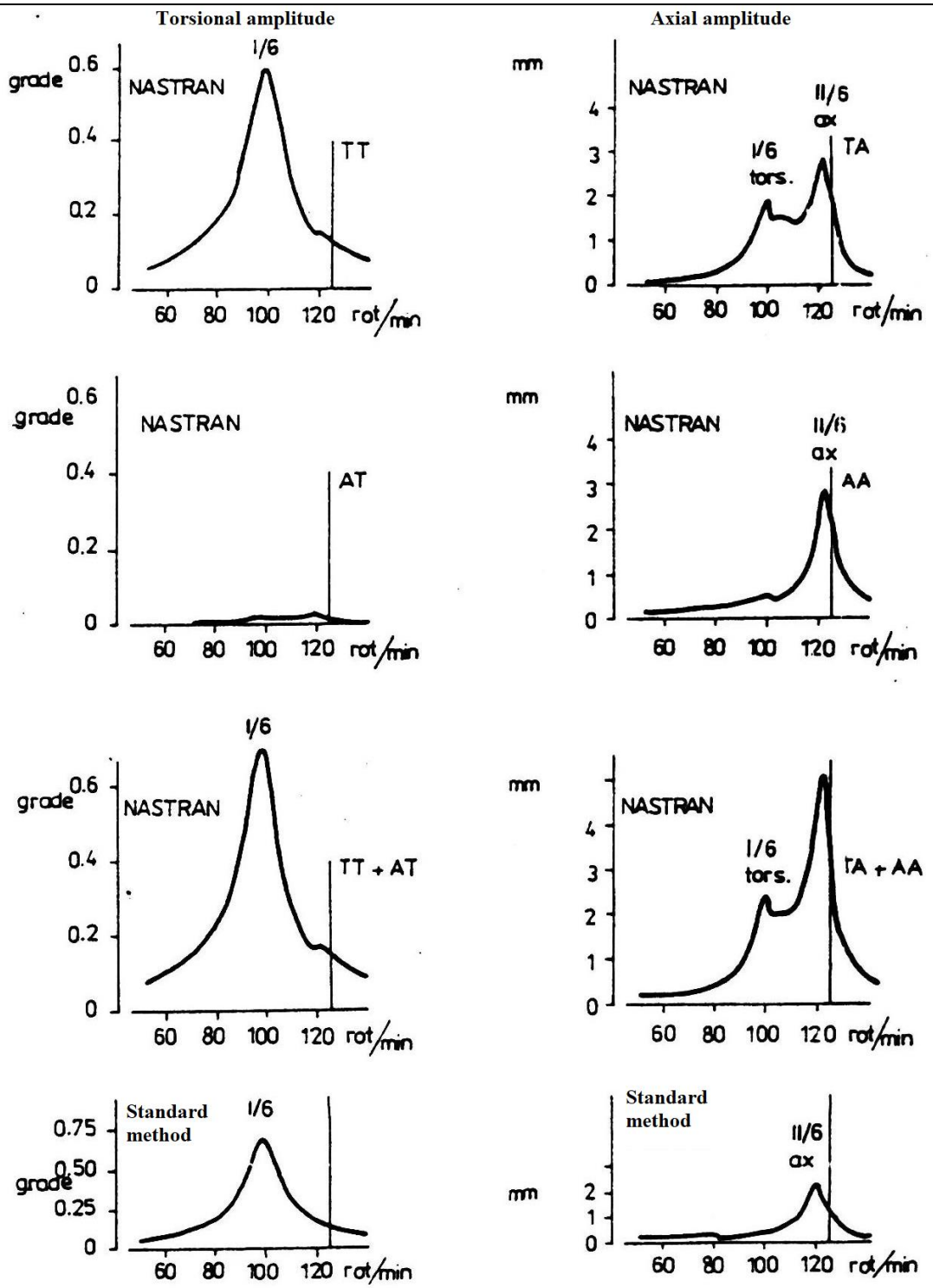

Figure 4.40: Axial and torsional vibrations amplitudes comparison for a Sulzer 6RTA58 main engine fitted with and axial vibration compensator

4.5 Experimental results for main engine shaft line vibrations measurements

Experimental validation of the proposed mathematical model proposed for the calculus of shaft line coupled vibrations of marine main engine has been done by applying a simple comparison method between the axial vibration amplitudes resulted after applying the presented methodology in the previous paragraph and the ones measured onboard during sea trials.

In order to do so an electronic set of equipment has been used, fitted with a probe that has a *vibration transducer*, preferably a *piezoelectric accelerometer*. This transducer does not need a reference point during the measurement process (as shown in the 4.42 figure). during measurements a *recorder with magnetic band* has also been used and its band has been interpreted in lab conditions. By using this type of device, a portable *7007 F recorder*, manufactured by Brule and Kjaer in Denmark a measurement chain element has been eliminated, this being the load *pre-amplifier*, which is already incorporated in the recording machine mentioned above.

When the spectral analysis is being done in the lab a *dualchannel real time analyzer* has been used, manufactured by Bruel and Kjaer, model 2034. After processing and handling the magnetic band the real time analyzer has trans ponded the recorded data from the time-amplitude domain into the amplitude-frequency domain, by using the FFT techniques (*Fast Fourier Transform*) displaying needed data straight to the operator.

The processed data have been generated by using a *numerical plotter* manufactured by Bruel and Kjaer, 2319 model. The measuring chain has been presented in the 4.43 figure observing the fact the inferior branch has been applied onboard the ship and the superior one has been applied in lab conditions as mentioned in the No. [118] reference. This way measurements have been made at an axial vibratory level for the K6SZ 52/105 main engine.

Shaft line axial vibrations measurements have been carried out after the owner has claimed that he has registered an amplifying of the vibration level onboard one of

his ships. Afterwards an axial vibration compensator has been fitted at the bow extremity of the main engine in both modes measurements being done in river navigation conditions.

These measurements have been carried out for the following operating regimes of the main engine:

- 100 rpm (corresponding with the starting value of critical rotational speed zone);

- 115 rpm (corresponding with the ending value of the critical rotational speed zone);

- 140 rpm (corresponding with the cruising speed).

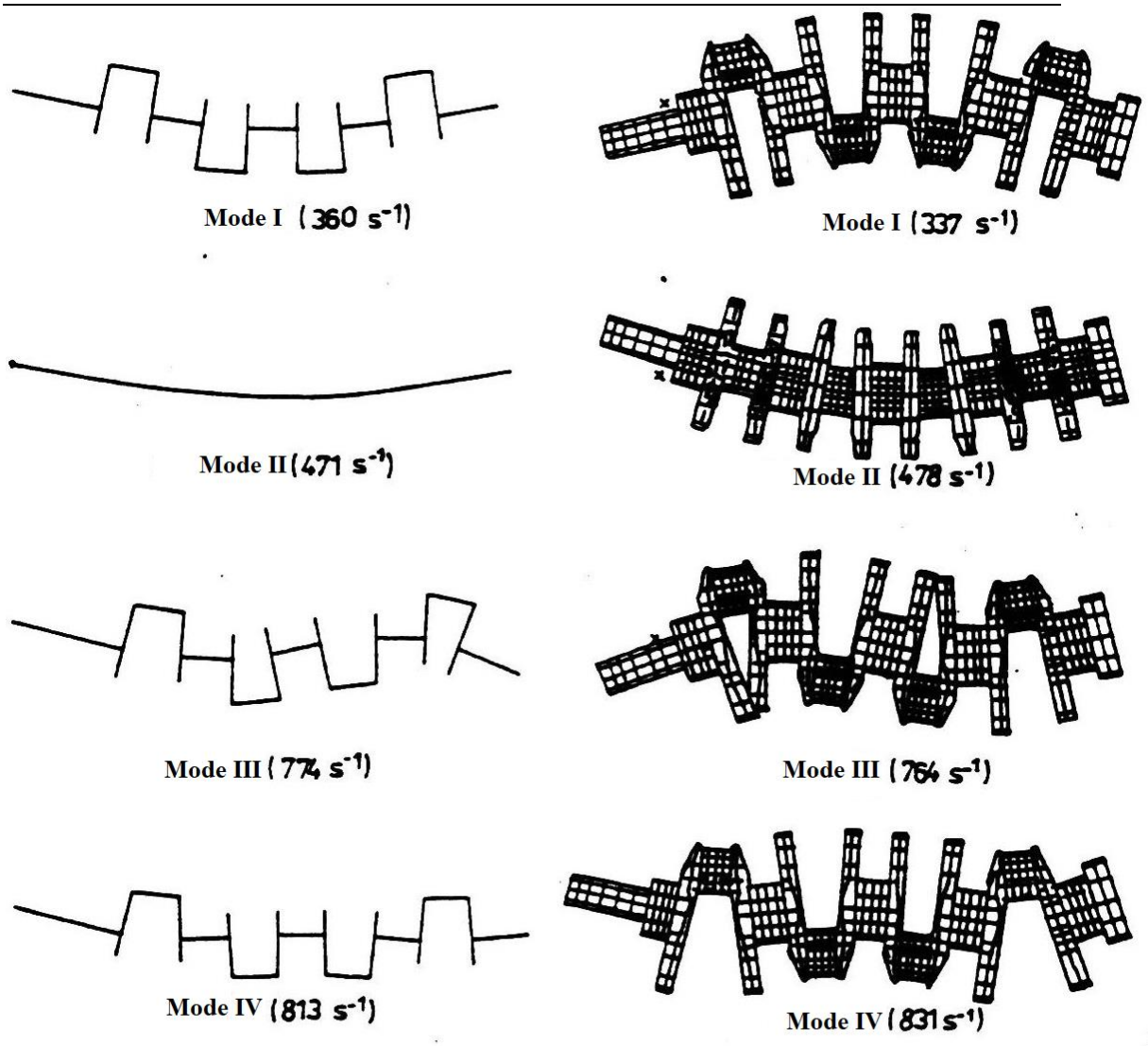

Figure 4.41: Comparison between the first vibration modes for a for stroke engine, these being calculated with ANSYS software for a simplified (left) and complex (right) structure

Axial vibration measurements have been recorded on a magnetic band and processed afterwards in the Sounds and Vibrations Laboratory of ICEPRONAV Galati Institute the results being presented and compared afterwards with the reference values specified in the No. [103] and [118] references and in the 4.44 figure and in 4.15 table.

Thus, by applying the MEF based calculus the first own pulsation regimes have been discovered by obtaining the amplitude values shown in the 4.16 table. Additional, it has to be mentioned that the measured values of the axial vibration amplitude are specific for the crankshaft corresponding with the situation in which a compensator is not fitted.

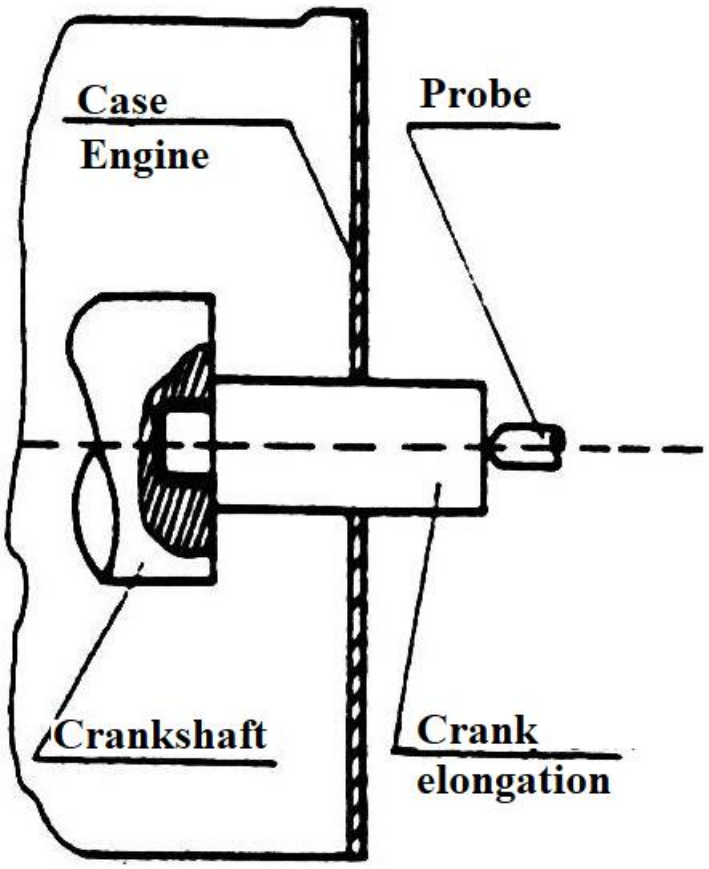

Figure 4.42: Accelerometer fitting diagram at the free end of the engine needed measure the axial vibration amplitude

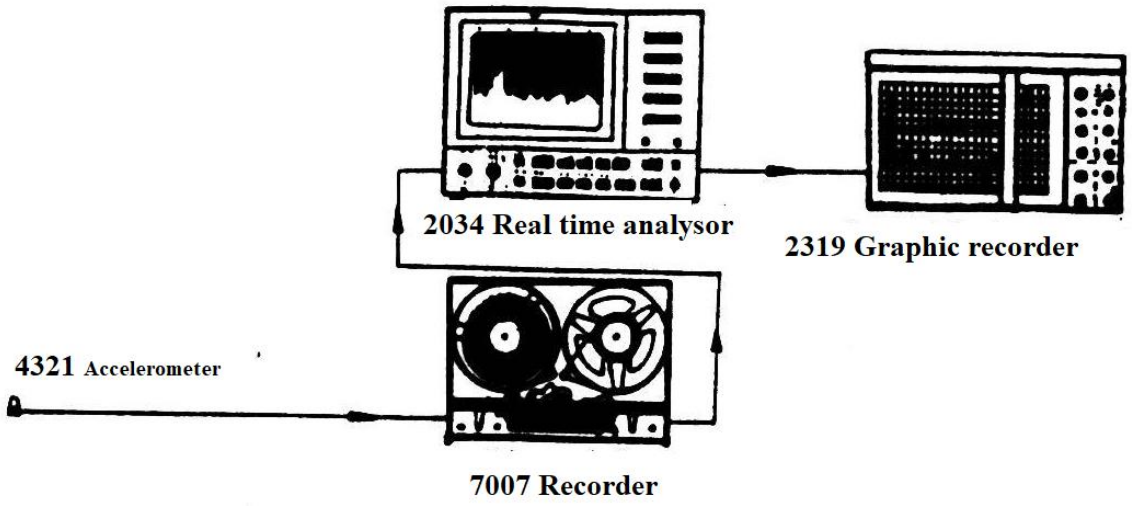

Figure 4.43: Measuring chain diagram for the system used to measure axial vibrations on the MAN K6SZ 52/105 main engine

It can be seen that around the 115 rpm rotational speed value a critical domain is being recorded for the real functioning conditions of the K6SZ 52/105 main engine and this confirms the above stated as well as through 2nd order own pulsation values previously mentioned. Truly, the rotational speed corresponding to this mode is: n_0 = *9.55 rpm,* ω_0 = *756,723 rpm*, and the rotational resonance with the harmonic order component with a $k = 6$ order is $n_6 = 6\ X\ 115 = 690\ rpm$, thus the ratio between the two rotational speed, as shown in the No. [89] reference is $\beta = n_6 / n_0 = 0{,}91$ and this value justifies the previous stated affirmation. Coupled vibrations calculus is being done only for the rotational speed corresponding to the nominal operating domain, for which the compensating effect can be neglected. It can be noticed that at a 140 rpm rotational speed the value difference between measurements and calculus is being placed around 9%, the compensating effect being lower and lower.

Extrapolating the results for the K6SZ 52/2015 main engine in the proximity of the nominal domain at the initial 6RND90 main engine for which the complex vibration calculus has been done, at the same functioning regime, the experimental validation of the proposed calculus model can be confirmed.

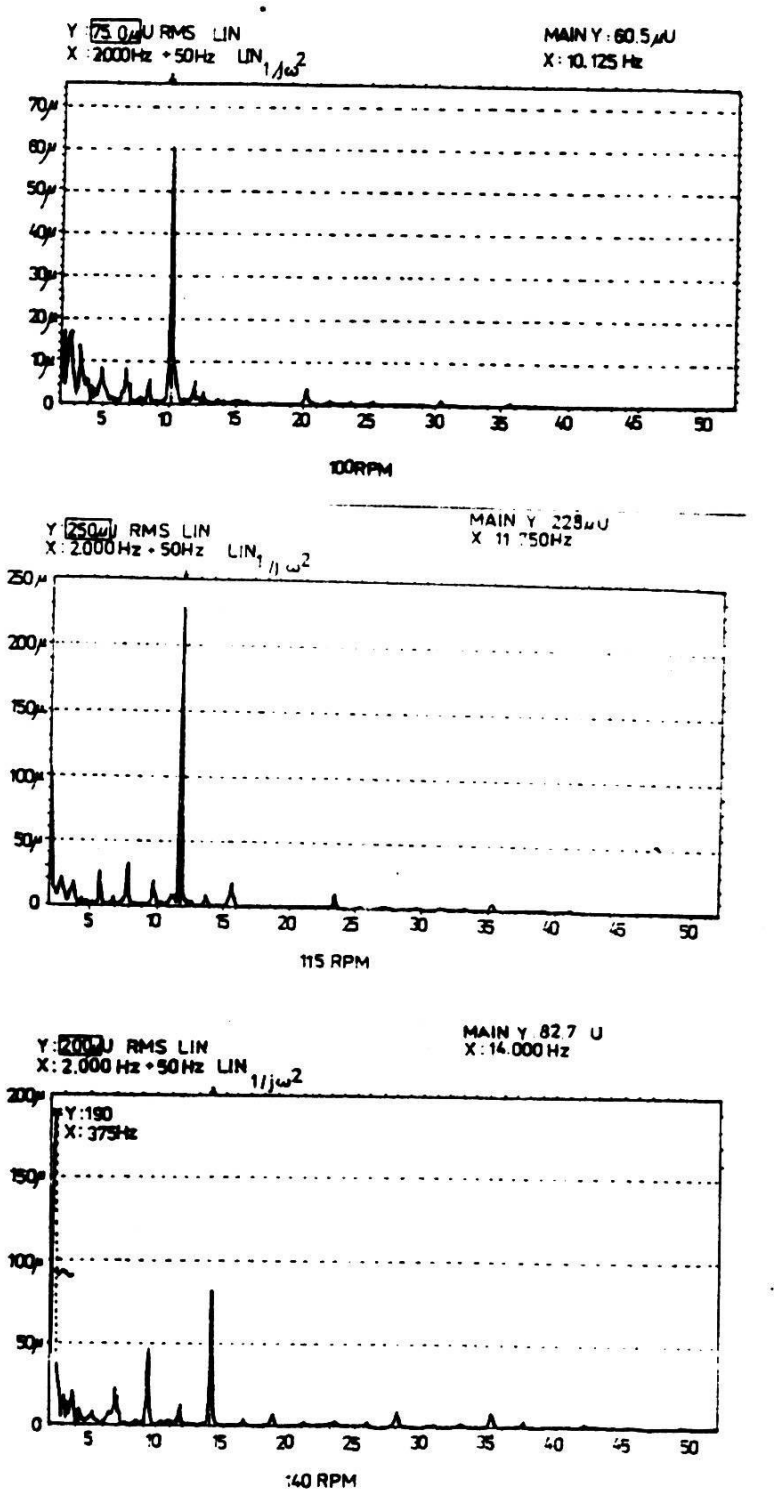

Figure 4.44: Axial vibrations spectrograms at the free end of the MAN K6SZ 52/105 main engine

Table 4.15: A comparison between axial vibrations amplitudes measured for the K6SZ 52/105 main engine in both cases, with and without axial vibrations compensator

Main engine regime [rpm]	Measured parameters			
	Frequency [Hz]	Amplitude [mm]		
		Without compensator	With compensator	Allowed values
100	10.25	0.865	0.065	0.318
115	11.75	2.740	0.228	0.318
140	14.00	0.726	0.082	0.318

Table 4.16: A comparison between axial vibrations amplitudes measured for the K6SZ 52/105 main engine and the ones calculated using MEF without an axial vibration compensator

Main engine regime [rpm]	Measured parameters			
	Frequency [Hz]	Amplitude [mm]		
		Measured	Calculated	Allowed values
100	10.25	0.865	-	0.318
115	11.75	2.740	-	0.318
140	14.00	0.726	0.793	0.318

References:

1. Bărănescu, G. *Teoria echilibrajului motoarelor cu ardere internă în linie*, Editura Academiei Române, București, 1975;

1. Apostolescu N., Taraza, D. *Bazele cercetării experimentele a maşinilor termice*, Editura Didactică și Pedagogică, București, 1979;

2. Barbu, M. *Câmpurile fizice ale navelor. Acțiuni și contraacțiuni*, Editura Militară, București, 1991;

3. Bayhan, M., Buzbuchi, N. *Engine Vibration Effects on Exhaust System and Sound Damping*, Volumul celei de-a VII-a Conferințe naționale de vibrații mecanice, Timișoara, 1993;

4. Bayhan, M., Buzbuchi, N. *Development and Application of Marine Engine*, Volumul "Sesiunea de comunicări științifice", Universitatea "Dunărea de Jos", Galați, 1993;

5. Bădescu, R. *Integrale utilizate în mecanică, fizică, tehnică și calculul lor*, Editura Tehnică, București, 1968;

6. Bățaga, N. *Motoare termice*, Editura Didactică și Pedagogică, București, 1979;

7. Bidoaie, J., Scarlet, G., Popovici, J.S., Totolici, S. *Bearing Forces Calculation*, Proceedings of the National Symposium of Ships Hydrodynamics, Galați, 1983;

8. Bonz, W. *Die Erregung der Längsschiwingungen von Kurbewellen*, MTZ, Jahrq 21 Heit 3 August, Berlin, 1960;

9. Bratu, P. *Sisteme elastice de rezemare pentru mașini și utilaje*, Editura Tehnică, București, 1990;

10. Brayard, J. *Avant projet de l'hélice standard, sillage et suction*, ENSTA, Paris, 1975;

11. Brătianu, C. *Metode cu elemente finite*, Editura Academiei Române, București, 1983;

12. Broch, J.T. *Mechanical Vibration and Shock Measurement*, K. Larsen & Son, Glodstrup, Denmark, 1984;

13. Bryndum, L., Jakobsen, S.B. *Vibration Characteristics of Two-Stroke Low Speed Diesel Engines*, MAN B&W, Copenhagen, 1987;

14. Buzbuchi, N. *Torsional Vibration of Marine Diesel Engines Shafting Systems. Software Reference Manual*, National Technical University of Athens Publishing House, Greece, 1995;

15. Buzbuchi, N., Oanță, E. *Matrix Methods in Studying the Torsional Vibration of the Marine Engines Shafting Systems. Software Reference Manual*, National Technical University of Athens Publishing House, Greece, 1996;

16. Buzbuchi, N. *Dinamica sistemelor de propulsie navalã*, Tipografia Institutului de Marinã Civilã Constanța, 1998;

17. Buzbuchi, N., Dinescu, C. *Vibrațiile motoarelor navale*, Tipografia Institutului de Marinã Civilã, Constanța, 1993;

18. Buzbuchi, N., Dinescu, C. *Complemente de* d*inamica motoarelor navale*, Editura Alas, Cãlãrași, 1995;

19. Buzbuchi, N., Taraza, D., Lyridis, D. *Theoretical and Experimental Study of the Torsional, Bending and Axial Coupled Vibration of Marine Diesel Engine Shafting System"*, Bulletin of the Marine Engineering Society in Japan (MESJ), the Fifth International Symposium on Marine Engineering ISME, Yokohama, 1995; a VIII-a Sesiune de Comunicări Științifice, Academia Navalã "Mircea cel Bãtrân", Constanța, 1995;

20. Buzbuchi, N., Taraza D., Lyridis, D. *Improvement of Marine Diesel Engine Dynamic Behaviour on Design and Operating Stage*, Institute of Marine Engineering Trans., London, 1995;

21. Buzbuchi, N. *Analiza surselor de excitație a vibrațiilor complexe ale liniilor de arbori antrenate de motoarele navale*, Buletinul Tehnic al Registrului Naval Român, nr. 3-4, București, 1995;

22. Buzbuchi, N., Boiangiu, M., Țoloiu, V.A. *Simulation of Coupled Vibrations in Two-Stroke Engine Crank Shafting*, Buletinul Tehnic al Registrului Naval Român, nr. 3-4, București, 1998;

23. Buzbuchi, N., Oanțã, E., Țoloiu, V.A. *Analytical and Numerical Methods in Studying the Shaft Alignment of the Internal Combustion Engine*, Romanian Journal of Technical Sciences Applied Mechanics, Editura Academiei Române, 1997;

24. Buzbuchi, N., Oanþã, E., Țoloiu, V.A. *Comparative Methods for Calculation of Marine Engine Shafting System*, Buletinul Tehnic al Registrului Naval Român, nr. 2, București, 1997;

25. Buzbuchi, N., Oanțã, E., ªoloiu V.A. *Dynamic Behaviour of the High Power Engine Shafing by Means of MTM*, the 8-th Conference with international participation VEHICLE AND ENVIRONEMENT CONAT-96, 10 pag., Brașov, 1996;

26. Buzbuchi, N. *Cuplarea vibrațiilor torsionale cu cele axiale și de încovoiere ale liniilor de arbori ale motoarelor cu ardere internã navale*, Referat de doctorat nr. 1, Universitatea "Politehnica" București, 1993;

27. Buzbuchi, N. *Echipamente și tehnici de mãsurare a vibrațiilor*, Referat de doctorat nr. 2, Universitatea "Politehnica" București, 1993;

28. Buzbuchi, N., Taraza, D. *On Vibration Analysis in Ship Installations with Two-Stroke Diesel Engines*, the Transaction Volume of the Motor and Motor Vehicle Engines, Izmir, 1993;

29. Buzbuchi, N. *Reversibilitatea elicelor navale*, Volumul "Sesiunea de comunicãri ºtiinþifice", Universitatea "Ovidius", Constanța, 1991;

30. Buzbuchi, N., Pruiu, A. *Cuplarea vibrațiilor torsionale și de încovoiere ale liniilor de arbori acționați de motoarele cu ardere internã navale"*, Volumul "Calculul și construcția motoarelor", a V-a Consfãtuire națională: "Creativitate în construcția, fabricația și repararea automobilelor", Pitești, 1993;

31. Buzbuchi, N., Bayhan, M. *Metode matriceale în studiul vibrațiilor torsionale ale liniilor de arbori ale motoarelor navale*, Volumul "Sesiunea de comunicãri științifice", Universitatea "Dunãrea de Jos", Galați, 1993;

32. Buzbuchi, N., Bayhan, M. *Efectul vâscozitãții asupra amortizãrii vibrațiilor torsionale ale liniilor de arbori ale motoarelor navale auxiliare*, Volumul "Sesiunea de comunicãri științifice", Universitatea "Dunãrea de Jos", Galați, 1993;

33. Buzdugan, Gh., Fetcu, L., Radeș, M. *Vibrații mecanice*, Editura Didactică și Pedagogică, București, 1982;

34. Buzdugan, Gh., Mihălescu, E., Radeș, M. *Vibration Measurement*, Martinus Nijhoff Publishers, Dordrecht, the Neenderlands & Editura Academiei, Bucharest, 1986;

35. Buzdugan, Gh., Mihăilescu, E., RadeȘ, M. *Măsurarea vibrațiilor*, Editura Academiei Române, București, 1979;

36. Buzdugan, Gh.: *Izolarea antivibratorie a mașinilor"*, Editura Academiei Române, București, 1980;

37. Buzdugan, Gh. *Izolarea antivibratorie*, Editura Academiei Române, București, 1993;

38. Carafoli, E., Oroveanu, T. *Mecanica fluidelor*, Editura Academiei Române, București, 1955;

39. Carafoli, E., Constantinescu, V.N. *Dinamica fluidelor incompresibile*, Editura Academiei Române, București, 1981;

40. Constantinescu, N.C., Dăneț, G. *Metode noi pentru calcule de rezistență*, Editura Tehnică, București, 1990;

41. Constantinescu, V.N., Gălețușe, St. *Mecanica fluidelor și elemente de aerodinamică*, Editura Didactică și Pedagogică, 1983;

42. Darabont, A., Văiteanu, D. *Combaterea poluării sonore și a vibrațiilor"*, Editura Tehnică, București, 1983;

43. Dumitrescu, H., Georgescu, A., Dumitrache, Al., Ghiță, Gh., Ceangă, V., Popovici, J.S., Nicolescu, B. *Calculul elicei*, Editura Academiei Române, București, 1990;

44. Fihtengolþ, G.M. *Curs de calcul diferențial și integral"*, Editura Didactică și Pedagogică, București, 1965;

45. Gafițeanu, M., Crețu, S., Drăgan, B. *Diagnosticarea vibroacustică a mașinilor și utilajelor*, Editura Tehnică, București, 1989;

46. Gafițeanu, M., Focșa, V., Merticaru, V., Biborosch, L. *Vibraþii și zgomote*, Editura "Junimea", Iași, 1980;

47. Gafițeanu, M., Poterașu, V.F., Mihalache, N. *Elemente finite și de frontierã cu aplicații la calculul organelor de mașini"*, Editura Tehnicã, 1987;

48. Gârbea, D. *Analizã cu elemente finite*, Editura tehnicã, București, 1990;

49. Gârlașu, Șt., Popp, C., Ionel, S. *Introducere în analiza spectralã și de corelație"*, Editura "Facla", Timișoara, 1982;

50. Georgescu, A. *Aproximații asimptotice*, Editura Tehnicã, București, 1989;

51. Gomez, G.P., Adalid, J.G. *Optimizacion del rendimiento de propulsor aislado de las helices de los buques"*, "Ingineria naval", nr. 687, 1992;

52. Gray, A., Mathews, G.B. *Funcții Bessel și aplicațiile lor în fizicã*, Editura Tehnicã, București, 1958;

53. Greenwald, B. *Teoria, calculul și construcția motoarelor pentru autovehicule rutiere*, Editura Didacticã și Pedagogicã, București, 1980;

54. Harris, M.C., Crede, E.Ch.: *Șocuri și vibrații*, Editura Tehnicã, București, 1969;

55. Heinz Kern, G. *Längsschwingungen von Kurbelwellen großer Schiffsdieselmotoren*, MTZ, Jahrq 1, Helt 2 Februar, Berlin, 1969;

56. Ivan, M. *Bazele calcului liniar al structurilor*, Editura "Facla", Timișoara, 1985;

57. Ixaru, L. Gr. *Numerical Methods for Differential Equations and Applications"*, Editura Academiei Române, București, 1984;

58. Jenzer, J., Welte, Y. *Coupling Effect between Torsional and Axial Vibration in Installations with Two-Stroke Diesel Engines*, New Sulzer Diesel, Winterthur, Switzerland, 1991;

59. Jenzer, J. *Vibration Analysis for Modern Ship Machinery*, New Sulzer Diesel, Winterthur, Switzerland, 1991;

60. Jenzer, J., Frossard de Saugny, H. *On the Dynamics of Diesel Power Plant*, New Sulzer Diesel, Winterthur, Switzerland, 1991;

61. Kovach, M. *Motor Vehicle Engines*, Editions Mir, Moscow, 1979;

62. MacCamhoil, M. *Static and Dynamic Balancing of Rigid Rotors*, Brüel & Kjaer, Naerum, Denmark, 1990;

63. Maier, V., *Mecanica și construcția navei*, Editura Tehnicã, București, 1986;

64. Mangeron, D., Poterașu, V.F., Vulpe, A. *Teoria optimizării structurilor cu aplicații*, Editura "Junimea", Iași, 1980;

65. Memet, F., Buzbuchi, N. *Coupled Vibrations of the Two-Stroke Marine Engine Shafting*, Bulletin of the Eighth International Congress of IMAM, Istanbul Technical University, Maritime Faculty, 1997;

66. Olariu, V., Brãtianu, C. *Modelare numericã cu elemente finite*, Editura Tehnicã, București, 1986;

67. Nestorides, E.J.A. *A Handbook on Torsional Vibration*, University Press, Cambridge, 1958;

68. Pascariu, I. *Elemente finite: concepte, aplicații"*, Editura Militarã, București, 1985;

69. Parlevliet, Th. *Modell zur Berechnung der erzwungenen Biege-und Torsionsschwingungen von Kurbelwellen unter Berücksichtigung der Ölverdrängungsdämpfung und Steifigkeit in den Grundlagern*, Doktor-Ingenieur genehmigte Dissertation, Technischen Universität Berlin, 1981;

70. Pestel, E.C., Leckie, F.A. *Matrix Methods in Elastomecnics*, McGgrow-Hill Book C-ny Inc., New York, 1963;

71. Petrila, T., Gheorghiu, C.I. *Metode element finit și aplicații"*, Editura Academiei Române, București, 1987;

72. Pitrop, N., Buzbuchi, N. *Calculul pulsațiilor proprii ale liniilor de arbori prin metoda elementelor finite*, Volumul "Sesiunea de comunicări Științifice", Institutul de Marinã Civilã, Constanța, 1993;

73. Ponomariov, S.D. *Calculul de rezistență în construcția de mașini"*, vol. III, Editura Tehnicã, București, 1987;

74. PopoviciI, J.S., Prever, R., Totolici, Șt., Trincas, G. *Unstady Hydrodynamics Propeller Forces: Validalion among Theoretical Calculations, Experiments and Full-Scale Measurements*, "Tecnica italiana", nr.2, Trieste, 1993;

75. Posea, N. *Calculul dinamic al structurilor*, Editura Tehnicã, București, 1991;

76. Pounder, C.C. *Marine Diesel Engines*, Newnes-Butterworth, London, 1976;

77. Pruiu, A., Buzbuchi, N. *Influența calării elicei asupra echilibrajului motoarelor navale de propulsie*, Volumul "Calculul și construcția motoarelor", a V-a Consfătuire națională: "Creativitate în construcția automobilelor", Pitești, 1993;

78. Radeș, M. *Diagnosis of an Auxiliary Diesel Engine Vibration Problem with Signature Analysis*, "Machine vibration", Springer-Verlag London Limited, 1992;

79. Rãdoi, M., Deciu, E. *Mecanica*, Editura Didacticã și Pedagogicã, 1981;

80. Rijic, I.C. *Tabele de integrale, sume, serii și produse"*, Editura Tehnicã, București, 1955;

81. Ripianu, A. *Mișcările vibratorii ale arborilor cotiți și drepți"*, Editura Tehnicã, București, 1969;

82. Ripianu, A., Crãciun, I. *Osii, arbori drepți și cotiți"*, Editura Tehnicã, București, 1977;

83. Ripianu, A. *Calculul cinematic și dinamic al arborilor cotiți"*, Editura "Dacia", Cluj, 1981;

84. Rodrigues, E. *Methodes de calcul des structures*, ENSTA, Paris, 1972;

85. Sialș, Gh. *Vibrații mecanice*, Editura Tehnicã, București, 1968;

86. Silaș, Gh. *Sisteme vibropercutante*, Editura Tehnicã, București, 1986;

87. Smirnov, V. *Cours de mathématiques supérieures*, tome II, Éditions Mir, Moscou, 1970;

88. Smoleanski, M.L. *Tabele de integrale nedefinite*, Editura Tehnicã, București, 1972;

89. Stuart, R.D. *Introducere în analiza Fourier, cu aplicații în tehnicã"*, Editura Tehnicã, București, 1971;

90. Șabac, Gh. *Matematici speciale*, Editura Didacticã și Pedagogicã, București, 1981;

91. Taraza, D. *Dinamica motoarelor cu ardere internã*, Editura Didacticã și Pedagogicã, București, 1985;

92. Taraza, D., Buzbuchi, N., Popovici, J.S. *Calculation of the Harmonic Structure of Marine Propeller Torque and Thrust*, International Off-Highway & Powerplant Congress & Exposition, Milwaukee, Wisconsin, 1994;

93. Taraza, D. *Possibilities to Reconstruct Indicator Diagrams by Analyis of Angular Motion of the Crankshaft*, International Off-Highway & Powerplant Congress & Exposition, Milwaukee, Wisconsin, 1993;

94. Taraza, D. *Estimation of the Mean Indicated Pressure from Measurement of the Crankshafts Angular Speed Variation*, International Off-Highway & Powerplant Congress & Exposition, Milwaukee, Wisconsin, 1993;

95. Taraza, D., Buzbuchi, N. *Considerații asupra vibrațiilor complexe ale motoarelor navale*, Volumul celei de-a VII-a Conferințe naþionale de vibrații mecanice, Timișoara, 1993;

96. Taraza, D., Buzbuchi, N. *Studiul vibrațiilor torsionale ale liniilor de arbori ale motoarelor navale prin metoda modalã*, Volumul "Sesiunea de comunicări științifice", Institutul de Marinã Civilã, Constanța, 1993;

97. Vanșeidt, V.A. *Motoare Diesel*, Editura Tehnicã, București, 1959;

98. Voinea, R., Voiculescu, D., Ceașu, V. *Mecanica*, Editura Didacticã și Pedagogicã, București, 1983;

99. Wakabayashi, K., Shimoyamada, K., Kodama, T., Honda, Y., Iwamoto, S. *A Numerical Computation for Vibration Displacements and Stresses of Crankshaft with a Shear Rubber Torsional Damper* International Congress and Exposition, Detroit, Michigan, 1993;

100. Yeo, S.D., Han, C.S., Lee, K.W., Cho, D.B.,Cheon, J. *Three Dimensional Crankshaft Vibration Analysis Including Gyroscopic Effect*, International Congress & Exposition, Detroit, Michigan, 1993;

101. Wang, P.C. *Metode numerice în mecanica construcțiilor*, Editura tehnicã, București, 1970;

102. Wang, P.C. *Numerical and Matrix Methods in structural Mechanics*, New-York, London, Sydney, John Wiley & Sons Inc., 1965;

103. *** *Reccomandations en vue de limiter les effets des vibrations à bord des navires*, Bureau Veritas, N.I., Juin, 1979;

104.*** *Service Instructions for Sulzer Diesel Engines, type RND 90*, Sulzer Brother Ltd., Winterthur, Switzerland, 1986;

105. *** *Reguli pentru clasificarea și construcția navelor maritime"*, Registrul Naval Român, București, 1990;

106. *** *Rules for the Constructions and Classification of Steel Ships*, Lloyd's Register of Shipping, London, 1968;

107. *** *Rules for the Constructions and Clasification of Steel Ships"*, Det Norske Veritas, Oslo, 1980;

108. *** *Master Catalogue-Electronic Instruments*, Brüel & Kjaer, Larsen & Son, Glodstrup, Denmark, 1989;

109. *** *Instrumente pentru mãsurãtori de sunet, vibrații, iluminare, mediu ambiant termic și gaze, pentru analize de semnal și diagnoze medicale*, Catalog rezumat, Brüel & Kjaer, Larsen & Son, Glostrup, Denmark, 1991;

110. *** *Introduction to Underwater Acoustics*, Application notes, Bruel & Kjaer, Naerum, Denmark, 1990;

111. *** *An Intoduction to Vibration Aspects of Two-Stroke Diesel Engines in Ships*, MAN B&W a/s, Copenhagen, Denmark;

112. *** *Calculation for Torsional Vibration*, Sumitomo Heavy Industries Ltd., Tamashima Machinery Div., Okayama, Japan;

113. *** *Navires, ports et chantiers*, Journal de la Marine Marchande, Paris, 1985-1990;

114. *** *Buletin de informare tehnicã*, BITNAV-ICEPRONAV, Galați, 1985-1993;

115. *** *Buletin tehnic*, Registrul Naval Român, București, 1985-1998;

116. *** *Sudostroenie*, Moskva, 1985-1990;

117. *** *Motorship*, the Motor Ship Publishing Office, London, 1987-1994;

118. *** *Diagnosticarea prin vibrații a stării tehnice a motoarelor și echipamentelor navale. Analiza fiabilității acestora*, contract de cercetare 1098/93, Institutul de Marinã Civilã Constanța, ICEPRONAV Galați, 1993-1994.

5. STRUCTURAL RESISTANCE VIBRATIONS OF MARINE MAIN ENGINES

A particular phenomenon for marine main engines, also highlighted in Chapter 3 is the occurrence of bending vibrations on the structural resistance elements of these engines.

The complexity of studying the above mentioned vibration types is a consequence of the constructive complicated structural shape of engine structures and the variable characteristic of all loads applied on it.

5.1 Bending vibrations excitation sources for structural elements of main engines

The origin of these type of vibrations has been presented in the 3.2.2 subchapter, these being the so-called *lateral forces and momentum*, and in that chapter the main own vibrating modes have been presented as well.

Further one it must be mentioned that the main source of excitation are the rolling momentum acting in the motion plan of each engine drive, which are being generated by the inertial effects of gas pressure. The dimensional value for the momentum is identical with the engine momentum (as mentioned in the 2.1 paragraph). On the general overview the harmonic component formula with a *k* order can be written for this momentum as:

$$M_{rs_k} = \left|M'_k\right| \sin\left(k\omega\tau + \beta_k\right) \quad (5.1)$$

In the above formula the module and the initial phase are being deducted has having the same formulas presented in reference No. [7]:

$$\begin{cases} \left|M'_k\right| = \left|M_k\right| \dfrac{\sin\dfrac{ik\delta}{2}}{\sin\dfrac{k\delta}{2}} \\ \beta_k = \varphi_k - \dfrac{(i-1)k\delta}{2} \end{cases} \qquad (5.2)$$

with the $|M_k|$ - the harmonic component module with a k order for the engine momentum, i - the cylinder number, δ - the angular off-set between two successive combustions and φ_i - the initial phase for the engine momentum as presented in (2.2) and (2.39) formulas.

The after mentioned component can be considered as being the effect of a lateral force with a variable harmonic expressed as:

$$F_{rs_k} = \frac{M_{rs_k}}{H} = \frac{\left|M'_k\right|}{H}\sin\left(k\omega\tau + \beta_k\right) \qquad (5.3)$$

this force would act straight on the cylinder axis, more precisely: at the extremity of the resistance structure, at a H distance towards the horizontal plan that includes the crankshaft axis (as presented in the 3.4 figure).

As it has been shown in the mentioned paragraph the qualitative approximation for the harmonic capacity taken into consideration in order to stimulate the structural elements is being given by the excitation degree defined in an analogical manner by the (4.103) formula, from which:

$$E_k = \sqrt{\left(\sum_{j=1}^{i}\phi_{k_j}\sin\alpha_{k_j}\right)^2 + \left(\sum_{j=1}^{i}\phi_{k_j}\cos\alpha_{k_j}\right)^2}, \qquad (5.4)$$

where θ_{kj} has the same specification as the one in the cited formula, while X_{kj} represents the own bending vibration modes for the engine structural resistance elements:

$$X_{k_j} = \begin{bmatrix} 1 & 1 & \cdots & 1 \end{bmatrix}^T \qquad (5.5)$$

for the *H* mode and:

$$X_{k_j} = \left[1 \quad \cdots 0 \quad \cdots \quad -1\right]^T \qquad (5.6)$$

for the *X* mode.

It has to be mentioned that the *X* mode the vector is null on the corresponding line of the cylinder *[i/2] + 1*.

5.2 Bending free and forced vibrations for structural resistance elements of marine main engines

In order to calculate the own pulsation regimes for structural elements the Myklestad method is being used, as mentioned in the No. [22] reference which is used for structure sketching by meshing the elements in a certain number of concentrated mass elements bounded between them by flexible areas, while the obtained oscillating system is directly dependent on the vibration type of the entire structure. The main issue is represented by mentioning the boundary conditions for the lower element stiffness (at the base of the structure). Experimental measurements allowed the evaluation of own frequencies for the structural elements and very close values have been noticed, such as the ones for an embedded plate, having a ratio between the height of the engine *H* and it's length *L*. Thus, for the Sulzer 6RND90 main engine the following data will be used:

- Height: H = 8,5 m;
- Length: L = 11,3 m;
- H/L ratio: 0,75 m;
- The own frequency H module;
- In shipyard: $\omega_H = 44.6\ s^{-1}$;
- In sea trials: $\omega_H = 40.2\ s^{-1}$;
- The own frequency X module;
- In shipyard: $\omega_H = 85.4\ s^{-1}$;

- In sea trials: $\omega_H = 83.5\ s^{-1}$;

Comparing with this method the modern calculus techniques based on MEF as mentioned in the references No. [3], [7], [10], [17] and [20] ensure a more precise evaluation of own pulsations for the entire structural assembly, because it substitutes the simplified calculus model represented by the concentrated mass system with one which is much closer to the real one. Mainly, this method ensures the expression of Lagrange equations for a conservative force system in a matrix formulation. A homogenous system is being obtained needed to calculate own pulsations regime. By imposing the condition that the system admits different solutions comparing with the normal one, the own pulsation regime for the structural elements are being obtained.

The effective calculus implies the meshing of the entire structure in finite elements having a square plate shape (as shown in the 5.1 figure which is valid for small powered engines, in generally, being tied up with more complex meshing situations for slower propulsion engines presented in the 3.6 figure).

According with the above mentioned figure an *(e)* element with the *a*, *b* and *h* thickness is being considered and for all its nodes the following independent parameters are being chosen:

- w – the displacement along the Oz axis;
- $\theta_x = -\partial w/\partial y$ - rotation around the Ox axis;
- $\theta_y = -\partial w/\partial x$ - rotation around the Oy axis.

For the *w* displacement a function with the following formula is being accepted:

$$w = a_1 + a_2 x + a_3 y + a_4 x^2 + a_5 xy + a_6 y^2 + a_7 x^3 + a_8 x^2 y + a_9 xy^2 + a_{10} y^3 + a_{11} x^3 y + a_{12} xy^3 \quad (5.7)$$

or the equivalent matrix:

$$w = X\,a \qquad (5.8)$$

in which:

$$\begin{cases} X = \begin{bmatrix} 1 & x & y & x^2 & xy & y^2 & x^3 & x^2y & xy^2 & y^3 & x^3y & xy^3 \end{bmatrix} \\ a = \begin{bmatrix} a_1 & a_2 & a_3 & a_4 & a_5 & a_6 & a_7 & a_8 & a_9 & a_{10} & a_{11} & a_{12} \end{bmatrix}^T \end{cases} \quad (5.9)$$

The a_i coefficients $i = 1 - 12$, are being calculated by imposing boundary conditions regarding displacements in the element nodes. By grouping the displacements and the rotation of all nodes of finite elements *(e)* in the column vector:

$$w^{(e)} = \begin{bmatrix} w_1 & w_2 & w_3 & w_4 & \theta_{1x} & \theta_{2x} & \theta_{3x} & \theta_{4x} & \theta_{1y} & \theta_{2y} & \theta_{3y} & \theta_{4y} \end{bmatrix}^T \quad (5.10)$$

the obtained value is:

$$w^{(e)} = Ba \quad (5.11)$$

Where B is a 12X12 matrix which has elements depending on the nodes coordinates. By applying the reverse matrix on the left side of the above formula B, $B^{-1} = H$, this one not being solitaire, results:

$$a = H w^{(e)} \quad (5.12)$$

The displacements are being considered as being time nodal functions, starting with the (5.8) and (5.22) formulas, thus, the w displacement becomes:

$$w(x, y, \tau) = X H w^{(e)} \quad (5.13)$$

By expressing the general Hooke law, which is a feature of the tensions plan status the following results:

$$\begin{cases} \sigma_x = \dfrac{E}{1-\nu^2}\left(\varepsilon_x + \nu\varepsilon_y\right) \\ \sigma_y = \dfrac{E}{1-\nu^2}\left(\nu\varepsilon_x + \varepsilon_y\right) \\ \tau_{xy} = \dfrac{E}{2(1+\nu)}\gamma_{xy} \end{cases} \quad (5.14)$$

where υ is the Poisson coefficient, written in a matrix formulation as:

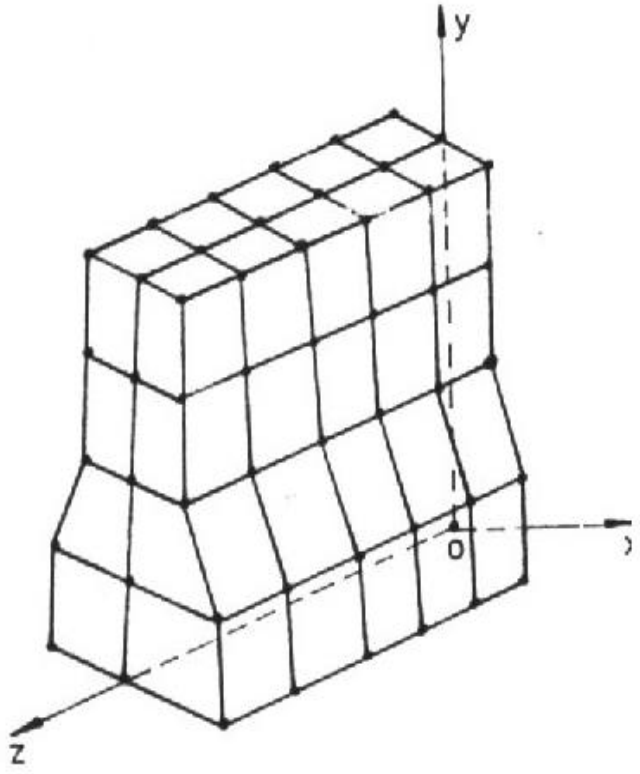

$$\begin{matrix}\sigma_x \\ \sigma_y \\ \tau_{xy}\end{matrix} = \frac{E}{1-\nu^2}\begin{matrix}1 & \nu & 0 \\ \nu & 1 & 0 \\ 0 & 0 & \frac{1-\nu}{2}\end{matrix}\begin{matrix}\varepsilon_x \\ \varepsilon_y \\ \gamma_{xy}\end{matrix} \qquad (5.15)$$

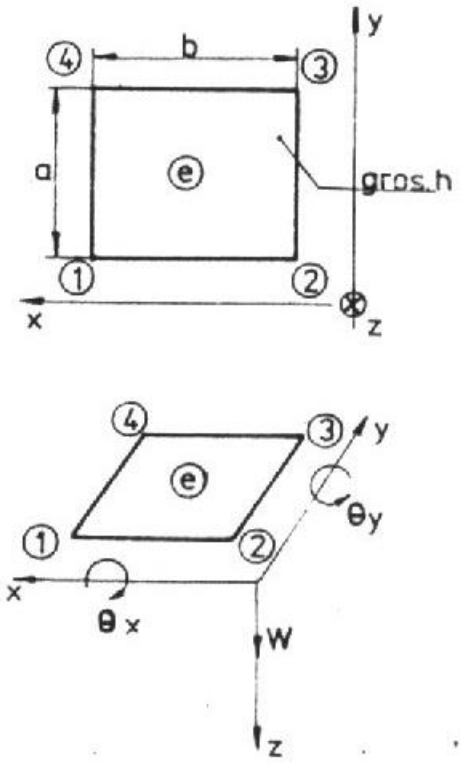

Figure 5.1: Finite elements structural meshing for a marine engine, finite elements having square plate shape

D symbolizes the flexibility plate matrix, written as:

$$D = \frac{Eh^3}{1-\nu^2}\begin{bmatrix} 1 & \nu & 0 \\ \nu & 1 & 0 \\ 0 & 0 & \dfrac{1-\nu}{2} \end{bmatrix} \quad (5.16)$$

The *C* vector for the curve is defined as:

$$C = \left[\frac{\partial^2 w}{\partial x^2} \quad \frac{\partial^2 w}{\partial y^2} \quad 2\frac{\partial^2 w}{\partial x \partial y} \right]^T \quad (5.17)$$

Applying the (5.7) equation the elements of the *C* are:

$$\begin{cases} \partial^2 w/\partial x^2 = 2a_4 + 6a_7 x + 2a_8 y + 6a_{11} xy \\ \partial^2 w/\partial y^2 = 2a_6 + 2a_9 x + 6a_{10} y + 6a_{12} xy \\ \partial^2 w/\partial x \partial y = a_5 + 2a_8 x + 2a_9 y + 3a_{11} xy \end{cases} \qquad (5.18)$$

From the (5.17) and (5.18) formula the following is obtained:

$$C = \begin{bmatrix} 0 & 0 & 0 & 2 & 0 & 0 & 6x & 2y & 0 & 0 & 6xy & 0 \\ 0 & 0 & 0 & 0 & 0 & 2 & 0 & 0 & 2x & 6y & 0 & 6xy \\ 0 & 0 & 0 & 0 & 2 & 0 & 0 & 4x & 4y & 0 & 6x^2 & 6y^2 \end{bmatrix} a = Ga$$

(5.19)

The potential deformation energy can be expressed as:

$$U = \frac{1}{2}\int_V \left(\sigma_x \varepsilon_x + \sigma_y \varepsilon_y + \tau_{xy} \gamma_{xy}\right) dV \qquad (5.20)$$

By taking the above relation and based on the (5.14) formula, the following results:

$$U = \frac{E}{2\left(1-\nu^2\right)}\int_V \left(\varepsilon_x^2 + \varepsilon_y^2 + 2\nu \varepsilon_x \varepsilon_y + \frac{1-\nu}{2}\gamma_{xy}^2 \right) dV \qquad (5.21)$$

Particular deformation and displacement formulas are:

$$\begin{cases} \varepsilon_x = \partial u/\partial x \\ \varepsilon_y = \partial v/\partial y \\ \gamma_{xy} = \partial v/\partial x + \partial u/\partial y \end{cases} \qquad (5.22)$$

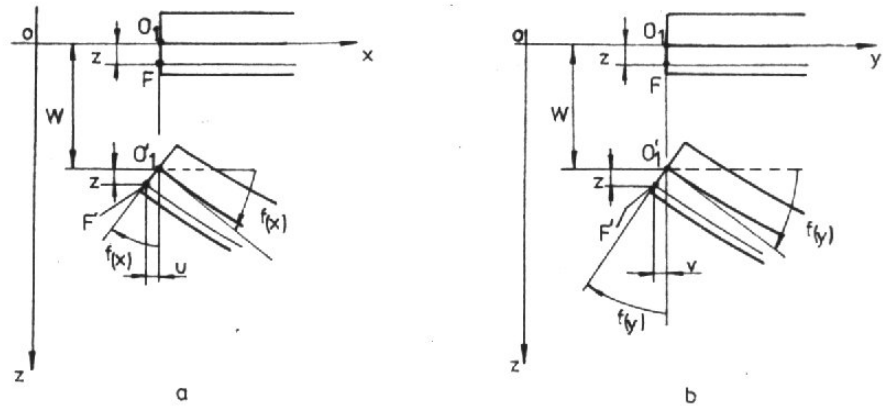

Figure 5.2: Stabilization diagram for correlations between modal displacements

Based on the non-deformability hypothesis of plate median surface, of normal straights and small displacements it can be proven that between the *u and v* displacements, as well as the transversal displacement *w* there are some form of dependencies (as seen in the above figure):

$$\begin{cases} u = -z\left(\partial w/\partial x\right) \\ v = -z\left(\partial w/\partial y\right) \end{cases} \qquad (5.23)$$

Now, by replacing (5.23) in (5.22) the following is obtained:

$$\begin{cases} \varepsilon_x = -z\,\dfrac{\partial^2 w}{\partial x^2} \\ \varepsilon_y = -z\,\dfrac{\partial^2 w}{\partial y^2} \\ \gamma_{xy} = -2z\,\dfrac{\partial^2 w}{\partial x \partial y} \end{cases} \qquad (5.24)$$

thus, the potential deformation energy becomes:

$$U = \frac{Eh^3}{2\left(1 - \nu^2\right)} \int_0^a \int_0^b \left(\frac{\partial^2 w}{\partial x^2} \right)^2 + \left(\frac{\partial^2 w}{\partial y^2} \right)^2 + 2\nu \frac{\partial^2 w}{\partial x^2} \frac{\partial^2 w}{\partial y^2} + 2(1 - \nu) \left(\frac{\partial^2 w}{\partial x \partial y} \right)^2 dxdy \quad (5.25)$$

Using the (5.11), (5.16), (5.17), (5.18) and (5.20) the value for the *U* energy can be expressed in a matrix manner:

$$U=\frac{1}{2}\int_0^a\int_0^b C^T D\ \ C\ \ dxdy=\frac{1}{2}\int_0^a\int_0^b a^T G^T D\ \ G\ \ a\ \ dxdy=\frac{1}{2}\int_0^a\int_0^b \left(w^{(e)}\right)^T H^T G^T D\ \ G\ \ H\ \ w^{(e)}dxdxy= \\ =\frac{1}{2}\left(w^{(e)}\right)^T\left[H^T\left(\int_0^a\int_0^b G^T D\ \ G\ \ H\ \ dxdy\right)\right]w^{(e)}. \quad (5.26)$$

Using the following notation:

$$R^{(e)}=H^T\left(\int_0^a\int_0^b G^T D\ \ G\ \ dxdy\right)H \quad (5.27)$$

for the stiffness matrix of the *(e)* element, the (5.27) expression for the potential energy is being transformed into:

$$U^{(e)}=\frac{1}{2}\left(w^{(e)}\right)^T R^{(e)}w^{(e)} \qquad (5.28)$$

The corresponding kinetic energy for the vibrating movement which the plate generated is:

$$E=\frac{1}{2}\int_V \rho\left(\frac{\partial w}{\partial \tau}\right)^2 dV \quad (5.29)$$

where ρ is the material density. In all integral equations form this paragraph, *V* represents the volume. By introducing (5.13) formula in the above formula will result:

$$E=\frac{1}{2}\int_0^a\int_0^b \rho h\left(\frac{\partial w}{\partial \tau}\right)^T\left(\frac{\partial w}{\partial \tau}\right)\ \ dxdy=\frac{1}{2}\int_0^a\int_0^b \rho h\left(\dot{w}^{(e)}\right)^T H^T X^T X\ \ \ H\ \ \ \dot{w}^{(e)}dxdy= \\ =\frac{1}{2}\left(\dot{w}^{(e)}\right)^T\left[H^T\left(\int_0^a\int_0^b \rho h\ \ \ X^T X\ \ \ dxdy\right)H\right]\ \ \dot{w}^{(e)} \quad (5.30)$$

Using the following notation:

$$M^{(e)} = H^T \left(\int_0^a \int_0^b \rho h \quad X^T X \quad dxdy \right) H \quad (5.31)$$

The mass matrix for the *(e)* element, the kinetic energy will be:

$$E = \frac{1}{2} (w^e)^{(T)} M^{(e)} w^{(e)} = \frac{1}{2} w^T R w \qquad (5.32)$$

By adding up all energy values for al structural elements the following results:

$$\begin{cases} U = \frac{1}{2} \sum_{(e)} \left(w^e\right)^{(T)} R^{(e)} w^{(e)} = \frac{1}{2} w^T R w \\ E = \frac{1}{2} \sum_{(e)} \left(w^e\right)^{(T)} M^{(e)} w^{(e)} = \frac{1}{2} w^T M w \end{cases} \qquad (5.33)$$

Based on the formulas expressed above, the Lagrange equations will be:

$$\frac{\partial}{\partial \tau} \left(\frac{\partial E}{\partial \dot{w}} \right) - \frac{\partial E}{\partial w} + \frac{\partial U}{\partial w} = 0 \quad (5.34)$$

the following matrix form will be adopted:

$$Mw + Rw = 0 \qquad (5.35)$$

With the vibrating motion of the entire structure written as:

$$w = W \sin\left(\omega \tau + \varphi\right) \quad (5.36)$$

The (5.35) can also be written as:

$$\left(R - \omega^2 M\right) \; W = 0 \quad (5.37)$$

generating an equation in the ω unknown that has a solution that leads to the own pulsation regime for the entire structure.

In order to calculate the structural displacements influenced by forced vibrations the matrix equation will be:

$$Mw + Rw = 0 \qquad (5.38)$$

in which F is the nodal force vector for the entire structure. By rewriting the (5.38) formula in amplitude values the following formula will be obtained:

$$W = \left(R - \omega^2 M\right) \left|F\right| \quad (5.39)$$

for which the force module is initially considered in harmonic components, being given by the lateral forces (5.3), from which the vector expressed in the (5.39) formula is being obtained by adding up the interest harmonics, in the same manner as it has been done in the (4.146) formula. The presented methodology can be applied to a simpler structure, such as the Sulzer 6RTA58 main engine and this lead to vibrating modes in H and X, as stated in the No. [16] reference and the 5.3 figure in which the own pulsation values have also been highlighted.

5.3 Experimental results of bending vibration measurements for main elements structural elements

Bending vibrations of resistance structures of the Sulzer 5RD68 main engine and Sulzer 3AL25/30 auxiliary engines fitted on the cadet ships *Neptun* belonging to the Maritime University of Constanta, having a 5500 deadweight, have been calculated during sea trials. This is the first engine developing a 5500 HP power at a 135 rpm nominal rotation, while the power for the auxiliary engines is 550 HP at a 750 rpm nominal rotation speed.

The measurement chain is fitted with the following elements:

- Piezoelectric accelerometer, 4388 type, manufactured by Bruel and Kjaer;
- Preamplifier, 2623 type, manufactured by Bruel and Kjaer;
- 2625 Amplifier, manufactured by Bruel and Kjaer;
- Frequency analyzer, type 2120, manufactured by Bruel and Kjaer.
- 214 oscilloscope, manufactured by Tetronix.

The measurement points have been set in the superior points, the ones corresponding to the turbocharger, with their functioning being influenced by this type of vibrations, as shown in the 3.2.2 paragraph.

The 5.4 figure shows the measurement points for the auxiliary engines, while the 5.5 figure the ones for the main engine nominal operation range, while the result are shown in tables 5.1 to 5.5, being calculated after an algorithm mentioned in the No. [6] and [18] references.

It can be seen that the placing of displacements in the boundary limits imposed by the classification societies has been done correct.

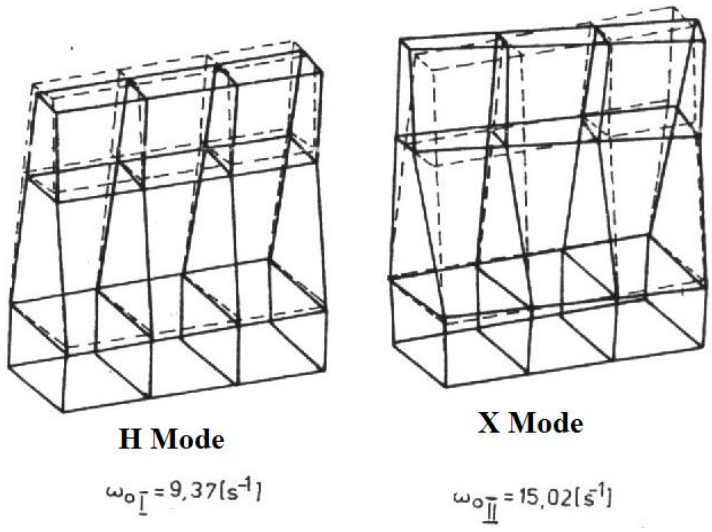

Figure 5.3: Vibration modes *H and X* for the structural resistance for a Sulzer 6RTA58 main engine

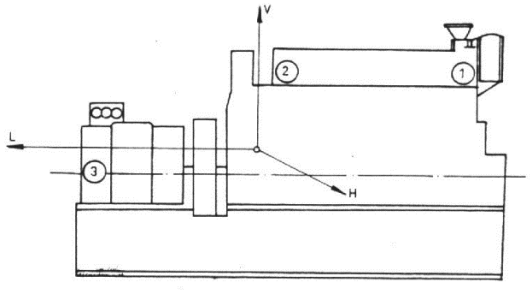

Figure 5.4: Measurement points placing for resistance structure vibrations in the case of a Sulzer 3AL25/30 main engine

Table 5.1: Resistance structure measurement results for a Sulzer 3AL

No. 1 Auxiliary engine	*n* = 750 rpm			Load = 295 kW
Measuring points	Displacement [mm]			Frequency [mm]
	V	L	H	
1	0.125	1.060	0.014	6.25
1	0.087	0.020	0.005	12.50
1	0.017	0.016	0.004	18.75
1	0.008	0.004	0.002	25.00
1	0.003	0.003	0.001	31.25
1	0.002	-	0.002	37.50
2	0.019	0.069	0.004	6.25
2	0.003	0.014	-	12.50
2	0.009	0.005	0.002	18.75
2	0.002	0.004	0.001	25.00
2	-	0.003	-	31.25
2	-	0.001	-	37.50
3	0.035	0.001	0.005	6.25
3	0.035	0.001	0.003	12.50
3	0.014	0.001	0.001	18.75
3	0.002	-	0.001	25.00
3	0.002	-	=	31.25
3	0.002	-	0.001	37.50

25/30 auxiliary engine No. 1

No. 2 Auxiliary engine	*n* = 750 rpm			Load = 295 kW
Measuring points	Displacement [mm]			Frequency [mm]
	V	L	H	
1	0.137	0.074	0.010	6.25
1	0.033	0.020	0.001	12.50
1	0.029	0.011	0.002	18.75
1	0.005	0.005	-	25.00
1	0.002	0.006	-	31.25
1	0.006	0.003	-	37.50
2	0.015	0.044	0.004	6.25
2	0.004	0.015	0.013	12.50

2	0.007	0.001	0.002	18.75
2	0.002	0.003	-	25.00
2	-	0.002	-	31.25
2	-	-	0.001	37.50
3	0.023	0.013	0.004	6.25
3	0.029	0.008	0.002	12.50
3	0.016	0.002	0.003	18.75
3	0.002	0.001	0.001	25.00
3	0.002	-	0.001	31.25
3	0.002	-	0.002	37.50

Table 5.2: Resistance structure measurement results for a Sulzer 3AL 25/30 auxiliary engine No. 2

Table 5.3: Resistance structure measurement results for a Sulzer 3AL 25/30 auxiliary engine No. 3

No. 3 Auxiliary engine	*n* = 750 rpm			Load = 295 kW
Measuring points	Displacement [mm]			Frequency [mm]
	V	L	H	
1	0.126	0.074	0.010	6.25
1	0.033	0.020	0.001	12.50
1	0.024	0.011	0.001	18.75
1	0.009	0.003	-	25.00
1	0.003	0.002	-	31.25
1	0.001	0.002	-	37.50
2	0.001	0.053	0.003	6.25
2	0.001	0.016	0.001	12.50
2	0.001	0.010	0.001	18.75
2	-	0.001	-	25.00
2	-	0.003	-	31.25
2	-	0.002	-	37.50
3	0.001	0.001	0.004	6.25
3	0.001	0.001	0.001	12.50
3	0.001	0.001	-	18.75
3	-	-	-	25.00
3	-	-	-	31.25
3	-	-	0.002	37.50

No. 4 Auxiliary engine	*n* = 750 rpm			Load = 295 kW
Measuring points	Displacement [mm]			Frequency [mm]
	V	L	H	
1	0.106	1.060	0.011	6.25
1	0.080	0.016	0.004	12.50
1	0.017	0.014	0.004	18.75
1	0.010	0.004	0.001	25.00
1	0.004	0.003	0.001	31.25
1	0.004	0.002	0.002	37.50
2	0.015	0.063	0.003	6.25
2	0.003	0.015	-	12.50
2	0.010	0.015	-	18.75
2	-	0.005	-	25.00
2	-	0.003	-	31.25
2	-	0.003	-	37.50
3	0.038	0.001	0.004	6.25
3	0.033	-	0.003	12.50
3	0.013	-	-	18.75
3	0.001	-	-	25.00
3	0.002	-	-	31.25
3	0.002	-	0.001	37.50

Table 5.4: Resistance structure measurement results for a Sulzer 3AL 25/30 auxiliary engine No. 4

Table 5.5: Resistance structure measurement results for a Sulzer 5RD68 main engine

Frequency [Hz]	Measuring point / Displacement amplitude [mm]					
	Bow turbocharger			Aft turbocharger		
	1 L	2 H	3 V	1 L	2 H	3 V
2.25	0.13	0.22	0.08	0.12	0.24	0.07
4.5	0.08	0.12	0.06	0.09	0.14	0.05
9	0.05	0.06	0.04	0.04	0.06	0.04
11.25	0.04	0.05	0.03	0.03	0.05	0.03

References:

1. Apostolescu N., Taraza, D. *Bazele cercetării experimentele a mașinilor termice*, Editura Didacticã și Pedagogicã, București, 1979;

2. Bărănescu, G. *Teoria echilibrajului motoarelor cu ardere internã în linie*, Editura Academiei Române, București, 1975;

3. Brayard, J., Muller, J. *Vibrations des structures*, ENSTA, Paris, 1974;

4. Brătianu, C. *Metode cu elemente finite*, Editura Academiei Române, București, 1983;

5. Broch, J.T. *Mechanical Vibration and Shock Measurement*, K. Larsen & Son, Glodstrup, Denmark, 1984;

6. Buzbuchi, N. *Echipamente și tehnici de măsurare a vibrațiilor*, Referat de doctorat nr. 2, Universitatea "Politehnica" București, 1993;

7. Buzbuchi, N., Dinescu, C. *Vibrațiile motoarelor navale*, Tipografia Institutului de Marinã Civilã, Constanța, 1993;

8. Buzbuchi, N., Dinescu, C. *Complemente de dinamica motoarelor navale*, Editura Alas, Cãlărași, 1995;

9. Buzbuchi, N., Taraza, D. *On Vibration Analysis in Ship Installations with Two-Stroke Diesel Engines*, the Transaction Volume of the Motor and Motor Vehicle Engines, Izmir, 1993;

10. Buzdugan, Gh., Mihãlescu, E., Radeș, M. *Vibration Measurement*, Martinus Nijhoff Publishers, Dordrecht, the Neenderlands & Editura Academiei, Bucharest, 1986;

11. Buzdugan, Gh., Fetcu, L., Radeș, M. *Vibrații mecanice*, Editura Didacticã și Pedagogicã, București, 1982;

12. Buzdugan, Gh., Mihãilescu, E., Radeș, M. *Măsurarea vibrațiilor*, Editura Academiei Române, București, 1979;

13. Buzdugan, Gh. *Izolarea antivibratorie a mașinilor*, Editura Academiei Române, București, 1980;

14. Bryndum, L., Jakobsen, S.B. *Vibration Characteristics of Two-Stroke Low Speed Diesel Engines*, MAN B&W, Copenhagen, 1987;

15. Gârbea, D. *Analizã cu elemente finite*, Editura tehnicã, București, 1990;

16. Jenzer, J. *Vibration Analysis for Modern Ship Machinery*, New Sulzer Diesel, Winterthur, Switzerland, 1991;

17. Jenzer, J., Frossard de Saugny, H. *On the Dynamics of Diesel Power Plant*, New Sulzer Diesel, Winterthur, Switzerland, 1991;

18. Niculescu, R., Buzbuchi, N. *Determinarea pulsațiilor proprii corespunzãtoare modului H de vibrație a structurii de rezistență motoarelor navale prin metoda elementelor finite*, Volumul "Sesiunea de comunicări științifice", Institutul de Marinã Civilã, Constanța, 1993;

19. Pestel, E.C., Leckie, F.A. *Matrix Methods in Elastomecnics*, McGgrow-Hill Book C-ny Inc., New York, 1963;

20. Posea, N. *Calculul dinamic al structurilor*, Editura Tehnicã, București, 1991;

21. Rodrigues, E. *Methodes de calcul des structures*, ENSTA, Paris, 1972;

22. Taraza, D. *Dinamica motoarelor cu ardere internã*, Editura Didacticã și Pedagogicã, București, 1985;

23. *** *Reguli pentru clasificarea și construcția navelor maritime"*, Registrul Naval Român, București, 1990.

24. *** *Reccomandations en vue de limiter les effets des vibrations à bord des navires*, Bureau Veritas, N.I., Juin, 1979.

Tipar executat în
Tipografia Universității Maritime din Constanța